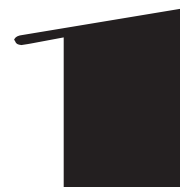




# VLÁKNA

# TEXTIL

## FIBRES AND TEXTILES



Volume **30**  
April  
**2023**

TECHNICAL  
UNIVERSITY  
OF LIBEREC

STU  
FCHPT



VÚTCH



CHEMITEX



**Indexed in:**

SCOPUS  
Chemical Abstract  
World Textile Abstracts  
EBSCO Essentials

ISSN 1335-0617  
print version

ISSN 2585-8890  
online version



# VLÁKNA A TEXTIL

<http://www.vat.ft.tul.cz>

## **PUBLISHED BY**

Technical University of Liberec, Faculty of Textile Engineering  
Slovak University of Technology in Bratislava, Faculty of Chemical and Food Technology  
Alexander Dubček University of Trenčín, Faculty of Industrial Technologies  
Slovak Society of Industrial Chemistry, Bratislava  
Research Institute of Man-Made Fibres, JSC, Svit  
VÚTCH – CHEMITEX, Ltd., Žilina  
Chemosvit Fibrochem, JSC, Svit

## **EDITOR IN CHIEF**

Maroš TUNÁK, Technical University of Liberec, CZ

## **EXECUTIVE EDITOR**

Veronika TUNÁKOVÁ, Technical University of Liberec, CZ

## **EDITORIAL BOARD**

Ľudmila BALOGOVÁ, VÚTCH – CHEMITEX, Ltd., Žilina, SK  
Marcela HRICOVÁ, Slovak University of Technology in Bratislava, SK  
Vladimíra KRMELOVÁ, A. Dubček University of Trenčín, SK  
Zita TOMČÍKOVÁ, Research Institute of Man-Made Fibres, JSC, Svit, SK  
Maroš TUNÁK, Technical University of Liberec, CZ  
Veronika TUNÁKOVÁ, Technical University of Liberec, CZ  
Tomáš ZATROCH, Chemosvit Fibrochem, JSC, Svit, SK

## **HONOURABLE EDITORIAL BOARD**

Vladimír BAJŽÍK, Technical University of Liberec, CZ  
Martin BUDZÁK, Research Institute of Man-Made Fibres, JSC, Svit, SK  
Anton GATIAL, Slovak University of Technology in Bratislava, SK  
Ana Marija GRANCARIĆ, University of Zagreb, HR  
Izabella KRUCIŇSKA, Technical University of Lodz, PL  
Anton MARCINČIN, Slovak University of Technology in Bratislava, SK  
Alenka M. LE MARECHAL, University of Maribor, SL  
Jiří MILITKÝ, Technical University of Liberec, CZ  
Darina ONDRUŠOVÁ, Alexander Dubček University in Trenčín, SK  
Olga PARASKA, Khmelnytskyi National University, UA  
Anna UJHELYIOVÁ, Slovak University of Technology in Bratislava, SK  
Victoria VLASENKO, Kyiv National University of Technologies and Design, UA

## **PUBLISHER**

Technical University of Liberec  
Studentska 1402/2, 461 17 Liberec 1, CZ  
Tel: +420 485 353615  
e-mail: [vat@tul.cz](mailto:vat@tul.cz)  
IČO: 46747885

## **ORDER AND ADVERTISEMENT OF THE JOURNAL**

Technical University of Liberec  
Faculty of Textile Engineering  
Studentska 1402/2, 461 17 Liberec 1, CZ  
Tel: +420 485 353615  
e-mail: [vat@tul.cz](mailto:vat@tul.cz)

## **TYPESET AND PRINT**

Vysokoškolský podnik, s.r.o., Voroněžská 1329/13, 460 01 Liberec 1, CZ

## **DATE OF ISSUE**

April 2023

## **APPROVED BY**

Rector's Office of Technical University of Liberec  
Ref. no. RE 18/23, 13th April 2023

## **EDITION**

First

## **PUBLICATION NUMBER**

55-018-23

## **PUBLICATION**

Quarterly

## **SUBSCRIPTION**

60 EUR

# VLÁKNA A TEXTIL

Volume 30, Issue 1, April 2023

**Special issue dedicated to the 23<sup>rd</sup> International Conference STRUTEX 2022  
„Structure and Structural Mechanics of Textile“  
held on November 30 – December 2, 2022 in Liberec, Czech Republic**

The presented publication from the 23<sup>rd</sup> International Conference STRUTEX 2022 is a collection of professional works of leading textile experts from all over the world, the Faculty of Textiles and also students of doctoral study programmes.

The papers are thematically divided into two chapters according to the conference sections. The first chapter contains papers focused on the topic Structure and structural mechanics of textiles. It includes publications focused on the structure of fibres and yarns, flat and spatial textiles, composites and biomechanics.

Chapter two covers innovations and applications of textile research in clothing, technical and medical textiles. All papers were selected by an editorial committee, which guaranteed their high professional standard.

PROF. ING. BOHUSLAV NECKÁŘ, DRSC.

## SCIENTIFIC COMMITTEE

PROF. LUBOŠ HES

PROF. S. M. ISHTIAQUE

PROF. OLDŘICH JIRSÁK

PROF. YORDAN KYOSEV

PROF. JIŘÍ MILITKÝ

PROF. BOHUSLAV NECKÁŘ

DR. VINCENT PLACET

PROF. JAKUB WIENER

ASSOC. PROF. LUKÁŠ ČAPEK

ASSOC. PROF. MARCIN BARBURSKI

ASSOC. PROF. BRIGITA KOLČAVOVÁ SIRKOVÁ

ASSOC. PROF. MAROŠ TUNÁK

Technical University of Liberec, Czech Republic

Indian Institute of Technology Delhi, India

Technical University of Liberec, Czech Republic

Technische Universität Dresden, Germany

Technical University of Liberec, Czech Republic

Technical University of Liberec, Czech Republic

University of Franche-Comté, France

Technical University of Liberec, Czech Republic

Technical University of Liberec, Czech Republic

Lodz University of Technology, Poland

Technical University of Liberec, Czech Republic

Technical University of Liberec, Czech Republic

Contributions have been accepted for publication without review. The authors are responsible for the professional and linguistic level of the contributions and translators.



# VLÁKNA A TEXTIL

Volume 30, Issue 1, April 2023

## CONTENT

- 5 **SAJJADIEH SABA, SAFARI FATEME, GHALEBI BAHARE AND SHANBEH MOHSEN**  
EFFECT OF TENSILE FATIGUE CYCLIC LOADING ON PERFORMANCE OF TEXTILE-BASED STRAIN SENSORS
- 11 **ŞARAPNAL DILEK AND BABAARSLAN OSMAN**  
INVESTIGATION OF THE USAGE OF ALTERNATIVE NEW GENERATION ECO-FRIENDLY FIBER BLENDS IN SYNTHETIC BASED DENIM FABRICS
- 18 **KOCAMAN RECEP TÜRKAY, PUTZKE ENRICO AND FICKER FRANK**  
WEAVEABILITY OF SPACER/DISTANCE FABRICS WITH HIGH PERFORMANCE FIBERS ON A TECHNICAL DOUBLE RAPIER JACQUARD WEAVING LOOM USING LANCETS
- 24 **FANG JIAHUI, KYOSEV YORDAN KONSTADINOV, LI YULING AND MA YANXUE**  
SIMULATION OF THE SEGMENT FILLING INSERTION FABRICS AT THE YARN LEVEL
- 30 **BOŇKOVÁ KAROLÍNA**  
NUMERICAL MODELLING OF TEXTILE STRUCTURES: POTENTIAL AND LIMITS
- 36 **İNCE MEHMET ERDEM, İNANIR SEVGI AND ERDOĞAN ESRA KUMSAL**  
COMFORTABLE AND PROTECTIVE HYBRID WEFT-KNIT PLATED FABRIC FROM GLASS AND WOOL/ACRYLIC YARNS
- 42 **LIU HAISANG, KYOSEV YORDAN AND JIANG GAOMING**  
PATTERN RELATED ISSUES IN THE MODELLING OF DEFORMED OVER SURFACE WARP KNITTED STRUCTURES WITH LONGER UNDERLAPS
- 49 **PONIECKA AGATA, BARBURSKI MARCIN, RANZ DAVID, CUARTERO JESÚS AND MIRALBES RAMON**  
NEW SOLUTIONS IN THE PRODUCTION OF COMPOSITES - MECHANICAL PROPERTIES OF COMPOSITES REINFORCED WITH TECHNICAL EMBROIDERY AND WOVEN FABRIC MADE OF FLAX FIBERS
- 54 **GABEN MAHDI AND GOLDFELD YISKA**  
DETECTING DAMAGED ZONES ALONG SMART SELF-SENSORY CARBON BASED TRC BY TDR
- 61 **YOSEF LIDOR AND GOLDFELD YISKA**  
INTELLIGENT TEXTILE AND FIBER REINFORCED MPC COMPOSITES FOR SHM
- 67 **OZDEMIR SUZAN, OZTEMUR JANSET, SEZGIN HANDE AND YALCIN-ENIS IPEK**  
THE EFFECT OF POLYMER TYPE AND FIBER ORIENTATION ON THE COMPLIANCE PROPERTIES OF ELECTROSPUN VASCULAR GRAFTS
- 72 **OZTEMUR JANSET, ÖZDEMİR SUZAN, SEZGIN HANDE AND YALCIN-ENIS IPEK**  
A PRELIMINARY STUDY EXAMINING THE BURST STRENGTH OF VASCULAR TUBULAR SCAFFOLDS
- 76 **PALAK HANDAN AND KAYA OGLU BURÇAK KARAGÜZEL**  
FABRICATION AND CHARACTERIZATION OF ELECTROSPUN ANTHOCYANIN-LOADED POLYLACTIDE NANOFIBERS
- 80 **KANIA ANNA AND BARBURSKI MARCIN**  
IMPROVING LOCAL THERMAL COMFORT IN BUILDINGS: A STUDY OF PROPERTIES OF HEATING TEXTILE COMPOSITES IN CONSTRUCTION INDUSTRY

- 84 **AGHADAVOOD ROYA, SHAHBAZ ZAHRA, KHEIRI TAHEREH, SHANBEH MOHSEN AND MARTINEK RADEK**  
DESIGN AND INVESTIGATION THE OPERATION OF TEXTILE BASED ELECTRODES FOR ELECTROTHERAPY
- 88 **PEKTAŞ KORAY, BALCI ONUR AND ORHAN MEHMET**  
SOLUTION BLOWN OF PLA NANOFIBER CONTAINING OZONATED MORMODICA OIL AND ITS MICROCAPSULES TO OBTAIN ANTIBACTERIAL MEDICAL TEXTILES SURFACES
- 93 **KORKMAZ AHMET AND BABAARSLAN OSMAN**  
CHITOSAN ADDED COMPOSITE VISCOSE YARN AND ITS POTENTIAL APPLICATION FOR DENIM FABRIC DEVELOPMENT
- 99 **ARSOY RAŞIT AND ASLAN SELÇUK**  
DESIGN OF ELECTRONICALLY CONTROLLED JACQUARD MACHINE FOR MULTI-SHED WEAVING MACHINES
- 105 **LEMMI TSEGAYE SH. AND BARBURSKI MARGIN**  
THERMAL AGING EFFECT ON THE PHYSIO-MECHANICAL PROPERTIES OF TEXTILES USED FOR THE REINFORCEMENT OF CONVEYOR BELTS
- 110 **SOOCHETA ANAGHA VAIDYA AND BHUNDOO SANSKRITA SINGH**  
INVESTIGATING THE APPLICATION OF TERRA DYE ON COTTON KNITTED FABRICS
- 120 **MELNYK LIUDMYLA AND KYZYMCHUK OLENA**  
NOVEL ELASTIC WARP KNITTED FABRIC WITH PERFORATION
- 126 **SEN KORHAN, KAYA AYSEGUL AND KANIK GOKSU**  
INVESTIGATION OF STRUCTURAL AND PERFORMANCE PROPERTIES OF HEMP-CONTAINING KNITTED FABRICS WITH DIFFERENT COMPOSITIONS
- 131 **BOGUŃ MACIEJ, ŚLEDZIŃSKA KATARZYNA, GIEŁDOWSKA MAŁGORZATA, KRÓL PAULINA, KAMIŃSKA IRENA AND MAGDZIARZ SYLWIA**  
POLYACRYLONITRILE NONWOVENS FOR THE PRODUCTION OF CARBON MATERIALS SUPPORTING THE REGENERATION OF BONE AND CARTILAGE TISSUES
- 134 **BŘEZINOVÁ HELENA, PECHOČIAKOVÁ MIROSLAVA AND GRABMÜLLEROVÁ JANA**  
IDENTIFYING THE MATERIALS IN ARCHAEOLOGICAL TEXTILES
- 138 **FISCHER HOLGER, SIGMUND INA, HARTWIG PETRA, DEDERER ESTHER AND MASCHINSKI ANNETT**  
STANDARDISING THE SAMPLE PREPARATION FOR ANALYSIS OF FIBRES AND PARTICLES BY STATIC IMAGE ANALYSIS
- 143 **TOMOVSKA ELENA AND HES LUBOS**  
SURFACE ROUGHNESS OF POLYAMIDE KNITTED FABRICS

# EFFECT OF TENSILE FATIGUE CYCLIC LOADING ON PERFORMANCE OF TEXTILE-BASED STRAIN SENSORS

SAJJADIEH SABA\*, SAFARI FATEME, GHALEBI BAHARE AND SHANBEH MOHSEN

Isfahan University of Technology, Department of Textile Engineering, Isfahan8415683111, Iran

## ABSTRACT

Textile-based strain sensors are a potential platform used in wearable devices for sensing and. 8 sensors containing monitoring the human body. These sensors not only have all the conventional sensors benefits but also, they are low-cost, flexible, light-weight, and easily adopted with three-dimensional shape of the body. Moreover, recent research has shown they are the best candidates for monitoring human's body motion. In this study, the effect of tensile fatigue cyclic loads on performance and sensitivity of textile-based strain sensors was investigated polyester/stainless steel staple fiber blend yarn as a conductive part with different structures were produced. The sensors varied in weft and warp density, percentage of stainless steel in conductive yarn, the number of conductive yarns, and weave pattern. The sensors were subjected to 500 cyclic loads operations and their tensile properties and sensitivity were investigated and compared before and after applying tensile fatigue cyclic loads. The results showed the textile-based strain sensors containing less percentage of stainless-steel fiber, lower number of conductive yarns, twill weave pattern and lower density in warp and weft direction have shown better performance after tensile fatigue cyclic loads.

## KEYWORDS

Tensile fatigue cyclic loading; Strain sensor; Smart textile; Conductive yarn; Woven fabric; Sensitivity.

\* Corresponding author: Sajjadieh S., e-mail: [s.sajadieh@tx.iut.ac.ir](mailto:s.sajadieh@tx.iut.ac.ir)

## INTRODUCTION

In the last decade, the products of the textile industry have found especial applications in the field of intelligent textiles, so the use of electrical fibers, yarns, and textiles is growing rapidly [16]. Electronic textiles (e-textiles) known as smart textiles are structures with conductive properties that can be used in a variety of applications such as sensors, communication, health care, computation, thermal purposes, protective clothing, wearable electronics, and fashion [7]. Electronic textiles can be produced by different methods such as weaving, knitting, embroidery and printing [10]. Sensors convert non-electrical physical or chemical quantities into electrical signals or other recognized electronic outputs [18]. Textile-based sensors especially strain sensors are desired because of their flexibility, ease of deformation, elastic recovery and fatigue resistance [18]. Strain deformation in e-textiles can be sensed in different mechanisms such as piezoelectricity, optical diffraction or interferometry, capacitance and piezoresistance. The most usual strain sensors in smart textiles are piezoresistive because of their manufacturing process and ease of use [11,19]. The "piezoresistive" term refers to

materials that change their electrical resistance by applying mechanical force due to microstructure change in conductive materials [3]. As mechanical force is applied to piezoresistive material, a mechanical deformation occurs. These deformations may change the electronic properties; therefore, the resistance will change [4]. As the force is removed, the electrical resistance regains regard to re-establishing structures [2]. The resistance can be evaluated by equation (1) which R is electrical resistance,  $\rho$  is the resistivity of material and A and L are the area and pathway length which the current flows respectively [12]. To evaluate the performance of a strain sensor, required information about the key parameters such as sensitivity, limit of detection (LOD), linearity, response time, and stability is needed [19].

$$R = \rho \frac{L}{A} \quad (1)$$

Fatigue is defined as the failure of a structure or component due to repetition and a load cycle which is less than a load to cause failure of the structure in a single application [14]. The failure occurs due to the cyclic nature of the load which causes microscopic material imperfections to grow into a

macroscopic crack [6]. Fabrics are subjected to tensile cyclic loads in different applications. Therefore, the study of the fatigue behavior of textiles in some applications such as sportswear is very important [17]. The fatigue failure in textiles usually is due to a reduction of elasticity during textile consumption. Fabric properties such as fabric density, weave design, yarn type and structure and material may affect the fatigue behavior of fabric [6].

There are many research work related textile-based strain sensors and their application. Shanbeh et al. produced woven strain sensors with different electrical conductivity and weft densities. They analyzed the effect of two different percentages of stainless-steel fibers in staple blend yarns that used in purpose-built strain sensors. They compared the sensitivity of strain sensors during 5 times cyclic loading. Their study showed that sensors containing less stainless-steel fiber have better performance. Moreover, the textile base strain sensor behavior during tensile cyclic loading wasn't stable. They claimed the electromechanical behavior of sensors under tensile loading is due to crimp, fiber migration, conductive fibers contact points and yarn diameter variation. [13]. Guo et al. presented four different textile-based strain sensors; two of them were conducted by coating and others by using conductive yarns in weaving process. Linear range of the sensor's work was reported [8]. Fen et al. developed a polyaniline (PANI)-coated polyurethane (PU) fiber with conductivity of  $10^{-2}\Omega/\text{cm}$ . They used fibers as a piezoresistive strain sensor which were subjected to 1500% strain deformation. The results showed that the resistivity was increased by applying strain but there were 3 different intensities. Furthermore, the fibers were under tensile cyclic loads on maximum 50% of strain level which results revealed the reversible response on the sensor. However, the reversibility wasn't absolute due to the hysteresis [5]. Liang et al. analyzed 16 knitted strain sensors' performance parameters such as sensitivity, linearity, hysteresis, responsiveness and fatigue during dynamic and static process. The sensors were made of three different materials consisting of a fabric coated with a conductive polymer, spun stainless steel yarn and silver-plated with different material composites. The sensors were tested at 10% strain and 100 times load-unload cycles. The results showed that sensors made of silver-plated yarn performed the best among other sensors. Moreover, sensors made of stainless-steel yarn performed the worst, because of knitted fabric properties [9]. Teyeme et al. developed a piezoresistive strain sensor from conductive fabric. The sensor had a stable dynamic response after 30 seconds, therefore they reported this sensor was suitable for slow-moving applications. They also found that the sensor wasn't sweat independent.

Thus, they conclude the sensor was not acceptable for sports applications [15].

In this work, we study effect of tensile fatigue cyclic loading on performance of textile-based strain sensors. Moreover, effect of different structural parameters of textile-based strain sensors on their performance during tensile fatigue cyclic loading was evaluated.

## EXPERIMENTAL

### Materials

Eight different textile-based strain sensors were woven by using two different conductive yarns produced by Xiamen JL-fiber Science and Technology Co. Ltd., Xiamen, China. The conductive yarn was polyester/stainless steel staple fiber blend. The fineness of stainless-steel fiber was  $12\mu\text{m}$ . Tensile properties of yarns were measured by Zwick tensile tester, which works based on constant rate of elongation. In Table 1, the properties of yarns are shown.

The sensors were produced by polyester filament yarn (75 den) as warp with two different densities (23 and 40 per cm). The conductive yarns were used as weft in combination with polyester filament/spandex yarns in two different densities (15 and 25 per cm). In designated textile-based strain sensors two different numbers of conductive yarns i.e. 9 and 20 was inserted. In Figure 1, the picture of one produced sample is illustrated. Moreover, the samples were produced with Plain and Twill (2/1) patterns. Optimax rapier weaving machine with 180 width and 450 PPM speed was used to produce all samples.

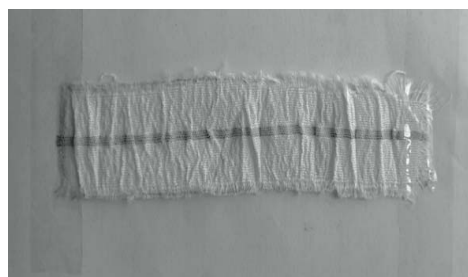


Figure 1. Textile-based strain sensor

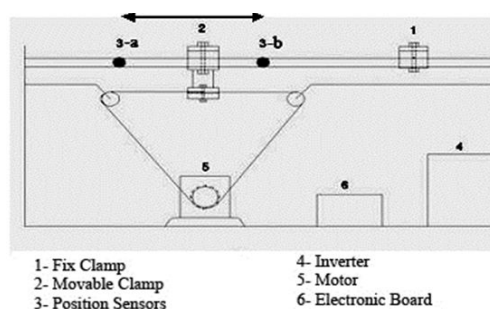


Figure 2. The schematic of equipment used for cyclic load [1]

**Table 1.** Mechanical and electrical properties of conductive yarns.

Yarn code	Percentage of stainless steel (%)	Nominal Count of yarn (Ne)	Breaking elongation (mm)	Breaking strength (cN)	Resistance ( $\Omega/m$ )	Yarn diameter ( $\mu m$ )
A	28	20	3.080	31.604	2982	248.25 $\mu m$
B	40	20	3.246	28.228	2307	249.46 $\mu m$

**Table 2.** Specifications of samples.

Sample code	Conductive yarn code	Number of conductive yarns	Weave pattern	Warp density (1/cm)	Weft density (1/cm)	Shrinkage (%)	Test speed (mm/min)	Breaking Strength (N)	Breaking Elongation (%)
1	A	9	Plain	40	15	32.4	230	56.20	174.76
2	A	20	Plain	40	15	24.2	230	78.04	129.26
3	B	9	Plain	40	15	29.5	230	55.63	154.87
4	B	20	Plain	40	15	21.3	230	61.00	128.30
5	A	9	Plain	40	25	29.6	140	175.02	89.70
6	B	9	Plain	40	25	15.7	130	187.49	82.56
7	B	9	Twill	40	25	15.7	210	143.10	251.07
8	B	9	Plain	23	25	16.5	140	146.22	152.08

## Methods

For measuring sensors' sensitivity and resistance variation of textile-based strain sensors during tensile test an electronic circuit was used which the strain sensor was one of the resistors series with other reference resistors as proposed by Guo et al. [8]. A purposed-built instrument was used for applying cyclic loads on sensors which is shown in Figure 2 [1]. The details operating method of instrument was explained in reference 1.

The dimension of textile-based strain sensors was  $25 \times 200$  mm. The samples were then subjected to wet relaxing process. Samples were immersed in  $90^\circ$  water for 10 minutes. Then, they were dried in ambient temperature and the shrinkage percentage was calculated by equation 2 which  $l_1$  is the initial length of sample and  $l_2$  is the length of sample after wet relaxation.

$$\text{shrinkage}(\%) = \frac{l_1 - l_2}{l_1} \times 100 \quad (2)$$

Tensile properties of samples were tested in weft direction based on ASTM-D5034 (2007) using Zwick tensile tester. In Table 2, the specifications of samples are shown.

The samples were tested in 10 cyclic loading at 50% of breaking strain level in weft direction. The resistance variation was recorded during cyclic test. The sampling rate was set at 10 per second similar to 10 Hz in frequency.

The sensitivity of each sensor was calculated using equation 3, which  $G$  is sensitivity of the sensor,  $V_{max}$  and  $V_{min}$  are the maximum and minimum voltage that has been recorded in each tensile cyclic load from beginning to end and  $\varepsilon$  is strain. The average sensitivity of 10 cycles was considered as sensor's sensitivity.

$$G = \frac{(V_{max} - V_{min}) / V_{min}}{\varepsilon} \quad (3)$$

Each sample was subjected to 500 tensile fatigue cyclic loads. They were loaded up to 50% of its breaking elongation and 3.4 Hz cyclic loading frequency was set, based on average running speed of a normal person.

The microtomy technique was used to evaluate the width cross-section of conductive yarns before and after tensile fatigue cyclic loads. The sensitivity of each sensor was also measured 24 hours after tensile fatigue cyclic loads test using mentioned methods

## RESULTS AND DISCUSSION

In Figures 3a and 3b, the voltage variation of textile-based strain sensors before and after tensile fatigue cyclic loading of two samples is shown. By applying tension to the fabric, the yarns are subjected to compressive forces at interchange points. This pressure may cause the variation of yarns' cross-section and the more possibility of contact between the stainless-steel fibers into the yarn. Although, the electro-mechanical properties of all samples during tensile cyclic loads revealed the same trend but the effect of structural parameters of samples on voltage variation was observed. The electro-mechanical variation of samples during tensile cyclic loads may be influenced by woven fabric shrinkage after wet relaxation.

Figure 4 displays the sensitivity of textile-based strain sensors before and after tensile fatigue cyclic loading. The increase of contact pressure between yarns into fabric structure during tensile force could be the reason for compactness of yarns and therefore more possibility of conductive fiber contacts into yarn structure. This phenomenon may

cause the decrease of sensitivity of samples during tensile cyclic loading.

As shown in Figure 4 the sensitivity of sample 2 after tensile fatigue cyclic loads decreased from 0.695 to 0.370 during 1<sup>st</sup> to 10<sup>th</sup> cyclic loading. Moreover, the sensitivity of sample 5 during tensile cyclic loading increased. The sensitivity (G) of eight textile-based strain sensors is shown in Table 3.

As can be seen in Table 3, the sensitivity of samples after tensile fatigue cyclic loading confirmed the structural variation of samples. It seems that the tensile fatigue cyclic loads in predetermined elongation may cause shrinkage removal of samples which cause the electro-mechanical variation of textile-based strain sensors.

It was observed that the sensitivity has a direct relation with conductivity of yarns before tensile fatigue cyclic loading, but this trend was not observed after tensile fatigue loading. The cross-section of conductive yarns (as shown in Figure 6) confirmed the fiber displacement in yarn cross-section which could be the reason for this phenomenon.

The textile-based strain sensor woven with plain pattern showed higher sensitivity compare with Twill 2/1 woven fabric before and after tensile fatigue cyclic loading. However, the sensitivity sample 7 woven with Twill pattern is more stable than plain ones (sample 6) that is maybe because of yarn float in fabric structure.

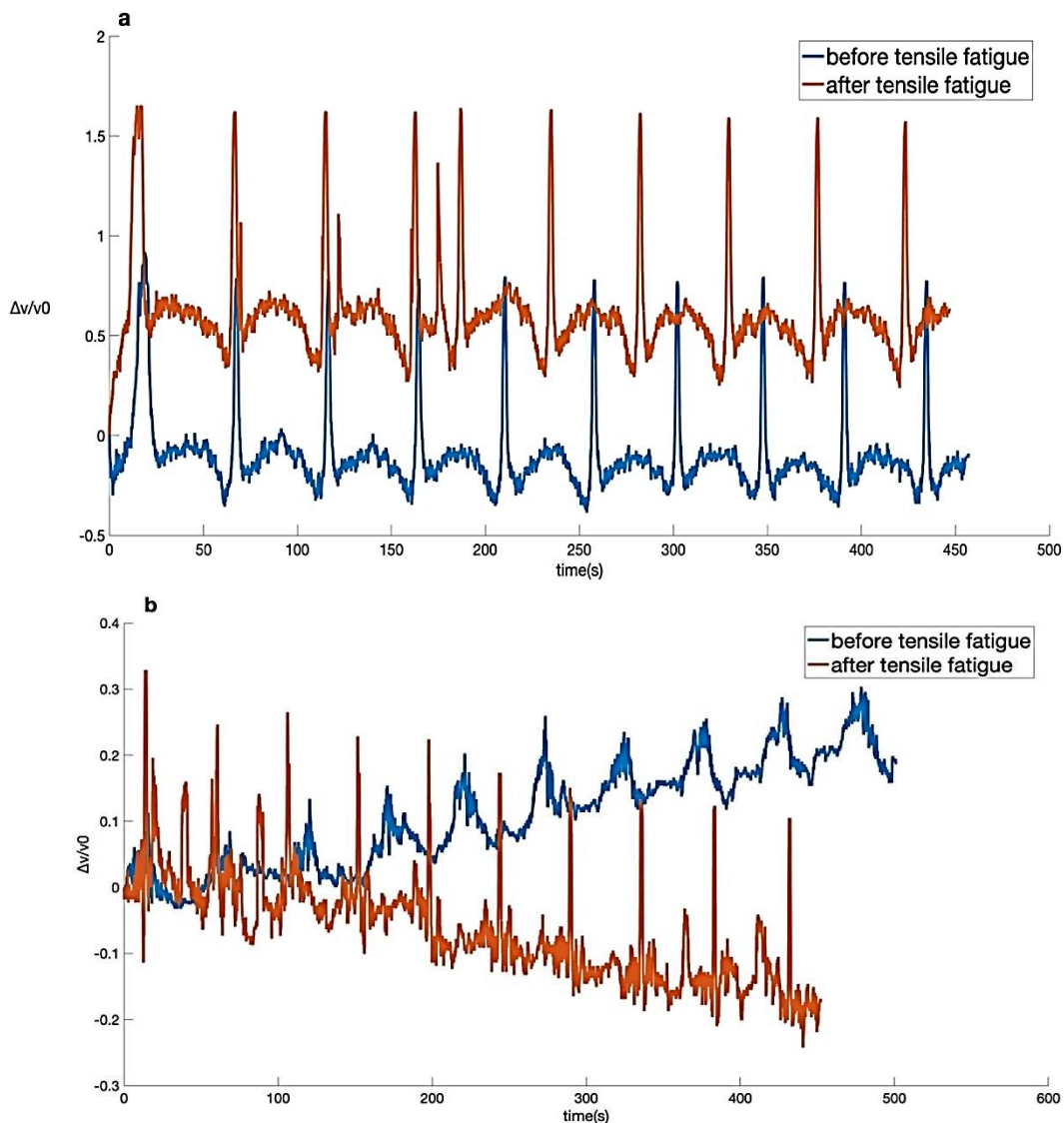


**Figure 3.** Voltage variation of two textile-based strain sensor during tensile cyclic loading before and after tensile fatigue cyclic loading. a) sample 5, b) sample 2. (The blue curve is before tensile fatigue cyclic loads and red curve after tensile fatigue cyclic loads.).

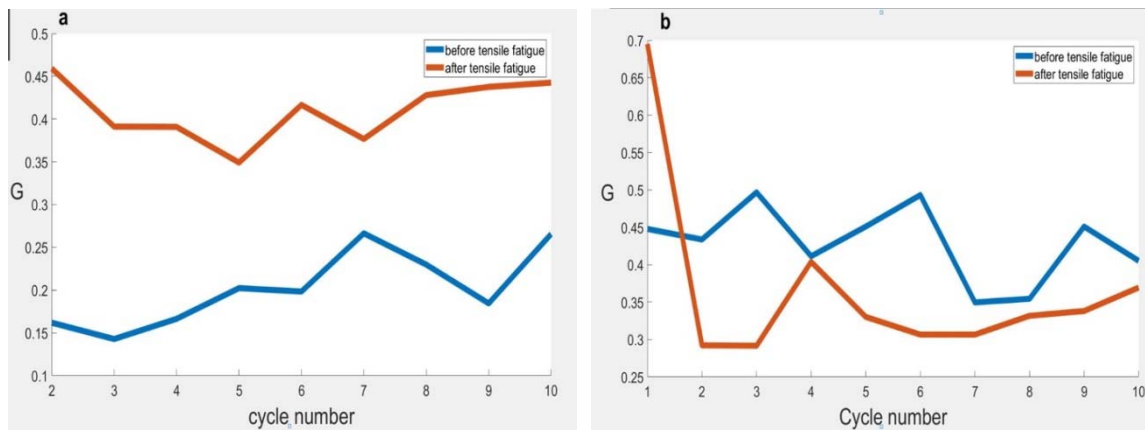


**Figure 4.** sensitivity (G) variation of two textile-based strain sensors during tensile cyclic loads before and after 500 tensile fatigue cyclic loading a) sample 5, b) sample 2. (The blue curve is before tensile fatigue cyclic loads and red curve after tensile fatigue cyclic loads.).

**Table 3.** The sensitivity (G) of textile-based strain sensors before and after tensile fatigue cyclic loads.

Sample code	Sensitivity of samples before tensile fatigue	Sensitivity of samples after tensile fatigue
1	0.156	2.29
2	0.131	0.409
3	0.138	0.171
4	0.273	5.22
5	0.205	0.420
6	0.131	0.409
7	0.409	0.402
8	0.838	0.358

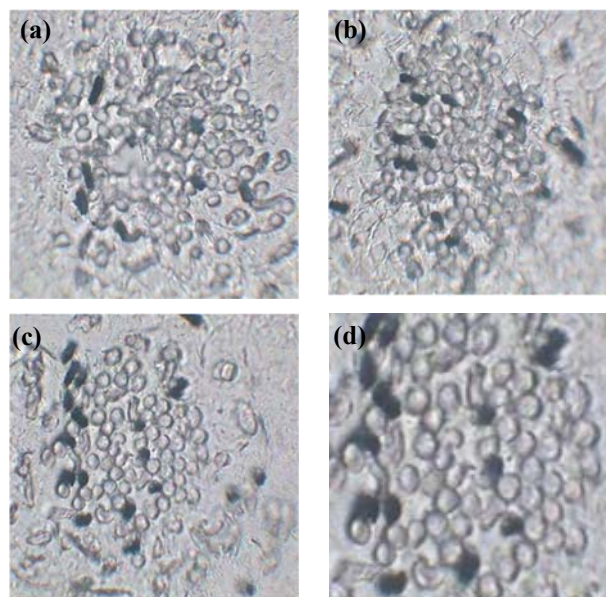


**Figure 6.** Conductive yarn cross-sections (a) before tensile fatigue cyclic loads of yarn A pulled out from sample 2, (b) after tensile fatigue cyclic loads of yarn A pulled out from sample 2, (c) before tensile fatigue cyclic loads of yarn B pulled out from sample 2, (d) after tensile fatigue cyclic loads of yarn B pulled out from sample 8.

It was found that by increasing the weft density, the sensitivity of textile-based strain sensors increased (As shown in Table 3). This trend can be because of lower shrinkage of woven fabrics with higher value of weft density. Moreover, by increasing the number of conductive yarns, the sensitivity or the voltage variation during tensile cyclic loading was increased.

This observation could be explained by lower shrinkage values of samples produced by higher number of conductive yarns. It seems that the structural variation of these samples was prominent because of tensile fatigue cyclic loading.

## CONCLUSIONS

In this study, 8 different textile-based strain sensors were produced by using weaving method. The sensitivity and electro-mechanical properties of samples during tensile cyclic loading showed the effectiveness of tensile fatigue cyclic loading. Moreover, the evaluation of cross-section of conductive yarns before and after tensile fatigue cyclic loading showed displacement of conductive fibers in yarn structure. Our finding confirmed the effect of percentage of conductive fibers in the yarn, weft and warp density, number of weft yarn, weave pattern on sensitivity and electro-mechanical properties of textile-based strain sensors after tensile fatigue cyclic loading. The minimum and maximum values of sensitivity before tensile fatigue loading was 0.131 and 0.409, respectively, but after tensile fatigue loading was 0.171 and 5.22. In future, we aim to work on effect of tensile fatigue cyclic loading parameters on sensitivity of textile-based strain sensors in different testing conditions.

## REFERENCES

- Adeli, B., Ghareaghaji, A. A., & Shanbeh, M. (2011). Structural evaluation of elastic core-spun yarns and fabrics under tensile fatigue loading. *Textile Research Journal*, 81(2), 137-147. <https://doi.org/10.1177/0040517510380104>
- Amjadi, M., Kyung, K.-U., Park, I. and Sitti, M. (2016). Stretchable, Skin-Mountable, and Wearable Strain Sensors and Their Potential Applications: A Review. *Adv. Funct. Mater.*, 26: 1678-1698. <https://doi.org/10.1002/adfm.201504755>
- Eaton, W. P., & Smith, J. H. (1997). Micromachined pressure sensors: review and recent developments. *Smart Materials and Structures*, 6(5), 530. <https://doi.org/10.1088/0964-1726/6/5/004>
- Eldessouki, M., Aysha, T., Ratičáková, M., Šašková, J., Padil, V. V., Ibrahim, M., & Černík, M. (2017). Structural parameters of functional membranes for integration in smart wearable materials. *Fibres & Textiles in Eastern Europe*. <http://dx.doi.org/10.5604/01.3001.0010.4631>
- Fan, Q., Zhang, X., & Qin, Z. (2012). Preparation of polyaniline/polyurethane fibers and their piezoresistive property. *Journal of Macromolecular Science, Part B*, 51(4), 736-746. <https://doi.org/10.1080/00222348.2011.609795>
- Flamm, M., Spreckels, J., Steinweger, T., & Weltin, U. (2011). Effects of very high loads on fatigue life of NR elastomer materials. *International Journal of Fatigue*, 33(9), 1189-1198. <https://doi.org/10.1016/j.ijfatigue.2011.03.008>
- Grancarić, A. M., Jerković, I., Koncar, V., Cochrane, C., Kelly, F. M., Soulat, D., & Legrand, X. (2018). Conductive polymers for smart textile applications. *Journal of Industrial Textiles*, 48(3), 612-642. <https://doi.org/10.1177/1528083717699368>
- Guo, L., Berglin, L., & Mattila, H. (2010). Textile strain sensors characterization-sensitivity, linearity, stability and hysteresis. *Nordic Textile Journal*, (2), 51-63.
- Liang, A., Stewart, R., & Bryan-Kinns, N. (2019). Analysis of sensitivity, linearity, hysteresis, responsiveness, and fatigue of textile knit stretch sensors. *Sensors*, 19(16), 3618. <https://doi.org/10.3390/s19163618>
- Oatley, Giles, Tanveer Choudhury, and Paul Buckman. 2021. "Smart Textiles for Improved Quality of Life and Cognitive Assessment" *Sensors* 21, no. 23: 8008. <https://doi.org/10.3390/s21238008>
- Raji, R. K., Miao, X., Zhang, S., Li, Y., & Wan, A. (2018). Influence of rib structure and elastic yarn type variations on textile piezoresistive strain sensor characteristics. *Fibres & Textiles in Eastern Europe*. <http://dx.doi.org/10.5604/01.3001.0012.2527>
- Seyedin, S., Zhang, P., Naebe, M., Qin, S., Chen, J., Wang, X., & Razal, J. M. (2019). Textile strain sensors: a review of the fabrication technologies, performance evaluation and applications. *Materials Horizons*, 6(2), 219-249. <https://doi.org/10.1039/C8MH01062E>
- Shanbeh, M., & Emadi, M. (2016). Effect of weft density and / percentage of stainless steel fiber content of weft yarn on electrical properties of woven fabric strain sensors. *The Journal of The Textile Institute*, 107(8), 958-966. <https://doi.org/10.1080/00405000.2015.1072384>
- Shanbeh, M., Hasani, H., & Manesh, F. Y. (2012). An investigation into the fatigue behavior of core-spun yarns under cyclic tensile loading. *Journal of Engineered Fibers and Fabrics*, 7(4), 155892501200700406. <https://doi.org/10.1177/155892501200700406>
- Teyeme, Y., Malengier, B., Tesfaye, T., & Van Langenhove, L. (2020). A Fabric-Based Textile Stretch Sensor for Optimized Measurement of Strain in Clothing. *Sensors*, 20(24), 7323. <https://doi.org/10.3390/s20247323>
- Voyce, J., Dafniotis, P., & Towlson, S. (2005). *Elastic textiles. In Textiles in sport* (pp. 204-230). Woodhead Publishing. <https://doi.org/10.1533/9781845690885.3.204>
- V. Šafářová, K. Malachová and J. Militký (2014). "Electromechanical analysis of textile structures designed for wearable sensors," *Proceedings of the 16th International Conference on Mechatronics - Mechatronika 2014*, pp.416-422
- Xiamoning, T., (2008). Electrical textile sensors for repeated large deformation. *International conference on experimental mechanics 2008*, 73754H. <https://doi.org/10.1117/12.839307>
- Zang, Y., Zhang, F., Di, C. A., & Zhu, D. (2015). Advances of flexible pressure sensors toward artificial intelligence and health care applications. *Materials Horizons*, 2(2), 140-156. <https://doi.org/10.1039/C4MH00147H>

# INVESTIGATION OF THE USAGE OF ALTERNATIVE NEW GENERATION ECO-FRIENDLY FIBER BLENDS IN SYNTHETIC BASED DENIM FABRICS

ŞARAPNAL DILEK<sup>1\*</sup> AND BABAARSLAN OSMAN<sup>2</sup>

<sup>1</sup> Çalık Denim Tekstil AŞ. R&D Department, Yeşilyurt/Malatya, Turkey

<sup>2</sup> Cukurova University, Engineering Faculty, Textile Engineering Department, Adana, Turkey

## ABSTRACT

Polyester yarn is made from post-consumer waste such as bottles, fabrics, etc., in the composition of polyester ethylene terephthalate (PET). Polyester (mainly polyethylene terephthalate, PET) is the most commonly employed textile fibre with over 50% share in total production of textile fibres. PLA is a biobased and biodegradable polymer produced from renewable resources. PLA is also a thermoplastic aliphatic compostable polyester. In this study, 75% Cotton - 25% PLA, 75% Lyocell - 25% PLA and 75% Cotton - 25% PET blended yarns were produced as rigid, corespun and dualcore in the ring spinning system. The fabrics were weaved with produced yarn. In the finishing processes, some of the fabrics were treated with caustic and some of the fabrics were only washed. Fabrics containing PLA and PET were compared with each other. Fabrics containing PLA and PET fiber were evaluated in terms of strength, elasticity, abrasion and pilling performances. Although the weft tensile and tear properties of Cotton-PLA blended fabrics are lower than Lyocell-PLA and Cotton-PET blends, it has been indicated that PLA blended yarns can be used as an alternative to PET based yarns and fabrics.

## KEYWORDS

Pla; Polyester; Lyocell; Blend Yarn and Fabrics; Fabric Performance.

---

\* Corresponding author: Şarapnal D., e-mail: [dilek.sarapnal@calikdenim.com](mailto:dilek.sarapnal@calikdenim.com)

## INTRODUCTION

One of the most common raw materials used in the global textile industry is Polyethylene terephthalate (PET) fiber, cotton fiber and their blends. Cotton and polyester staple fibers constitute 58% and 28% of staple yarns, respectively. [1] Polyester (mainly polyethylene terephthalate, PET). The most widely used textile fiber in total textile fiber production. In general, it has excellent performance properties. In addition to this feature, it is a non-biodegradable fiber that consumes fossil fuels [2]. Polylactic acid (pla) has been recognized as one of the solutions for the disposal of plastics, as it is produced from renewable resources and completely biodegrades at the end of its life [3]. In addition to offering advantages in the use of pet and cotton fiber blends, pet-cotton production has negative effects on the environment. Fabrics made using pla offer good moisture management properties for underwear, sportswear, active wear and fashion wear due to their excellent wicking ability, rapid moisture spreading and drying properties [4]. The dry tensile strength of lyocell fiber is greater than that of other

man-made cellulosic staples, not only its physical, mechanical and chemical properties are better than viscose fiber, but also environmentally friendly because the lyocell process uses non-toxic NMMO solvent [5].

The current study aims to comparison of eco-friendly pla fiber to cotton-pes blended fabrics, as well as the physical properties of pla fiber in lyocell-pla and cotton-pla blended fabrics will be compared.

## EXPERIMENTAL

### Materials

Pla, cotton, polyester and lyocell fibers were used in the production of the yarns used in this study. Polylactic acid (PLA, Palmetto Synthetics LLC), lyocell (TencelRB, Lenzing AG), PET and cotton fibres were sourced. The properties of selected fibres are given in Table 1 and characteristic strength-elongation curves are plotted in Table 1.

**Table 1.** Fiber details.

Parameters	Pla	Lyocell	Polyester	Cotton
Fineness (dtex)	1,66	1,7	1.53	0.11 (4.7mic)
Fibre length (mm)	38	38	38	29.3
Tenacity (cN.tex-1)	25	33	57.4	29.8
Elongation (%)	52	13	18	7.3

**Table 2.** Yarn type and compositions.

Yarn Code	Yarn Types	Sheath fiber composition	Yarn description
A1	Rigid	25% Pla+75% Lyocell	Ne 18/1 RK
A2	Corespun	Sheath fiber-25% Pla+75% Lyocell	Ne 18/1 RK 78 LYC
A3	Dualcore	Sheath fiber-25% Pla+75% Lyocell	Ne 18/1 55 dtex T400 78 LYC
B1	Rigid	25% Pla+75% Cotton	Ne18/1 RK
B2	Corespun	Sheath fiber-25% Pla+75% Cotton	Ne 18/1 RK 78 LYC
B3	Dualcore	Sheath fiber-25% Pla+75% Cotton	Ne 18/1 55 dtex T400 78 LYC
C1	Rigid	25% Pes+75% Cotton	Ne18/1 RK
C2	Corespun	Sheath fiber-25% Pes+75% Cotton	Ne 18/1 RK 78 LYC
C3	Dualcore	Sheath fiber-25% Pes+75% Cotton	Ne 18/1 55 dtex T400 78 LYC

18 Ne ring-spun rigid, core and dual core-spun yarn has been produced. 78dtex lycra® and 55dtex T400® (PET/PTT) are used in the production of core-spun and dual core-spun yarns.

The details of yarns are given in Table 2.

## Methods

Rigid, core-spun and dual-core yarns were produced in the ring-spinning process. The weaving process was completed on Picanol type machines.

Finishing processes of the woven fabrics have been completed. In addition to comparing the use of Pla and the use of Pes, the effect of the pre-treatment step on the fabric performance was also investigated. Fabric weaving details are given in Table 3.

The codes and explanations given to the fabrics according to the pre-processing steps are given in Table 4.

After conditioning the fabrics according to ASTM D 1776 for 24 hours (21°C±1 temperature, 65±2 % relative humidity), all tests were carried out.

For this study, tensile strength, tear strength, elasticity & growth, abrasion test results were evaluated.

ASTM D5034, ASTM D1424, ASTM D 3107, TS EN ISO 12947-2 standard methods were used to determine the performance of the fabric, respectively.

**Table 3.** Fabric details.

	CTPLA B1	CTPLA B2	CTPLA B3	CLYPLA A1	CLYPLAA 2	CLYPLAA 3	CTPES C1	CTPES C2	CTPES C3
Warp Yarn	14/1 RK Slub	14/1 RK Slub	14/1 RK Slub	14/1 RK Slub	14/1 RK Slub	14/1 RK Slub	14/1 RK Slub	14/1 RK Slub	14/1 RK Slub
Weft Yarn	B1 (Rigid)	B2 (Core-spun)	B3 (Dual core-spun )	A1 (Rigid)	A2 (Core-spun)	A3 (Dual core-spun )	C1 (Rigid)	C2 (Core-spun)	C3 (Dual core-spun )
Comb	70	70	70	70	70	70	70	70	70
Weft Density	21	21	21	21	21	21	21	21	21
Weave Types	3/1Z	3/1Z	3/1Z	3/1Z	3/1Z	3/1Z	3/1Z	3/1Z	3/1Z

Table 4. Pre-processing steps.

Fabric Code	Sheath fiber composition	Treatment Process
CTPLA B1-W	%25 Pla +% 75 Cotton	Washed
CTPLA B1-C	%25 Pla +% 75 Cotton	10 Be' Caustic
CTPLA B2-W	%25 Pla +% 75 Cotton	Washed
CTPLA B2-C	%25 Pla +% 75 Cotton	10 Be' Caustic
CTPLA B3-W	%25 Pla +% 75 Cotton	Washed
CTPLA B3-C	%25 Pla +% 75 Cotton	10 Be' Caustic
CLYPLA A1-W	%25 Pla+%75 Lyocell	Washed
CLYPLA A1-C	%25 Pla+%75 Lyocell	10 Be' Caustic
CLYPLA A2-W	%25 Pla+%75 Lyocell	Washed
CLYPLA A2-C	%25 Pla+%75 Lyocell	10 Be' Caustic
CLYPLA A3-W	%25 Pla+%75 Lyocell	Washed
CLYPLA A3-C	%25 Pla+%75 Lyocell	10 Be' Caustic
CTPES C1-W	%25 Pes +% 75 Cotton	Washed
CTPES C1-C	%25 Pes +% 75 Cotton	10 Be' Caustic
CTPES C2-W	%25 Pes +% 75 Cotton	Washed
CTPES C2-C	%25 Pes +% 75 Cotton	10 Be' Caustic
CTPES C3-W	%25 Pes +% 75 Cotton	Washed
CTPES C3-C	%25 Pes +% 75 Cotton	10 Be' Caustic

## RESULTS AND DISCUSSION

### Tensile properties of fabric

Strength values are important for denim fabrics. Warp tensile values in all Cotton/Pla, Tensile/Pla and Cotton/Pes groups were found to be lower in fabrics made with rigid weft compared to the experiments made with core-spun and dual core-spun weft.

The increase in the warp tensile values of the fabrics using core-spun and dual core-spun weft was due to the increase in the warp yarn density.

The lowest weft tensile values were observed in the Cotton/Pla group. The increase in tensile values of the Tencel/Pla group compared to the Cotton/Pla group is due to the fact that the Tencel fiber is more

durable than cotton.

It is possible that the Cotton/Pla group has less strength than the Cotton/Pes group, possibly because the Pla fiber is less durable than the polyester fiber.

Pla fiber is sensitive to alkaline treatments, but it has been determined that it does not significantly affect the tensile values between washing and 10 Be'causticizing processes as a finishing process. Tensile warp and weft test results are given in Figure 1 and Figure 2.

It has been determined that the Warp and Weft Tear test results are in line with the interpretations obtained in the tensile values. Tear warp and weft test results are given in Figure 3 and Figure 4.

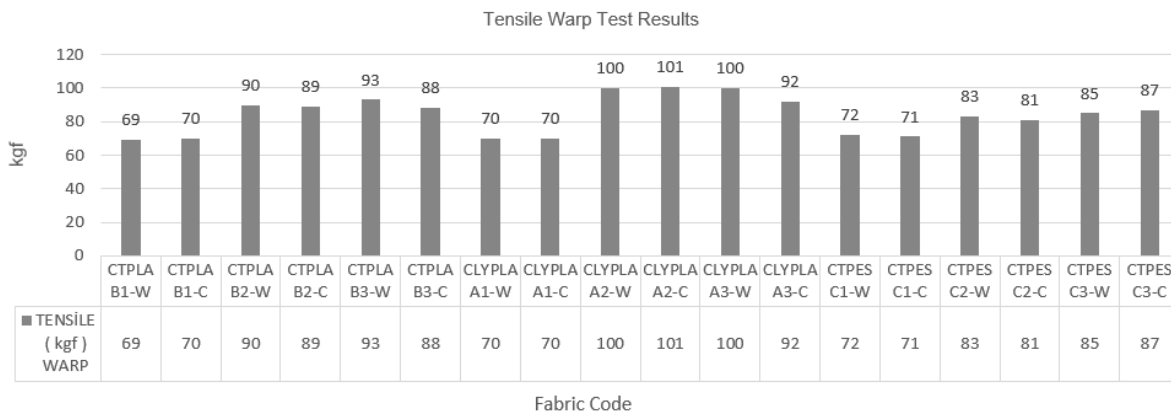


Figure 1. Warp tensile test results

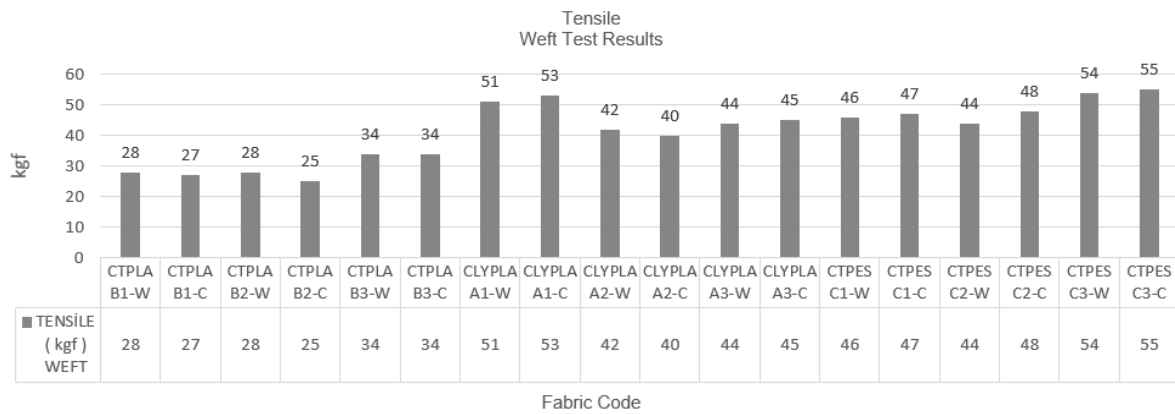


Figure 2. Weft tensile test results.

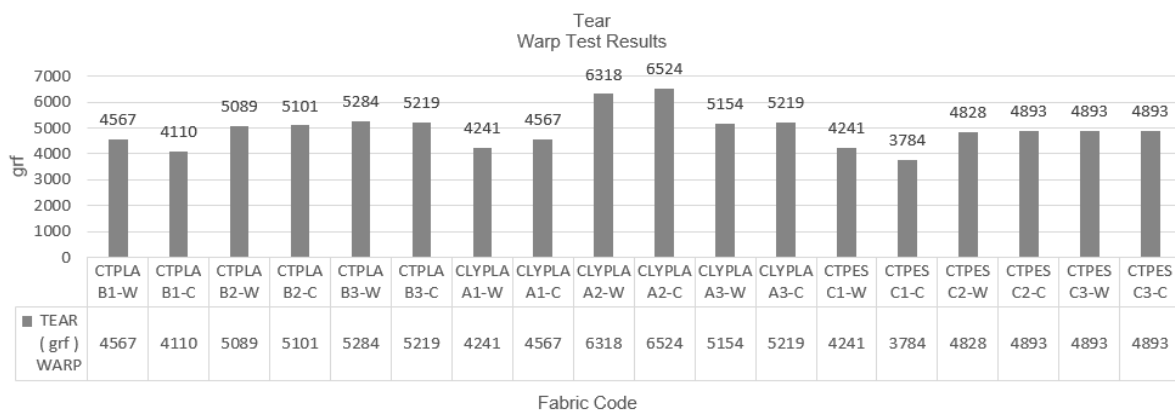


Figure 3. Warp tear test results.

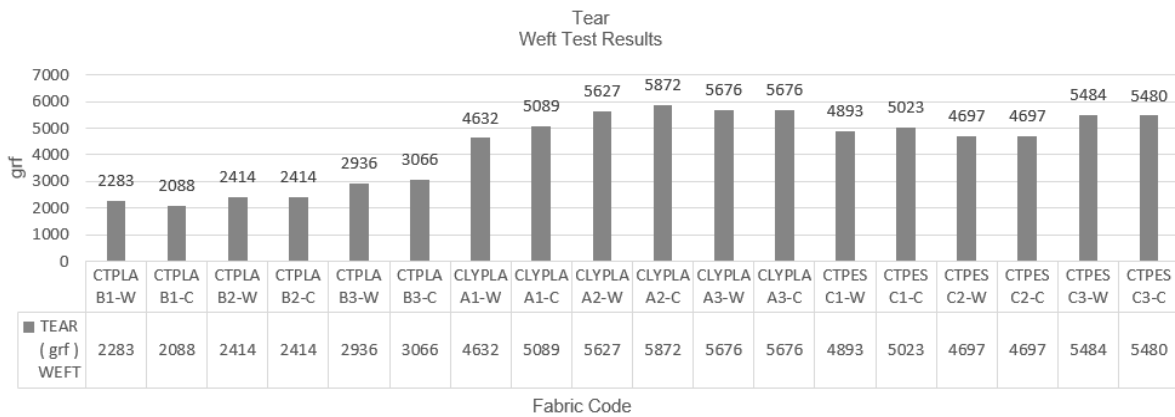


Figure 4. Weft tear test results.

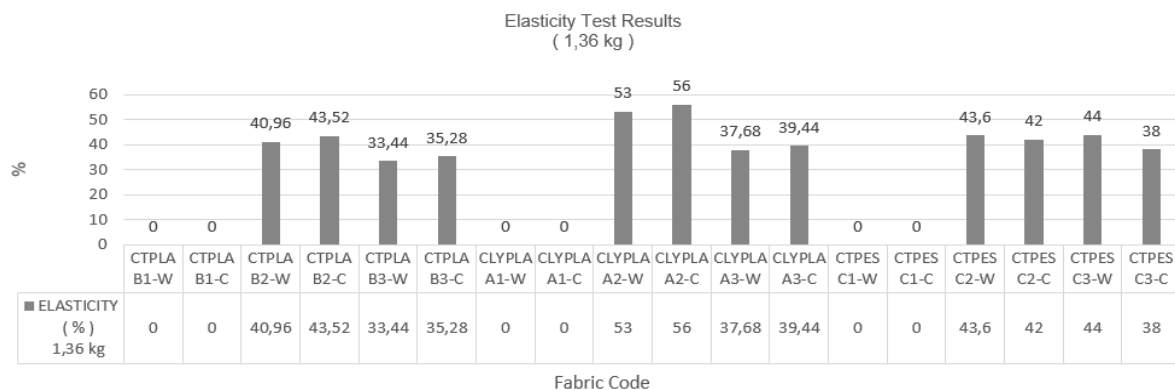


Figure 5. Elasticity test results.

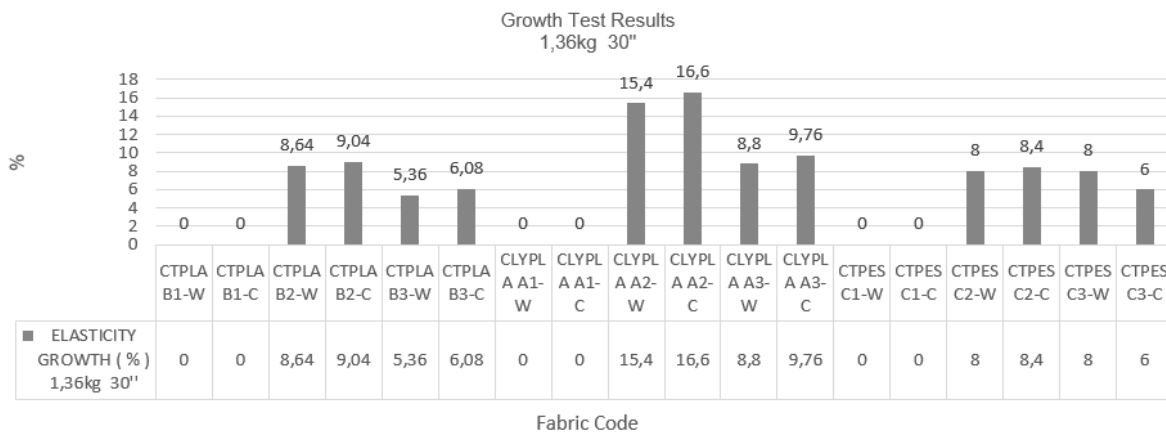


Figure 6. Growth test results.

### Elasticity and Growth results of fabrics

The elasticity values of the rigid fabrics are shown as zero. The elasticity value of the core-spun yarns of the cotton/Pla group and the Tencel/Pla group were higher than the elasticity value of the dualcore-spun yarns. In the Cotton/Pes group, elasticity the values of core-spun and dualcore-spun yarns were found to be close to each other.

It was seen that the lowest growth value was in the group with Cotton/Pla, the highest in the group containing Tencel/Pla fiber.

### Abrasion results of fabrics

The abrasion test was performed on the back side of the fabrics and up to 25000 cycles. No breakage was detected in the yarns until 25000 cycles. There was no difference between 10 Be'causticization and washing processes.

Figure 7 show the abrasion test results of treated 10 Be' denim samples. Washed fabrics also have a similar backside appearance.

Table 5. Abrasion test results

Fabric Code	Sheath fiber composition	Treatment Process	Abrasion	Fabric Face
CTPLA B1-W	%25 Pla +% 75 Cotton	Washed	>25000	Back
CTPLA B1-C	%25 Pla +% 75 Cotton	10 Be' Caustic	>25000	Back
CTPLA B2-W	%25 Pla +% 75 Cotton	Washed	>25000	Back
CTPLA B2-C	%25 Pla +% 75 Cotton	10 Be' Caustic	>25000	Back
CTPLA B3-W	%25 Pla +% 75 Cotton	Washed	>25000	Back
CTPLA B3-C	%25 Pla +% 75 Cotton	10 Be' Caustic	>25000	Back
CLYPLA A1-W	%25 Pla+%75 Lyocell	Washed	>25000	Back
CLYPLA A1-C	%25 Pla+%75 Lyocell	10 Be' Caustic	>25000	Back
CLYPLA A2-W	%25 Pla+%75 Lyocell	Washed	>25000	Back
CLYPLA A2-C	%25 Pla+%75 Lyocell	10 Be' Caustic	>25000	Back
CLYPLA A3-W	%25 Pla+%75 Lyocell	Washed	>25000	Back
CLYPLA A3-C	%25 Pla+%75 Lyocell	10 Be' Caustic	>25000	Back
CTPES C1-W	%25 Pes +% 75 Cotton	Washed	>25000	Back
CTPES C1-C	%25 Pes +% 75 Cotton	10 Be' Caustic	>25000	Back
CTPES C2-W	%25 Pes +% 75 Cotton	Washed	>25000	Back
CTPES C2-C	%25 Pes +% 75 Cotton	10 Be' Caustic	>25000	Back
CTPES C3-W	%25 Pes +% 75 Cotton	Washed	>25000	Back
CTPES C3-C	%25 Pla +% 75 Cotton	10 Be' Caustic	>25000	Back

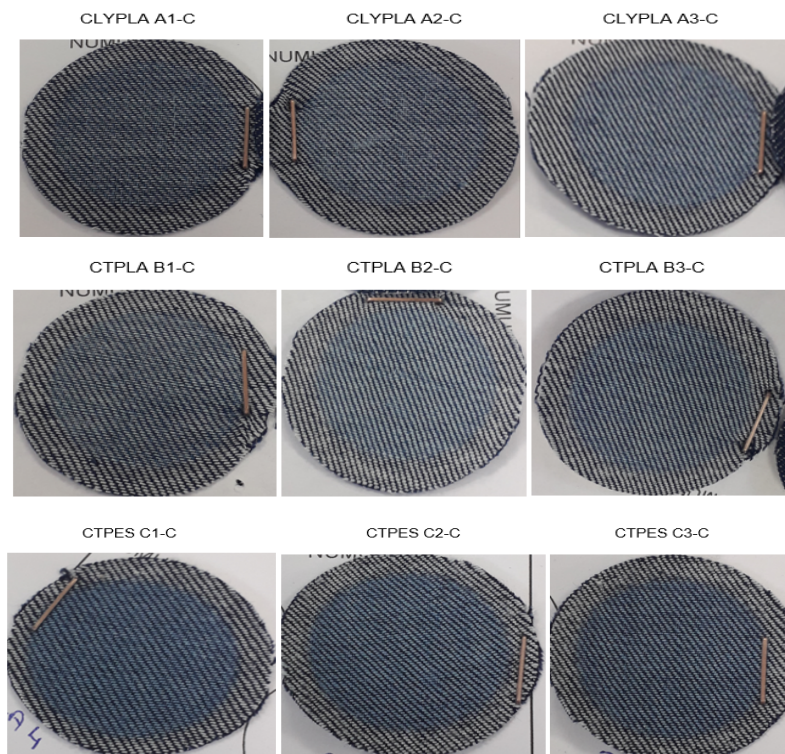


Figure 7. Abrasion test results of treated 10 Be' denim fabrics.

Table 6. Pilling test results.

Fabric Code	Sheath fiber composition	Treatment Process	Pilling	Fabric Face
CTPLA B1-W	%25 Pla +% 75 Cotton	Washed	4	Back
CTPLA B1-C	%25 Pla +% 75 Cotton	10 Be' Caustic	4	Back
CTPLA B2-W	%25 Pla +% 75 Cotton	Washed	4-5	Back
CTPLA B2-C	%25 Pla +% 75 Cotton	10 Be' Caustic	4-5	Back
CTPLA B3-W	%25 Pla +% 75 Cotton	Washed	4	Back
CTPLA B3-C	%25 Pla +% 75 Cotton	10 Be' Caustic	4	Back
CLYPLA A1-W	%25 Pla+%75 Lyocell	Washed	4-5	Back
CLYPLA A1-C	%25 Pla+%75 Lyocell	10 Be' Caustic	4	Back
CLYPLA A2-W	%25 Pla+%75 Lyocell	Washed	4-5	Back
CLYPLA A2-C	%25 Pla+%75 Lyocell	10 Be' Caustic	4-5	Back
CLYPLA A3-W	%25 Pla+%75 Lyocell	Washed	4-5	Back
CLYPLA A3-C	%25 Pla+%75 Lyocell	10 Be' Caustic	4-5	Back
CTPES C1-W	%25 Pes +% 75 Cotton	Washed	2-3	Back
CTPES C1-C	%25 Pes +% 75 Cotton	10 Be' Caustic	2-3	Back
CTPES C2-W	%25 Pes +% 75 Cotton	Washed	3	Back
CTPES C2-C	%25 Pes +% 75 Cotton	10 Be' Caustic	3	Back
CTPES C3-W	%25 Pes +% 75 Cotton	Washed	3	Back
CTPES C3-C	%25 Pes +% 75 Cotton	10 Be' Caustic	2-3	Back

### Pilling Test results of fabrics

When the pilling test results for the Cotton/Pla and Tencel/Pla groups were evaluated over the washing

and caustic treatments, results were close to each other. The pilling test results of the Cotton/Pes groups were found to be the lowest. There was no significant difference between 10 Be'Caustic and

washing processes.

## CONCLUSIONS

The use of Pla fiber instead of Pes fiber was investigated by applying different pretreatment processes. The strength values of Pla fiber blended fabrics and Pes fiber blended fabrics were compared. It has been observed that fabrics containing Pla fiber blend have lower strength than Pes fiber blended fabrics. When the 10 Be'causticizing process is compared with the fabrics that have only been washed, it has been observed that the 10 Be'causticizing process does not have a serious effect on the fabric strength values. When its physical properties are evaluated on the fabric, it has been determined that it can be used as an alternative to pes fiber because it is a biodegradable fiber. When Cotton/Pla blended yarns are evaluated in terms of strength, elasticity, pilling and abrasion test results, it is thought that Pla can be used to reduce the amount of cotton in the yarn. In this respect, it also contributes to sustainability.

## REFERENCES

1. Chapman, A., Hollins, O., et al. (2010). *Mistra future fashion review of life cycle assessments of clothing*. Oakdene Hollins Research & Consulting, Stockholm.
2. Blackburn, R. S. (2005). *Biodegradable and sustainable fibres*. Chicago, IL: Taylor & Francis US.
3. Yang, Y., Zhang, M., Ju,Z. (2020). Poly(lactic acid) fibers, yarns and fabrics: Manufacturing, properties and applications, *Textile Research Journal* 91(13-14), 1641-1669.  
<https://doi.org/10.1177/0040517520984101>
4. Prakash, C., Ramakrishnan, G., & Koushik, C. (2012). Effect of blend ratio of quality characteristics of bamboo/cotton blended ring spun yarn. *Daffodil International University Journal of Science and Technology*, 7(1), 34–37.  
<https://doi.org/10.3329/diujst.v7i1.9645>
5. Shishoo, R. (2012). *The Global Textile and Clothing Industry: Technological Advances and Future Challenges*, Sawston: Woodhead Publishing.

# WEAVEABILITY OF SPACER/DISTANCE FABRICS WITH HIGH PERFORMANCE FIBERS ON A TECHNICAL DOUBLE RAPIER JACQUARD WEAVING LOOM USING LANCETS

KOCAMAN RECEP TÜRKAY \*, PUTZKE ENRICO AND FICKER FRANK

Hochschule Hof - University of Applied Sciences, Institute for Materials Science, Kulmbacher Straße 76, 95213, Münchberg, Germany

## ABSTRACT

In this study, a technical double rapier weaving loom was used for the weaving of spacer/distance fabrics with a polyester multifilament based ground warp, binding yarns and with polyester and basalt weft yarns. The spacing of the distance fabrics was achieved by using lancets. Four different bindings were developed and three different lancet heights have been used for the spacing. Thus developed spacer/distance fabrics showed uniform spacing between layers with a total thickness from 11.1 mm to 18.5 mm and were characterized according to their compressive resistance and energy absorption properties.

## KEYWORDS

Woven spacer fabrics; Distance fabrics; Double rapier; Jacquard; Lancet.

---

\* Corresponding author: Kocaman R.T., e-mail: [recep.kocaman@hof-university.de](mailto:recep.kocaman@hof-university.de)

## INTRODUCTION

Woven spacer fabrics are three dimensional textile structures consisting of two separate outer layers that are combined using binding yarns - keeping a space between two outer layers. Woven spacer fabrics are produced mainly by means of face-to-face weaving technique. Two surfaces of ground warp yarns are connected with pile yarns and for a carpet weaving, two layers are separated with a cutting mechanism within this technique [1]. Distance fabrics can also be woven using lancets. Two or more weft yarns can be inserted simultaneously into two different sheds. The distance warp yarn interlaces through the top and bottom fabric and the distance between the layers can be adjusted using appropriate lancet height. False picks or catching wefts can also be used to define the distance between layers [2]. Woven spacer fabrics can also be produced with modified double rapier weaving looms in order to weave semi-finished lightweight woven constructions [1, 3, 4]. Different geometries for the integration of foam between adjacent layers can also be realized using double rapier weaving technology with lancet systems [5]. This study summarizes the findings of the basic research for the weaveability of spacer/distance fabrics with high performance fibers using lancet systems with double rapier weaving technology, their compressive stress and energy absorption properties.

## EXPERIMENTAL

### Materials

Polyester multifilament yarns (167 tex) purchased from Zwirnerei Nikol Weber GmbH were used as ground warp yarns, binding yarns and also as weft yarns. Basalt multifilament yarns (1200 tex and 2400 tex, MeltRock) were used as weft yarns for the weaving of spacer fabrics.

### Methods

Four types of weave patterns were used for the study. The weave patterns were developed using the software EAT Scope Design (EAT GmbH). With this software it is possible to develop the bindings also for double rapier weaving looms. Figure 1 shows the three-dimensional models of developed weave patterns independent of yarn count and their weft cross sections. Weaves differ from each other by weave pattern within top and bottom layer and number of binding yarn group. Weave number 1, 2 and 3 have two groups of binding yarns which have the same yarn count with the ground warp yarns, whereas weave number 4 has one group of binding yarn. Weave number 1 and 4 have one-up one-down weave with a step number 1 and have reinforcement yarns between in both layers. Weave number 3 has two-up two-down weave with a step number 2 and has one-up one-down reinforcement yarns between in both layers. Weave number 2 has

one-up one-down weave without stepping and also reinforcement yarns between.

A technical double rapier weaving machine (TF 20, Stäubli GmbH, Germany) was used for the weaving of spacer/distance fabrics. This machine has a UNIVAL 100 jacquard system which makes it possible to control each harness via servo motors. Every harness can be controlled independently. It also includes special rapiers for the insertion of high performance fibers like carbon, aramid, basalt and ceramic fibers. Levelled metal lancets were used for the spacing of distance fabrics. Lancets with three different levels, respectively 10 mm, 14 mm and 18 mm were chosen for the design of experiment. For an effective shed geometry adjustment and in order to assist the weaving of outer layers, two front weaving tables were adjusted with 2 mm distance from the top and from below for every lancet height. Basalt multifilament yarns with two different yarn counts and polyester multifilament yarn were used as weft yarns whereas polyester multifilament yarn

was also used as ground warp yarn and binding yarn. Machine speed was adjusted between 40 and 45 rpm during weaving. The double rapier weaving loom has a continuous and discontinuous linear take-up system. Weft densities of the woven patterns were defined during the weaving for an optimum fabric tension and these density values were noted. After each row of inserted weft yarns, distance fabrics were taken up discontinuously with a defined length. Figure 2 shows the used lancet system and the examples of woven distance fabrics.

Compressive stresses of the chosen distance fabric samples were measured according to the test method DIN-EN-ISO 3386-I. Therefore, 70 mm x 70 mm, samples were prepared and 3 samples were measured from each woven spacer fabric type. The samples were loaded 3 times up to 70% of its thickness and then unloaded, and at the fourth time loaded up to 70%. First loading cycle was taken into account for calculation of energy absorptions and efficiencies.

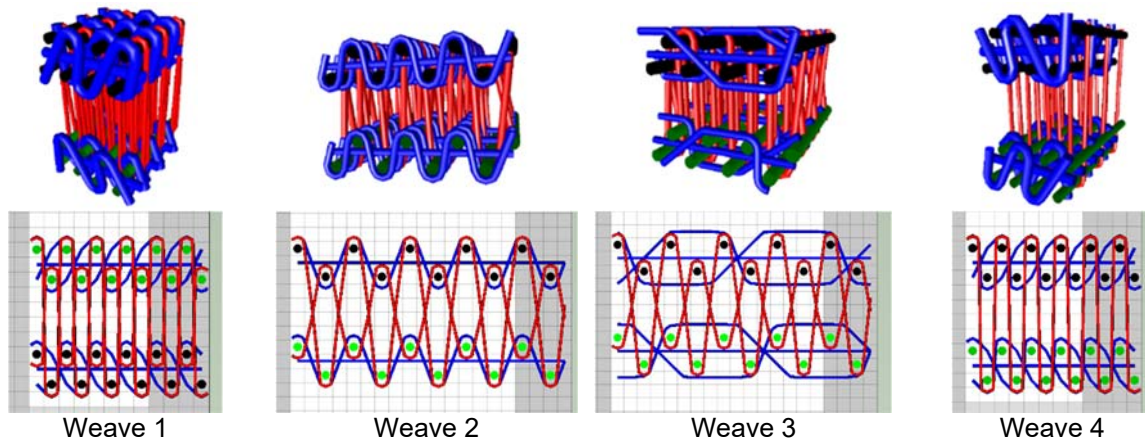


Figure 1: 3D models of developed weave patterns and their weft cross sections.

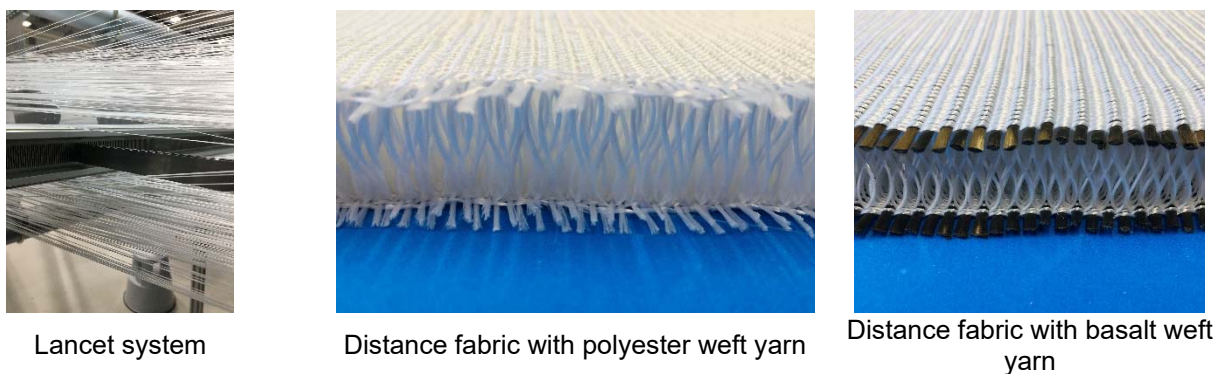


Figure 2: Lancet system and examples of woven distance fabrics.

## RESULTS AND DISCUSSION

### General findings

A uniform spacing was achieved in all of the woven distance fabrics. Weave pattern 3 with basalt weft yarn (2400 tex) could not be woven because of insufficient binding which showed up during

weaving. In general, weave patterns 3 and 4 showed visually looser structures with basalt weft yarns. Adjusted discontinuous take-up distances for each inserted weft row and measured thickness values of the woven samples are summarized in Table 1. According to the results, weave pattern 2 showed less fabric thickness values than the 18 mm lancet

height. This could be because of the type of binding which leads to a compact structure after the release of the woven sample from the lancet zone. Weave pattern 1 and weave pattern 2 showed sufficient binding and compact structures compared to pattern 3 and pattern 4. Generally, total fabric thickness values were up to 2 mm higher than the used lancet heights.

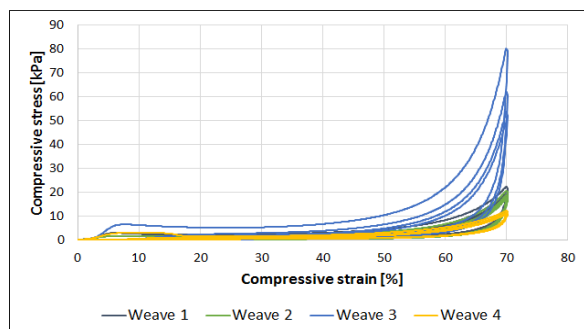
**Table 1.** Summary of the findings

Weave pattern	Lancet height	Take-up [mm/weft row]	Distance fabric thickness [mm]
Weave 1	18 mm	1.4 – 3.0	18.2 – 18.4
	14 mm	1.2 – 2.8	15.4 – 16.1
	10 mm	1.1 – 2.6	11.1 – 12.1
Weave 2	18 mm	1.8 – 3.4	15.2 – 16.7
	14 mm	1.4 – 3.1	15.1 – 15.4
	10 mm	1.4 – 2.8	11.5 – 12.7
Weave 3	18 mm	1.2 – 2.2	16.1 – 18.2
	14 mm	1.1 – 1.6	15.7 – 16.1
	10 mm	0.9 – 1.4	11.9 – 13.0
Weave 4	18 mm	1.2 – 3.0	17.0 – 18.5
	14 mm	1.0 – 2.8	14.6 – 15.3
	10 mm	1.0 – 2.2	11.7 – 12.4

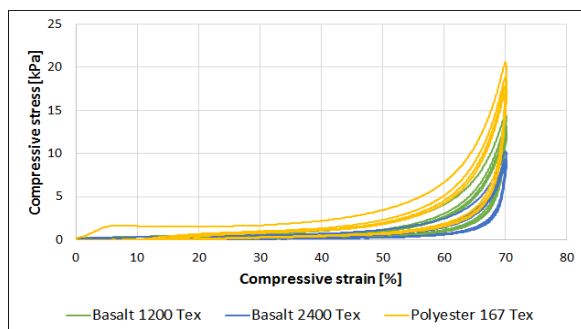
## Compressive resistance properties

Compressive resistance properties of chosen woven distance fabrics were characterized according to the weave pattern, used weft yarn and lancet height. Figure 3 shows the comparison of measured compressive stress values of chosen samples.

Test results show generally lower compressive stress values, because there is not a monofilament binding yarn in these structures. Binding yarns were also multifilament yarns and their yarn counts correspond to the ground warp yarns. All of the samples showed a long plateau stage, approximately up to 50 % of the total thickness. According to the results, weave pattern 3 showed the best compressive stress value when the weave patterns were compared (Figure 3(a)). Comparison of the samples with different weft yarn counts showed that the best compressive stress values were measured with the finest weft yarn; Polyester 167 tex, when the lancet height was 18 mm (Figure 3(b)). This could be due to a higher compact structure, using the finer weft yarns. Lower inner fabric thicknesses (lancet height: 10 mm, fabric thickness: 11.5 mm) showed better compressive stress values within the same weave pattern and weft yarn type (lancet height: 18 mm, fabric thickness: 18.5 mm) as shown in Figure 3(c). Weave pattern 1 with two groups of binding yarns showed better compressive stress values compared to weave pattern 4 with only one group of binding yarn as expected (Figure 3(d)). The best compressive resistance value was achieved within the weave pattern 3 with a polyester weft yarn and a fabric thickness of 11.6 mm (Lancet height: 10 mm) as shown in Figure 3(e).



**a)** Weft yarn: Polyester 167 Tex  
Lancet height: 18 mm



**b)** Weave pattern: Weave 2  
Lancet height: 18 mm

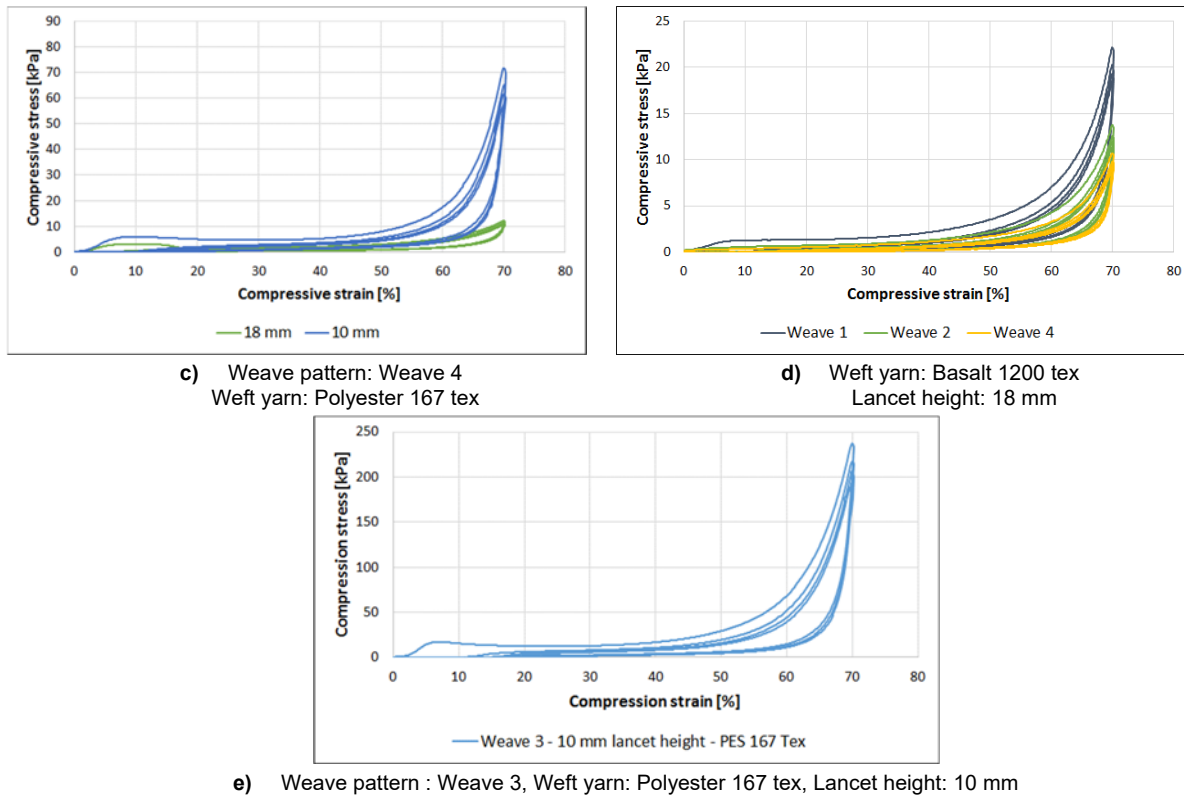


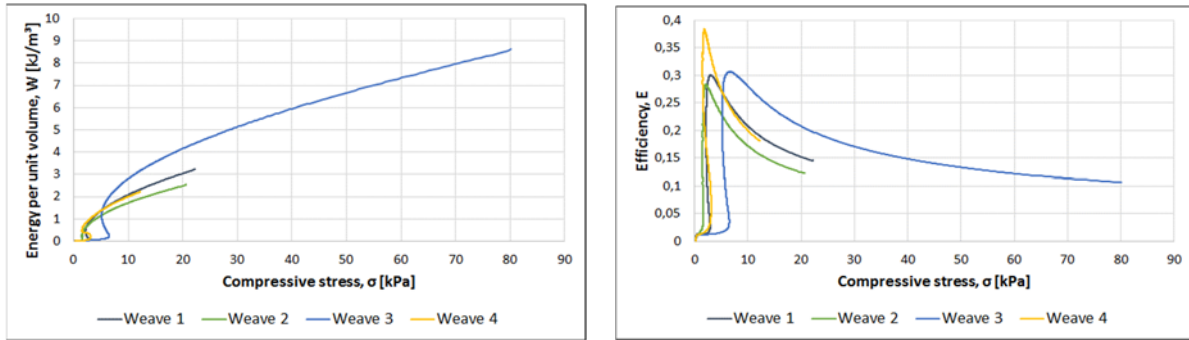
Figure 3: Comparison of compressive resistance values of chosen woven spacer fabrics.

### Energy absorption properties

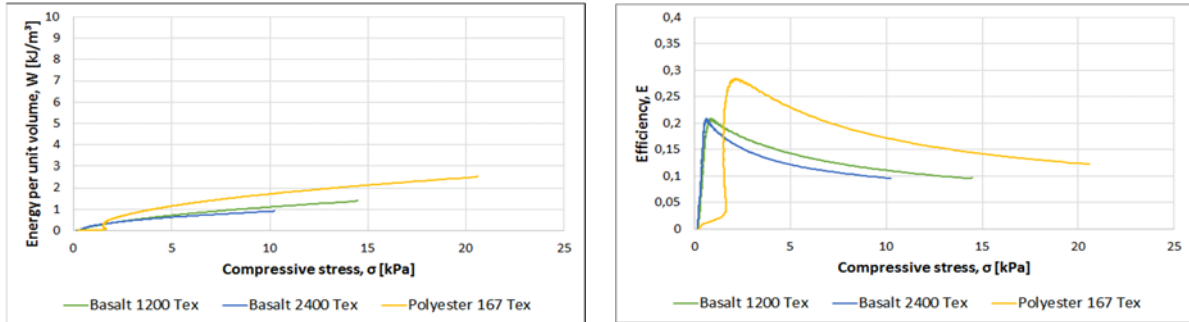
Calculation of the energy absorbed by a spacer/distance fabric under compression has a great importance. Compressive stress – strain diagrams can also show the energy absorption behavior, but using the energy absorption diagram will clearly show the absorbed energy per unit volume in order to understand the energy absorption property of a spacer fabric in a better way [6]. An energy absorption diagram shows the absorbed energy per unit volume as a function of the compressive stress and these kinds of diagrams were used in previous studies to show the energy absorption properties of foams, honeycomb structures and spacer fabrics [6, 7, 8]. Efficiency – compressive stress diagrams were also used to see energy absorption efficiency and the plateau stress [6, 7, 8]. A dramatic increase in the absorbed energy can be seen when the stress is towards the plateau stress in the efficiency – compressive stress diagrams and the stress maintains constant. Figure 4 shows the energy absorption diagrams of chosen samples (left) and their efficiency-compressive stress diagrams (right) which are calculated from the data of the first loading cycle.

The best energy absorption property was achieved within the weave pattern 3 with a polyester weft yarn in comparison of the weave pattern (Figure 4(a)).

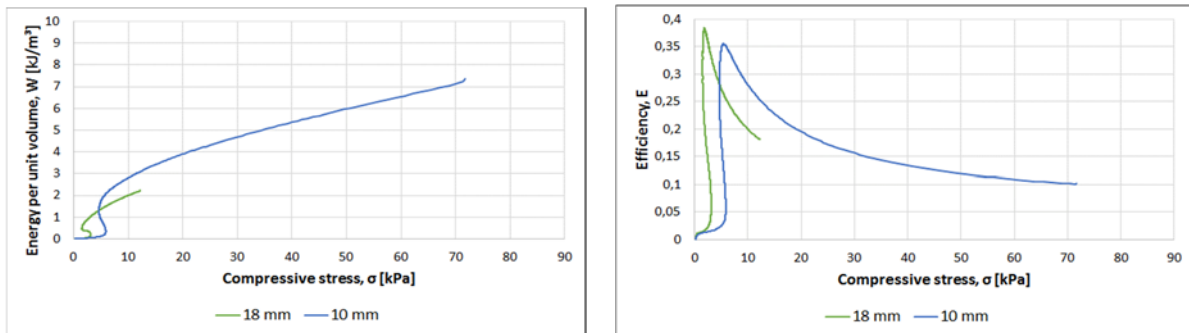
The plateau stress of this weave was approx. 7 kPa. Up to approx. 2 kPa, weave patterns 2 and 4 showed higher energy absorption efficiencies. On the other hand, woven spacer fabric with polyester weft yarn showed a higher plateau stress compared to basalt weft yarns (Figure 4(b)). Thicker woven spacer fabric showed a longer plateau zone and a lower plateau stress (Figure 4(c)). Thicker woven spacer fabric can absorb a defined amount of energy at lower stress. That means, thicker woven spacer fabric reaches its maximum efficiency point at a lower stress and energy level, which are approx. 1.71 kPa and 0.66 kJ/m<sup>3</sup>. Whereas the thinner woven spacer fabric reaches its maximum efficiency point at much higher stress and energy level, which are approx. 5.36 kPa and 1.9 kJ/m<sup>3</sup>. For this reason, both of these spacer fabrics have different working ranges. Comparison of weave pattern 1 with weave pattern 4 showed that the woven spacer fabric with two groups of binding yarns showed higher compressive stress and energy level and a higher efficiency, which is due to the effect of additional binding yarn system (Figure 4(d)). Weave pattern 3 with an 11.6 mm thickness (10 mm lancet height) and polyester weft yarn showed the highest plateau stress of approx. 15 kPa and the highest energy level of approx. 4.6 kJ/m<sup>3</sup> all among the woven spacer fabrics.



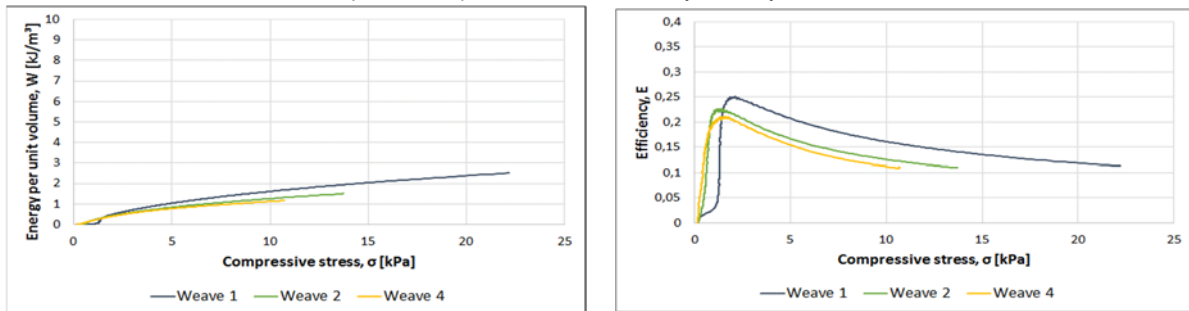
a) Weft yarn: Polyester 167 tex, Lancet height: 18 mm



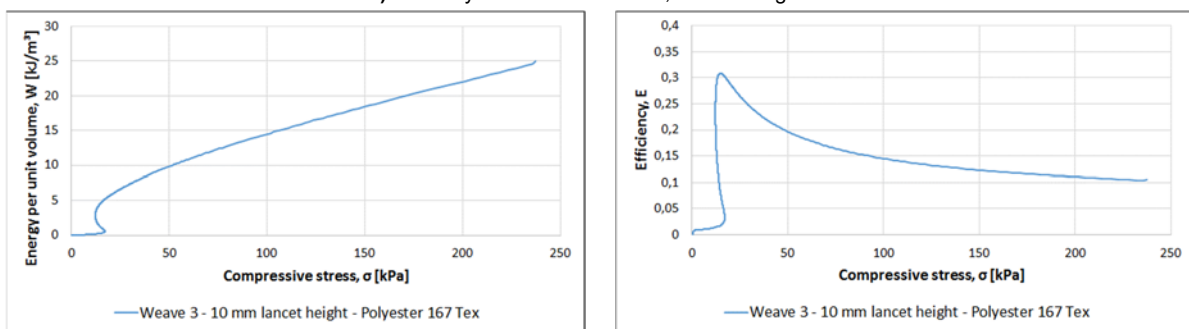
b) Weave pattern: Weave 2, Lancet height: 18 mm



c) Weave pattern: Weave 4, Weft yarn: Polyester 167 Tex



d) Weft yarn: Basalt 1200 tex, Lancet height: 18 mm



e) Weave 3, Weft yarn: Polyester 167 tex, Lancet height: 10 mm

Figure 4: Energy absorption (left) and efficiency (right) diagrams of chosen woven spacer fabrics.

## CONCLUSIONS

In this study the weavability of distance fabrics with high performance fibers like basalt yarns and polyester yarns on a technical double rapier weaving machine was discussed. Different woven fabric samples were compared according to their thicknesses and bindings. Important findings were summarized. Compressive resistance properties of chosen fabrics were compared according to their weave pattern type, weft yarn type and lancet height. Energy absorption properties of chosen samples were analyzed and compared according to the material, process and fabric parameters.

**Acknowledgements:** *This research received no specific grant from any funding agency in the public, commercial, or not-for-profit sectors. The authors are grateful to Mr. Uwe Schwittai and Mr. Harald Ott for the weaving of spacer/distance fabrics and Ms. Susanne Schödel-Guthke for the testing of the fabric samples. The responsibility for the content of this publication lies with the author(s).*

## REFERENCES

1. Torun, A.R. (2011). Advanced manufacturing technology for 3D profiled woven preforms. PhD Study. Dresden University of Technology (Dresden)
2. Maes, D. (2009). Applications of distance fabrics and multiple layer weaves in technical textiles. <http://www.technicaltextile.net>
3. Mountasir, A. (2016). Entwicklung einer flexiblen Webtechnologie zur Fertigung integral gewebter 3D Halbzeuge für Faserkunststoffbauteile komplexer Geometrie. PhD Study. Dresden University of Technology (Dresden)
4. Großman, K., Mühl, A., Löser, M., Cherif, C., Hoffmann, G., Torun, A.R. (2010). New solutions for the manufacturing of spacer preforms for thermoplastic textile-reinforced lightweight structures. *Prod. Eng. Res. Devel.* 4:589-597. <https://doi.org/10.1007/s11740-010-0267-9>
5. Lüling, C., Rucker-Gramm, P., Weilandt, A., Beuscher, J., Nagel, J., Schneider, J., Maier, A., Bauder, H., Weimer, T. (2021). Advanced 3D Textile Applications for the Building Envelope. *Applied Composite Materials.* 29:343-356. <https://doi.org/10.1007/s10443-021-09941-8>
6. Liu, Y., Hu, H., Zhao, L., Long, H. (2011). Compression behavior of warp-knitted spacer fabrics for cushioning applications. *Textile Research Journal.* 82(1):11-20. <http://dx.doi.org/10.1177/0040517511416283>
7. Bates, S., Farrow, I., Trask, R. (2016). 3D printed elastic honeycombs with graded density for tailorable energy absorption. *Proc. SPIE 9799, Active and Passive Smart Structures and Integrated Systems.* <https://doi.org/10.1117/12.2219322>
8. Avale, M., Belingardi, G., Montanini, R. (2001). Characterization of polymeric structural foams under compressive impact loading by means of energy-absorption diagram. *International Journal of Impact Engineering* 25:455-472. [https://doi.org/10.1016/S0734-743X\(00\)00060-9](https://doi.org/10.1016/S0734-743X(00)00060-9)

# SIMULATION OF THE SEGMENT FILLING INSERTION FABRICS AT THE YARN LEVEL

FANG JIAHUI<sup>1,2\*</sup>, KYOSEV YORDAN KONSTADINOV<sup>2</sup>, LI YULING<sup>1</sup> AND MA YANXUE<sup>1</sup>

<sup>1</sup> College of Textiles, Donghua University, Shanghai, 201620, China

<sup>2</sup> Technische Universität Dresden, Dresden, 01069, Germany

## ABSTRACT

Fabrics with segment filling insertion are finding application in several traditional luxurious textiles, clothing, and in the latest time as well for smart textiles. Segment filling allows the integration of conductive yarns for contacting areas, keeping the textile character of the structures. This work presents a method for 3D modeling woven structures with segment filling at the yarn level. The pattern image is analyzed by an image processing tool, written in Python, and used to create the initial weaving information. After that, the different regions are filled with suitable preselected weave types, such as plain, twill, or others. Finally, this data is used to compute the 3D coordinates of the weft and warp yarns, and saved in a suitable format. The 3D visualization is done by the TexMind Viewer, which allows its advanced version export in various formats for FEM, CFD, and other computations.

## KEYWORDS

Segment filling insertion fabrics; Yarn level; Product development; 3D simulation.

\* Corresponding author: Fang J., e-mail: [fangjiahui@163.com](mailto:fangjiahui@163.com)

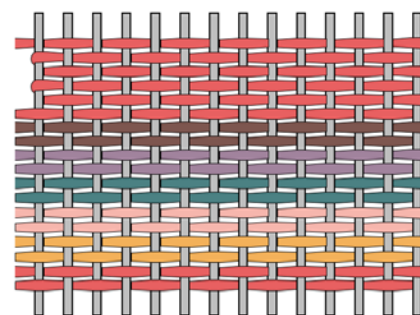
## INTRODUCTION

According to the filling insertion method [1], weaving looms can be divided into shuttle looms and shuttleless looms, the weaving looms were all based on the normal filling method until 2019. As shown in Figure 1, every weft is filled from one side to the other with one single yarn in fabrics with a plain weave. Meanwhile, many researchers have taken numerous approaches in yarn-level woven fabric modeling [2]-[4] based on the normal filling method [5]-[7].

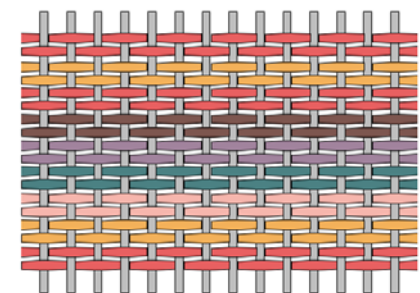
With the improvement of automatic techniques, segment filling insertion fabrics (see Figure 2) can be woven by a modified dobby loom in 2019 [8]. The segment filling insertion fabrics are pretty complex, different from the normal woven fabrics, where the fabrics are composed of yarn-level patterns based on repeated sections<sup>[9-10]</sup>. As each row is composed of several yarns of different colors, which can be turned back at any position.

The method for 3D simulation of woven structures with segment filling at the yarn level is systematically proposed in this work. Characterization of yarns in the segment filling insertion fabric as is shown in Fig. 2. For the simulation of segmental filling insertion fabrics, the challenge is that the trajectory of the weft yarn is flexible, i.e., it can start and end at any position, in addition, it is continuous between

different rows, the connection between the end of one row and the start of the next row is also much more complicated compared with normal woven fabrics.



(a) Fabrics woven by shuttle loom



(b) Fabrics woven by shuttleless loom

Figure 1. Normal filling insertion fabrics.

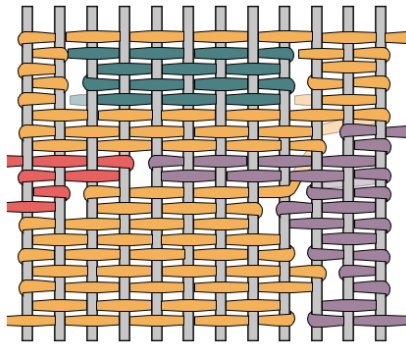
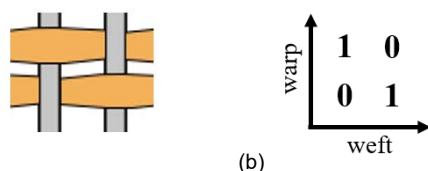


Figure 2. Segment filling insertion fabrics.

## EXPERIMENTAL

The simulation parameters are obtained through imaging analysis, area division, weave filling, and orientation property marks of key positions along the yarn trajectory. A topology-based model, similar to those reported for braided structures [11] or in the general case for any textile architecture [12] was developed as a parametric mathematical model and then implemented in a Python program.

In the past years, a matrix of '0' and '1' is generally applied to describe the structure of a fabric [13]. In simulation analysis as well as 3D modeling of fabrics [14-15], this matrix describes the position relationship of warp and weft yarns, that is, the Z coordinate in the 3D coordinate system. Taking plain weave fabric as an example, as shown in Figure 3, its basic organizational structure matrix is shown in Figure 3(b). For other parameters [16-17], such as yarn geometry (e.g. yarn length, fineness, yarn spacing, etc.), yarn mechanics (e.g. initial modulus, strength, elongation, etc.), yarn color parameters, etc. The common feature of the above simulation as well as the modeling of woven fabrics is that the normal weft yarns are continuous in the row as well as disconnected at both ends. For the calculation of the key coordinates of the yarn trajectory, it is not necessary to consider the relationship between wefts. More realistic methods for the representation of the yarns at the fiber level can be implemented in the future, as reported by Liu et al. [18], but in the current work, the specific areas of the weft yarn transition have to be considered and modeled more detailed.



(a) Schematic diagram of plain weave  
(b) Matrix code for organization chart

Figure 3. Plain weave and its corresponding matrix.

## Methods

In this study, the initial pattern (noted as matrix  $Z_{0ij}$ , as shown in Figure 4 (a)) is first processed by the algorithm to divide the color minimum region, and the color information of each part of the region can be extracted separately as well as saved in a new matrix of size  $i*j$ , noted as matrices  $Z_{1ij}$ ,  $Z_{2ij}$ ,  $Z_{nij}$  (as shown in Fig. 4(b)), where each part of the divided region is composed of one single continuous weft yarn. (For the segment filling insertion fabric, its area division standards mainly follow the shortest floating line, as well as the principle of the shortest entanglement, which involves a complex process issue, not discussed in detail in this paper.)

The original pattern image is analyzed by algorithms written in python, in this paper, the simulation model of the segment filling insertion fabric is mainly obtained by connecting the key points with Cubic Hermite spline, so the calculation of the key points in the 3D coordinate system is the core of this study.

The new matrix obtained by the algorithm fills the divided area with plain organization, noted as  $Y_{1ij}$ ,  $Y_{2ij}$ , ...,  $Y_{nij}$ , the matrix indicates the corresponding relationship between warp and weft in each row, the figure 'Δ' is '1' in the matrix, i.e., the weft is on top; 'o' corresponds to the matrix '-1', i.e., the weft is at the bottom; the blank is '0', i.e., the weft does not pass through the region, as shown in Figure 5, this matrix represents the topological information.

$Y_{111} = 1$ ,  $Y_{121} = -1$ , ..., the non-zero region of this matrix is the range covered by the weft, i.e., a continuous yarn coverage, moreover, the key points of the yarn are recorded in the matrix  $Weft1[P()]$ , where the coordinates of the key point  $P(X_P, Y_P, Z_P) = (i, j, Y_{nij})$ . The weave diagram is produced.

The coordinates of the weft at the last point of the previous row are marked as  $P(X_P, Y_P, Z_P)$ , the adjacent row of wefts (as shown in Figure 6(a)), or the non-adjacent row of wefts (as shown in Figure 6(b)). The starting point is Q.

The correct order of the key points is obtained by judging from Eq. 1. As shown in Figure 7.

$$Q = \begin{cases} Q_m, X_P \leq X_{Qm} \\ Q_m, X_{Qm} < X_P < X_{Qn} \cup (X_P - X_{Qm})^2 - (X_P - X_{Qn})^2 \leq 0 \\ Q_n, X_{Qm} < X_P < X_{Qn} \cup (X_P - X_{Qm})^2 - (X_P - X_{Qn})^2 > 0 \\ Q_n, X_{Qn} \leq X_P \end{cases} \quad (1)$$

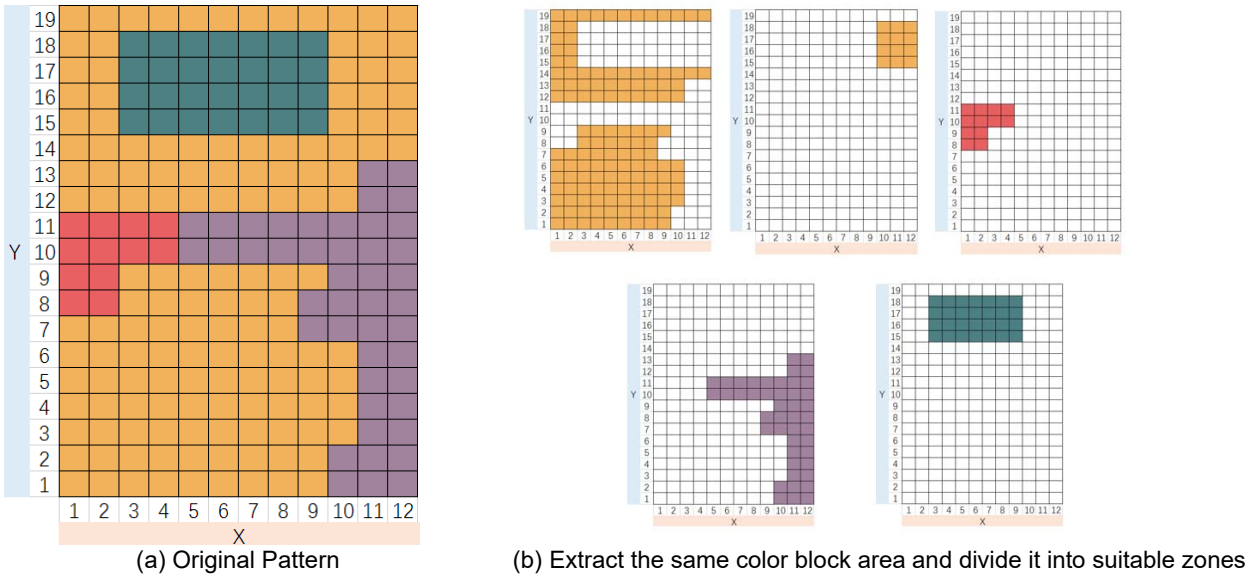


Figure 4. Original Pattern and the divided zones.

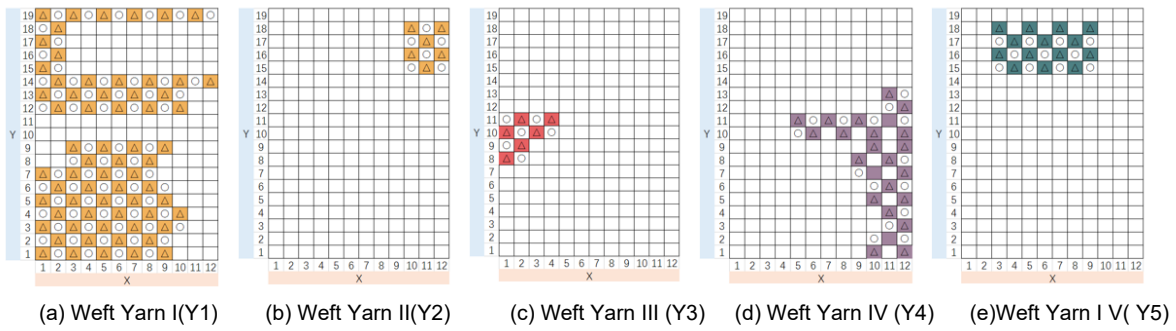


Figure 5. The weave diagram of each weft.

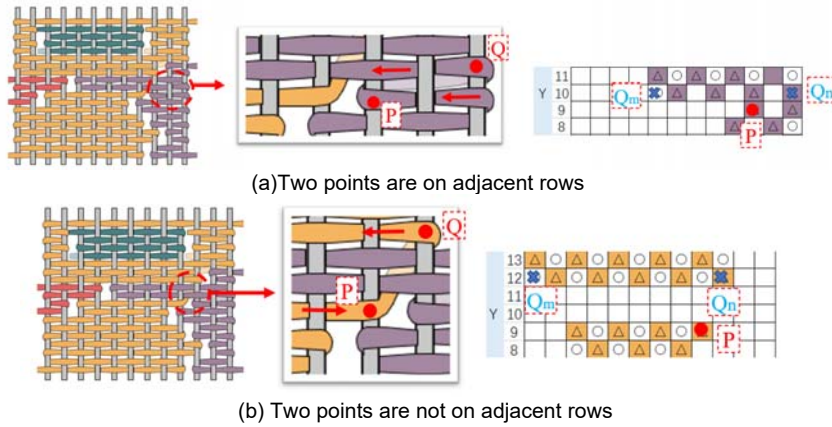


Figure 6. Connection of P and Q.

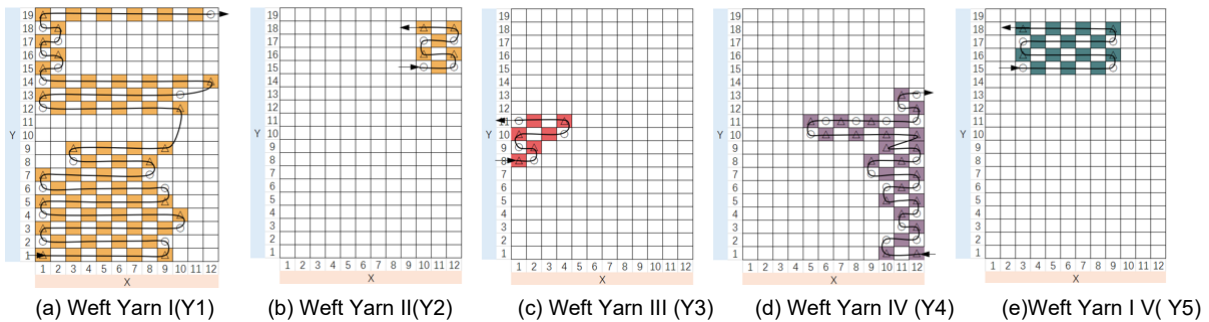


Figure 7. Determine the weft trajectory.

The weft yarn is continuously between rows, so the weft returned from the edge of the fabric. or create a floating line from one point (at the end of the previous row) to another point (the connection of the next row), which is another unique feature of the segmental filling insertion fabric. In the case of the weft return from the edge of the fabric, it is assumed that the next point is  $Q_n$ , i.e., a new control point  $N(X_N, Y_N, Z_N)$  needs to be inserted between the points  $P(X_P, Y_P, Z_P)$  and  $Q(X_Q, Y_Q, Z_Q)$  (as shown in Fig. 8). Thereby ensuring the trajectory variation of the yarn in the z-axis direction.

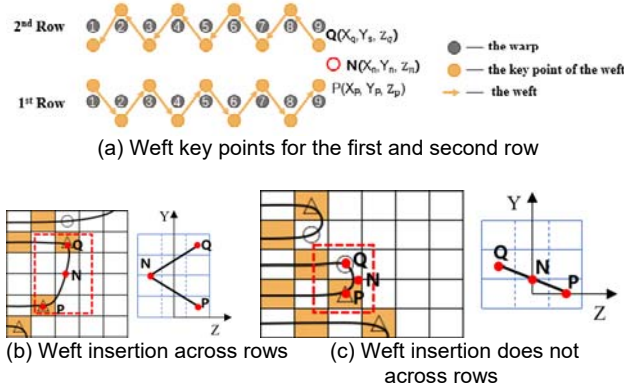


Figure 8. Insert a new control point N based on Points P and Q.

If the floating line is generated, i.e., a new control point N needs to be inserted between points P and Q, meanwhile, the Z coordinates of points P and Q are also to be compared, then the coordinates of the N point can be calculated.

$$\begin{cases} X_N = \frac{X_P + X_Q}{2} \\ Y_N = \frac{Y_P + Y_Q}{2} \\ Z_N = \begin{cases} \frac{Y_P + Y_Q}{2}, Z_P * Z_Q < 0 \\ -\frac{Y_P + Y_Q}{2}, Z_P * Z_Q > 0 \end{cases} \end{cases} \quad (2)$$

Meanwhile, the next weft is determined by calculating the relative position in the X-axis, followed the Eq. 2, starting from the left or right.

Finally, we got the key points of the yarn recorded in the matrix, suppose the yarn starts from (m,n) and ends at (w,v), the points through the yarn was saved in order in the matrix Weft1 = [P1( $X_m, Y_n, Z_P$ ), P2( $X_{m+1}, Y_n, Z_P$ ), ..., Pi( $X_i, Y_n, Z_P$ ), N( $\frac{X_P + X_Q}{2}, \frac{Y_P + Y_Q}{2}, Z_N$ ), P( $X_Q, Y_Q, Z_Q$ ), ..., P( $X_w, Y_v, Z_P$ )]. Moreover, all the simulation information is saved in the fabric matrix as follows, Fab = [Wefts[P1(),P2(),..., Pm()], Warps[P1(),P2(),..., Pn()],yarn parameters map].

### Simulation Parameters

In addition to some parameters [19-20] that need to be analyzed from the original pattern, some additional parameters have to be input by the designer to simulate the fabric, as shown in Table 1.

Table 1. Specifications of 3D fabric.

	Input parameters	Output
Yarn parameters	Color map Warp radius r1 Weft radius r2	Simulation file
Fabric parameters	Warp density/ Warp gap Weft density/ Weft gap	

The number of warp and weft can be obtained after analysis the pattern. Meanwhile, the matrix information can be gained by further calculations. Many parameters can be calculated, such as, the warp length can be calculated from the yarn fineness and the size of the pattern. Integration of parameters in python to complete the simulation of the fabric as shown in Fig. 9.

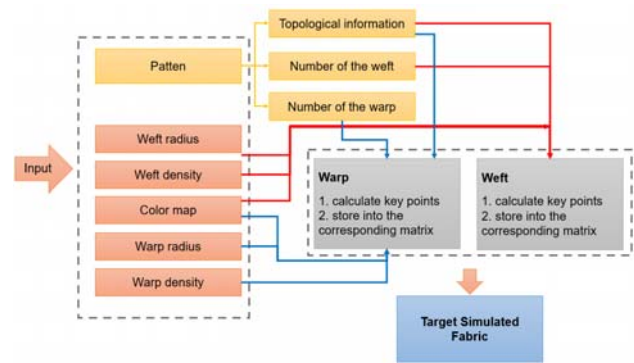


Figure 9. Calling and handling of parameters.

## RESULTS AND DISCUSSION

In this study, parameters are collected mainly by analyzing pattern as well as the input from the designer, then the Z-axis coordinates are obtained by filling the segmented area with unit matrix organization, besides, the different rows are connected by inserting auxiliary points; the weft trajectories are obtained from the key point sequence. Finally, yarn parameters are added to complete the simulation of the segmented filling insertion fabric.

The simulated segment filling insertion fabric is displayed by the TexMind Viewer, as shown in Figure 10. The floating yarns are generated between non-adjacent areas in the back view. Two simulated fabrics with the same warp density but different weft densities are named F1 and F2.

The method proposed in this study, the simulation not only reflected the characteristics of the segment filling insertion fabric but also can be a guide for the fabric design and rationality check of the weaving process. This work solves the following problems in the simulation process: Determination of the sequence point Q in the process of weft yarn transferred to another row; Calculation of the correct auxiliary points by P and Q; The combination of yarn

parameters as well as topological information matrix to obtain the simulated fabric.

However, the work still has some shortcomings, the bending of warp yarn is not considered in the

simulation process and there are details that can continue to be optimized subsequently. More parameters can be added to improve the accuracy of the simulation.

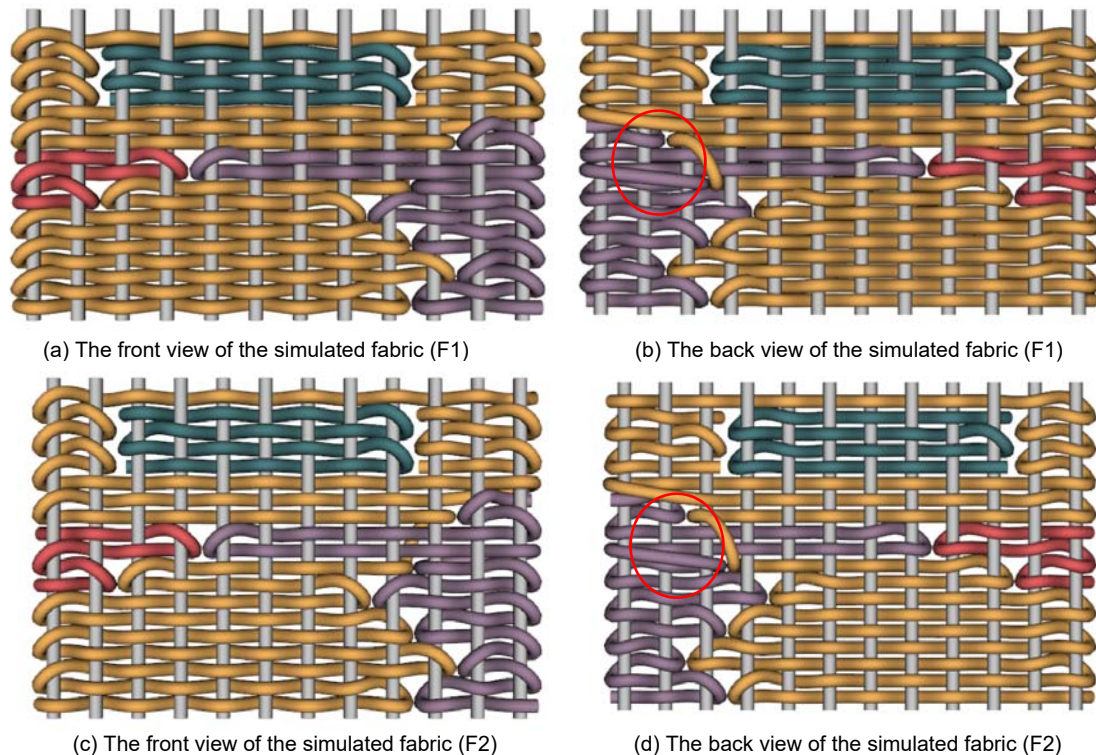


**Figure 10.** The front view and the back view of the two simulated fabrics.

## CONCLUSIONS

Yarn-level simulation can assist in the design and weaving of the fabric, converting the original 2D weave diagram into a 3D intuitive visual effect, which is very significant for fabric-assisted design. Modeling in 3D visualization at the yarn level is more friendly for the designers, because they can make reasonable modifications to the design by the 3D model. Besides, yarn-level modeling can be also used to simulate the physical properties of textiles. The structure of the segment filling insertion fabric has infinite possibilities, which can make the fabric more diverse, as different color areas can be woven with different functional yarns.

**Acknowledgements:** This research stay in Germany of Jiahui Fang for study was supported by 'the Fundamental Research Funds for the Central Universities' (Grant No.: 2232020E-10) and 'China Scholarship Council'

## REFERENCES

- Mao X.H, Bao M.(2005) Weaving Volume II. China Textile Publishing House (Beijing).
- Dong, Z., & Sun, C. T. (2009). Testing and modeling of yarn pull-out in plain woven Kevlar fabrics. *Composites Part A: Applied science and manufacturing*, 40(12), 1863-1869. <https://doi.org/10.1016/j.compositesa.2009.04.019>
- Leaf, J., Wu, R., Schweickart, E., James, D. L., & Marschner, S. (2018). Interactive design of periodic yarn-level cloth patterns. *ACM Transactions on Graphics (TOG)*, 37(6), 1-15. <https://doi.org/10.1145/3272127.3275105>
- Jauffrès, D., Sherwood, J. A., Morris, C. D., & Chen, J. (2010). Discrete mesoscopic modeling for the simulation of woven-fabric reinforcement forming. *International journal of material forming*, 3(2), 1205-1216. <http://dx.doi.org/10.1007%2Fs12289-009-0646-y>
- Tripathi, L., Chowdhury, S., & Behera, B. K. (2022). Modeling and simulation of impact behavior of 3D woven solid structure for ballistic application. *Journal of Industrial Textiles*, 51(4\_suppl), 6065S-6086S. <https://doi.org/10.1177/1528083720980467>
- Özdemir, H., & Başer, G. (2008). Computer simulation of woven fabric appearances based on digital video camera recordings of moving yarns. *Textile Research Journal*, 78(2), 148-157. <http://dx.doi.org/10.1177/0040517507080692>
- Özdemir, H., & Başer, G. (2009). Computer simulation of plain woven fabric appearance from yarn photographs. *The Journal of The Textile Institute*, 100(3), 282-292. <https://doi.org/10.1080/00405000701757529>
- Fang, J., Ma, Y., Li, Y., et al. (2021). Design and development of urban cultural and creative products with segment filling insertion. In *Journal of Physics: Conference Series*: 1790(1): 012032. [doi:10.1088/1742-6596/1790/1/012032](https://doi.org/10.1088/1742-6596/1790/1/012032)
- Nilakantan, G., Keefe, M., Bogetti, T. A., Adkinson, R., & Gillespie Jr, J. W. (2010). On the finite element analysis of woven fabric impact using multiscale modeling techniques. *International Journal of Solids and Structures*,

- 47(17), 2300-2315.  
<https://doi.org/10.1016/j.ijolstr.2010.04.029>
10. Rief, S., Glatt, E., Laourine, E., Aibibu, D., Cherif, C., & Wiegmann, A. (2011). Modeling and CFD-simulation of woven textiles to determine permeability and retention properties. *AUTEX Research Journal*, 11(3), 78-83.
  11. Kyosev Y. Generalized geometric modeling of tubular and flat braided structures with arbitrary floating length and multiple filaments. *Textile Research Journal*. 2016;86(12):1270-1279.  
<https://doi.org/10.1177/0040517515609261>
  12. Kyosev, Y., Topology-Based Modeling of Textile Structures and Their Joint Assemblies, Springer Nature Switzerland AG, 2019, 238 p,  
<https://doi.org/10.1007/978-3-030-02541-0>
  13. Dash, B. P., Behera, B. K., Mishra, R., & Militky, J. (2013). Modeling of internal geometry of 3D woven fabrics by computation method. *Journal of the Textile Institute*, 104(3), 312-321.  
<https://doi.org/10.1080/00405000.2012.720850>
  14. Wielhorski, Y., Mendoza, A., Rubino, M., & Roux, S. (2022). Numerical modeling of 3D woven composite reinforcements: A review. *Composites Part A: Applied Science and Manufacturing*, 154, 106729.  
<https://doi.org/10.1016/j.compositesa.2021.106729>
  15. Manjunath, R. N., & Behera, B. K. (2017). Modelling the geometry of the unit cell of woven fabrics with integrated stiffener sections. *The Journal of The Textile Institute*, 108(11), 2006-2012.  
<https://doi.org/10.1080/00405000.2017.1308785>
  16. Lee, S. K., Byun, J. H., & Hong, S. H. (2003). Effect of fiber geometry on the elastic constants of the plain woven fabric reinforced aluminum matrix composites. *Materials Science and Engineering: A*, 347(1-2), 346-358.  
[https://doi.org/10.1016/S0921-5093\(02\)00614-7](https://doi.org/10.1016/S0921-5093(02)00614-7)
  17. Daelemans, L., Faes, J., Allaoui, S., Hivet, G., Dierick, M., Van Hoorebeke, L., & Van Paepegem, W. (2016). Finite element simulation of the woven geometry and mechanical behaviour of a 3D woven dry fabric under tensile and shear loading using the digital element method. *Composites Science and Technology*, 137, 177-187.  
<http://dx.doi.org/10.1016/j.compscitech.2016.11.003>
  18. Liu, H., Kyosev, Y., & Jiang, G. (2022). Yarn level simulation of warp-knitted clothing elements – first results and challenges. *Communications in Development and Assembling of Textile Products*, 3(2), 115-126.  
<https://doi.org/10.25367/cdatp.2022.3.p115-126>
  19. Cirio, G., Lopez-Moreno, J., Miraut, D., & Otaduy, M. A. (2014). Yarn-level simulation of woven cloth. *ACM Transactions on Graphics (TOG)*, 33(6), 1-11.  
<https://doi.org/10.1145/2661229.2661279>
  20. Nilakantan, G., & Gillespie Jr, J. W. (2012). Ballistic impact modeling of woven fabrics considering yarn strength, friction, projectile impact location, and fabric boundary condition effects. *Composite Structures*, 94(12), 3624-3634.  
<http://dx.doi.org/10.1016/j.compstruct.2012.05.030>

# NUMERICAL MODELLING OF TEXTILE STRUCTURES: POTENTIAL AND LIMITS

BOŇKOVÁ KAROLÍNA\*

Technical University of Liberec, Department of Textiles and Structures, Studentská 2, 461 17 Liberec, Czech Republic

## ABSTRACT

Numerical modelling, namely finite element modelling, is a standardised tool in many branches of engineering. In textile engineering, due to the complexity of the structure, many limitations occur in using this approach. Despite the limitations the finite element modelling of textiles has huge potential for the future. This contribution deals with FE modelling of tensile test in wale and course direction of single jersey knitted fabric. The meso level of the structure was chosen for the model, so it could be possible to track the behaviour of yarn interlacement during the simulated deformation. The virtual model was created according to parameters of single jersey knitted fabric sample, which was produced from polyester monofilament. By using monofilament instead of staple yarn, contacts between fibres in yarn could be excluded in FE model preparation. Two different computational programs were used for simulations – MSC Marc Metant for implicit computing approach and ANSYS LS-DYNA for explicit computing approach. The results from implicit and explicit solver were compared and discussed. Validation of models was done and results were included in the discussion. Due to big deformations of textiles, explicit solver appears to be more suitable for finite element modelling in textile engineering.

## KEYWORDS

Finite element method; Implicit and explicit solver; Textile structures; Modelling; Tensile test; Knitted fabric.

\* Corresponding author: Boňková K., e-mail: [karolina.bonkova@tul.cz](mailto:karolina.bonkova@tul.cz)

## INTRODUCTION

Textile structures are extremely variable which is one of the reasons why it is possible to find them in nearly every industrial sector from clothing industry, automotive to biomechanics etc. Modelling of textiles is a challenging topic for many reasons and one of them is their multi-scale structure character [1, 2]. Textile structures can be divided into three main groups – linear, planar and 3D shaped textiles. Each group can be further described on three levels – macro, meso and micro scale. Macro-scale describes overall shape of the textile, so for example if it is yarn, woven fabric or some 3D braided structure. Meso-scale investigates the core structure of the textile, how yarns are interlaced so basically it describes pattern of the yarn arrangement. Micro-scale model tracks how individual fibres are arranged around each other.

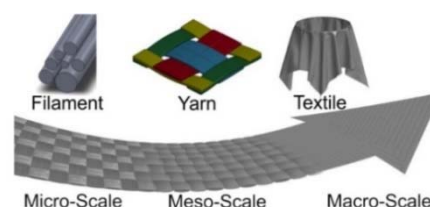


**Figure 1.** Representation of micro, meso and macroscale of textiles [1]

Textiles have inhomogeneous character and their mechanical behavior can be described mainly as viscoelastic. Thanks to these attributes the general geometry depiction of textile structures is complicated to describe, because of its changeability. For example a shape of an individual staple yarn is different than the same yarn which is weaved in fabric. Many studies have been done about this topic and in conclusion, geometry models of textile structures are always simplified at some level in comparison with the real geometry. By using computer tomography data and reconstruction of textile structure it is possible to create virtual textile model with exact geometry [3], but this method is time consuming and usually only small part of the

textile is modelled. Another aspect is, that even though we have high performance computational technology, it still is not efficient enough to capture all scales of the structure at the same time. Such model would be extremely demanding for the data and processing memory. Because of that we are able to model textiles usually on one or maximally two structural levels at the same time.

Creating virtual 3D model of textiles is first step for finite element modelling in which even more limitations occur such as description of material models, types of used elements, number of elements, contacts and more. Complex multiscale simulations are used in FE modelling of textiles, when results from one scale simulation are used as input data for another scale simulation [3]. According to work [4], the most important aspects for quality simulation on one scale with good corresponding results are:

- a realistic geometric model of textile structure,
- realistic boundary conditions,
- a realistic contact surface between yarns without penetration,
- physically measured yarn mechanical data used as input for material model.

Most of the studies which include FE modelling of textiles are oriented on woven fabrics which are commonly used as a reinforcement in textile composites [5]. Work of [6] studied optimization of geometrical model of knitted structures designated as an input for FE modelling. Similarly work [5] investigated mechanical behavior of knitted textiles and their geometrical modifications. Unfortunately neither of these works have FE models validated by experiment.

## EXPERIMENTAL

### Materials and methods

PERLON Polyester monofilament of diameter 0.1 mm was used to produce single jersey knitted fabric. Tensile test of monofilament was done to obtain information about its mechanical properties (Instron 4411, testing length 250 mm, testing speed 500 mm/min, 10 tested samples). Average tensile strength was 734 MPa and average modulus was 1950 MPa.

Single jersey knitted fabric was manufactured using Shima Seiki SRY 123LP machine with gauge G14. Relaxed fabric had 32 loops/50 mm in course direction and 98 loops/100 mm in wale direction so geometry of a single loop could be described by width 1.56 mm and height 1.02 mm.

**Table 1.** Parameters used for generating of geometry – models of single jersey knitted fabric samples

	Model for wale direction	Model for course direction
Number of courses	49	15
Number of wales	10	32
Loop width [mm]	1.56	
Loop height [mm]	1.02	
Monofile diameter [mm]	0.1	
Element length for export [mm]	0.2	

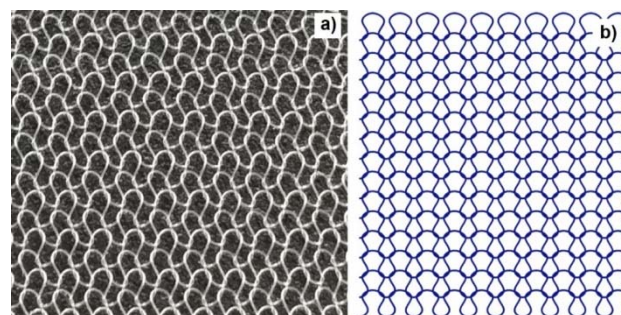


**Figure 2.** a) Single jersey knitted fabric from polyester monofilament, b) 3D virtual model of the textile

### Preparation of FE models

Two computational solvers were used – MSC Marc Metant (implicit solver) and ANSYS LS-DYNA (explicit solver). Two models were prepared, tensile test of virtual sample in course and tensile test of virtual sample in wale direction. In both softwares the same input geometry, material properties, boundary conditions, computational method and job results were set. Since programs offer different settings, models differed a little bit in used element and contact description but both were chosen as similar as possible.

#### a) Geometry

The geometry of the single jersey fabric was prepared in program TexMind WeftKnitting3D. Two models were prepared – one as a sample for tensile test in course direction and second as a sample for tensile test in wale direction. As an input information for the program, parameters shown in Table 1 were used.

#### b) Meshing, material and contact

Beam elements were used. Beam had circular cross-section with diameter 0.1 mm. Average element length was 0.2 mm. In MSC Marc Metant element type 52 (Euler-Bernoulli beam) was used and in ANSYS LS-DYNA beam formulation 1 (Hughes-Liu) was chosen.

Linear elastic material model was chosen and described with values of modulus  $E = 1950 \text{ MPa}$ , Poisson's ratio  $\mu = 0.3$  and density  $\rho = 1365 \text{ kg/m}^3$ .

In MSC Marc Metant, beam to beam touching contact was chosen. Friction coefficient was set to value 0.1.

In ANSYS LS-DYNA, automatic general contact was chosen. Static and dynamic friction coefficient were set to value 0.1.

### c) Boundary conditions and job results

In both tensile tests edge nodes were disabled in every degree of freedom on one side (symbolized by cross) – this side represented static clamp of tensile testing machine. Other edge nodes were allowed in every rotational degree of freedom, one sliding degree of freedom in one direction and two remaining directions were disabled (symbolized by arrow). This side of model represented the edge of sample fixed in moving clamps of tensile testing machine. In LS-DYNA boundary conditions were applied directly on the nodes, in MCS Marc nodes were connected to one Rigid body element on each side.

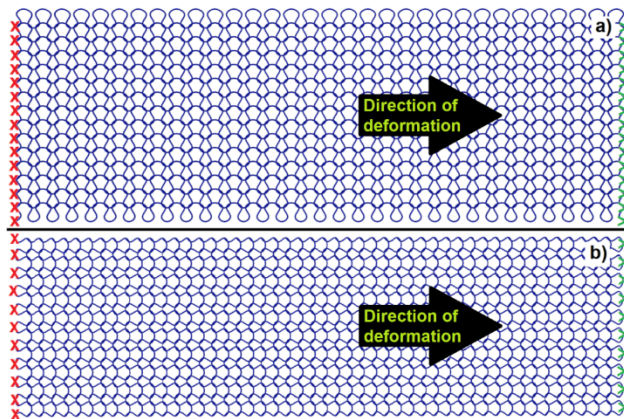


**Figure 3.** Boundary conditions a) course direction, b) wale direction

In both tests (tensile test in course and wale direction) models were elongated by 15 mm. Tests were controlled by displacement of destined nodes.

Displacement and reaction force were monitored as results of simulations.

## Validation

For validation ADMET MTESTQuattro (TM) machine with 10lb head was used. For each direction (course, wale) 10 samples were prepared and tested. One sample had 90x15 mm dimensions for comfortable fixation to the clamps. The machine set up and sample can be seen in Figure 4. Clamps had coarse surface, so during testing there was no problem with slipping of the sample from the clamps. Testing length was 50 mm and testing speed was 40 mm/min.

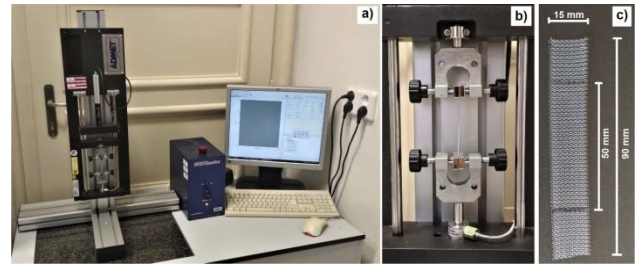


**Figure 4.** a) Testing machine setup, b) fixed sample in clamps, c) sample dimensions

## RESULTS AND DISCUSSION

**Table 1.** Results of tensile tests – validation experiment and simulations

	Tensile test in wale direction		Tensile test in course direction	
	Displacement [mm]	Force [N]	Displacement [mm]	Force [N]
Validation Experiment	15	0.57	15	0.37
			7.83	0.67
MSC Marc Metant	15	2.96	15	0.04
ANSYS LS-DYNA	15	1.09	15	0.38
			29.5	0.65

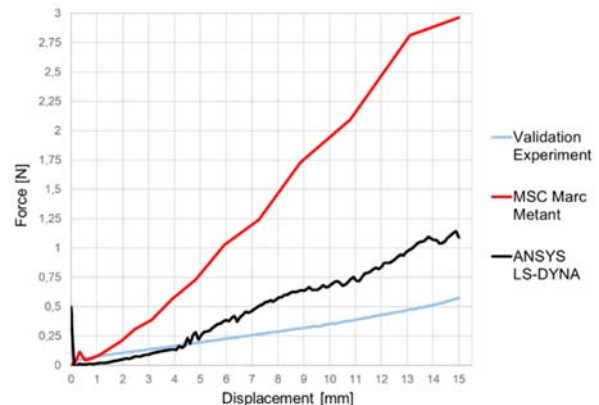


**Figure 5.** Comparison of tensile curves computed in MSC Marc, LS-DYNA and from validation experiment – testing in wale direction

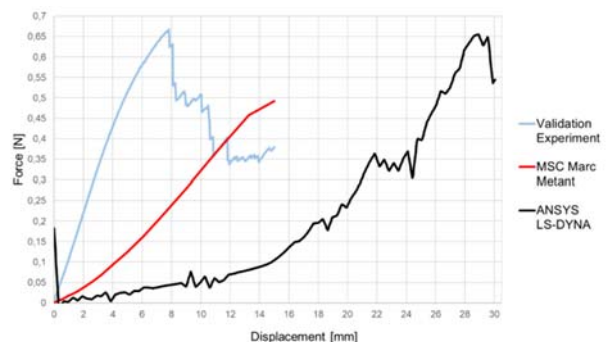


**Figure 7.** Comparison of tensile curves computed in MSC Marc, LS-DYNA and from validation experiment – testing in course direction

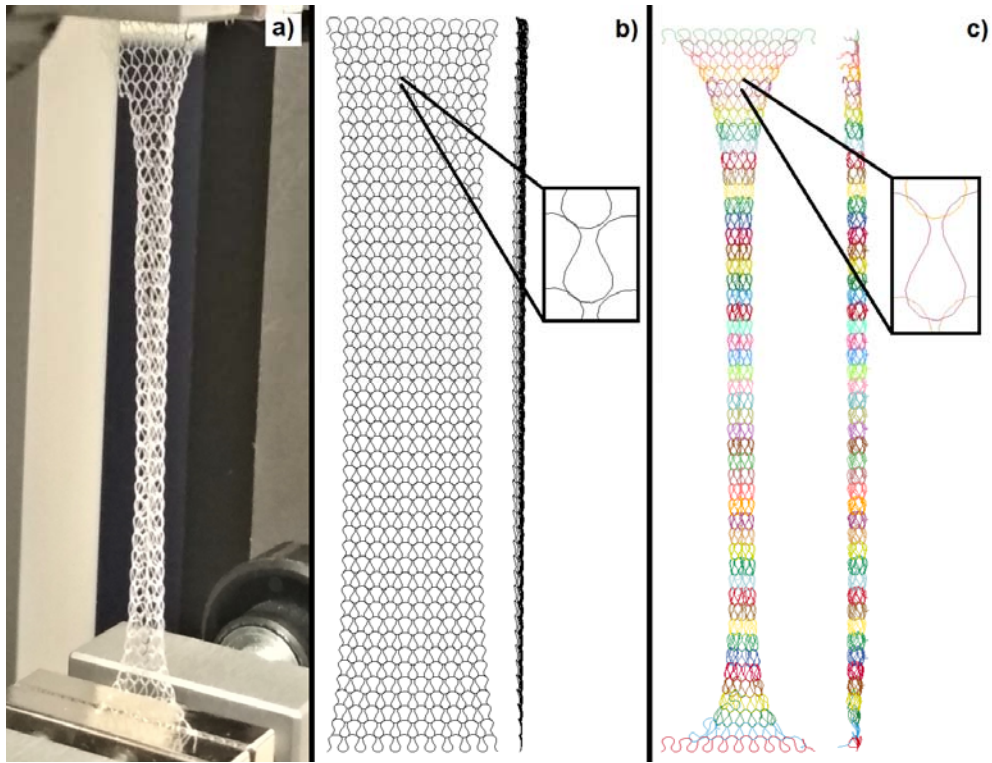


**Figure 6.** Visual comparison of deformed samples: a) validation experiment, b) MSC Marc simulation, c) LS-DYNA simulation – testing in wale direction

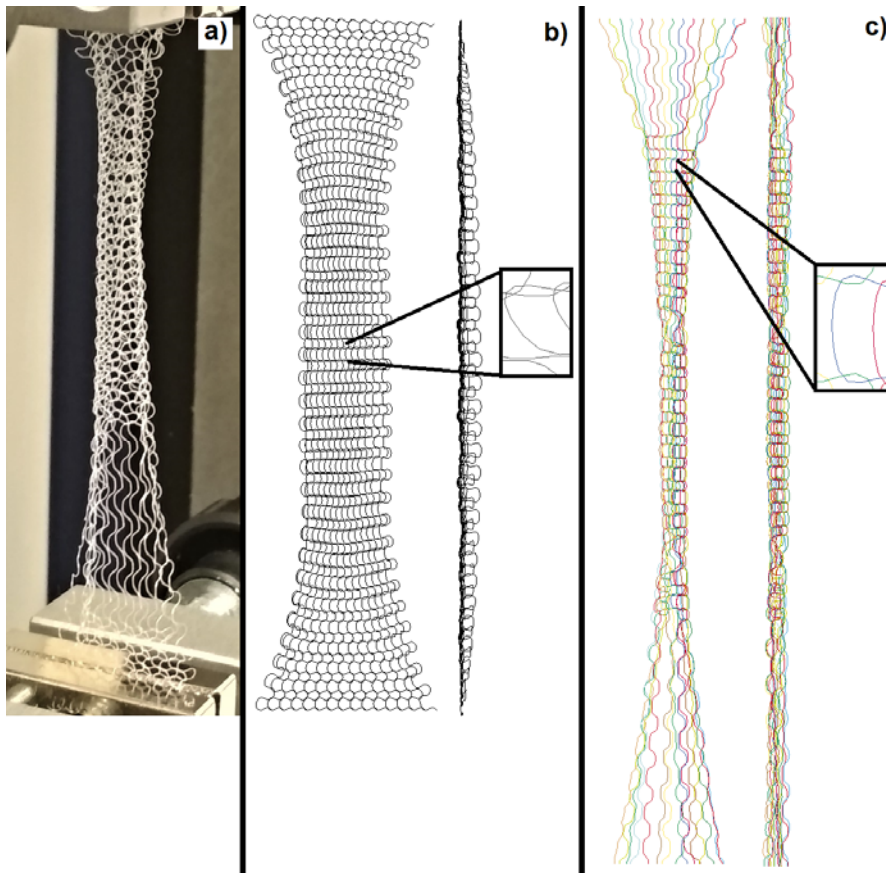


**Figure 8.** Visual comparison of deformed samples: a) validation experiment, b) MSC Marc simulation, c) LS-DYNA simulation – testing in course direction

Tensile test in wale direction: In Figure 6 c) it can be seen, that LS-DYNA visual representation of deformed sample corresponds with the real deformed sample very well. The elongated model sample is curled, narrow only in area of boundary conditions (same as nearby clamps) and some of the edge loops are pulled out. In LS-Dyna model no penetration of beams occurred. On the other hand, MSC Marc model after deformation is mainly narrow, minimally curled on the edges and the edge loops mostly remained in the initial shape. During the simulation there were even problems with penetration of the beams thorough all settings which supposed to prohibit that. From results we can see, that the MSC Marc model is not applicable and that the implicit solver with mentioned settings is not usable. In Figure 5 comparison of tensile curves in wale direction is shown. MSC Marc's result curve is extremely up dimensioned in comparison with the validation experiment. LS-DYNA's result curve is more accurate but the predicted value of the reaction force is still nearly twice bigger than the experimental value.

Tensile test in course direction: As it can be seen in Figure 8 a), the real sample at elongation of 15 mm is damaged by many pulled out loops. Neither model was able to simulate this at 15 mm elongation. Both models were visually compact and none of the loops were pulled out. Due to this, both simulations were repeated but with the elongation of 30 mm. The MSC Marc model was not able to simulate the slippage of the loops even with the higher deformation and plus beam penetrations occurred again. On the other hand, LS-DYNA model accurately predicted the slippage of loops during the higher deformation, even with the curled edges of the model which are appearing also in the real specimen. Again, the model did not have any penetrations of beams. In Figure 7 comparison of tensile curves in course direction is shown. Both simulated result curves are under dimensioned in comparison with the experimental curve, however the LS-DYNA's result curve with the 15 mm offset from the origin of the coordinate system, with some instabilities, is getting closer to the experimental curve and at its end it has nearly the same value of reaction force. LS-DYNA's value of reaction force is 0.65 N and the experimental value is 0.67 N.

Usually single jersey fabric is more elastic in course direction. Ratio of number of loops in a course is 1.5 times bigger than in a wale of the manufactured fabric. Due to that, experimental results from tensile tests show that the fabric is more rigid in course direction and more elastic in wale direction. After relaxation of the fabric, original width of the loop 1.81 mm shrank to 1.56 mm. Inner forces of the monofilament are certainly influenced by the shrinkage and FE model is not capable to predict

these forces just from the input geometry model, which affects the results. As it can be seen in Figure 2, due to the bending stiffness of the monofilament, knitted fabric loops are not in a narrow position as it is in the case of the generated geometry model. There is also a difference between loop length even though that the geometry model was generated according to real parameters of the fabric. Average measured loop length is 4.62 mm and the modelled loop length is 3.93 mm. These geometric differences have influence on the results. Also simplified material model and friction model affect the simulated results.

## CONCLUSIONS

Two finite element models of single jersey knitted fabric were prepared in computational software MSC Marc Metant with implicit solver and in computational software ANSYS LS-DYNA with explicit solver. Tensile test in a course and in a wale direction were simulated in both programs with as similar settings as possible. Validation of the models was done using ADMET MTESTQuattro machine which has great sensitivity so the experimental results have good accuracy. It appears that MSC Marc was not able to provide good results even with complex settings and penetrations of beams occurred during the simulations. ANSYS LS-DYNA performed great visual simulations of deformations of modelled samples which corresponded very well with real deformation of the specimen during the validation experiment. Simulated tensile curves were less corresponding with the experiments however that is influenced by the simplified geometry of the knitted fabric and simplified material model. In this case it can be said that the explicit solver is more suitable for modelling of textile mechanical deformations. For future simulations, more accurate input geometry, more complex material model as for example linear piecewise material should be used and analyzed. Also, inner forces of the yarn after the relaxation of the knitted fabric should be considered and incorporated in FE simulations. Finite element modelling of mechanical behavior of textile structures is possible but experimental validation is necessary. FE simulations can be highly inaccurate without validation and models like that can be very misleading for the research.

**Acknowledgements:** *This contribution was written at the Technical University of Liberec, Textile Faculty with the support of Student Grant Competition (project SGS-2022-6062 "Textile replacements designated for the chest wall reinforcement after bone defects"), which financially supported finite element course in computing program ANSYS LS-DYNA.*

## REFERENCES

1. Döbrich, O., Gereke, T., Cherif, Ch. (2015). Textile and Composite Modelling on a nearMicro-scale: Possibilities and Benefits. 10th European LS-DYNA Conference 2015, Würzburg, Germany [online 17.10.2022] <https://www.dynalook.com/conferences/10th-european-ls-dyna-conference/4%20Materials%20I%20-%20Endless%20Fibers/01-Doebrich-TechnicalUnivDresden-P.pdf>
2. Komeili, M., & Milani, A. S. (2011). Finite Element Modeling of Woven Fabric Composites at Meso-Level under Combined Loading Modes. In (Ed.), *Advances in Modern Woven Fabrics Technology*. IntechOpen. <https://doi.org/10.5772/17333>
3. Sodhani, D., Reese, S., Jockenhövel, S., Mela, P., Stapleton, S. E. (2018) Multi-scale modelling and simulation of a highly deformable embedded biomedical textile mesh composite, *Composites Part B: Engineering*, 143. 113-131. <https://doi.org/10.1016/j.compositesb.2018.01.010>.
4. Lin, H., Clifford, M., Long, A., Lee, K., Guo, N. (2012). A finite element approach to the modelling of fabric mechanics and its application to virtual fabric design and testing. *Journal of The Textile Institute*, 103. 1-14. <https://doi.org/10.1080/00405000.2012.660755>.
5. Liu, D., Christe, D., Shakibajahromi, B., Knittel, Ch., Castaneda, N., Breen, D., Dion, G., Kotsos, A. (2017) On the role of material architecture in the mechanical behavior of knitted textiles, *International Journal of Solids and Structures*, 109.101-111. <https://doi.org/10.1016/j.ijsolstr.2017.01.011>.
6. Wadekar, P., Perumal, V., Dion, G., Kotsos, A., Breen, D. (2020). An optimized yarn-level geometric model for Finite Element Analysis of weft-knitted fabrics. *Computer Aided Geometric Design*, vol. 80, <https://doi.org/10.1016/j.cagd.2020.101883>.

# COMFORTABLE AND PROTECTIVE HYBRID WEFT-KNIT PLATED FABRIC FROM GLASS AND WOOL/ACRYLIC YARNS

İNCE MEHMET ERDEM<sup>1\*</sup>, İNANIR SEVGI AND ERDOĞAN ESRA KUMSAL

<sup>1</sup> Gaziantep University, Textile Engineering Department, 27310, Şehitkamil, Gaziantep, Turkey

## ABSTRACT

In this study, hybrid weft-knit plated fabrics were produced by co-feeding glass and wool/acrylic blend yarns. While the wool/acrylic yarn in contact with skin is expected to provide comfort, the glass yarn next to the environment is to provide protection. The physical, structural, air permeability, bursting strength, and the protection against flame properties of glass plus wool/acrylic plated fabric were compared with the reference fabrics consisting completely of glass or wool/acrylic blend yarn. Two factors: the yarn composition and the cam setting of the knitting machine were considered. Two-ply of glass yarn was fed to the each face of the reference glass fabric, and a single-ply of wool/acrylic yarn was fed to the each face of the reference wool/acrylic fabric. On the other hand, while the hybrid plated fabric's back face accommodated two-ply of glass yarn, its front face involved a single-ply of wool/acrylic yarn. Two different cam settings, loose and tight, were selected. The physical and the structural properties of the fabrics were measured. Then, air permeability, bursting strength, and the protection against flame tests were performed. Test results were subjected to detailed statistical data analysis and how they were affected by the yarn composition and the cam setting was presented with visual and self-explanatory graphs.

## KEYWORDS

Glass yarn; Weft knit fabric; Plated fabric; Protective fabric; Air permeability.

\* Corresponding author: İnce M.E., e-mail: [meince@ncsu.edu](mailto:meince@ncsu.edu), [eince@gantep.edu.tr](mailto:eince@gantep.edu.tr)

## INTRODUCTION

While textile fabrics only provided covering when they first appeared, now this expectation evolved into functionality. By functionality, it is understood that the fabric not only covers and comforts the individual, plus protects him against dangers from the outside. This expectation has increased the need for the hybrid fabrics where the natural yarns that provide comfort and the synthetic yarns that offer protection are used together. The wool fiber stands out with its comfort and insulation feature. On the other hand – as a result of its affordable price, moderate mechanical properties, high protection against flame and chemicals – glass fiber is widely used in technical textile applications. However, due to its hard and brittle structure, the glass fiber experiences high level of breakage in the fabric formation processes [4, 7, 8, 11]. The contact of broken fiber ends with the skin causes itching and discomfort. In addition, the moisture absorption performance of glass fiber is very low, which significantly lowers its comfort feeling. On the other hand, its compatibility with human skin, moisture absorption capacity, and thermal insulation capability renders the wool fiber very valuable in comfortable clothing.

Woven fabrics require laborious weaving preparation processes such as weft yarn preparation, warping, sizing, tying and drawing-in. However, these pre-processes are not required for weft knitted fabrics. Therefore, the production cost of weft knitted fabric is considerably lower than that of woven fabric. Woven and weft knitted fabrics are also quite different from each other in terms of fabric structure and performance. The weft knitted fabric, which consists of meshed loops, easily stretches when exposed to any in-plane or out-of-plane load and easily takes the desired three-dimensional shape. This makes it possible to produce comfortable clothing from weft knitted fabric that drapes the body without any folding, and wrinkling [3, 6, 12-15].

The fabric pattern is one of the critical features that determine the performance of the fabric. The pattern of the weft-knit fabric is determined by the number and the position of different types of stitches inside the knit repeat, and the cam setting. Besides, the cam setting controls the fabric tightness through determining the size of the loops. Therefore, it is possible to produce weft knitted fabrics in numerous architectures by playing with the fabric pattern and the cam settings [1-2, 5, 9-10].

In this study, it was planned to produce protective and comfortable weft knitted fabric with different tightness using glass and wool/acrylic yarns. Due to the disturbing effect of the glass fiber in contact with the skin, the plated weft-knit fabric structure was selected. In the plated fabric structure, the wool/acrylic yarn was used on the surface of the fabric in contact with the body, while glass yarn was used on the other side (outer) of the fabric. It was anticipated that glass yarn provides protection against dangers from outside, while wool/acrylic yarn in contact with the skin is thought to provide comfort by establishing the desired micro-climate between the body and the fabric.

## EXPERIMENTAL

### Materials

In this study, E-glass multifilament yarn with a single-ply yarn count of 136 tex, and individual fiber diameter of 9 microns was used. Nm 7 count, high bulk, 50/50% wool/acrylic blend yarn was used as the yarn that would provide wearability and comfort to the fabric. Plated weft-knit fabrics were produced by Brother KH-864, hand-operated, 5E gauge knitting machine. The plating yarn feeder used in the production of all fabrics and the different yarn compositions fed to the feeder are given in Figure 1.

We focused on two factors. The first one is the yarn composition, and the other is the cam setting of the knitting machine. While the yarn composition had

three sublevels (completely glass yarn, completely wool/acrylic blend yarn, and the combination of glass and wool/acrylic blend yarn), the cam setting had only two sublevels (loose and tight cam settings). In the production of completely glass yarn fabric, 2-ply of glass yarn was fed into both the front and rear eyes of the plating yarn feeder (Figure 1). In glass plus wool/acrylic yarn (hybrid) fabric; while a single-ply of wool/acrylic yarn was fed to the rear eye of the feeder, 2-ply of glass yarn was fed to the front eye. Finally, in the fabric consisting completely of wool/acrylic yarn, a single-ply of wool/acrylic yarn was fed to both the front and rear eyes of the feeder. The yarn composition was coded as given below:

WA: single-ply wool/acrylic yarn, G: single-ply glass yarn;

GG/GG: 4-ply of glass yarn fabric (2-ply of glass yarn on both the front and back faces of the fabric).

WA/GG: The front face is a single-ply of wool/acrylic yarn, while the back face is 2-ply of glass yarn fabric.

WA/WA: 2-ply of wool/acrylic yarn fabric (a single-ply of wool/acrylic yarn on both the front and back faces of the fabric).

Two fabric tightness levels, 4 (tight fabric) and 8 (loose fabric) were selected as the cam setting. Thus, a total of 6 (3x2) different weft-knit plated fabrics were produced. The images of the fabrics are given in Figure 2.

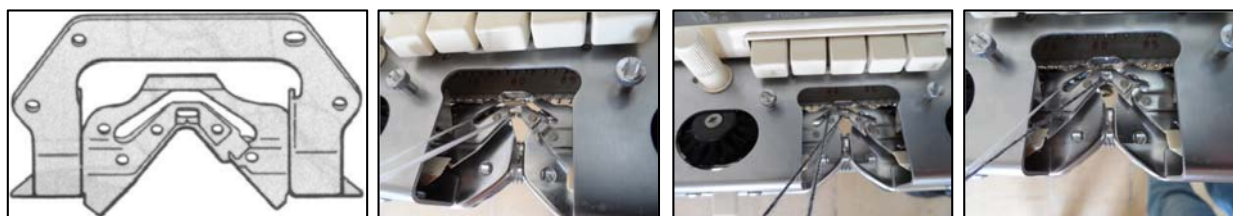


Figure 1. The plating yarn feeder and different yarn compositions fed to the feeder.

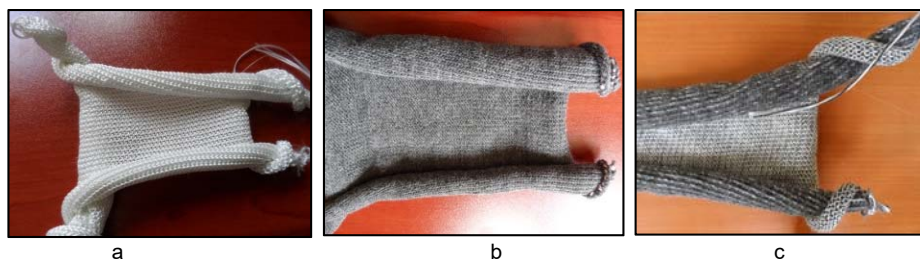


Figure 2. The completely glass yarn GG/GG fabric (a), the completely wool/acrylic yarn WA/WA (b), the hybrid WA/GG fabric (c).

### Methods

A digital thickness gauge device with a presser foot diameter of 21.15 mm and a compression pressure

of 2 kPa was used to measure the fabric thickness. BS 5441 standard was followed for length measurement. ASTM D737 was followed and the SDL ATLAS M021A test device was used in the air

permeability tests. The circular fabric test area was taken as 20 cm<sup>2</sup> and the pressure drop was chosen as 200 Pa. Bursting strength test was performed on the knitted fabrics according to BS EN ISO 13938-1. A dome with an internal diameter of 30.5 mm and a corresponding internal area of 7.3 cm<sup>2</sup> was selected. The "Surface Ignition" test procedure was performed on the knitted fabrics via following the BS EN ISO 15025 standard. A specified flame with an application time of 10-second was performed on the back (purl loop) face of the all fabrics, thus the glass yarn surface of the wool/acrylic plus glass yarn (hybrid WA/GG) fabric sample was exposed to the flame.

Yarn composition changed the fabric thickness at a statistically significant level (Figure 3 and Table 1). While the bulky structure of the wool/acrylic yarn increased the fabric thickness, the thin and regular structure of the glass yarn decreased the fabric thickness. The addition of wool/acrylic yarn to the fabric structure also increased the fabric thickness variation (standard deviation).

The addition of glass yarn to the weft knitted fabric decreased the loop length (Figure 4 and Table 2). This is attributed to the thin and low-volume nature of the glass yarn. In other words; the addition of wool/acrylic blend yarn, which has a voluminous structure, to the fabric increased the loop length.

## RESULTS AND DISCUSSION

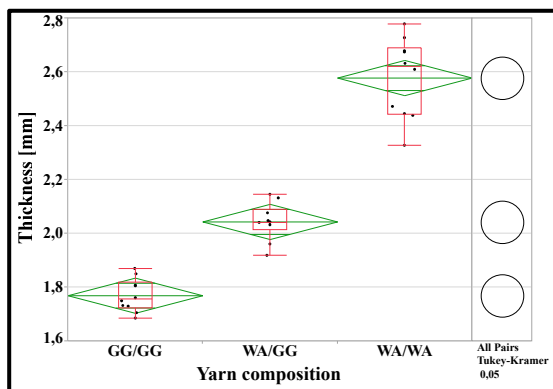


Figure 3. The effect of yarn composition on thickness.

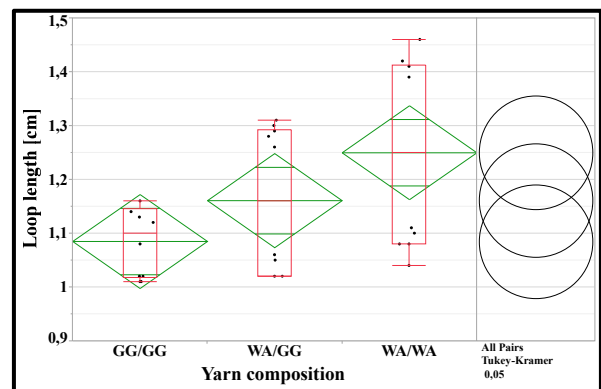


Figure 4. The effect of yarn composition on loop length.

**Note:** The horizontal green line dividing the green diamond corresponds to the mean, while the distance between the lower and upper corners of the green diamond shows the confidence interval based on the 95% confidence level. One comparison circle for the mean calculated at each sublevel level is given in the right-hand column. The circles representing means that differ significantly from each other ( $\alpha = 0.05$ ) either do not intersect or intersect slightly.

Table 1. The effect of yarn composition on thickness.

Property	Yarn composition				n	mean	sd	LL	UL	p-value
Thickness [mm]	WA/WA	A			10	2.58	0.15	2.51	2.64	<0.0001
	WA/GG		B		10	2.04	0.07	1.98	2.11	
	GG/GG			C	10	1.77	0.06	1.70	1.83	

**Note:** Levels that are not combined with the same alphabetic capital letter differ significantly from each other ( $\alpha = 0.05$ ). n: number of measurements, sd: standard deviation, LL: lower limit, UL: upper limit. The limits were established according to the 95% confidence level. A p-value less than 0.05 is an indication that the difference between at least two levels is statistically significant and is colored red.

Table 2. The effect of yarn composition on loop length.

Property	Yarn composition				n	mean	sd	LL	UL	p-value
Loop length [mm]	WA/WA	A			10	1.25	0.18	1.16	1.34	0.0362
	WA/GG		A	B	10	1.16	0.14	1.07	1.25	
	GG/GG			B	10	1.08	0.06	1.00	1.17	

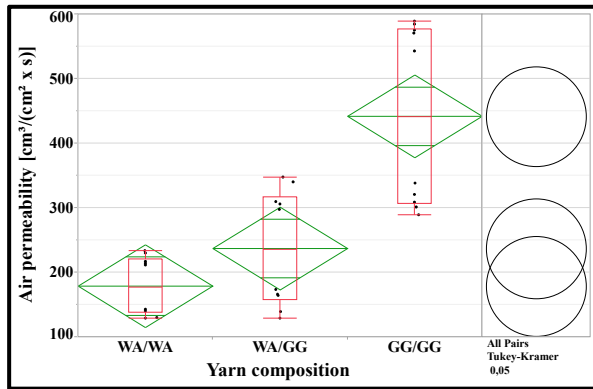


Figure 5. The effect of yarn composition on air permeability.

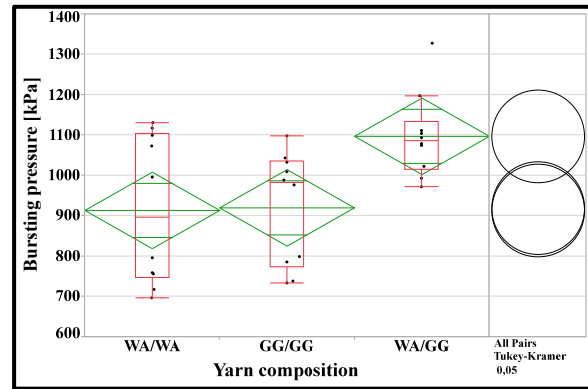


Figure 6. The effect of yarn composition on the bursting pressure.

Table 3. The effect of yarn composition on air permeability.

Property	Yarn composition			n	mean	sd	LL	UL	p-value
Air permeability [cm <sup>3</sup> /(cm <sup>2</sup> xs)]	GG/GG	A		10	441,70	138,64	377,61	505,79	<0,0001
	WA/GG		B	10	237,00	89,44	172,91	301,09	
	WA/WA		B	10	178,70	45,28	114,61	242,79	

Table 4. The effect of yarn composition on bursting pressure.

Property	Yarn composition			n	mean	sd	LL	UL	p-value
Bursting pressure [kPa]	WA/GG	A		10	1097.28	103.40	1002.50	1192.00	0.0133
	GG/GG		B	10	919.97	139.85	825.20	1014.70	
	WA/WA		B	10	913.74	183.58	819.00	1008.50	

The addition of wool/acrylic yarn, which is more voluminous and thicker than glass yarn, to the fabric structure closed the pores of the fabric and reduced air permeability (Figure 5 and Table 3). However, no statistically significant difference was observed between the air permeability of the purely wool/acrylic yarn (YA/YA) fabric and the wool/acrylic yarn plus glass yarn (YA/CC) fabric. Moreover, the addition of glass yarn to the fabric structure increased the air permeability variation of the fabric.

Figure 6 and Table 4 show the effect of yarn composition on fabric bursting strength (pressure). Hybrid plated (WA/GG) fabric with 2-ply of glass yarn on the back face and a single-ply of wool/acrylic yarn on the front face showed the highest bursting pressure. The hybrid plated fabric also exhibited the lowest bursting pressure variation, demonstrating a stable bursting performance. On the other hand, completely glass yarn (GG/GG) fabric and completely wool/acrylic yarn (WA/WA) fabric exhibited the lowest bursting pressure. The interaction of the glass yarn with the knitting elements while the yarn was being forced to take the loop form had resulted in fiber breakage, which showed itself as a decrease in bursting strength of the fabric. It is promising that the hybrid plated (WA/GG) fabric, consisting of a single-ply of wool/acrylic plus two-ply of glass yarn, exhibited the highest (statistically significant level higher than the

other fabrics) and the most stable (lowest variation) bursting pressure.

The yarn composition affected the afterflame time at a statistically significant level (Figure 7 and Table 5). Completely wool/acrylic yarn (WA/WA) fabrics exhibited an average afterflame time of 123 seconds, while completely glass yarn (GG/GG) fabrics exhibited an average of zero afterflame time, that is, GG/GG fabrics did not ignite. While WA/WA fabrics burned completely, GG/GG fabrics preserved their integrity. The promising result here is that the hybrid (WA/GG) fabric and the completely glass yarn (GG/GG) fabric exhibited statistically the same average afterflame time. This is because that tightly knitted hybrid (WA/GG) fabric at the 4 cam setting did exhibit lack of flaming after the flame removal (i.e. afterflame time of zero second). Therefore, the tightly knitted (at 4 cam setting level) hybrid plated (WA/GG) fabric behaved similar with the completely glass yarn (GG/GG) fabric and did not exhibit flaming (i.e. not ignited) after the flame was removed at the end of 10 seconds.

Figure 8 shows the burned images of completely glass yarn GG/GG fabrics knitted at 4 cam settings. Glass fibers that turned into black at the flame application point but kept their integrity exhibited a decreasing yellowing with distance from the flame point.

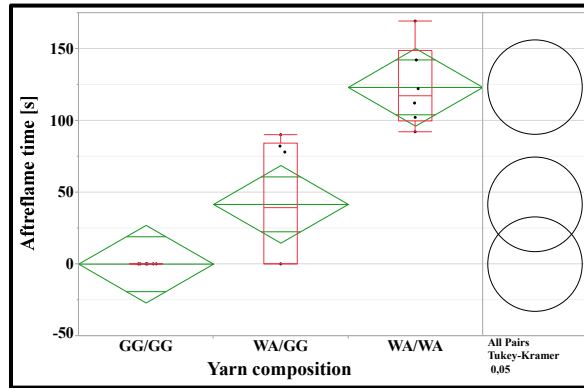


Figure 7. The effect of yarn composition on afterflame time.

Table 5. The effect of yarn composition on afterflame time.

Property	Yarn composition			n	mean	sd	LL	UL	p-value
Afterflame time [s]	WA/WA	A		10	123.17	28.29	96.12	150.21	<0.0001
	WA/GG		B	10	41.67	45.81	14.62	68.71	
	GG/GG		B	10	0.00	0.00	-27.05	27.05	



Figure 8. Pictures taken after the burning test of completely glass yarn GG/GG fabric knitted at 4 cam settings.



Figure 9. The photos of the burned WA/GG hybrid fabric knitted at 4 cam setting.

Figure 9 shows the photos of the burned WA/GG fabric knitted at 4 cam setting. Flame propagation in WA/GG hybrid fabric remained within a limited area. The tight fabric structure and the presence of 2-ply of glass yarn on the surface where the flame is applied stopped the flame propagation. While the wool/acrylic yarn became charred at the flame application point, this charring decreased as moved away from the application point.

## CONCLUSIONS

In this study, weft-knit plated hybrid fabrics with different tightness were produced from glass and wool/acrylic yarns. In the hybrid plated fabric, while front face of the fabric formed from single-ply of wool/acrylic yarn, the back face formed from 2-ply of glass yarn. The physical, structural, air permeability, bursting strength, and protection against flame properties of the hybrid fabric were compared with the reference fabrics those consisted of only 4-ply of glass or only 2-ply of wool/acrylic yarn. The hybrid fabric exhibited comparable air permeability performance with the fabric from completely wool/acrylic yarn, while it demonstrated statistically significantly better bursting pressure than the reference fabrics from completely glass or wool/acrylic yarns. The hybrid fabric with tight cam setting also showed the similar flame resistance with the fabric from completely glass yarns.

**Acknowledgements:** We would like to thank Scientific Research Projects Management Unit (BAPYB) of Gaziantep University for their financial support to this study under the project number of MF.ÖKAP.21.11. This study was supported in the category of research project with undergraduate student participation. The second and third authors are the current undergraduate students of Textile Engineering Department of Gaziantep University.

## REFERENCES

1. Abounaim, Md., Hoffmann, G., Diestel, O., Cherif, C. (2010), Thermoplastic composite from innovative flat knitted 3D multi-layer spacer fabric using hybrid yarn and the study of 2D mechanical properties. *Composites Science and Technology*, 70(2), 363-370. <http://dx.doi.org/10.1016/j.compscitech.2009.11.008>
2. Alpyildiz, T., İçten, B. M., Karakuzu, R., Kurbak, A. (2009). The effect of tuck stitches on the mechanical performance of knitted fabric reinforced composites. *Composite Structure*, 89(3), 391-398. <http://doi.org/10.1016/j.compstruct.2008.09.004>
3. Ciobanu, L. (2011). Development of 3D Knitted Fabrics for Advanced Composite Materials. In *Advances in Composite Materials – Ecodesign and Analysis*. Brahim Attaf (Editor), InTech. 161-192. <https://doi.org/10.5772/14876>
4. Hu, H., Zhu, M. (2005). A study of the degree of breakage of glass filament yarns during the weft knitting process. *AUTEX Research Journal*, 5(3), 141-148.
5. Kane, C. D., Patil, U. J., Sudhakar, P. (2007). Studies on the influence of knit structure and stitch length on ring and compact yarn single jersey fabric properties. *Textile Research Journal*, 77(8), 572-582. <https://doi.org/10.1177/0040517507078023>
6. Ko, F. K. (2000). 3-D textile reinforcements in composite materials. In *3-D textile reinforcements in composite materials*. Antonio Miravete (Editor), Boca Raton: CRC Press, 9-42.
7. Lau, K. W., Dias, T. (1994). Knittability of high-modulus yarns. *The Journal of the Textile Institute*, 85(2), 173-190. <https://doi.org/10.1080/00405009408659018>
8. Liu, X-M., Chen, N-L., Feng, X-W. (2009). Investigation on the knittability of glass yarn. *The Journal of The Textile Institute*, 100(5), 440-550. <https://doi.org/10.1080/00405000701877657>
9. Marmaralı, A. B. (2004). Atkı Örmeciliğine Giriş. E.Ü. Tekstil ve Konfeksiyon Araştırma – Uygulama Merkezi (İzmir).
10. Marmaralı, A., Kretzschmar, S. D. (2004). Örne Terimleri ve Tanımlamaları. E.Ü. Tekstil ve Konfeksiyon Araştırma – Uygulama Merkezi (İzmir).
11. Savci, S., Curiskis, J. I., Pailthorpe, M. T. (2001). Knittability of glass fiber weft-knitted preforms for composites. *Textile Research Journal*, 71(1), 15-21. <https://doi.org/10.1177/004051750107100103>
12. Savci, S., Curiskis, J. I., Pailthorpe, M. T. (2000). A study of the deformation of weft-knit preforms for advanced composite structures Part 1: Dry preforms properties. *Composites Science and Technology*, 60(10), 1931-1942. [https://doi.org/10.1016/S0266-3538\(00\)00077-4](https://doi.org/10.1016/S0266-3538(00)00077-4)
13. Savci, S., Curiskis, J. I., Pailthorpe, M. T. (2000). A study of the deformation of weft-knit preforms for advanced composite structures Part 2: The resultant composite. *Composites Science and Technology*, 60(10), 1943-1951. [https://doi.org/10.1016/S0266-3538\(00\)00078-6](https://doi.org/10.1016/S0266-3538(00)00078-6)
14. Savci, S., Curiskis, J. I., Pailthorpe, M. T. (1999). Formability of weft knitted preforms. International Committee on Composite Material (ICCM) 12 Conference, paper 841.
15. Zhong, T., Hu, Hong. (2007). Formability of weft-knitted fabrics on hemisphere. *AUTEX Research Journal*, 8(4). 245-251.

# PATTERN RELATED ISSUES IN THE MODELLING OF DEFORMED OVER SURFACE WARP KNITTED STRUCTURES WITH LONGER UNDERLAPS

LIU HAI SANG<sup>1,2\*</sup>, KYOSEV YORDAN<sup>2</sup> AND JIANG GAOMING<sup>1</sup>

<sup>1</sup> Jiangnan University, College of Textile Science and Engineering, Wuxi, Jiangsu, Lihu Ave. 1800, Binhu, 214122 China

<sup>2</sup> TU Dresden, Institute of Textile Machinery and High Performance Material Technology, Chair of Development and Assembly of Textile Products, Dresden, Sachsen, Hohe Str. 6, 01069, Germany

## ABSTRACT

The yarn level modelling of warp knitted structures is a complex process. For structures placed on the plane, it is well investigated and there are a few software solutions and papers reported. This paper considers the simulation of warp knitted structure, deformed in the 3D space. Especially the modelling of the areas of high curvature are detailed observed. Underlaps with longer lengths makes an unreal visualization for simulation results. Different pattern with different length of the underlaps are modelled with original algorithm developed by the authors. Modelling and visualization problems in the areas with long underlaps are discussed and possible solutions are proposed.

## KEYWORDS

3D simulation; Modelling; Curved surface; High curvature; Visualization; Fabric structure.

---

\* Corresponding author: Liu H., e-mail: [sophie@stu.jiangnan.edu.cn](mailto:sophie@stu.jiangnan.edu.cn)

## INTRODUCTION

In the era of continuous development of digital textiles, more and more scholars have focused on the simulation of fabrics. In the course of fabric simulation, 3-dimensional(3D) simulation has made a great progress in the recent years, which has become increasingly important in numerous application areas in production. 3D simulation is commonly used in fabric design, apparel design, etc., which is convenient for designers and consumers to obtain visualization results, helping us better understand the shape and structure of fabrics.

There are many softwares on the market for clothing design with fabric display, such as *Clo3D*, *Marvelous Designer*, *Revobit*, etc. All of them use texture mapping methods to add textures to clothing. Similarly, many scholars used texture mapping, transferring the flat patterns to complex models [1-3]. But the detailed textile structure was not well represented.

Yarn-level 3D simulation solved this problem well. Researchers conducted studies on flat fabrics. Peng et al. [4] simulated the weft knitted pattern and proposed the loop deformation. The structures of various types of flat warp-knitted fabrics were well demonstrated by 3D simulation [5]. Based on this, Liu et al. [6] added the jacquard parameters to

simulate more complex warp knitting patterns. The above simulation research on flat fabrics had laid a good foundation for warp knitting simulation.

For knitted products with complex shapes, Yuksel et al. [7] meshed the existing models. Different shapes of meshes corresponded to different knitting structures. Wu et al. [8] labeled those meshes with knitting direction, filling the meshes with similar matching loops. Also loop force deformation were well analyzed to reach a more detailed result [9,10]. These 3D simulation above focused on weft knitted fabrics, which was a good reference for our research of warp knitted fabric simulation.

The authors also paid attention to the warp knitted fabric simulation. Renkens et al. [11] modelled the double needle-bed warp knitted fabrics using a mathematical method. Liu et al. [12] spread out a double-layer fabric and then rolled it into a tube with geometry calculation. They mainly discussed the fabric tube shape rather than the stitch details. Many flat models with stitch shape details were mentioned in the Kyosev's book [5,14]. Also, warp knitting stitch size was measured and the stitch model was established [14]. But only stitch main body was sized and underlaps were out of consideration.

During the simulation development and the practical experience with model simulation by ourselves, we

find that some pattern related issues need to be improved when we establish the fabric models according to different knitting parameters for patterns.

## EXPERIMENTAL

### Modelling basis

In this paper, we develop our research based on our previous works<sup>[12,15]</sup>. The tubular fabric was spread out into a plane. And a spatial relationship of the stitch grids between the tube mesh and the plane mesh was derived to mapping the stitch coordinate on the tube. Then geometry tubes in Three.js, a lightweight cross-browser JavaScript library, were used to realize the fabric simulation.

### Pattern related issues

Although the simulation results are good, we find some patterns related issues need to be improved. Figure 1 shows an example from our previous work<sup>[15]</sup>. As we all know, the stitches in the warp knitted fabrics are connected with underlaps. But different patterns are made of different chain

notation. Some underlaps is short, like the structure 1-0/1-2//. Some underlaps are longer like 1-0/2-3// and 1-0/4-5//, whose underlaps span several wales. There are high curvature areas at when fabrics are rolled into a tube in Figure 1(a). Stitches are simulated well with the 8-points model. But the underlap is lying in an unusual place, especially for longer underlaps.

For a better visualization, we extract the underlap paths from a side view in Figure 1(b). In the structure 1-0/1-2//, the underlap is short so that they fit tightly to the deformed surface. But as the underlaps get longer in 1-0/2-3// and 1-0/4-5//, the space become larger between underlaps and deformed surface. It is because the connecting yarns between two stitches are simulated by a straight line with two points. Actually, stitches on a real-world fabric fit well to the surface within the common underlap lengths. For a more realistic simulation results, some improvements need to be made.

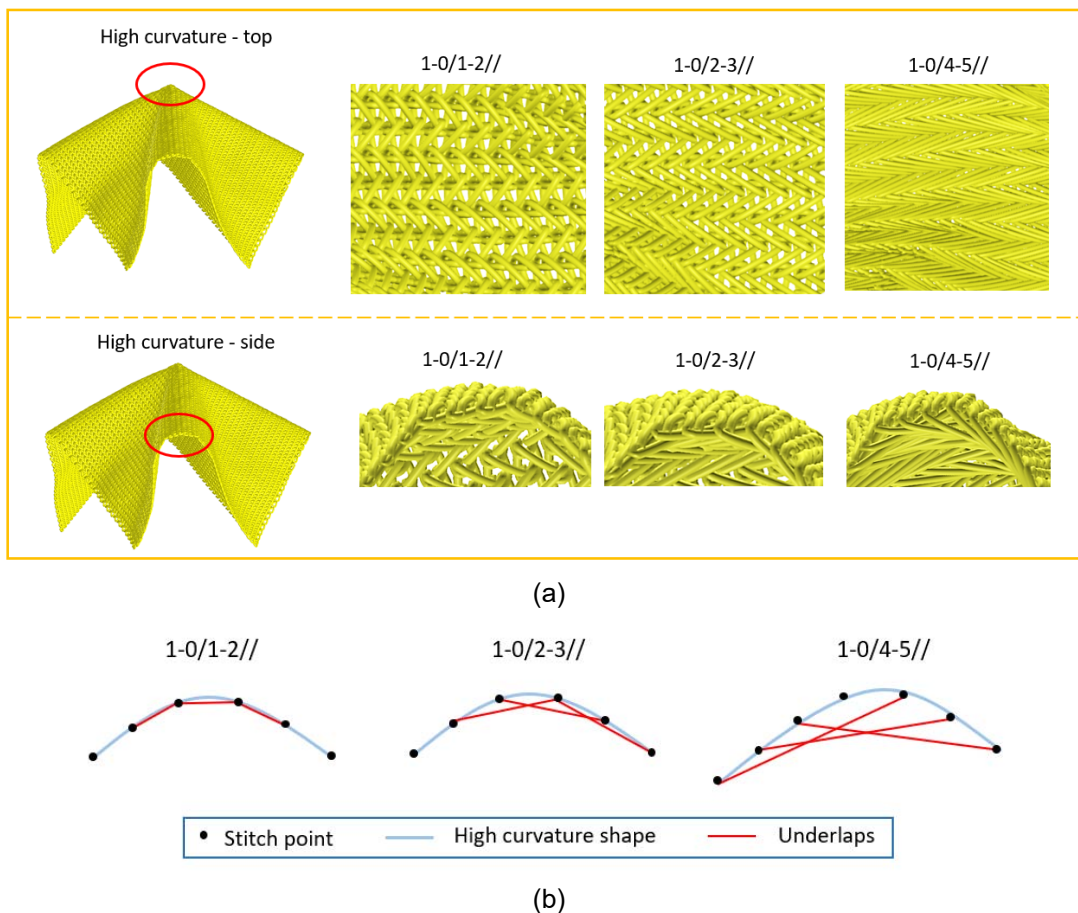


**Figure 1.** Pattern related issues with high curvature and long underlaps in 3D simulation: (a)simulation results with different underlap length [15]; (b) Statement of underlaps with different lengths on the high curvature shape.

## Methods

The stitch grids not always in the same plane as mentioned in Section 2.2. The long underlaps are overhang from the deformed surface. But the number of points on the underlap is changed to avoid unnecessary calculations.

Figure 2 is a schematic from the top view, where the fabric is bent into a curved surface. Figure 2(a) shows two stitches on a plane fabric, the straight underlap is exactly on the fabric surface. Figure 2(b) shows stitches on the same curvature surface. The vertical vectors of stitch grid that toward the outside of the model surface is represented as green lines. When the vector angle of two connected stitches is larger, the underlap is farther away from the fabric surface. In Figure 2(c), the deformed surfaces have different curvature with two stitch vertical vector remains the same. The higher the curvature is, the more inaccurate the simulated underlap is.

In order to solve this problem, some control points are added to the underlap model, modifying the stitch model as shown in Figure 3. The points connecting the underlaps is very near to the stitch bottom center that can almost be ignored, so the underlap is regarded as an edge of the underlap triangle when calculating the added points. The underlap is divided into several segments. Because the triangles including the underlap segments are similar triangles, added points can be calculated by Eq.1 according to the wale distance ratio. Thus, the underlap can be pulled from the original shape, fitting the deformed surface well. In this example, the distance ratio  $e = \frac{w}{4w} = 0.25$ .

$$\begin{cases} P = e \times (P_2 - P_1) + P_1 \\ e = (P - P_1)/(P_2 - P_1) \end{cases} \quad (1)$$

Where,  $P$  is the added point,  $P_1$  and  $P_2$  are stitch points connecting underlap,  $e$  is the distance ratio.

In the other case, the stitches are on the bent fabric, not on the regular tube. There is an example for fabrics knitted by 1-0/4-5// in Figure 4. Different from the round fabric, the added points depend on the normal vectors of stitches. All the normal vectors are towards the same side of the fabric.

Seeing the Figure 4 - Vector relationship, bent I is the occasion where the normal vector angle  $\alpha$  is less than  $180^\circ$ .  $V_1$ ,  $V_2$  and  $V_3$  are the normal vectors of stitches. When the vector angle  $\alpha_1$  is larger than the value  $\beta$ , added points are put on the underlap lapping pass these two stitches.  $\beta$  is a specified angle value. The details of a tested yarn are shown in underlap triangle. And  $V_2$  becomes the first vector to compose the vector angle with the normal vector of the next stitch. For  $V_2$  and  $V_3$ , the angle  $\alpha_2$  is less than the value  $\beta$ , so there is no added point at this position. Then it continues combining with the next stitch vector. When calculating the added points on the plane fabric, the underlap is also regarded as an edge of a triangle according to Eq.1. In bent II, when the angle  $\alpha_2$  of two normal vectors  $V_4$  and  $V_5$  is larger than  $180^\circ$ , the underlap is at the other side of the fabric. The added points are directly added on the underlap. Then  $V_5$  Then it continues combining with the next stitch vector.

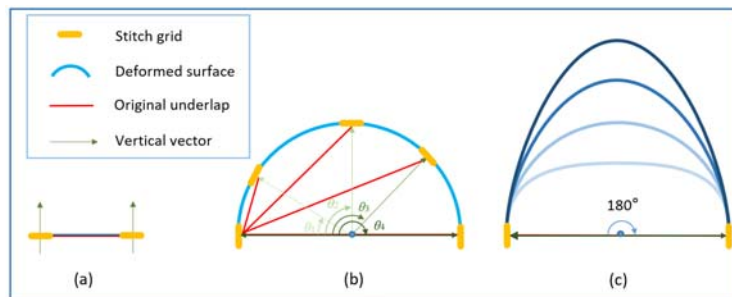


**Figure 2.** Stitch statement and the underlap positions. (a)Plane fabric; (b)Stitches on the same curvature surface; (c)The same stitches with different curvature surfaces.

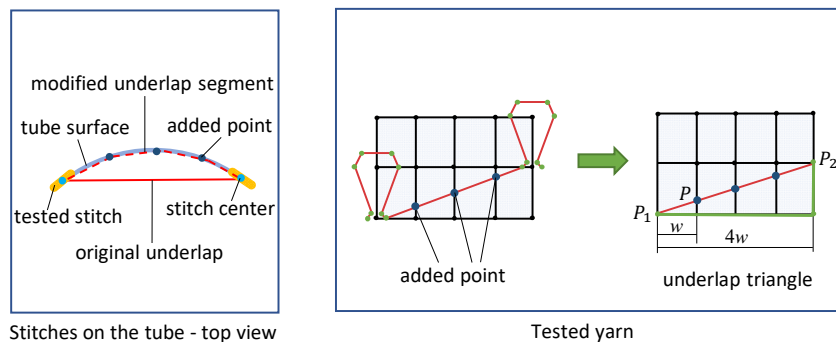


**Figure 3.** The modified stitch models with added control points on the underlap.

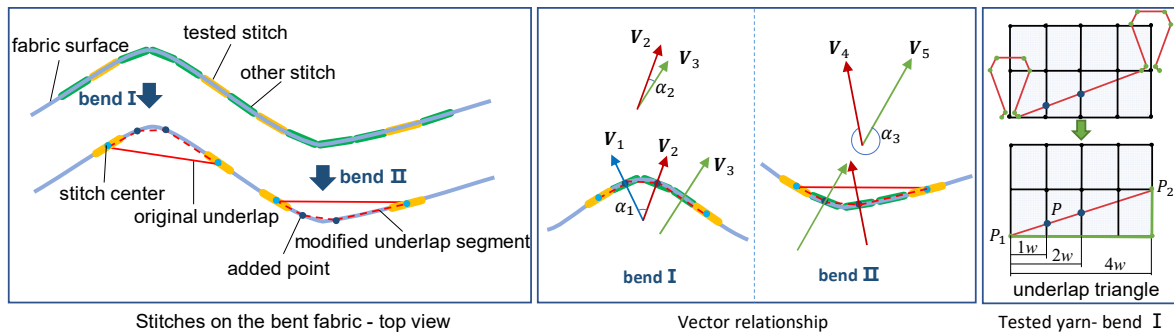


Figure 4. The modified stitch models on the bent fabric.

## RESULTS AND DISCUSSION

### Tubes

Figure 5 shows some simulation results for different underlaps on the same curvature of the regular tubes. The structure 1-0/1-2// is special because there is no added point on the underlap. The green triangles mark the red stitch position in the tested yarns. The maximum vertical distances from underlaps to stitches are listed in Table 1. This measurement size for the modified group is the average of each underlap segments. The modified

models seem thinner than the original ones, which means underlaps are closer to the surface. Each structure saves 48~79% distance. The longer the underlap, the more efficient improvement the modified model shows. For a fabric in the size of 15 wales × 10 courses (150 stitches), the time efficiency is recorded in Table 1. Although underlaps with added points takes longer calculation time, the differences are within an acceptable range of 10%. From the side view of these tubes in Figure 5, they look similar for one single yarn. But yarns in the modified simulation result are more neatly arranged.

Table 1. Size and time efficiency comparison for the tube models.

Structure	Thickness			Calculation time/15 wales × 10 courses		
	Original/px	Modified/px	Differences/%	Original/ms	Modified/ms	Differences/%
1-0/2-3//	0.257	0.132	48.64	12.867	13.559	5.39
1-0/3-4//	0.366	0.134	63.39	13.856	14.709	6.15
1-0/4-5//	0.413	0.140	66.10	15.560	16.468	5.83
1-0/5-6//	0.525	0.144	72.57	14.636	15.660	7.00
1-0/6-7//	0.703	0.147	79.09	15.474	16.993	9.82

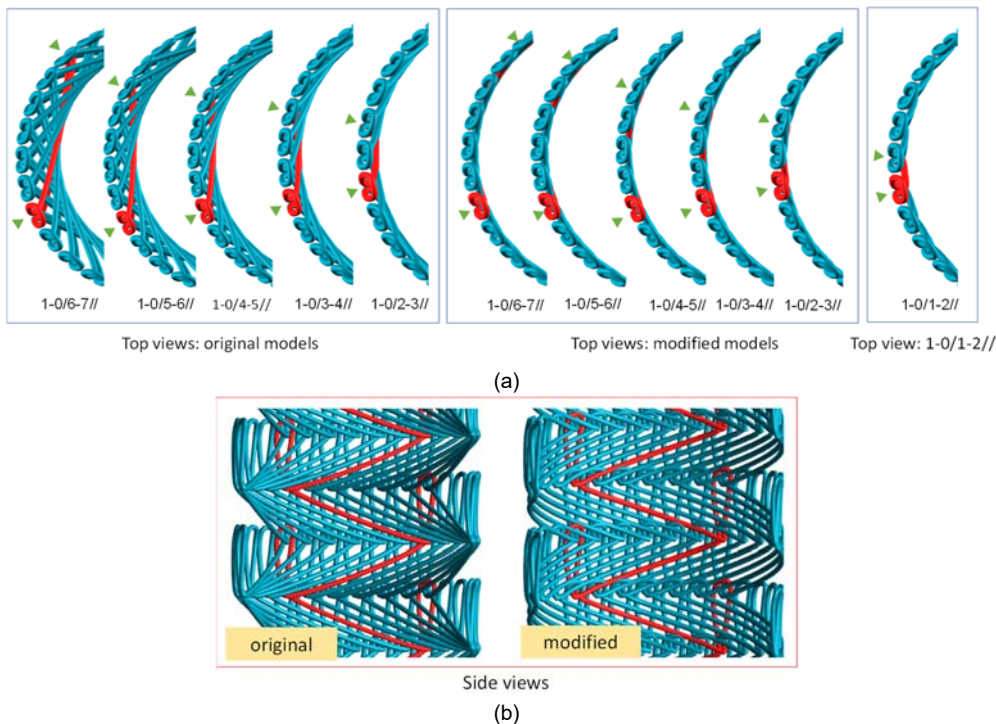


Figure 5. Simulation results of the original model and the modified model for regular tubes. (a) from top views; (b) from side views.

### Bent fabric

In order to get the specified angle value  $\beta$ , fabrics are bent at certain angles. Figure 6 shows a group of fabrics with the bent angle of  $60^\circ$  before modified. The fabrics are bent at between the 7<sup>th</sup> and the 8<sup>th</sup> wales. The fabrics become thicker as the underlaps become longer. Both top views and side views of a structure 1-0/4-5// are also shown in Figure 6 as a visual example.

Figure 7(a) is the vertical length (the maximum thickness of the fabric) from the underlaps to the fabric faces at several angles from  $0^\circ$  to  $165^\circ$  with the tested angle step  $15^\circ$ . For the short underlap structures 1-0/1-2// and 1-0/2-3//, the underlap become away from the fabric before the angle  $75^\circ$ . And then the underlap becomes closer to the fabric surface. This decrease is more obvious in the longer

underlap structures. But for these structures, the turning angle is  $90^\circ$ . Take the structure 1-0/6-7// for example in Figure 7(b), when the bend angle becomes larger, the underlap triangle becomes smaller, resulting in a shorter distance trend to the fabric. It is because when the bend angle is larger, two fabric pieces get closer to each other. That is why the turning angle exists at  $75^\circ$  and  $90^\circ$ .

The added points can be omitted when the distance short enough. The differences are listed in Table 2 comparing with the flat fabric ( $0^\circ$ ). Structures are named from 0 to 5, which is relating to the stitch interval number the underlap passes. The differences under 10% are regarded as an acceptable range for the underlap simulation. The underlaps at the angle differences larger than 10% need added points to pull them back. Thus, the specified angle value  $\beta$  is obtained in Table 3.

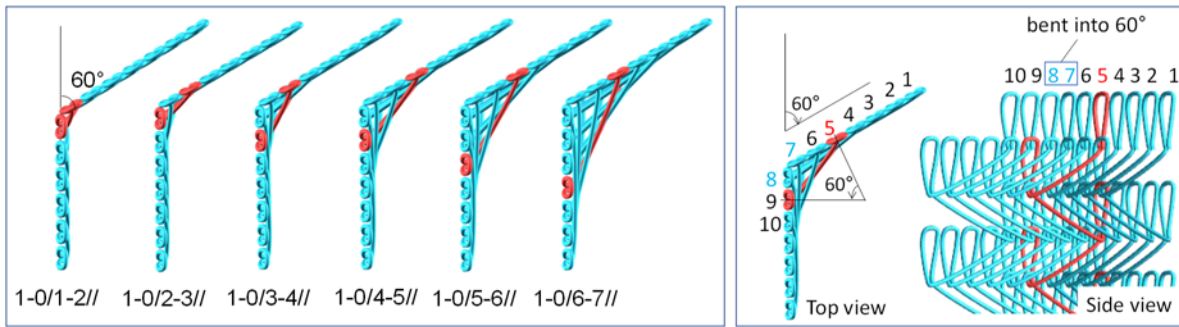
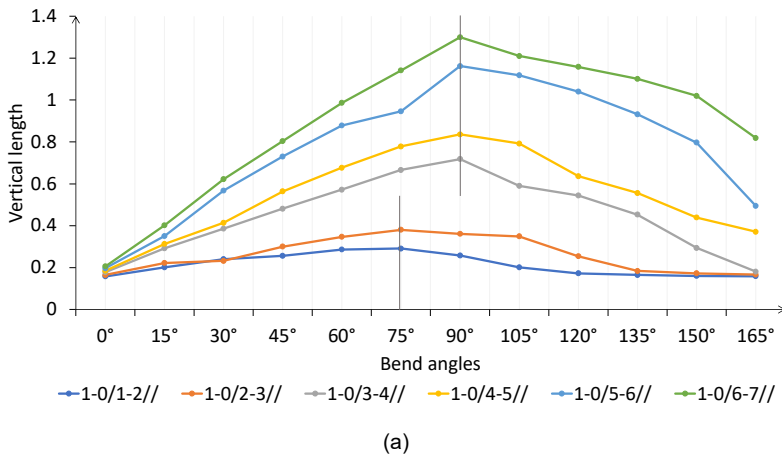
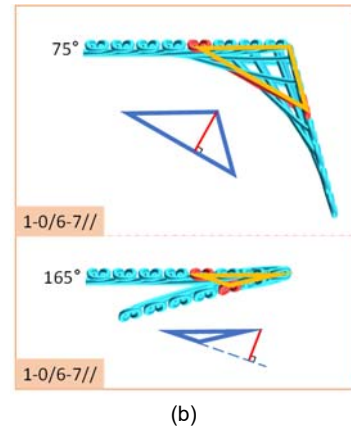


Figure 6. Bent fabrics at  $60^\circ$  before modified.



(a)



(b)

Figure 7. Vertical length measurement results. Vertical length of bent fabrics at different angles.

Table 2. Vertical distance differences comparing with the flat fabric.

Stitch interval number	15°	30°	45°	60°	75°	90°	105°	120°	135°	150°	165°
0	27.22	51.90	62.03	81.01	84.18	63.29	27.22	9.49	4.43	1.27	0.63
1	34.55	40.61	81.82	110.30	130.30	118.79	111.52	53.94	11.52	4.85	1.21
2	64.04	116.85	170.22	221.35	274.16	303.37	231.46	205.62	154.49	65.17	1.69
3	69.19	123.78	204.86	265.95	320.54	351.89	328.11	243.78	200.54	137.30	100.54
4	78.17	188.32	270.56	345.69	380.20	489.85	467.51	427.92	373.10	304.57	151.27
5	95.15	201.94	290.29	378.64	453.88	531.07	487.38	462.14	434.47	395.15	297.57

Table 3.  $\beta$  ranges.

Stitch interval number	$\beta$
0	$\left\{ \begin{array}{l} \beta = 0^\circ \text{ or } \beta > 120^\circ, \text{ no added points} \\ \text{else, added points} \end{array} \right.$
1	$\left\{ \begin{array}{l} \beta = 0^\circ \text{ or } \beta > 150^\circ, \text{ no added points} \\ \text{else, added points} \end{array} \right.$
2	$\left\{ \begin{array}{l} \beta = 0^\circ \text{ or } \beta > 165^\circ, \text{ no added points} \\ \text{else, added points} \end{array} \right.$
3	$\left\{ \begin{array}{l} \beta = 0^\circ, \text{ no added points} \\ \text{else, added points} \end{array} \right.$
4	
5	

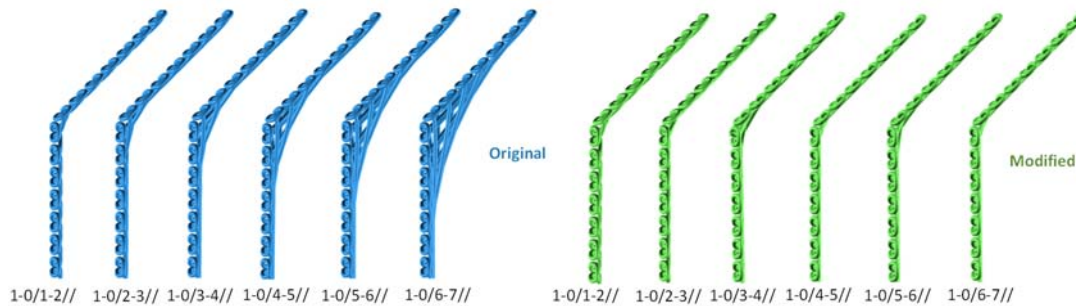


Figure 8. Comparison between original models and modified models at the bend angle of 45°.

Figure 8 shows another example of the bent fabric at the bend angle of 45°. The added points are calculated according to the above regulars. All underlaps are pulled closer to the fabrics after modifying the models, which proves the method proposed in this paper is effective for a better visualization.

### CONCLUSIONS

During our 3D simulation for warp knitted fabrics, a pattern related issues with underlaps on deformed surface is discussed. The longer the underlap will get an inaccurate simulation result. Thus, the vertical vectors of stitch grids on the deformed surface are analyzed. And the original stitch model is modified with additional control points on the underlaps. For the tube fabric, points are added at each wale that the underlaps pass. For the bent fabric, the points are added according to the vertical normal vector angles of stitches. Fabrics with several angles of normal vectors are analyzed. Relationships between points and stitch interval number are established and demarcation angles  $\beta$  are obtained. The size comparison results declare that underlaps are pulled back to the fabric well. The results show this method has a positive effectiveness in visualization.

**Acknowledgements:** The authors thank TU Dresden and Jiangnan University for supporting this work for their laboratories and advanced apparatus. This work was supported by National Science Foundation of China (61902150), Taishan Industry Leading Talents (tscy20180224) and China Scholarship Council (No.202106790059).

### REFERENCES

- Yuksel, C., Lefebvre, S., & Tarini, M. (2019). Rethinking texture mapping. *Computer Graphics Forum*, 38(2), 535-551. <https://doi.org/10.1111/cgf.13656>
- Xu, Y., Yang, S., Sun, W., Tan, L., Li, K., et al. (2019). 3d virtual garment modeling from rgb images. In 2019 IEEE International Symposium on Mixed and Augmented Reality (ISMAR), 37-45. <https://doi.org/10.48550/arXiv.1908.00114>
- Mir, A., Alldieck, T., & Pons-Moll, G. (2020). Learning to transfer texture from clothing images to 3D humans. 2020 IEEE/CVF Conference on Computer Vision and Pattern Recognition (CVPR), 7021-7032. <https://doi.org/10.1109/cvpr42600.2020.00705>
- Peng, J., Jiang, G., Xia, F., Cong, H., & Dong, Z. (2020). Deformation and geometric modeling in three-dimensional simulation of fancy weft-knitted fabric. *Textile Research Journal*, 90(13-14), 1527-1536. <https://doi.org/10.1177/0040517519894749>
- Kyosev, Y. (2019). *Warp knitted fabrics construction*. (1 ed.). CRC Press(Boca Raton). <https://doi.org/10.1201/9780429094699>
- Liu, H., Jiang, G., & Dong, Z. (2020). Lapping modeling of looped warp knitted jacquard fabrics based on web. *Journal of Engineered Fibers and Fabrics*, 15(43), 1-13. <http://dx.doi.org/10.1177/1558925020979300>
- Yuksel, C., Kaldor, J. M., James, D. L., & Marschner, S. (2012). Stitch meshes for modeling knitted clothing with yarn-level detail. *ACM Transactions on Graphics (TOG)*, 31(4), 1-12. <https://doi.org/10.1145/2185520.2185533>
- Wu, K., Gao, X., Ferguson, Z., Panozzo, D., & Yuksel C. (2018). Stitch meshing. *ACM Transactions on Graphics (TOG)*, 37(4): No. 130, 1-14. <https://doi.org/10.1145/3197517.3201360>
- Weeger, O., Sakhaei, A. H., Tan, Y. Y., Quek, Y. H., Lee, T. L., et al. (2018). Nonlinear multi-scale modelling, simulation and validation of 3D knitted textiles. *Applied Composite Materials*, 25(4), 797-810. <https://doi.org/10.1007/s10443-018-9702-4>

10. Ielina, T., Galavska, L., Ausheva, N., & Dzikovich, T. (2021). 3d modelling of untwisted multifilament threads, curved in a knitted loop. *Deutsche Internationale Zeitschrift für zeitgenössische Wissenschaft*, (22), 74-79. <http://dx.doi.org/10.24412/2701-8369-2021-22-74-79>
11. Renkens, W., & Kyosev, Y. (2011). Geometry modelling of warp knitted fabrics with 3D form. *Textile Research Journal*, 81(4), 437-443. <https://doi.org/10.1177/0040517510385171>
12. Liu, H., Jiang, G., & Dong, Z. (2022). Mesh modeling and simulation for three-dimensional warp-knitted tubular fabrics. *The Journal of The Textile Institute*, 113(2), 303-313. <https://doi.org/10.1080/00405000.2020.1871184>
13. Kyosev, Y. (2019). *Topology-based modeling of textile structures and their joint assemblies*. (1 ed.). Springer International Publishing(Switzerland). <https://doi.org/10.1007/978-3-030-02541-0>
14. Liu, H., Jiang, G., & Dong, Z. (2021). A shortened development process method for warp-knitted yarn-dyed shirt fabric. *Textile Research Journal*, 91(3-4), 443-455. <https://doi.org/10.1177/0040517520937372>
15. Liu, H., Kyosev, Y., & Jiang, G. (2022). Yarn level simulation of warp-knitted clothing elements—first results and challenges. *Communications in Development and Assembling of Textile Products*, 3(2), 115-126. <https://doi.org/10.25367/cdatp.2022.3.p115-126>

# NEW SOLUTIONS IN THE PRODUCTION OF COMPOSITES - MECHANICAL PROPERTIES OF COMPOSITES REINFORCED WITH TECHNICAL EMBROIDERY AND WOVEN FABRIC MADE OF FLAX FIBERS

PONIECKA AGATA<sup>1</sup>, BARBURSKI MARCIN<sup>1\*</sup>, RANZ DAVID<sup>2</sup>, CUARTERO JESÚS<sup>3</sup> AND MIRALBES RAMON<sup>2</sup>

<sup>1</sup> Lodz University of Technology, Faculty of Material Technologies and Textile Design, Institute of Architecture of Textiles, Zeromskiego 116, Post code: 90-924 Lodz, Poland

<sup>2</sup> University of Zaragoza, Department of Design and Manufacture Engineering, C/María de Luna, Post code: 50018 Zaragoza, Spain

<sup>3</sup> University of Zaragoza, Department of Mechanical Engineering, C/María de Luna, Post code: 50018 Zaragoza, Spain

## ABSTRACT

The main purpose of the article is to present the new possibilities of producing natural fiber composite reinforcement. In this case, a computer embroidery machine by ZSK type JCZA 0109-550 was used. A technical embroidery with a stitch length of 2 mm was made on the machine. The embroidery was made of flax roving with a linear density of 400 tex. The woven fabric was made of the same flax roving as the embroidery, with a surface mass of 400 g/m<sup>2</sup>. Composites were then produced from the technical embroidery and woven fabric using the infusion method with epoxy resin. The individual configurations differed from each other in the orientation of the roving in the embroidery samples. Samples for tensile strength and tensile elongation tests consisted of 4 layers, while samples for the DCB test consisted of 6 layers, with the addition of a separating foil between the 3rd and 4th layer. Composites were then subjected to strength tests - tensile strength, tensile elongation and DCB test (Double Cantilever Beam test), on the INSTRON machine. During the action of force along the direction of the fibers, composites containing technical embroidery as reinforcement were characterized by higher strength than composites containing woven fabric as reinforcement. Additionally, embroidery is a barrier to the formation of interlayer cracks. Technical embroidery is made on the basis of Tailored Fiber Placement (TFP) technology. This technology allows optimizing the mechanical values of the composite reinforcement.

## KEYWORDS

Technical embroidery; Flax fibres; Composites; Mechanical properties; Tailored fiber placement.

---

\* Corresponding author: Barburski, M., e-mail: [marcin.barburski@p.lodz.pl](mailto:marcin.barburski@p.lodz.pl)

## INTRODUCTION

The composite production technology is faced with the challenge of minimizing the resulting production waste. This idea is reflected in the Tailored Fiber Placement (TFP) method, which includes technical embroidery. It consists in placing the medium on the surface of a flat textile product in any direction of the X and Y axes. The embroidery can also reach a certain dimension in the direction of the Z axis by overlapping embroidery layers. The height of the stacking sequence can be up to 8 mm. The amount of production waste in this kind of preforms is minimized thanks to the production of a precisely designed pattern, without the need to cut an element from a larger surface. The main waste generated during the production of technical embroidery is non-woven fabric or other types of backing on which the embroidery was made. The amount of this waste

can be reduced by using an appropriate hoop size [1]. Electric wires, optics, glass or carbon fibers, electrically conductive yarns and others are used to perform technical embroidery increasing the performances of the final application [2].

Technical embroidery is now mainly used in textronics, to create heating mats (e.g., in car seats), connecting sensors, shielding, conductive interconnections and interfaces. Technical embroidery can be also used to create antennas or as an alternative to solid copper to make a coil for unilateral nuclear magnetic resonance systems. [3–7].

In the case of the following tests, linen roving was used to make the samples. The use of this material in the production of composites has increased significantly since 2012 [8]. Composites containing

natural fibers exhibit a high level of vibration damping and a low weight [9-10].

The characteristics of the reinforcement itself, used for the production of composites, i.e. the arrangement of the fibers, the type of weave, the linear density of the yarn, the density of the yarn arrangement in the fabric, have an impact on the out-plane fracture toughness of the composite. Z-pinning, fiber stitching and the use of 3D fabrics can enhance these properties. The disadvantage of these methods is a reduction in tensile strength, a reduction in the modulus of elasticity and fatigue performance [11-18]. The answer to these disadvantages is the use of technical embroidery technology. As proven in previous studies, the use of technical embroidery for the production of composite reinforcements improves strength of composites, compared to ones containing woven fabric as reinforcement. [19-20].

**EXPERIMENTAL**

**Materials**

The GiS BasePack version 10 program was used to make the embroidery pattern. The embroidery were made on a ZSK embroidery machine, type JCZA 0109-550 (Figure 1a). This machine is equipped with a W-type head designed for technical embroidery.

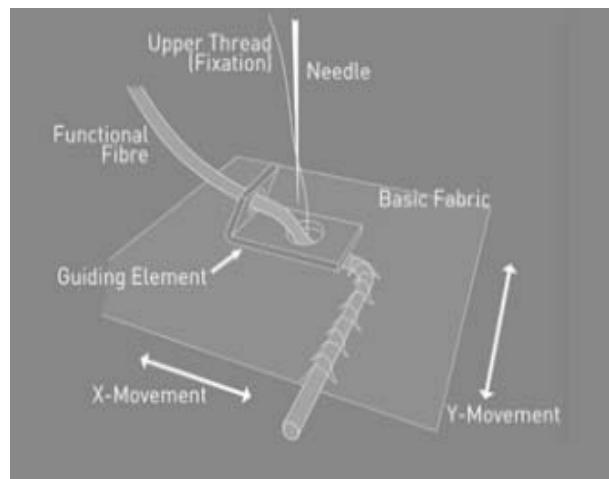
The rule of the operation of this head is shown in Figure 1b.

The subject of the research was composites containing two types of flax fiber reinforcements: technical embroidery and woven fabric. The embroidery was made with the use of Safilin linen roving with a linear weight of 400 tex. Gunold monofilament with a linear weight of 11 tex was used to make the fastening zig-zag stitch. The length of the zig-zag stitch was 2 mm and the width was 1.2 mm. In the case of manufacturing samples for the DCB test, an induced crack was created, leaving an area without stitching yarns and placing a plastic foil after making three layers of embroidery, and then three more layers of embroidery were placed. The tensile strength of the flax roving was 7,37 cN/tex and the tensile elongation was 1,69 %. Embroidery was made on a base of cotton fabric with an area weight of 280 g/m<sup>2</sup> and non-woven fabric with an area weight of 35 g/m<sup>2</sup>. The flax woven fabric was made from the same roving used for the embroidery. The surface mass of the fabric was 400 g/m<sup>2</sup>. All reinforcement samples were then impregnated with the following resin system: SR GreenPoxy 33 epoxy resin and SD4772 hardener at a ratio of 100:32. Composite samples were made using the infusion method.

In total, the following variants for tensile strength and tensile elongation tests were prepared:



(a)



(b)

**Figure 1.** (a) - ZSK embroidery machine, type JCZA 0109-550 [own source]; (b) - Scheme of laying the medium on the base [21].

**Table 1.** Configurations for tensile strength and tensile elongation tests.

Reinforcement	technical embroidery	technical embroidery	technical embroidery	woven fabric	woven fabric
Fiber orientation	0°	±45°	90°	0/90°	±45°

For interlaminar fracture toughness test, the following variants were prepared:

**Table 2.** Configurations for interlaminar fracture toughness test.

Reinforcement	technical embroidery	woven fabric
Fiber orientation	0°	0/90°

## Methods

The tensile strength and tensile elongation tests were performed according to the PN-EN ISO 527-4 standard [22]. The samples were stretched at a constant speed until the breakage was attained. The relative elongation at maximum force, maximum force, breaking force and relative elongation at break values were collected during the testing. The tests were carried out using a 100 kN load cell on an INSTRON universal testing machine, model 8032. A 50 mm gauge length extensometer was used to measure the specimens' elongation. The test parameters were as follows: grips distance: 100 mm; speed of testing: 1 mm/min; sample size 250×25×3.5 mm; number of samples: 5 of each variant. The test findings are presented in the graph of tensile stress as a function of elongation.

Mode I interlaminar fracture toughness test (DCB - Double Cantilever Beam Test) was carried out based on the ASTM D 5528-01 standard [23]. The test consisted of opening by the crosshead movement, until the samples broke. During stretching, the values of the load ( $P$ ) and delamination length ( $\delta$ ) were recorded. The test was stopped when the delaminating crack spreads to at least 45 mm from the apex of the initial fracture or when the crack growth at delamination was from 3 to 5 mm. The tests were conducted on a INSTRON universal testing machine with a 50 kN load cell. The velocity of the test was 5 mm/min. The test parameters were as follows: grips distance 0 mm; speed of testing: 5 mm/min; sample size: 160×25×5 mm; number of samples: 5 of each variant.

Both tests were made on the INSTRON universal testing machine, presented in Figure 2a and 2b.



(a)



(b)

Figure 2a and 2b. 2a - Tensile strength and tensile elongation test; 2b - Interlaminar fracture toughness test [own source].

## RESULTS AND DISCUSSION

### Tensile strength and tensile elongation tests

Tensile strength and tensile elongation values are presented on the Figure 3.

As shown in Figure 3, based on performed tests, it can be concluded that the tensile strength is greatest when a force is applied along the fibers ( $0^\circ$  variant). In these variants, most fibers are involved in the stretching process. The composite with technical embroidery placed at an angle of  $0^\circ$  to the acting force showed by far the highest tensile strength (142 MPa). Its strength was almost twice as high as that of a composite containing woven fabric as reinforcement, although the woven fabric contains two systems of threads in its structure - weft and warp. The strength of the composite with embroidery placed at an angle of  $90^\circ$  to the acting force as reinforcement turned out to be by far the smallest. In this case, none of the roving fibers is involved in the stretching process. Only the resin and the base on which the embroidery was made is responsible for the strength of the sample. In the case of samples  $\pm 45^\circ$ , the strength of the embroidery variants and the woven fabric were on a similar level.

However, the failure strain in  $\pm 45^\circ$  woven samples is twice than in  $\pm 45^\circ$  embroidery samples. This is due to the fact that the roving in the woven fabric structure has a significant crimp, which increases the elongation. In addition, when a tensile force is

applied, shear and bending forces first act in the composite. The fibers in the composite first have to travel from the  $\pm 45^\circ$  direction to the  $0^\circ$  direction - then they are subjected to a tensile force. In the case of composites containing embroidery as reinforcement, the  $0^\circ$  system showed a greater elongation than the  $90^\circ$  system. This is due to the tensile force along the axis of the fibers.

### Interlaminar fracture toughness

In Figure 4 it can be clearly seen that the composite containing woven fabric as reinforcement showed a greater degree of delamination. For about the first 2 millimeters of opening the sample, both variants showed almost identical characteristics. On the

other hand, at about 4 mm opening, the composite containing embroidery as reinforcement cracks. The embroidery is therefore a barrier to delamination of the sample. The composite containing the fabric as reinforcement was delaminated - it broke when it opened about 35 mm.

In the case of samples containing embroidery as reinforcement, the type of the crack formed was also influenced by the sample manufacturing technology itself. The roving layers themselves could be divided in half, while one of the parts always contained fabric, fleece and a backing thread - which increased the strength of this layer. The crack always occurred in the layer not containing these systems.

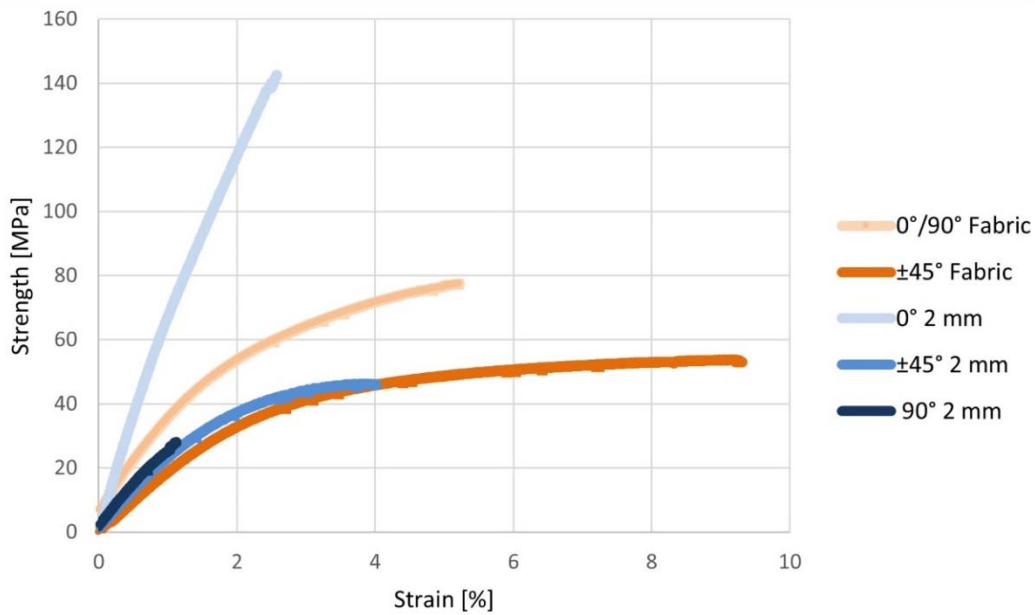


Figure 3. Tensile strength and tensile elongation of produced samples.

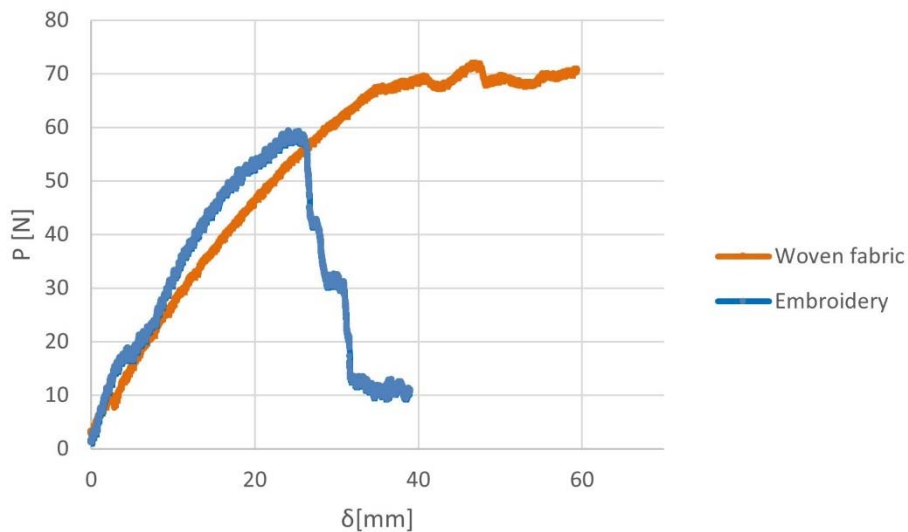


Figure 4. Interlaminar fracture toughness of produced samples.

## CONCLUSIONS

The use of embroidery as a reinforcement of a composite increases its tensile strength in the direction of fiber stretching, compared to a composite containing woven fabric as reinforcement. Whereas composites containing woven fabric as reinforcement, in each variant of fiber arrangement, showed higher strain.

As a result of the conducted tests, it can be concluded that the vertical stitching of embroidery prevents the delamination of the composite, because the composite with technical embroidery as reinforcement does not undergo the opening process during the test.

It is possible to adjust the strength properties of the composite, containing technical embroidery as reinforcement, to the expected loads affecting the finished product. This fact should be considered when designing finished products with embroidered patterns as reinforcement. In the case of beam systems, it is recommended to arrange the strengthening medium in the direction of the acting tensile forces.

## REFERENCES

1. Poniecka, A., Barburski, M., Urbaniak, M. (2021). Mechanical properties of composites reinforced with technical embroidery made of flax fibers. *AUTEX Research Journal*  
<https://doi.org/10.2478/aut-2021-0025>
2. Mecnika, V., Hoerr, M., Krievins, I., Jockenhoevel, S., Gries T. (2014). Technical Embroidery for Smart Textiles, Review. *Materials Science Textile and Clothing Technology*, 9, 56-63.  
<http://dx.doi.org/10.7250/mstct.2014.009>
3. Abbas, B., Khamas, S.K., Ismail, A., Sali, A. (2019). Full Embroidery Designed Electro-Textile Wearable Tag Antenna for WBAN Application. *Sensors*, 19(11), 2470.  
<https://doi.org/10.3390/s19112470>
4. Linz, T., Vieroth, R., Dils, Ch., Koch, M., Braun, T., Friedrich Becker, K., et al. (2008). Embroidered Interconnections and Encapsulation for Electronics in Textiles for Wearable Electronics Applications. *Advances in Science and Technology*, 60, 85–94.  
<http://dx.doi.org/10.4028/www.scientific.net/AST.60.85>
5. Shafti, A., Ribas Manero, R.B., Borg, A.M., Althoefer, K., Howard, M.J. (2017). Embroidered Electromyography, A Systematic Design Guide. *IEEE Transactions on Neural Systems and Rehabilitation Engineering*, 25 (9), 1472–1480.  
<https://doi.org/10.1109/tnsre.2016.2633506>
6. Morris, R.H., McHale, G., Dias, T., Newton, M.I. (2013). Embroidered coils for magnetic resonance sensors. *Electronics*, 2(2), 168–177.  
<https://doi.org/10.3390/electronics2020168>
7. Zhang, M., Zhao, M., Jian, M., Wang, C., Yu, A., Yin, Z., et al. (2019). Printable Smart Pattern for Multifunctional Energy-Management E-Textile. *Matter*, 1(1), 168-179.  
<https://doi.org/10.1016/j.matt.2019.02.003>
8. Monteiro, S., Candido, V., Braga, F. (2016). Sugarcane bagasse waste in composites for multilayered armor. *European Polymer Journal*, 78, 173–185.  
<http://dx.doi.org/10.1016%2Fj.eurpolymj.2016.03.031>
9. Cristaldi, G., Latteri, A., Recca, G. (2010). Composites based on natural fibre fabrics. In, *Woven fabric engineering*, Dubrovski, P.D., InTech, Rijeka, 317–342.  
<http://dx.doi.org/10.5772/10465>
10. Buksnowitz, C., Adusumalli, R., Pahler, A., Sixta, H., Gindl, W. (2012). Acoustical properties of Lyocell, hemp, and flax composites. *J. Reinf. Plast. Compos.*, 29, 3149–3154.  
<https://doi.org/10.1177/0731684410367533>
11. Liu, Q., Hughes M. (2008). The fracture behaviour and toughness of woven flax fibre reinforced epoxy composites. *Composites Part A Applied Science and Manufacturing*, 39(10), 1644-1652  
<https://doi.org/10.1016/j.compositesa.2008.07.008>
12. Bensadoun, F., Verpoest, I., Vuure, A.W. Van. (2017). Interlaminar fracture toughness of flax epoxy composites. *J Reinf Plast Compos*, 36(2), 121–136.  
<https://doi.org/10.1177/0731684416672925>
13. Mouritz, A.P. (2007). Review of z-pinned composite laminates. *Compos A*, 38, 2383–97.  
<https://doi.org/10.1016/j.compositesa.2007.08.016>
14. Rong, M.Z., Zhang, M.Q., Liu, Y., Zhang, Z.W., Yang, G.C., Zeng, H.M. (2001). Effect of stitching on inplane and interlaminar properties of sisal/epoxy laminates. *J Compos Mater*, 36, 1505–26.  
<https://doi.org/10.1177/0021998302036012163>
15. Mouritz, A.P., Bannister, M.K., Falzon, P.J., Leong, K.H. (1999). Review of applications for advanced three-dimensional fibre textile composites. *Composites Part A*, 30, 1445–1461.  
[https://doi.org/10.1016/S1359-835X\(99\)00034-2](https://doi.org/10.1016/S1359-835X(99)00034-2)
16. Allegri, G., Zhang X. (2007). On the delamination suppression in structural joints by z-fibre pinning. *Composites Part A: Applied Science and Manufacturing*, 38, 1107–1115.  
<https://doi.org/10.1016/j.compositesa.2006.06.013>
17. Dell'Anno, G., Treiber, J.W.G., Partridge, I.K. (2016). Manufacturing of composite parts reinforced through-thickness by tufting. *Robotics and Computer-Integrated Manufacturing*, 37, 262-272.  
<http://dx.doi.org/10.1016/j.rcim.2015.04.004>
18. Sickinger, C., Herrmann, A. (2001). Structural Stitching as a method to design high-performans composites in future, 11th International Textextil-Symposium for Technical Textiles, Nonwovens and Textile-Reinforced Materials, Germany, 23.-26.04.2001
19. Poniecka, A., Barburski, M., Urbaniak, M. Mechanical properties of composites reinforced with technical embroidery made of flax fibers. *AUTEX Research Journal*  
<https://doi.org/10.2478/aut-2021-0025>
20. Poniecka, A., Barburski, M., Ranz, D., Cuartero, J., Miralbes, R. (2022). Comparison of mechanical properties of composites reinforced with technical embroidery, UD and woven fabric made of flax fibers. *Materials*, 15 (7469), 1-18.  
<https://doi.org/10.3390/ma15217469>
21. Document available on a web page. Retrieved 3 January 2021. Web site: [www.technicalembroidery.co.uk](http://www.technicalembroidery.co.uk)
22. EN ISO 527-4:1997; *Plastics—Determination of tensile properties—Part 4: Test conditions for isotropic and orthotropic fi-bre-reinforced plastic composites*. Available online: <https://www.iso.org/standard/4595.html> (accessed on 15 March 2021).
23. ASTM D 5528-01 *Standard Test Method for Mode I Interlaminar Fracture Toughness of Unidirectional Fiber-Reinforced Polymer Matrix Composites*

# DETECTING DAMAGED ZONES ALONG SMART SELF-SENSORY CARBON BASED TRC BY TDR

GABEN MAHDI AND GOLDFELD YISKA\*

Faculty of Civil and Environmental Engineering, Technion – Israel Institute of Technology, Haifa, 32000, Israel

## ABSTRACT

The study aims to investigate the ability of smart self-sensory carbon roving to detect damaged zones in TRC structures. State of the art monitoring procedures are based on integrative measurements and accordingly are limited in detecting only the occurrence of damage. This study aims to handle this limitation and offers to adopt the Time Domain Reflectometer (TDR) technique. The TDR concept is widely used in Bayonet Nut Coupling (BNC) cables to identify defects along the cable (opens, shorts, etc.). The current study adopts its principle to carbon rovings. To simulate the BNC cable configuration, the study offers to connect two parallel carbon rovings to the TDR Data Acquisition (DAQ) system. The proposed monitoring technique is investigated by loading two textile reinforced MPC beams under uniaxial tensile loading. Results show the potential of the suggested technique to locate damage zones in TRC structures and highlights its limitation.

## KEYWORDS

Time domain reflectometer; Smart carbon rovings; AC measurements; Crack identification technique.

---

\* Corresponding author: Goldfeld Y., e-mail: [yiska@technion.ac.il](mailto:yiska@technion.ac.il)

## INTRODUCTION

Intelligent concrete structures with self-sensory capabilities are increasingly relevant in today's-built environment. The technology of carbon-based textile reinforced concrete (TRC) is a potential candidate for the development of such intelligent structures. Textile reinforcement technology is based on a biaxial textile mesh of alkali-resistant glass (AR-glass), carbon or basalt rovings with a high tensile strength and high resistance to corrosion. It allows to construct thin-walled, light and durable concrete elements [2,10,14]. Since the carbon rovings are electrically conductive, they can be used both as the main reinforcement system and as the sensory agent [1,4,5,13,16,17]. The potential of using carbon rovings as an integrated sensory agent has been presented in the literature for various sensory purposes such as: detecting cracking [7], estimating strain [7,13,16,17], monitoring the mechanical loading [1,4,5], identifying infiltration of water through cracked zones [6,12], etc. The commonly used approaches for the electrical measurement are based on direct current (DC) electrical circuits by two-probes monitoring setup [13], four-probes monitoring setup [16], Wheatstone bridge configurations [7,17], or by alternating current (AC) electrical circuits [4,5]. These studies proved the feasibility of the smart sensory concept and focused on the correlation between measured changes in the

electrical resistance (ERC), the electrical inductance or the electrical impedance of the carbon roving and the structural response. All the above-mentioned monitoring systems yield integrative measurements quantities that cannot localize damage along the structure. This study aims to detect the damaged zones by adopting the principles of the Time Domain Reflectometer (TDR) technique to smart carbon based TRC structures.

The principle of TDR is traditionally used in Bayonet Nut Coupling (BNC) cables to identify defects along the cable. The electrical configuration of BNC cables consists of a copper wire and an insulation barrier. The latter is placed at a constant distance from the copper wire, and the resistance per unit length is constant and equals to 50 Ohms. This study offers to adopt the idea of the BNC configuration by using embedded continuous carbon rovings to locate damage along TRC elements. Damage in this study defines as cracks. Two parallel carbon rovings are connected to a designated data acquisition (DAQ) system, one roving functions as the signal and the other as the insulation.

The carbon rovings have a unique micro-structure, which is divided into two zones: the inner (core) filaments and external (sleeve) filaments [8,11,15]. The sleeve filaments break due to cracking, which yields changes in the electrical current density

distribution along the roving. This phenomenon results in an increase of the impedance. In addition, the impedance is not a constant value along the carbon roving and depends on the length of the roving. These properties may limit a direct implementation of the BNC concept which will be reflected by the monitoring capabilities.

To isolate the influence of the electrical properties of the cement body, the study uses magnesium phosphate cement (MPC) matrix. MPC is a production of acid-based solution, dead burnt magnesia, potassium-based phosphate and ammonium-based phosphate [4]. MPC matrix is characterized by a relatively high impedance value compared to conventional cement-based matrix [4]. As a result, it is a better choice to reduce external environmental emissions.

To demonstrate the proposed sensory concept, the study experimentally investigates two textile reinforced MPC elements under uniaxial tensile loading tests and presents the potentials of the proposed monitoring system.

**MATERIALS AND METHOD**

This study uses a generic production process of textile reinforced cement elements [4-7,12,17]. The mechanical and electrical properties of the textile and the production process of the textile reinforced MPC specimens are discussed in this section.

**Carbon-based textile**

Following [4-7,12,17], the current study uses a generic textile mesh. The textile consists of six carbon rovings in the longitudinal direction (0°) and AR-glass rovings in the transverse direction (90°). The textile has a warp-knitted grid structure with a mesh size of 7-8 mm. The stitch type is pillar. The mechanical and electrical properties of the carbon and the AR-glass rovings are given in Table 1.

**Table 1.** Material properties of the AR-glass and the carbon rovings [5].

	<b>AR-Glass roving</b>	<b>Carbon roving</b>
Specific mass density [kg/m <sup>3</sup> ]	2,680	1,810
Modulus of elasticity [GPa]	72	270
Filament Tensile strength [MPa]	1,700	5,000
Filament diameter	19 μm	7 μm
Linear Density [tex]	2,400	1,600
Electrical resistance [Ω/m]	Infinity	13

**MPC matrix with additive short aramid fibers**

The study uses a commercial matrix of mono-potassium phosphate acid produced by ICL Group Ltd. Its commercial name is Phosment. In addition, to improve the ductility of the matrix short aramid fibers (AF) were added to the mixture. The volume fraction of the fibers is determined as 0.5%. The study uses a commercial AF named Technora CF32 produced by Teijin Frontier company Ltd. The short AF are 3mm length 12 filaments: 12 μm diameter, the tenacity - 2.3-2.5 N/tex, mass density - 1.39 g/cm<sup>3</sup>, tensile strength - 3.2-3.5 GPa, modulus of elasticity - 65-85 GPa, elongation break - 3.9-4.5%. The MPC matrix was prepared with a ratio of 1:4 water to dry material.

The tensile and flexural strengths of the matrix (MPC +0.5% short AF) specimens were determined at 14 days according to EN 196-1:2005 [3]. The tensile and compression strengths are 6.611 ± 0.434 MPa and 61.929 ± 6.172 MPa, respectively.

**Carbon-based textile reinforced MPC beams**

Two beams are investigated. In each beam, a single textile layer is placed. The geometrical properties of both beams are 500 mm long, 50 mm wide and 8 mm thick. The textile layer is placed in the middle of the cross-section of the beams. The beams are cast in a special mold that enables to slightly pretensioned the textile upon casting, see Fig. 1.

**Loading setup**

The beams are loaded under a uniaxial tensile loading with a displacement control rate 0.5 mm/min by Instron model 5966. In order to avoid local stress at the ends of the beams, aluminum panels were attached to the ends of the beams, see also [8]. A special uniaxial device was used (Instron screw side action tensile grips model 1710-116) the widths of the supports are 50 mm and they were positioned 20 mm from the beams' edges. Along the loading process, the applies load, the displacement, the impedance spectrum and the crack propagation using the digital image correlation (DIC) technique are measured (LaVision DaVis 10). The loading scheme is shown in Fig. 2.

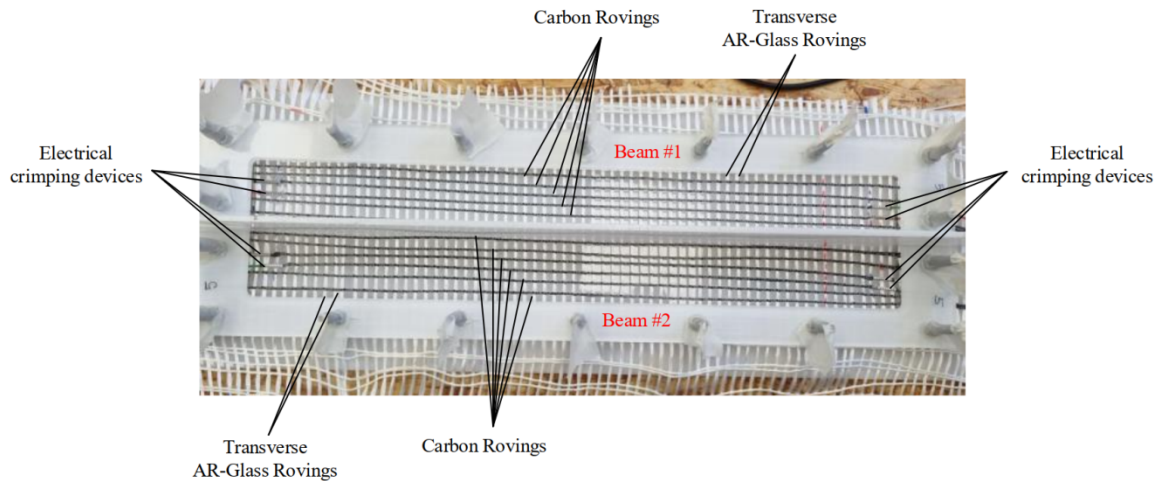


Figure 1. Casting mold for two beams.

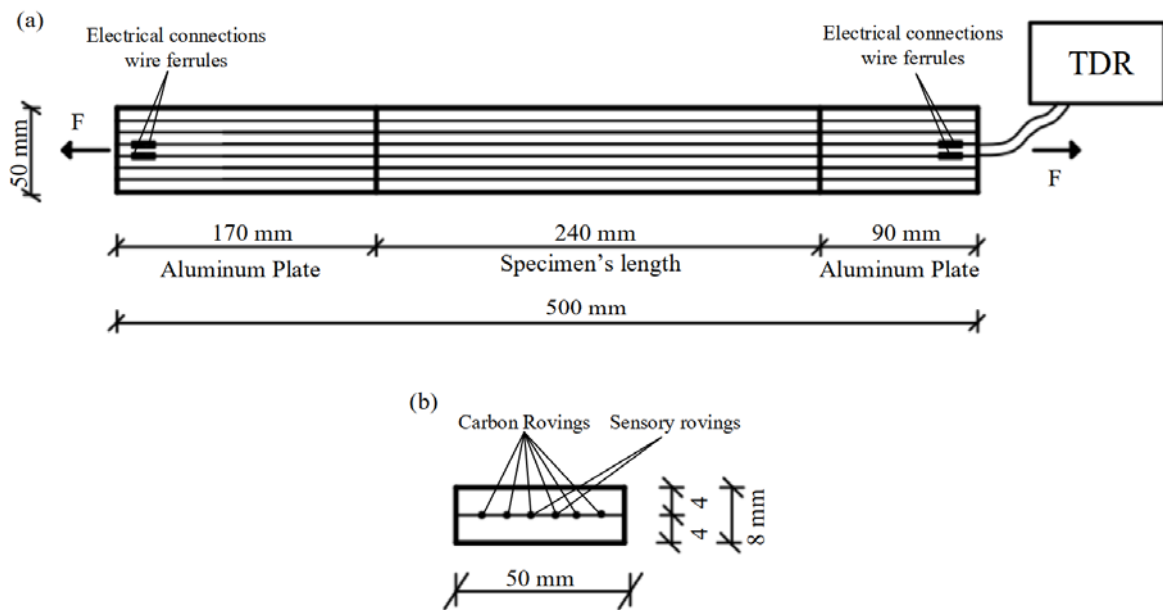


Figure 2. Experimental layout: (a) Uniaxial tensile loading beam; (b) Typical cross-section.

## SENSING CONCEPT

The study argues that by using TDR analysis, the location of damaged zones along textile reinforced MPC structures can be identified. The idea is based on sending energy pulses by an electrical current into a BNC cable. When the energy pulse encounters a damage, a portion of it is reflected. The reflection time is translated into the position of the damage. Opposed to BNC cables whose resistance per length is constant, the resistance of a carbon roving changes along the roving and depends on the structural health.

The study uses a Fieldfox Handheld Analyzer N9918B with a frequency range of 200kHz-500Mhz with 1600 reading points. Since the resistance of the carbon roving increases with the roving's length, a calibration process determines the location of the damage. The calibration is performed by a magnetic

field on a selected known zone along the element. The obtained calibrations are as follow:

$$\text{Beam A: Crack location [mm]} = 0.2231 \cdot \text{TDRindex} - 56.66 \quad (1)$$

$$\text{Beam B: Crack location [mm]} = 0.2583 \cdot \text{TDRindex} - 45.665 \quad (2)$$

The sensory process is performed by the following main three steps:

First, the measured values are determined by the following processes:

- The impedance spectrums from the TDR were measured every 1 Hz.
- The difference between every two consecutive impedance spectrums was calculated, they referred as impedance spectrum change (ISC).
- For each ISC, the peak to peak (PTP) value was calculated.

Second, the threshold values are estimated by the following process:

- The first 200 ISC were evaluated at an unloaded position and aim to estimate the noise level. The noise level evaluated by the maximum PTP of the readings (for each ISC). In our case the noise level for beam A and beam B are 0.016  $\Omega$  and 0.011  $\Omega$ , respectively.
- After the loading started, each PTP value higher than 30% of the noise level, is eligible for further investigation and considered as potential damage events.

Third, the identification of damage events is performed by:

- At the potential events the maximum PTP was investigated. Since the formation of cracks yields an integrative increase of the ISC [4,5], it is assumed that the occurrence of damage events should yield a local maximum in the ISC. In such a case, the index of the maximum PTP determines the damaged zone by the calibration presented in Eqs. [1] and [2].

## RESULTS AND DISCUSSION

Results of the experimental investigation are given in Figs. 3-6. The impedance response spectrum is measured in a frequency range of 200kHz-500MHz, with 1600 points, in a rate of 1 Hz. Fig. 3a and Fig. 5a present the load-deflection curve, the dashed vertical lines represent the formation of cracks. Cracks are considered as damage and their formation are called event #. Fig. 3b and Fig. 5b present the propagation of the cracks (measured by the DIC technique) versus the vertical deflection of beams A and B, respectively. Fig. 3c and Fig. 5c present the peak-to-peak values of the ISC for beams A and B, respectively. Therefore, the figures present the first and second main steps of the identification procedure. Fig. 4 and Fig. 6 represent a comparison between the identified position of damage by using the TDR analysis (the third step) and the actual position by using the DIC technique for beams A and B, respectively.

From the structural point of view, Fig. 3a and Fig. 5a, it is seen that both beams have similar structural responses. Beam A and beam B have four and three events, respectively. Each event represents a formation of a micro crack. The objective of the monitoring system is to identify these events.

From Fig 3c and Fig. 5c, it is seen that in both beams all the damage events are successfully identified. It is seen that in case of beam A, along

with the actual events an additional event was identified, marked in a red circle in the Fig. 3c.

According to the third step for each potential event the PTP profile and its peak was investigated. The position of the damaged zone is calculated by the obtained index and transformed to physical location by the calibration formulas. From Fig. 4a and 6a it is observed that in both beams the first damage zone is successfully identified. Yet, the locations of the next damaged zones were failed to be detected. These results are associated to the degradation of energy pulse along the carbon roving due to two main reasons: first, loss of the energy pulse after an encounter of the previous damage. In our case, a portion of the energy pulse as the first damage occurred; second, since in carbon rovings, the impedance changes along the roving, the ability to distinguish and locate damage zones that are located relatively far from the energy source reduces.

These observations demonstrate the potential of using TDR analysis to locate damaged zones in reinforced MPC structures. Yet, advanced investigation is needed to yield a robust monitoring system.

## CONCLUSIONS

The paper presented a preliminary demonstration of using TDR technique to locate cracked zones in TRC structures. The goal was to explore the ability of the technique to identify the damaged zones in TRC beams. Two specimens were loaded under uniaxial tensile loading and were monitored along the loading process. It was demonstrated that TDR technique can successfully identify the occurrence of all damage events. The first damaged zones were also successfully identified, while the exact location of the next damaged zones could not be identified. The reasons are associated to the loose of energy signal and the distance from the energy source. Despite of that, this investigation demonstrated the potential of using of TDR analysis for structural health monitoring applications. These preliminary results open the way for the development of advanced investigations that will further bring the concept of selfsensory carbon roving into realization.

**Acknowledgements:** *This research was supported by the ISRAEL SCIENCE FOUNDATION (grant No. 1663/21). The authors are thankful for the help of Eng. Barak Ofir and of the technical and administrative staff of the National Building Research Institute at the Technion. The authors acknowledge the support provided by ICL Group Ltd for providing the MPC mixture (Phosment) and by Teijin Frontier company Ltd for providing the short aramid fibers.*

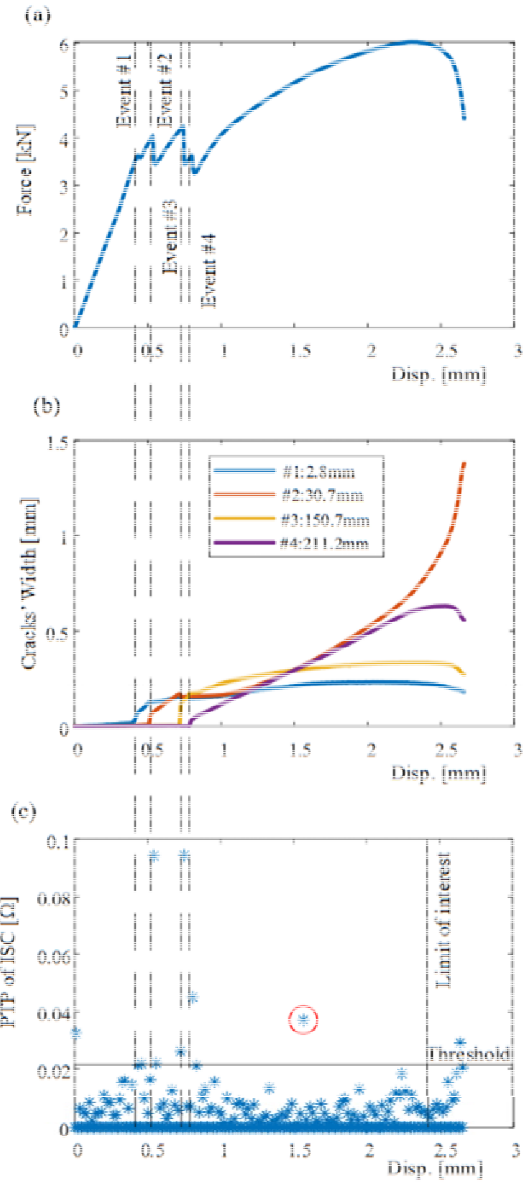


Figure 3. Mechanical and TDR analysis of Beam A: (a) Load- deflection curve; (b) PTP of ISC; (c) Cracks' propagation.

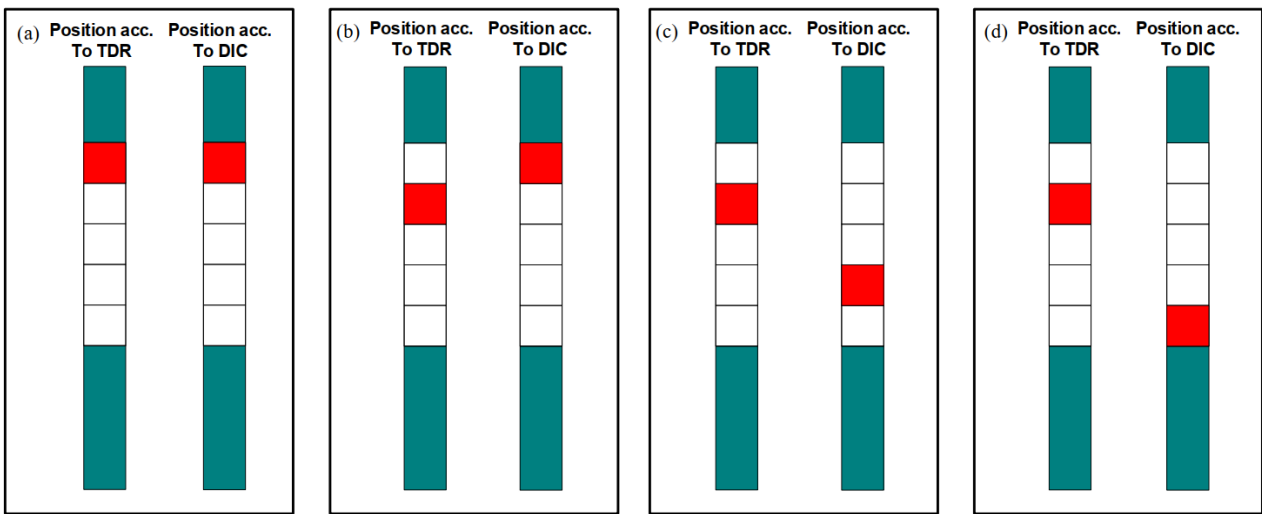


Figure 4. Position of damage comparison between the proposed method and the actual damage by DIC results for Beam A: (a) Event #1; (b) Event #2; (c) Event #3; (d) Event #4.

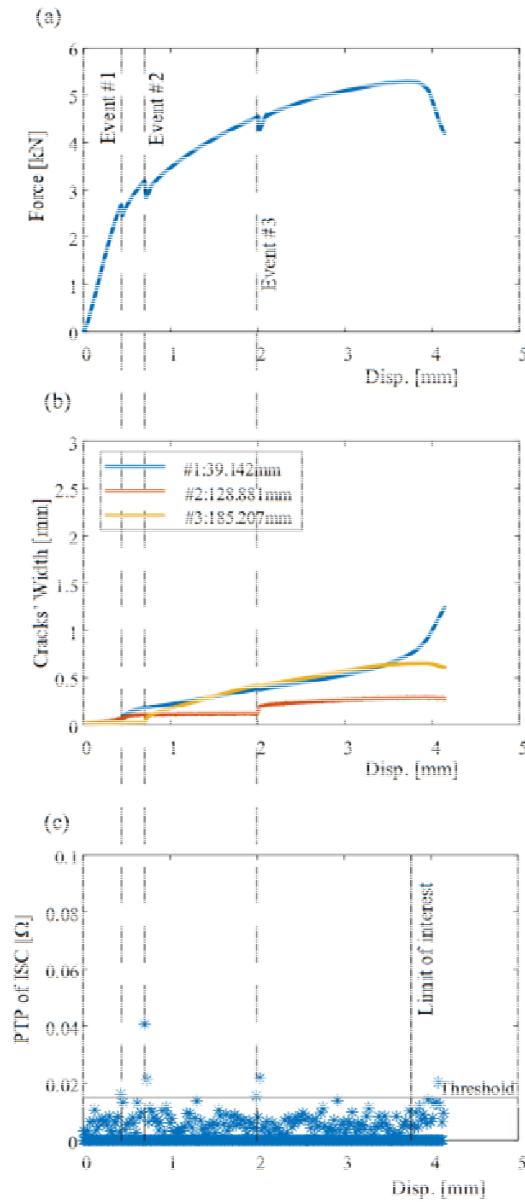


Figure 5. Mechanical and TDR analysis of Beam B: (a) Load- deflection curve (b) PTP of ISC; (c) Cracks' propagation.

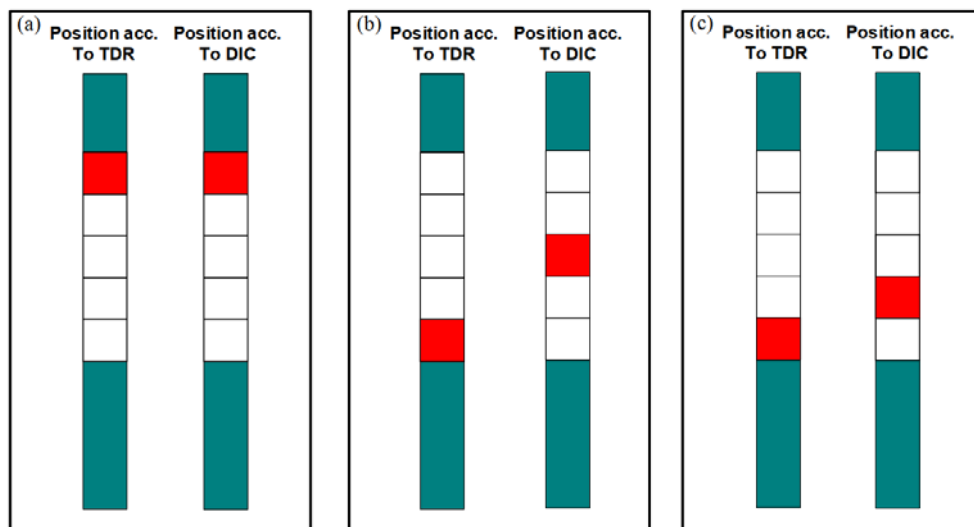


Figure 6. Position of damage comparison between the proposed method and the actual damage by DIC results for Beam B: (a) Event #1; (b) Event #2; (c) Event #3.

## REFERENCES

1. Christner, C., Horoschenkoff, A., Rapp, H., (2012). Longitudinal and transvers strain sensitivity of embedded carbon fiber sensors, *Journal of Composite Materials*. 47 (2), 155-167  
<https://doi.org/10.1177/0021998312437983>
2. De Andrade Silva, F., Butler, M., Mechtcherine, V., Zhu, D., Mobasher, B., (2011). Strain rate effect on the tensile behavior of textile-reinforced concrete under static and dynamic loading. *Materials Science and Engineering: A*, 528(3), 1727-1734.  
<http://dx.doi.org/10.1016/j.msea.2010.11.014>
3. En, B. S., (2005). 196-1. (2005). Methods of testing cement. Determination of strength. British Standards Institute.
4. Gaben, M., Goldfeld, Y., (2022). Enhanced self-sensory measurements for smart carbon-based textile reinforced cement structures. submitted for publication.  
<https://doi.org/10.1016/j.measurement.2023.112546>
5. Gaben, M., Goldfeld, Y., (2022). Self-sensory carbon-based textile reinforced concrete beams– Characterization of the structural-electrical response by AC measurements. *Sensors and Actuators A: Physical*, 334, 113322.  
<https://doi.org/10.1016/j.sna.2021.113322>
6. Goldfeld, Y., Perry, G., (2018). Electrical characterization of smart sensory system using carbon based textile reinforced concrete for leakage detection. *Materials and Structures*, 51(6), 170.  
<http://dx.doi.org/10.1617/s11527-018-1296-7>
7. Goldfeld, Y., Yosef, L., (2019). Sensing accumulated cracking with smart coated and uncoated carbon based TRC, *Measurement*. 141, 137-151.  
<https://doi.org/10.1016/j.measurement.2019.04.033>
8. Häußler-Combe, U., Hartig, J., (2007). Bond and failure mechanisms of textile reinforced concrete (TRC) under uniaxial tensile loading. *Cement and Concrete Composites*, 29(4), 279-289.  
<https://doi.org/10.1016/j.cemconcomp.2006.12.012>
9. Hegger, J., Voss, S., (2008). Investigations on the bearing behavior and application potential of textile reinforced concrete. *Engineering Structures*, 30, 2050-205.  
<https://doi.org/10.1016/J.ENGSTRUCT.2008.01.006>
10. Peled, A., Bentur, A. (2003). Fabric structure and its reinforcing efficiency in textile reinforced cement composites. *Composites Part A: Applied Science and Manufacturing*, 34(2), 107-118.  
[https://doi.org/10.1016/S1359-835X\(03\)00003-4](https://doi.org/10.1016/S1359-835X(03)00003-4)
11. Perry, G., Dittel, G., Gries, T., Goldfeld, Y., (2021). Monitoring capabilities of various smart self sensory carbon-based textiles to detect water infiltration. *Journal of Intelligent Material Systems and Structures*, 1045389X211006901.  
<https://doi.org/10.1177/1045389X211006901>
12. Quadflieg, T., Stolyarov, O., Gries, T., (2016). Carbon rovings as strain sensors for structural health monitoring of engineering materials and structures. *Journal of strain analysis for engineering design*, 51(7), 482-492.  
<https://doi.org/10.1177/0309324716655058>
13. Shames, A., Horstmann, M., Hegger, J., (2014). Experimental investigations on Textile-Reinforced Concrete (TRC) sandwich sections. *Composite Structures*, 118, 643-653.  
<http://dx.doi.org/10.1016/j.compstruct.2014.07.056>
14. Soranakom, C., Mobasher, B., (2009). Geometrical and mechanical aspects of fabric bonding and pullout in cement composites. *Materials and structures*, 42(6), 765-777.  
<http://dx.doi.org/10.1617/s11527-008-9422-6>
15. Wen, S., Wang, S., Chung, D. D. L., (1999). Carbon fiber structural composites as thermistors. *Sensors and Actuators A: Physical*, 78(2-3), 180-188.  
[https://doi.org/10.1016/S0924-4247\(99\)00240-X](https://doi.org/10.1016/S0924-4247(99)00240-X)
16. Yosef, L., Goldfeld, Y., (2020). Smart self-sensory carbon-based textile reinforced concrete structures for structural health monitoring. *Structural Health Monitoring*, 1475921720951122.  
<https://doi.org/10.1177/1475921720951122>

# INTELLIGENT TEXTILE AND FIBER REINFORCED MPC COMPOSITES FOR SHM

YOSEF LIDOR\* AND GOLDFELD YISKA

Technion - Israel institute of technology, Faculty of civil and environmental engineering, Haifa 32000, Israel

## ABSTRACT

This study develops novel intelligent composite structural elements combining three advanced technologies: magnesium phosphate cement (MPC) matrix, smart-self sensory carbon-based textile reinforcement system, and additive short-dispersed fibers. In such system, the carbon rovings simultaneously serve as the main reinforcement system and the sensory agent. The material properties of the MPC matrix include minimization of environmental effects, high flexural strength and enhanced rheological properties which is an advantage in textile reinforcement system. From the sensory point of view, MPC is electrically insulated matrix which enhances the measured electrical signal from the carbon rovings.

Experimental investigation demonstrates the advanced capabilities of the new hybrid structures. The investigation compares between the structural and electrical responses of textile reinforced MPC elements and TRC elements under flexural loading. The structural-electrical correlation enables to further explore new composite configurations and to develop enhanced smart self-sensory systems. The study demonstrates that by merging MPC mixture with textile and fiber reinforcement systems, it is possible to design and construct thin-walled, elements with advanced structural and self-sensing capabilities.

## KEYWORDS

Intelligent structures; Advanced structural response; Enhanced sensory capabilities; Textile and fiber reinforcement.

---

\* Corresponding author: Goldfeld Y., e-mail: [Yiska@technion.ac.il](mailto:Yiska@technion.ac.il)

## INTRODUCTION

The technology of textile reinforced cementitious structures (TRC) is based on the synergy between the high compressive strength of the concrete and tensile strength of the textile. The technology enables to construct thin-walled structural elements with advanced structural performance, to reduce the amount of consumed building materials, with the benefit to integrate structural health monitoring (SHM) systems [8-9,12,14,16]. To further enhance the structural and sensory capabilities of the TRC technology, the current study investigates the use of magnesium phosphate cement (MPC) which is a perfect candidate for development of smart TRC structures.

MPC is an eco-friendly material that is characterized by a high early strength [15,18], high corrosion resistance and advanced bonding with existing concretes. These qualities were mainly used for development of rapid retrofitting existing concrete structures and roads [19]. Recent studies investigated the possibility to merge MPC mixture with textile for strengthening of reinforced concrete elements [22]. Furthermore, the improved rheological and electrical properties of the MPC is

advantageous for textile reinforced composites from both structural [4] and sensory aspects [20]. The current study investigates the combination of MPC matrix with textile and fiber reinforcement systems for development of light, and optimal structural elements with integrated self-monitoring system.

Generally, textile reinforced cementitious structures are based on Portland cement (PC) matrix. The level of impregnation of the matrix into the roving cross-section affects the load transfer mechanism and govern the overall structural response [10-11,17]. It is affected by the properties of the matrix and the bundle of filaments that characterize rovings, and results in partial roving impregnation. Accordingly, the roving is usually divided into two sub rovings that called sleeve and core [21]. The load transfer mechanism of the sleeve filaments is based on adhesion with the concrete matrix, while the core filaments carry stress by cohesion with the neighboring filaments. The volume fraction of sleeve to core filaments significantly affects the overall structural response. Therefore, the research in this focus on exploring the bond mechanism and the parameters that governed it [3,13]. The resultant macrostructural response of TRC composites can be divided into four main states according to the ACK

model. State I, is the healthy state; State II, in which distributed multiple microcracks are formed, is the design state of the element; State III, in which the existing cracks expand and propagate, is related to the damage state; and State IV, in which the rovings are pulled out from the matrix, leads to failure of the element [1].

PC based TRC structures were investigated for SHM purposes such as monitoring the load pattern [2], distinguishing between micro and macro-cracks [5] and detecting accumulated damage [7]. Further research investigated the effect of textile configuration, which change the textile-matrix bond mechanism, on the SHM capabilities [6]. The current study argues that the advanced rheological and electrical properties of MPC matrix enhance the bond mechanism, and accordingly will be reflected by advanced monitoring capabilities. The study investigates three types of composites: textile reinforced PC matrix (TRC), textile reinforced MPC (TR-MPC) and TR-MPC with additive short aramid fibers. The experimental investigation is based on monotonic flexural loading tests and focuses on the effect of the composite configuration on the structural and electrical responses, and the correlation between them.

**EXPERIMENTAL INVESTIGATOIN**

**Materials**

The study aims to develop new textile reinforced composite elements, with enhanced structural and sensory capabilities. The investigation focuses on three different types of matrices: Portland cement

(PC); plain MPC; and MPC with 0.5% of additive short aramid fibers. The PC matrix is classified as a fine-grained matrix. This study uses a commercial mixture (Sika grout 214). The MPC matrix is a commercial potassium-based mixture (K-MPC) called Phosment, produced by ICL LTD. The short aramid fibers (AF) are commercial product of Teijin Fournier LTD, called Technora and their typical length is 3mm. The material properties of the AF are given in Table 1. In case of TR-MPC with additive AF, the fibers were added to the water and then mixed with the dry MPC powder.

The PC and MPC mixtures were prepared with water to dry material ratios of 1:8 and 1:4, respectively. The flexural and compression strengths of the matrices were tested at age of 28 days by using 40/40/160 mm and 50/50/50 mm specimens. The mean compression and flexural strengths and standard deviation of PC, MPC, and MPC with short AF are:  $(6.33 \pm 0.1, 67.99 \pm 0.14)$ ,  $(9.90 \pm 0.42, 69.35 \pm 1.5)$ ,  $(11.29 \pm 0.95, 72.75 \pm 2.64)$ .

The textile reinforcement is a generic glass-carbon bi-axial mesh with mesh size of 7-8 mm [4-7] The warp direction is composed of 6 AR-glass rovings and 2 carbon rovings, while in the weft direction only AR-glass rovings are positioned. The material properties of the textile and short fibers are given in Table 1.

The geometrical dimensions of the beam specimens are length 300mm, width 70mm, height 15 mm. Each beam is reinforced with a single textile layer, located 5 mm above the lower face of the beam. The textile layer is slightly pretensioned in the mold before casting, see Fig. 1.

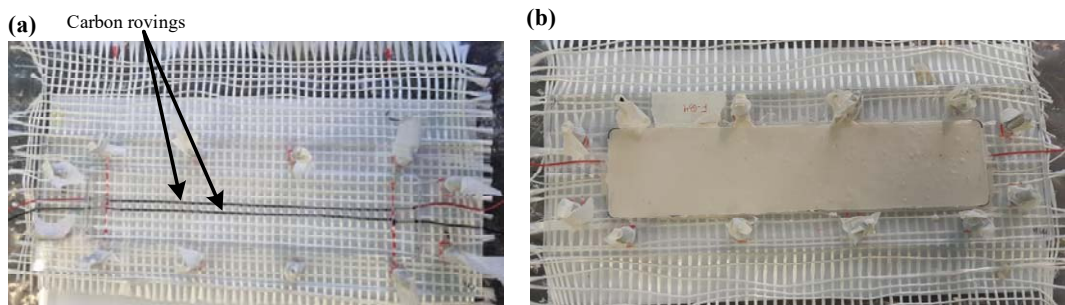


**Figure 1.** Beam specimen in the mold: (a) Before casting, (b) After casting.

**Table 1.** Material properties of the textile and short fibers [4,5].

	AR-Glass roving	Carbon roving	Aramid fibers (3 mm length)
Specific mass density [g/cm <sup>3</sup> ]	2.68	1.8	1.39
Modulus of elasticity [GPa]	72	270	65-85
Filament Tensile strength [GPa]	1.7 (elongation 2.4%)	5 (elongation 1.7%)	3.2-3.5 (elongation 3.9-4.5%)
Filament diameter	19 μm	7 μm	12 μm
Linear density [Tex]	2,400	1,600	-
Electrical resistance [W/m]	Infinity	13	Infinity

**Methods**

The study investigates three different cementitious composites: PC based TRC, textile reinforced MPC (TR-MPC) and TR-MPC with additive short fibers. The specimens were experimentally tested in monotonic flexural loading tests by using a four-points bending scheme [4-7,20]. The beams span length was 210 mm and the distance between the load points was 70 mm. The experiment is performed in a displacement control mode in loading rate of 0.1 mm/min by using an Instron loading machine (Model 5966), see Fig. 2(a). The specimens were loaded from the healthy state and up to the ultimate load capacity, the experiments were terminated at a drop of 15% of the ultimate load. The DIC method was used to monitor the displacement field at the front face of the beam, and to analyze the formation and propagation of cracks. The front face of each beam is photographed along the experiment for the DIC analysis (1 photo every 3 seconds).

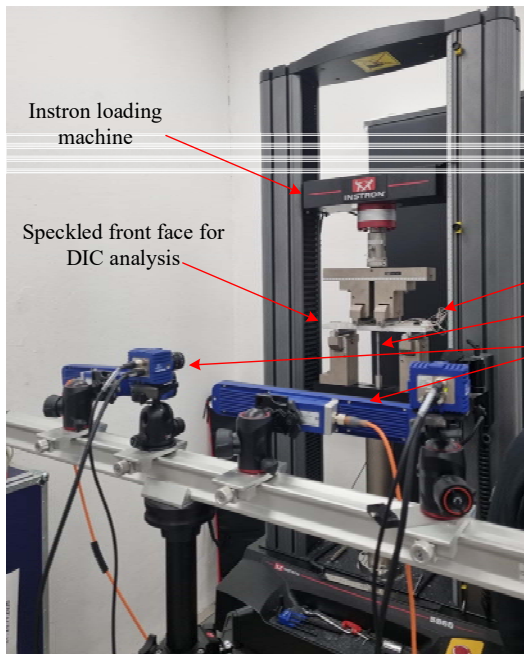
The study utilizes the piezoresistive capabilities of the carbon rovings. The sensory concept is adopted from [6] and is based on DC measurements by using a Wheatstone bridge electrical circuit. Each carbon roving functions as electrical resistor that is connected to an individual bridge. The measured voltage changes across the bridge is used to evaluate the integrative electrical resistance change (ERC) of the carbon roving, by using the following equation, see also Fig. 2(b):

$$R_x = V_{in} \frac{R_c}{V_b + \left(\frac{R_b}{R_a + R_b}\right) V_{in}} - R_c - R_d \quad (1)$$

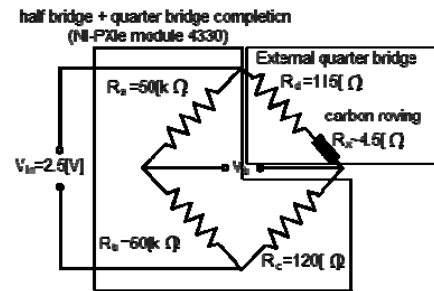
Where  $R_x$  is the rovings integrative resistance,  $V_{in}$  is the excitation voltage,  $R_a$ ,  $R_b$ ,  $R_c$ ,  $R_d$  are known resistors, and  $V_b$  is the measured voltage change across the bridge. The ERC is measured relative to the electrical resistance at the beginning of the experiment, which represents the healthy state. The study also adopts the compensation procedure of environmental parameters such as temperature and moisture by using a non-loaded reference beam [6]. Accordingly, the ERC which is solely related to structural-mechanical change is calculated as follows:

$$\Delta R = R_x - R_0 - \Delta R_{reference} \quad (2)$$

The study explores the structural performance and the structural-electrical correlation for each of the composite beams. The structural electrical correlation is based on two integrative values. The first is the ERC, which is measured over the length of roving, and the second is the strain at the front face of the beam, that is correspondingly calculated over the length of the roving. It means that according to this sensory concept, only an integrative measure of the structural health is obtained, which limit the possibility to identify the exact location of a crack. Yet, it was demonstrated that the integrative measurements yield sufficient information that can be used for SHM purposes [4-7].



(a)



(b)

**Figure 2.** (a) Experimental test setup: Specimen, loading machine and DIC system, (b) DC measurement by Wheatstone's bridge scheme [6].

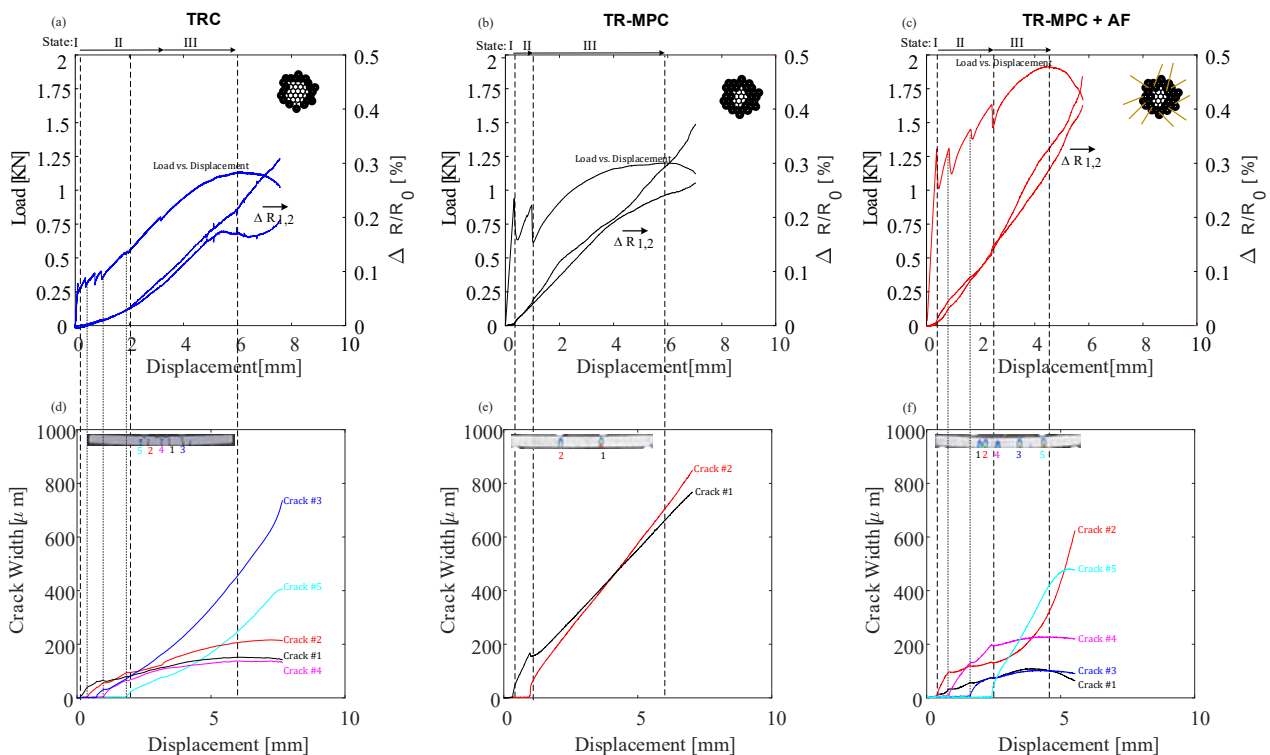
## RESULTS AND DISCUSSION

Fig. 3(a-c) presents the structural and electrical response of the three composite beams. The figure also presents the formation and propagation of cracks along the experiment, see Fig. 3 (d-f). The structural-electrical correlation is presented in Fig.4 by the measured relative ERC versus the integrative strain along the roving. The results highlight several observations:

First, from Fig. 3 it is seen the structural response of the three composites can be divided into the four main structural states that characterized textile reinforced cement beams. Yet, each beam is characterized by a different structural response. The differences between the beams are explained by the matrix properties and especially by the different bond-mechanism between the textile-fiber reinforcement and the matrix. In state I, the differences in the first cracking loads are associated with the higher flexural strength of the MPC matrix (0.92-1.3 KN for TR-MPC and 0.33 KN for the TRC). In state II, the differences are observed by the number and severity of the cracks. While in case of TRC multiple micro-cracks (up to 150 mm) are formed, in the TR-MPC the matrix is relatively brittle which result in formation of only two macro-cracks, see Fig. 3(d-e). This behavior is improved by adding short AF to the MPC matrix Fig. 3(c,f). The contribution of the short AF in this state is reflected

by higher ductility and by adding new cross links with the matrix that result in multiple microcracks and wider range of State II. In state III, the improved bond mechanism of MPC composites is expressed by enhanced strain hardening behavior and higher ultimate loads that are carried by the improved composite elements (1.21-1.91 KN for TR-MPC and 1.13 KN for the TRC).

Second, it is observed that there is a consistent increase in the ERC signal of the three specimens. Yet differences between the trend and intensity of the signals are also observed. In case of MPC based specimens (Fig. 3(b,c)) the intensity of the ERC signal is higher along the entire structural-electrical response (0.26-0.31% for TR-MPC and 0.19% for the TRC at the ultimate load). Furthermore, while in TRC specimen (Fig. 3a) the trend of the ERC is dependent on the structural state, in the TR-MPC the trend is relatively linear. These differences are associated with the structural states and the microstructural mechanism of each composite configuration. In case of TRC the mechanism is changing from sleeve controlled in state II, to core controlled in state III, while in TR-MPC the contribution of the sleeve filaments remains consistent along the entire response, see Fig. 3(b-c).



**Figure 3.** Structural and electrical response of TRC, TR-MPC and TR-MPC +AF: (a-c) load vs. displacement and ERC of the carbon rovings, (d-f) crack formation and propagation analysis.

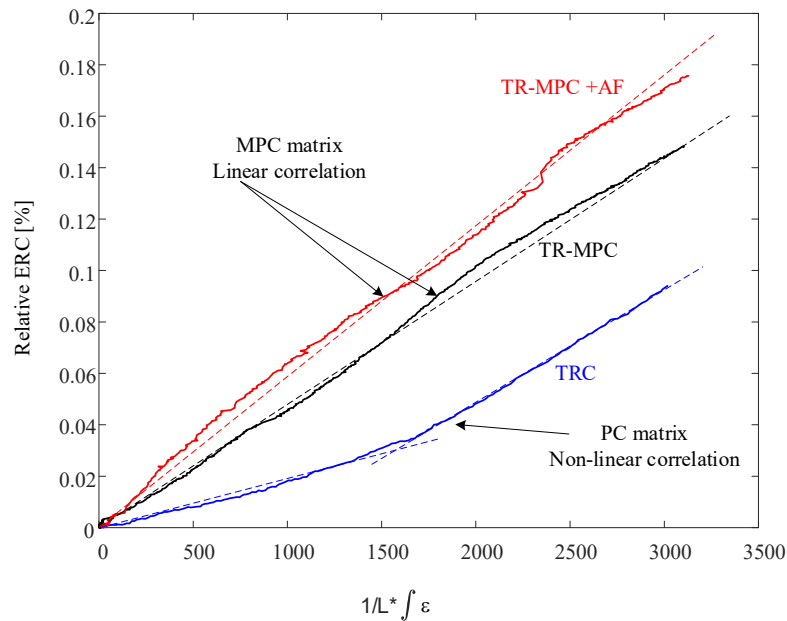


**Figure 4.** Comparison of the composites structural-electrical correlation: Linear correlation of MPC matrices and nonlinear correlation PC matrix

Third, the different composite configurations yield different structural-electrical correlations. It is associated with the bond mechanism of each composite, and especially the active sub rovings in each state, see Fig. 4. In case of TRC, the active sub-roving changes from sleeve to core (State II - State III). As a result, the structural-electrical correlation yields a non-linear correlation function [7]. In case of TR-MPC, the improved rheology is expressed by relatively high-volume fraction of sleeve filaments that are active along the response. It leads to a linear structural-electrical correlation, see Fig. 4. Furthermore, the contribution of the short AF leads to enhanced textile-matrix bond and higher ERC, which is expressed by higher trend of the structural-electrical correlation.

The above results show the advantage of MPC based composites from both the structural and sensory points of view. The improved rheological and electrical properties of the MPC matrix [4,20] result in enhanced structural response and sensing capabilities. The structural-electrical correlation reflects the unique bond mechanism of each composite.

## CONCLUSIONS

This study investigated the structural and sensory capabilities of intelligent MPC based composite elements that were made of three types of matrices: PC, MPC and MPC with short additive fibers, reinforced with glass-carbon textile. The structural and electrical behaviors of the composites were

investigated in flexural tests from a healthy state and up to the ultimate load. It is seen that the enhanced material properties of the MPC matrix resulted in advanced performance of the thin-walled element compared to the PC based TRC. The MPC based composites exhibited higher cracking loads and ultimate carrying loads. The contribution of the short fibers to the TR-MPC was expressed in enhanced cracking pattern and higher ultimate loads which indicated on the improved textile-matrix bond mechanism. Accordingly, the TR-MPC elements were characterized by enhanced sensory capabilities. It was expressed by higher ERC signal along the entire structural response, linear electrical trend, and higher SNR values. The differences in mechanical and sensory capabilities of the composites are associated with the matrix properties and the contribution of the dominant sub-roving to the structural-electrical correlation in each composite.

**Acknowledgements:** *This research was supported by the Israeli Ministry of Construction and Housing. The authors acknowledge the support provided by ICL Group Ltd for providing the MPC mixture (Phosment) and by Teijin Frontier company Ltd for providing the short aramid fibers. The authors also acknowledge the support provided to this study by the American Technion Society within the framework of the Interdisciplinary Eco-Engineering Research Center: Philip and Harriet Klein Contribution. The study was conducted at the Technion with the assistance of Eng. Barak Ofir and the technical staff of the National Building Research Institute, their help is gratefully acknowledged.*

## REFERENCES

1. Aveston J., Cooper G., Kelly A., (1971) "The properties of fibre composites", in Conference Proceedings of the National Physical Laboratory, IPC Science and Technology Press Ltd., Guildford, England, pp. 15–26
2. Christner C., Horoschenkoff A., and Rapp H. (2012). Longitudinal and transvers strain sensitivity of embedded carbon fiber sensors, *Journal of Composite Materials*, 47(2):155-167, 2012.  
<https://doi.org/10.1177/0021998312437983>
3. Gao S.L., Mäder, E. and Plonka, R. (2004). Coatings for glass fibers in a cementitious matrix, *Acta Materialia*, Vol. 52, No. 16, pp. 4745-4755.  
<http://dx.doi.org/10.1016/j.actamat.2004.06.028>
4. Goldfeld, Y., Biton, R. (2022). Experimental study of thin-walled composite elements made of magnesium phosphate cement reinforced by fibers and textile, Submitted for Publication.
5. Goldfeld, Y., Quadflieg, T., Ben-Aarosh, S., and Gries, T. (2017a). Micro and macro crack sensing in TRC beam under cyclic loading. *Journal of Mechanics of Materials and Structures*, 12(5), 579-601.  
<https://doi.org/10.2140/jomms.2017.12.579>
6. Goldfeld Y., Yosef L. (2019). Sensing accumulated cracking with smart coated and uncoated carbon based TRC, *Measurement*, 141:137-151.  
<https://doi.org/10.1016/j.measurement.2019.04.033>
7. Goldfeld Y., Yosef L. (2020). Electrical–structural characterization of smart carbon-based textile reinforced concrete beams by integrative gauge factors. *Strain*. 2020;56:e12344  
<https://doi.org/10.1111/str.12344>
8. Hegger J. and Voss S., "Investigations on the bearing behavior and application potential of textile reinforced concrete." *Eng. Struct.* 30 (7) (2008) 2050–2056.
9. Hegger J., Kulas C., Raupach M. And Büttner T., "Tragverhalten und Dauerhaftigkeit einer schlanken Textilbetonbrücke". *Beton- und Stahlbetonbau* 106 (2) (2011b) 72–80.  
<http://dx.doi.org/10.1002/best.201000082>
10. Lepenies, I., Meyer, C., Schorn, H., & Zastrau, B. (2007). Modeling of load transfer behavior of AR-glass-rovings in textile reinforced concrete. *Special Publication*, 244, 109-124.
11. Mobasher, B., Peled, A., and Pahilajani, J., Pultrusion of fabric reinforced high fly ash blended cement composites, in Sixth Rilem Symposium on Fibre-Reinforced Concrete (FRC), BEFIB 2004, Varenna, Italy, September 20–22, 2004.
12. Mobasher B., Dey, V., Cohen, Z., and Peled A. (2014) "Correlation of constitutive response of hybrid textile reinforced concrete from tensile and flexural tests", *Cement & Concrete Composites*, 53:148-161.  
<https://doi.org/10.1016/j.cemconcomp.2014.06.004>
13. Perry, G., Dittel, G., Gries, T., and Goldfeld, Y. (2020). Mutual effect of textile binding and coating on the structural performance of TRC beams. *Journal of Materials in Civil Engineering*, 32(8), 04020232.  
[http://dx.doi.org/10.1061/\(ASCE\)MT.1943-5533.0003331](http://dx.doi.org/10.1061/(ASCE)MT.1943-5533.0003331)
14. Silva F. D. A., Butler M., Mechtcherine V., Zhu D., and Mobasher B.. "Strain rate effect on the tensile behavior of textile-reinforced concrete under static and dynamic loading". *Mater. Sci. Eng.* 528 (3) (2011) 1727–1734.  
<http://dx.doi.org/10.1016/j.msea.2010.11.014>
15. Sugama T., and Kukacka L.E. (1983). Characteristics of magnesium polyphosphate cements derived from ammonium polyphosphate solutions. *Cement and Concrete Research* Vol. 13, pp. 499-506.  
[https://doi.org/10.1016/0008-8846\(83\)90008-X](https://doi.org/10.1016/0008-8846(83)90008-X)
16. Tysmans T., Adriaenssens S., Wastiels J., "Form finding methodology for force modelled anticlastic shells in glass fibre textile reinforced cement composites". *Eng Struct* 33 (2011) 2603–11.  
<http://dx.doi.org/10.1016/j.engstruct.2011.05.007>
17. Tysmans, T., Adriaenssens, S., Cuypers, H., and Wastiels, J., Structural analysis of small span textile reinforced concrete shells with double curvature, *Composites Science and Technology*, 69, 1790–1796, 2009.  
<http://dx.doi.org/10.1016/j.compscitech.2008.09.021>
18. Walling S.A., and Provis J. L. (2016). A discussion of the papers "Impact of hydrated magnesium carbonate additives on the carbonation of reactive MgO cements" and "Enhancing the carbonation of MgO cement porous blocks through improved curing conditions", by C Unluer and A Al-Tabbaa". *Cem. Concr. Res.* 79 (2016) 424–426.  
<http://dx.doi.org/10.1016/j.cemconres.2015.09.010>
19. Yang Q., Zhu B., Wu X., (2000). "Characteristics and durability test of magnesium phosphate cement-based material for rapid repair of concrete". *Materials and Structures* 33 (4) (2000) 229-234.  
<http://dx.doi.org/10.1007/BF02479332>
20. Yosef L., Goldfeld Y., (2022). "Effect of Matrix Electrical and Micro-Structural Properties on the Self-Sensory Capabilities of Carbon-Based Textile Reinforced Composites", submitted for publication.  
<https://doi.org/10.1016/j.jobe.2023.105909>
21. Zastrau, B., Lepenies, I., & Richter, M. (2008). On the multi scale modeling of textile reinforced concrete. *Technische Mechanik-European Journal of Engineering Mechanics*, 28(1), 53-63.
22. Zhu C.J., Fang S., Ng P.L., Pundliene I., and Chen J.J, (2020). "Flexural Behavior of Reinforced Concrete Beams Strengthened by Textile Reinforced Magnesium Potassium Phosphate Cement Mortar". *Front. Mater.* 7:272.  
<https://doi.org/10.3389/fmats.2020.00272>

# THE EFFECT OF POLYMER TYPE AND FIBER ORIENTATION ON THE COMPLIANCE PROPERTIES OF ELECTROSPUN VASCULAR GRAFTS

OZDEMIR SUZAN\*, OZTEMUR JANSET, SEZGIN HANDE AND YALCIN-ENIS IPEK

Istanbul Technical University, Textile Engineering Department, Istanbul, Turkey

## ABSTRACT

Vascular diseases are a major source of fatalities globally. However, the lack of accessibility of autologous vessels and the poor efficacy of commercial small-diameter vascular grafts limit surgical alternatives. Researchers therefore aimed to develop vascular prostheses that meet all requirements. Apart from the benefits of tissue-engineered grafts, significant obstacles that still hinder successful grafting include compliance mismatch, dilatation, thrombus development, and the absence of elastin. Among these issues, compliance mismatch between native vessel and artificial vascular scaffold has been mentioned in the literature as a possible cause of intimal hyperplasia, suture site rupture and endothelial and platelet cell damage. As a result, the usage of suitable materials and optimized fabrication techniques are required to achieve better control over the characteristics and functionality of the grafts. In particular, in the case of electrospun vascular grafts, the compliance can be adjusted throughout a broad range of values by adjusting the electrospinning parameters such as material selection, fiber orientation, porosity, and wall thickness. In this study, the electrospun vascular grafts consisting of pure PCL, PLA, and their blends were produced by using two different rotation speeds to achieve the oriented and non-oriented scaffolds. The impact of polymer type and fiber orientation on the compliance properties was evaluated. The results revealed that both material selection and fiber alignment have a significant effect on the compliance levels. PCL100\_R grafts had the highest compliance value whereas the PCLPLA50\_O scaffold had the lowest.

## KEYWORDS

Vascular grafts; Electrospinning; Compliance mismatch; Intimal hyperplasia.

\* Corresponding author: Ozdemir S., e-mail: [ozdemirsu@itu.edu.tr](mailto:ozdemirsu@itu.edu.tr)

## INTRODUCTION

Cardiovascular diseases, which account for 32% of all fatalities worldwide, will continue to be the leading global cause of disability and death, according to experts' predictions for the future [1, 2]. There is an urgent and significant need in clinics for tissue engineered small-diameter (<6 mm) blood vessel substitutes due to a lack of availability of autologous vessels and effective commercial products used for bypass surgeries, such as vascular prostheses made of polyethylene terephthalate (PET) or expanded polytetrafluoroethylene (ePTFE), which have low clinical efficacy and a high failure rate after implantation [3, 4].

Tissue engineering faces a great challenge when attempting to replicate the unique design and distinctive mechanical characteristics of the vascular wall in order to fulfill the functional needs of the native tissue [5]. There are several design criteria that affect the properties of vascular grafts, including material selection and constructional parameters including fiber diameters, pore sizes, fiber

orientation, wall thickness, and etc. [6]. In tissue engineering applications, the selection of biomaterials has an important role in providing the basic structure for mechanical properties, cell interactions, biocompatibility, biodegradability, anti-toxicity, and cell growth [7]. While natural biodegradable polymers are very successful in biocompatibility and cell activities, synthetic polymers stand out with their properties such as high strength and controllable degradation rate. Each biopolymer has advantages as well as drawbacks that need to be addressed, and the necessity of combining two or more polymers has been raised as a solution [8]. Polycaprolactone (PCL), which has a highly flexible structure and a long biodegradation period to allow the scaffold enough time for the formation of neo-tissue, is highly demanded for tissue engineering applications [9]. On the other hand, polylactic acid (PLA) is a biomaterial that is usually favored due to its great biocompatibility and outstanding mechanical qualities. However, PCL has lower biocompatibility than PLA, and factors like the brittleness of PLA make the combination of these

two materials appealing [10]. Surface production methods and parameters are as important as the selection of biomaterials for the applicability of scaffolds. Electrospinning method is a frequently preferred surface fabrication technique for obtaining three-dimensional structures in different constructions by the modification of various collector systems because it is a simple mechanism to adjust the fiber diameter, pore size and wall thickness of the samples, to obtain fiber orientation, and to facilitate the use of many biopolymers [11]. Thus, all the production parameters should be determined clearly to manufacture the ideal vascular graft that has sufficient characteristics that contribute to the material's performance.

In literature, morphological and biological studies are typically given top priority, whereas mechanical aspects are typically just briefly discussed. To improve the clinical efficacy of vascular grafts exposed to physiological stresses and avoid graft failure due to intimal hyperplasia, thrombosis, aneurysm, blood leakage, and occlusion, sufficient mechanical characteristics that are equivalent to native vessels must be achieved for grafts [12]. The mechanical properties of the scaffold, such as suturability, compliance, tensile strength, burst pressure, and blood permeability, are significantly influenced by the material and architecture of the scaffold [13]. In particular, one of the main reasons for graft failure over extended periods of implantation is compliance mismatch between the native artery and the inelastic artificial graft at the anastomosis sites, which produces low blood flow rates and turbulent blood flow in small-diameter vascular prostheses [14]. The blood flow fluctuations in the vascular scaffold and the stress concentration at the anastomosis regions are caused by the incompatible dimension changes of the vascular prosthesis and the native blood vessel as a reaction to pressure variations inside the lumen, which is known as compliance mismatch [15]. Low patency rates are caused by these mechanical problems, which also contribute to the scaffold material's thrombogenicity, inadequate endothelialization, luminal constriction, and thrombosis, which are triggered by intimal hyperplasia [14]. It is notably difficult to create vascular prostheses that are both elastic and strong enough to resist blood pressure because burst strength and compliance are frequently inversely proportional [16]. Numerous studies in the literature demonstrate that the compliance is determined by the material selection and construction characteristics, such as wall thickness, the number of layers, and the orientation of the fibers within the layers [17-19]. Johnson et al. (2015) produced vascular grafts from various

polymers and wall thicknesses. The compliance values revealed that both the polymer type and wall thickness were effective on the compliance levels. An increase in wall thickness reduced the compliance values, whereas using flexible materials improved the results [17]. Li et al. (2017) designed composite vascular graft prototypes by integrating a flexible PLA knitted fabric as an inner layer with a soft PCL matrix as an outer layer. The compliance value of all the samples was found to be below 2%/100 mmHg [20]. Also, the measured compliance values of some of the native human blood vessels are given in Table 1.

**Table 1.** Compliance values of native human blood vessels.

Type of Blood Vessel	Compliance	References
Saphenous vein	1.5%/100 mmHg	[21]
Coronary artery	0.0725%/mmHg	[22]
Femoral artery	3.8–6.5%/100mmHg	[23]

In this study, both the radially-oriented and randomly-distributed electrospun fibrous vascular grafts that were made of neat PCL, PLA, and their blend with a weight ratio of 50:50 were fabricated to assess the impact of the polymer selection and the fiber orientation on the compliance properties.

## EXPERIMENTAL STUDY

### Materials

The neat or the blended form of PCL (Mn 80,000) and PLA (Mn 230,000; Ingeo 2003 D with 4.3 mol% D-lactide content) were dissolved in a solvent system consisting of chloroform (CH)/acetic acid (AA)/ethanol (ETH) with 8/1/1 wt. at a concentration of 8% w/w. All the polymers and the solvents were supplied from the Sigma Aldrich.

### Methods

#### Surface fabrication

The prepared neat PCL, neat PLA and PCL/PLA (50:50) solutions were stirred for 4 hours with a magnetic stirrer and immediately electrospun by using electrospinning system supplied from Inovenso, Turkey (Nanospinner, Ne100<sup>+</sup>). The neat and blended polymer solutions were transferred by a 10 ml plastic syringe through a distance from the needle tip which was kept at 20 cm. The mandrel with a rotational speed of 200 rpm and 10000 rpm were used for the fabrication of tubular scaffolds with randomly distributed and radially oriented fibers, respectively. Tubular scaffolds have 6mm inner diameter and the spinning time for all samples was fixed at 40 minutes. The sample codes and details are given in Table 2.

**Table 2.** Samples codes and details.

Sample codes	Blending ratio of PCL/PLA (%)	Rotational speed of the collector (rpm)	Fiber orientation
PCL100_R	100/0	200	Randomly distributed
PCL100_O	100/0	10000	Radial orientation
PCLPLA50_R	50/50	200	Randomly distributed
PCLPLA50_O	50/50	10000	Radial orientation
PLA100_R	0/100	200	Randomly distributed
PLA100_O	0/100	10000	Radial orientation

### Compliance

The custom-designed device used to test compliance provided air flow at a physiologically equivalent pressure. After the balloon was inserted through the samples, they were mounted by the sleeves to the nozzles and supplied with air from the system. The pulsatile intraluminal pressure was established at the diastolic and systolic pressures of 80 mmHg and 120 mmHg, respectively. The photos of the samples at these pressures were taken by a camera system, and the diameters at each pressure were measured by the Image J software system. After that, the compliance values were calculated by the formula below;

$$\%compliance = \frac{R_{p2} - R_{p1}}{P_2 - P_1} \times 10^4 \quad (1)$$

$R_{p1}$  = pressurized radii at diastolic pressure [mm]  
 $R_{p2}$  = pressurized radii at systolic pressure [mm]  
 $p_1$  = diastolic pressure [mmHg]  
 $p_2$  = systolic pressure [mmHg]

### RESULTS AND DISCUSSION

The compliance values of each sample group were given with their standard deviations in Table 3. It was clearly observed from the results that the radial fiber orientation reduced the compliance values of the scaffolds. This situation was expected as the oriented fibers are already under stress in that direction and they cannot be stretched as in the randomly oriented fibers [3]. Grasl et al. (2021) also manufactured electrospun vascular grafts made of polyurethane (PU) and PLLA with fiber orientations in different directions and measured the compliance values. It was observed that in PU samples, fiber orientation in any direction caused a reduction in compliance values, whereas PLLA showed similar compliance levels in any direction because of its stiff structure. For example, in PU scaffolds with radially oriented fibers, the compliance was  $4.1 \pm 0.4$  mmHg %/100 mmHg whereas it was  $29.7 \pm 5.5$  mmHg %/100 mmHg in the PU scaffolds with randomly distributed fibers. On the other hand, in PLLA samples the compliance was  $1.3 \pm 0.4$  mmHg %/100

mmHg for the radial orientation whereas it was  $1.4 \pm 0.4$  mmHg %/100 mmHg for the samples with no fiber orientation [24].

On the other hand, scaffolds made of PCL have the highest compliance values in all directions, whereas blended scaffolds showed the lowest compliance among all the samples. As the PCL is a flexible and pliable biopolymer with high strain values, higher compliance results were expected from the PCL100 scaffolds. In addition, PLA is a brittle and stiff material with lower elongation values, PLA100 showed lower compliance than PCL prostheses [25]. In the PCLPLA50 samples, the lowest compliance values were observed because of the mechanical failure caused by the immiscible characteristics of the polymer components. As the blending cannot be reached properly, the phase separation occurs because of the weak adhesion forces between the polymer chains in these scaffolds during the electrospinning process [26].

When the obtained compliance values were compared with the values of the native vessels, it was clear that compliance values of the samples of randomly distributed fibers were higher than those of the saphenous vein and coronary artery, with a compliance of 1.5%/100 mmHg and 0.0725%/mmHg, respectively [21,22]. Additionally, oriented samples also had higher compliance values than the coronary artery. Despite the fiber orientation lowers the compliance, it also known that it contributes to mechanical characteristics of the scaffolds such as tensile strength and burst pressure [27]. Thus, both of the structures can be utilized for different approaches in multilayer vascular graft strategies.

**Table 3.** Compliance values of the scaffolds at a pressure range of 80 -120 mmHg.

Sample codes	Compliance $\pm$ SD (%/100 mmHg)
PCL100_R	2,494 $\pm$ 0,791
PCL100_O	1,155 $\pm$ 0,553
PCLPLA50_R	1,542 $\pm$ 0,783
PCLPLA50_O	0,864 $\pm$ 0,350
PLA100_R	1,603 $\pm$ 1,326
PLA100_O	1,078 $\pm$ 0,353

## CONCLUSIONS

In this study, PCL, PLA, and PCL/PLA blended samples were fabricated by using two rotational speeds to achieve scaffolds with randomly distributed and radially oriented fibers. The effect of the polymer type and the fiber orientation of the samples was confirmed by the compliance test results. It was seen that PCL100\_R had the highest compliance value among all the samples, as it has much more elastomeric polymer and fibers without high tension. On the other hand, the PCLPLA50\_O sample had the lowest compliance values because of the incompatibility of the polymer blending and stretched fibers by orientation. Although the samples with randomly oriented fibers had adequate compliance levels, combining the advantages of both structures by designing multilayered grafts should be considered to optimize the other mechanical and biological characteristics of these scaffolds.

**Acknowledgements:** This study is funded by TUBITAK Project (Grant no:121M089) and ITU Scientific Research Project (Grant no: 43368).

## REFERENCES

- Fayon, A., Menu, P., & el Omar, R. (2021). Cellularized small-caliber tissue-engineered vascular grafts: looking for the ultimate gold standard. In *npj Regenerative Medicine* (Vol. 6, Issue 1). Nature Research. <https://doi.org/10.1038/s41536-021-00155-x>
- Tran, N., Le, A., Ho, M., Dang, N., Thi Thanh, H. H., Truong, L., Huynh, D. P., & Hiep, N. T. (2020). Polyurethane/polycaprolactone membrane grafted with conjugated linoleic acid for artificial vascular graft application. *Science and Technology of Advanced Materials*, 21(1), 56–66. <https://doi.org/10.1080/14686996.2020.1718549>
- Nezarati, R. M., Eifert, M. B., Dempsey, D. K., & Cosgriff-Hernandez, E. (2015). Electrospun vascular grafts with improved compliance matching to native vessels. *Journal of Biomedical Materials Research - Part B Applied Biomaterials*, 103(2), 313–323. <https://doi.org/10.1002/jbm.b.33201>
- Ye, L., Takagi, T., Tu, C., Hagiwara, A., Geng, X., & Feng, Z. (2021). The performance of heparin modified poly( $\epsilon$ -caprolactone) small diameter tissue engineering vascular graft in canine—A long-term pilot experiment in vivo. *Journal of Biomedical Materials Research - Part A*, 109(12), 2493–2505. <https://doi.org/10.1002/jbm.a.37243>
- Nerem, R. M., & Seliktar, D. (2001). Vascular tissue engineering. In *Annual Review of Biomedical Engineering* (Vol. 3, pp. 225–243). <https://doi.org/10.1146/annurev.bioeng.3.1.225>
- Yalcin Enis, I., & Gok Sadikoglu, T. (2018). Design parameters for electrospun biodegradable vascular grafts. In *Journal of Industrial Textiles* (Vol. 47, Issue 8, pp. 2205–2227). SAGE Publications Ltd. <https://doi.org/10.1177/1528083716654470>
- Yu, E., Mi, H. Y., Zhang, J., Thomson, J. A., & Turng, L. S. (2018). Development of biomimetic thermoplastic polyurethane/fibroin small-diameter vascular grafts via a novel electrospinning approach. *Journal of Biomedical Materials Research - Part A*, 106(4), 985–996. <https://doi.org/10.1002/jbm.a.36297>
- Shalumon, K. T., Deepthi, S., Anupama, M. S., Nair, S. v., Jayakumar, R., & Chennazhi, K. P. (2015). Fabrication of poly (l-lactic acid)/gelatin composite tubular scaffolds for vascular tissue engineering. *International Journal of Biological Macromolecules*, 72, 1048–1055. <https://doi.org/10.1016/j.ijbiomac.2014.09.058>
- Mohamed, R. M., & Yusoh, K. (2015). A Review on the Recent Research of Polycaprolactone (PCL). *Advanced Materials Research*, 1134, 249–255. <https://doi.org/10.4028/www.scientific.net/amr.1134.249>
- Patrício, T., Domingos, M., Gloria, A., & Bártolo, P. (2013). Characterisation of PCL and PCL/PLA scaffolds for tissue engineering. *Procedia CIRP*, 5, 110–114. <https://doi.org/10.1016/j.procir.2013.01.022>
- Li, S., Sengupta, D., & Chien, S. (2014). Vascular tissue engineering: From in vitro to in situ. In *Wiley Interdisciplinary Reviews: Systems Biology and Medicine* (Vol. 6, Issue 1, pp. 61–76). <https://doi.org/10.1002/wsbm.1246>
- Johnson, R., Ding, Y., Nagiah, N., Monnet, E., & Tan, W. (2019). Coaxially-structured fibres with tailored material properties for vascular graft implant. *Materials Science and Engineering C*, 97, 1–11. <https://doi.org/10.1016/j.msec.2018.11.036>
- Hasan, A., Memic, A., Annabi, N., Hossain, M., Paul, A., Dokmeci, M. R., Dehghani, F., & Khademhosseini, A. (2014). Electrospun scaffolds for tissue engineering of vascular grafts. In *Acta Biomaterialia* (Vol. 10, Issue 1, pp. 11–25). Elsevier Ltd. <https://doi.org/10.1016/j.actbio.2013.08.022>
- Hiob, M. A., She, S., Muiznieks, L. D., & Weiss, A. S. (2017). Biomaterials and Modifications in the Development of Small-Diameter Vascular Grafts. *ACS Biomaterials Science and Engineering*, 3(5), 712–723. <https://doi.org/10.1021/acsbiomaterials.6b00220>
- Zhang, Y., Li, X. S., Guex, A. G., Liu, S. S., Müller, E., Malini, R. I., Zhao, H. J., Rottmar, M., Maniura-Weber, K., Rossi, R. M., & Spano, F. (2017). A compliant and biomimetic three-layered vascular graft for small blood vessels. *Biofabrication*, 9(2). <https://doi.org/10.1088/1758-5090/aa6bae>
- Fernández-Colino, A., Wolf, F., Rütten, S., Schmitz-Rode, T., Rodríguez-Cabello, J. C., Jockenhoevel, S., & Mela, P. (2019). Small Caliber Compliant Vascular Grafts Based on Elastin-Like Recombinamers for in situ Tissue Engineering. *Frontiers in Bioengineering and Biotechnology*, 7. <https://doi.org/10.3389/fbioe.2019.00340>
- Devan Ohst, J. J. (2015). Development of Novel, Bioresorbable, Small-Diameter Electrospun Vascular Grafts. *Journal of Tissue Science & Engineering*, 06(02). <https://doi.org/10.4172/2157-7552.1000151>
- Kim, S. H., Mun, C. H., Jung, Y., Kim, S. H., Kim, D. I., & Kim, S. H. (2013). Mechanical properties of compliant double layered poly(L-lactide-co- $\epsilon$ - caprolactone) vascular graft. *Macromolecular Research*, 21(8), 886–891. <https://doi.org/10.1007/s13233-013-1095-5>
- Matsuda, T., Ihara, M., Inoguchi, H., Kwon, I. K., Takamizawa, K., & Kidoaki, S. (2005). Mechano-active scaffold design of small-diameter artificial graft made of electrospun segmented polyurethane fabrics. *Journal of Biomedical Materials Research - Part A*, 73(1), 125–131. <https://doi.org/10.1002/jbm.a.30260>
- Li, C., Wang, F., Douglas, G., Zhang, Z., Guidoin, R., & Wang, L. (2017). Comprehensive mechanical characterization of PLA fabric combined with PCL to form a composite structure vascular graft. *Journal of the Mechanical Behavior of Biomedical Materials*, 69, 39–49. <https://doi.org/10.1016/j.jmbbm.2016.11.005>
- McClure, M. J., Simpson, D. G., & Bowlin, G. L. (2012). Tri-layered vascular grafts composed of polycaprolactone, elastin, collagen, and silk: Optimization of graft properties. *Journal of the Mechanical Behavior of Biomedical Materials*, 10, 48–61. <https://doi.org/10.1016/j.jmbbm.2012.02.026>
- Bouchet, M., Gauthier, M., Maire, M., Aji, A., & Lerouge, S. (2019). Towards compliant small-diameter vascular

- grafts: Predictive analytical model and experiments. *Materials Science and Engineering C*, 100, 715–723.  
<https://doi.org/10.1016/j.msec.2019.03.023>
23. Xing, M. Y., Yu, C. L., Wu, Y. F., Wang, L., & Guan, G. P. (2020). Preparation and characterization of a polyvinyl alcohol/polyacrylamide hydrogel vascular graft reinforced with a braided fiber stent. *Textile Research Journal*, 90(13–14), 1537–1548.  
<https://doi.org/10.1177/0040517519896753>
24. Grasl, C., Stoiber, M., Röhrich, M., Moscato, F., Bergmeister, H., & Schima, H. (2021). Electrospinning of small diameter vascular grafts with preferential fiber directions and comparison of their mechanical behavior with native rat aortas. *Materials Science and Engineering C*, 124.  
<https://doi.org/10.1016/j.msec.2021.112085>
25. Zahedi, P., Karami, Z., Rezaeian, I., Jafari, S. H., Mahdavian, P., Abdolghaffari, A. H., & Abdollahi, M. (2012). Preparation and performance evaluation of tetracycline hydrochloride loaded wound dressing mats based on electrospun nanofibrous poly(lactic acid)/poly( $\epsilon$ -caprolactone) blends. *Journal of Applied Polymer Science*, 124(5), 4174–4183.  
<https://doi.org/10.1002/app.35372>
26. Carvalho, J. R. G., Conde, G., Antonioli, M. L., Dias, P. P., Vasconcelos, R. O., Taboga, S. R., Canola, P. A., Chinelatto, M. A., Pereira, G. T., & Ferraz, G. C. (2020). Biocompatibility and biodegradation of poly(lactic acid) (PLA) and an immiscible PLA/poly( $\epsilon$ -caprolactone) (PCL) blend compatibilized by poly( $\epsilon$ -caprolactone-*b*-tetrahydrofuran) implanted in horses. *Polymer Journal*, 52(6), 629–643.  
<https://doi.org/10.1038/s41428-020-0308-y>
27. Ozdemir, S., Yalcin-Enis, I., Yalcinkaya, B., & Yalcinkaya, F. (2022). An Investigation of the Constructional Design Components Affecting the Mechanical Response and Cellular Activity of Electrospun Vascular Grafts. *Membranes*, 12(10), 929.  
<https://doi.org/10.3390/membranes12100929>

# A PRELIMINARY STUDY EXAMINING THE BURST STRENGTH OF VASCULAR TUBULAR SCAFFOLDS

OZTEMUR JANSET\*, ÖZDEMİR SUZAN, SEZGIN HANDE AND YALCIN-ENIS IPEK

Istanbul Technical University, Textile Engineering Department, Istanbul, Turkey

## ABSTRACT

In this study, neat PCL, neat PLA and PLA/PCL (50/50) based tubular surfaces are produced by electrospinning to simulate the native blood vessel structure and to investigate the effects of both graft material and fiber orientation on burst strength. The burst pressure values of these vascular graft structures that designed with both randomly oriented fibers and oriented fibers, measured by a custom-burst pressure tester, and the results are compared. The results show that fiber orientation have a great influence on burst pressure, regardless of the type of biomaterial. It is determined that grafts with oriented fibers have at least twice the burst strength than those with random fibers. The findings indicate that changing the graft material has also an effect on burst strength. When the results are analyzed by polymer type, although the PLA100\_O sample has the highest burst strength among all oriented fiber sample groups, it is better to determine the vascular graft candidate by taking into account radial elasticity.

## KEYWORDS

Vascular graft; Fiber orientation; Burst pressure; Mechanical properties; Electrospinning.

---

\* Corresponding author: Oztemur J., e-mail: [oztemurj@itu.edu.tr](mailto:oztemurj@itu.edu.tr)

## INTRODUCTION

According to data from the World Health Organization, among various chronic and non-chronic diseases, cardiovascular diseases have a mortality rate of 31%, making them the most common cause of death [1]. Although blood vessel replacement is the most popular and recommended treatment for cardiovascular diseases, its usage is constrained due to a shortage of accessible vessel resources, donor site morbidity, vasoplasma problems, dimensional incompatibility, and poor quality [2]. Vascular grafts now assist the development of the native artery by enabling surviving cells to adhere, develop, and proliferate. While materials like polyethylene terephthalate (PET), polytetrafluoroethylene (PTFE), and polyurethane (PU) have been effectively employed in large-diameter grafts in the past, an adequate success rate for small-caliber grafts has not been attained [3]. The use of these materials in small-diameter vascular grafts results in large-scale thrombosis (tendency to produce clots), restenosis (stenosis of the vessel and consequent blood flow limitation), and various infections. They also have properties like insufficient structural porosity, insufficient cell adhesion and proliferation, and low

level radial elasticity [4]. For this reason, researchers are looking for novel vascular graft materials that can imitate the injured artery in all of its characteristics.

Due to its exceptional mechanical qualities, including high elongation, slow biodegradation time, biocompatibility, and cell survival, polycaprolactone (PCL) is a particularly desirable material for vascular graft applications [5]. Moreover, another aliphatic polyester, polylactic acid (PLA), is also in demand because of its high strength, biocompatibility, and biodegradability [6].

On the other hand, vascular grafts are successful to the extent that they can mimic native vessels and approximate the artificial tissue to native tissues in all their properties. The designed vascular grafts should match the native vascular structure, which is a very complex structure, in terms of physical, histological, topographic and biological properties as well as mechanical properties [7]. The vascular structure, which is subjected to many loads such as blood pressure and stress cycling, must have burst strength to prevent aneurysmal expansion [8]. The burst pressure values of the saphenous artery and the internal mammary artery can be seen in Table 1 (Table 1).

**Table 1.** Burst strength values of native human blood vessels.

Type of Blood Vessel	Burst Pressure (mmHg)	Reference
Saphenous vein	1599±877	[9,10]
Internal mammary artery	3196±1264	[9]

Studies on vascular graft designs that include burst strength are regularly reported in the literature. The burst strength values in the study by Gao et al. (2019), in which they developed PCL and poly(lactide-co-glycolide) (PLGA) blend-based vascular grafts, were found to be extremely similar to the human blood vessel strength properties, and the burst resistance was over 1500 mmHg [11]. Yalcin-Enis et al. (2017) designed surfaces with randomly oriented fibers and oriented fibers using PCL and poly(L-lactide) caprolactone (PLC) with various molecular weights, and then they examined the mechanical strength of those surfaces. The study's findings showed that the molecular weight and surface orientation both affected the burst strength of the graft formations [12].

The graft structures developed within the scope of the study aim to examine the effects of the raw materials and the fiber orientation on burst strength, as well as an imitation of the native vessel structure with synthetic materials. In this context, tubular scaffolds are produced from both neat PLA and PCL and blend forms of these materials in 50/50 ratios, and the effects of material and fiber orientation on the burst strength of scaffolds are examined.

## EXPERIMENTAL

### Materials

PCL (Mn 80,000), PLA (Mn 230,000; Ingeo 2003 D with 4.3 mol% D-lactide content), and the components of solvent systems (chloroform (CHL), ethanol (ETH), and acetic acid (AA)) are supplied from Sigma Aldrich.

### Methods

Neat PCL, neat PLA, and PLA/PCL (50/50) are dissolved in CHL/ETH/AA (8/1/1 wt.) at 8% polymer concentrations. Each polymer solution system is stirred for 2 hours at room temperature. Tubular vascular graft structures with 6 mm diameter are fabricated using electrospinning set-up with rotating feeding unit that supplied from Inovenso, Turkey (Nanospinner, Ne100+).

Moreover, graft surfaces are produced at two different rotational speeds; 200 rpm for randomly oriented fibers and 10000 rpm for oriented fibers. Sample codes and descriptions are given in Table 2. For textile fabrics, the burst strength analysis is often applied in a planar form. Due to their constrained size, tubular samples cannot be tested using this

implementation. For that reason, the burst pressure properties of the tubular graft structures are measured by custom design burst tester (Inovenso, Turkey, Figure 1) developed within the scope of the study. The following succinctly describes the measuring methodology for the burst pressure in the aforementioned device; the sample is secured to the ends, and pressure from the air inlets is applied to it. The pressure value is then read from the screen and recorded when the sample bursts.

**Table 2.** Sample codes and descriptions.

Sample Code	PCL ratio (%)	PLA ratio (%)	Production Rotational Speed (rpm)	Fiber Orientation
PCL100_O	100	0	10000	Oriented
PCL100_R	100	0	200	Random
PCLPLA50_O	50	50	10000	Oriented
PCLPLA50_R	50	50	200	Random
PLA100_O	0	100	10000	Oriented
PLA100_R	0	100	200	Random

## RESULTS AND DISCUSSION

Burst strength test results are given in the Table 3. As can be clearly seen from the table, the burst resistance of vascular graft samples with fiber orientation is considerably higher than those of samples with randomly distributed fibers. Examining the burst pressure readings of each sample group reveals that the fiber orientation increases the burst pressure value of each sample by two to three times. This situation is also encountered in vascular graft studies in the literature. Tubular grafts were created by McClure et al. (2009) using a variety of biomaterials, including neat PCL, PCL:silk, neat polydioxanone (PDO), and PDO:silk-based, at two distinct rotational speeds, 500 and 8000 rpm. According to the study, grafts produced at high rotational speeds (8000 rpm), independent of the kind of material used, had greater burst pressure value (3095, 2009, 3336, and 1256 mmHg for PCL, PCL:silk, PDO, and PDO:silk, respectively) with better-aligned fibers than grafts with randomly aligned fibers (2202, 1237, 1152 and 834 mmHg for PCL, PCL:silk, PDO, and PDO:silk, respectively) [13]. Grasl et al. (2021), on the other hand, produced thermoplastic polyurethane (PUR) and polylactid acid (PLLA) based vascular graft structures with both circumferential and axial fiber orientation as well as random fibers. In both PUR and PLLA graft samples, it was observed that the burst resistance was better on the surfaces with oriented fibers (894 mmHg for PUR, and 7641 mmHg for PLLA as circumferentially oriented, and 606 mmHg for PUR and 1587 mmHg for PLLA as axially oriented) compared to the surfaces with random fibers (200 mmHg for PUR, and 570 mmHg for PLLA) [14].

The ideal vascular graft should be similar to native arteries to minimize issues related to mismatch, have enough mechanical strength to resist arterial pressures, and pulse-rate blood flow to prevent aneurysms [15]. Moreover, human saphenous vein burst strength is frequently used as a benchmark for the burst strength of other manufactured grafts since it is considered the "gold standard" of vascular grafts [13]. The PCL100\_O, PCLPLA50\_O, and PLA100\_O samples are found to be highly successful in terms of burst resistance and their burst pressure values are found greater than the burst resistance of the human saphenous vein which is 1599 mmHg [9,10].

**Table 3.** Burst pressure results of vascular graft samples with standard deviations (SD).

Sample	Burst Pressure ± SD (mmHg)
PCL100_O	1449,0±10,6
PCL100_R	730,3±94,45
PCLPLA50_O	2001,0±44,6
PCLPLA50_R	702,5±39,7
PLA100_O	2362,5±109,6
PLA100_R	936,5±10,6

On the other hand, the data also demonstrate how the type of biomaterial affects burst resistance. The PLA100\_O and the PLA100\_R are found to have the highest burst strengths among the all sample groups with orientated fibers and random fibers, respectively. This is a result of PLA's improved mechanical properties [16]. Although PLA has a great mechanical strength, its stiff structure prevents it from possessing the flexibility that vascular grafts should have [6]. PCL, on the other hand, has a relatively lower burst resistance than PLA. The beneficial effect of the PCL/PLA combination becomes apparent at this point. As can be seen in Table 3, PCLPLA50\_O has a sufficient burst resistance at about 2001 mmHg. In addition, it was noticed during testing that this sample (PCLPLA50\_O) has a much more flexible structure than PLA100\_O.

## CONCLUSIONS

The purpose of the study is to produce PCL, PLA, and PCL/PLA-based vascular graft constructions in two different rotational speeds (at 200 and 10000 rpm) to test the burst strength of tubular structures with both orientated fibers and randomly distributed fibers. In order to develop a structure that closely mimics the behavior of the native vessel, it is first determined how fiber orientation and material selection influence burst pressure. When the results are examined, it is seen that oriented fibers are effective in burst resistance and PLA100\_O has the highest value with 2362 mmHg. However, in native artery replacement, the elastic structure of the material is of great importance as well as the burst

resistance of the material. Since the rigid structure of PLA does not match the characteristic elastic structure of the native artery, PCLPLA50\_O sample is thought to be a more suitable substitute among the samples produced considering both properties. Nevertheless, examining the radial elasticity of the material to be used in vascular grafts is important in terms of material selection.

**Acknowledgements:** This study is supported by the TUBITAK (The Scientific and Technological Research Council of Turkey) under grant no: 121M309 and ITU Scientific Research Projects under grant no: 43368.

## REFERENCES

- Ghiasi, M. M., Zendeheboudi, S., & Mohsenipour, A. A. (2020). Decision tree-based diagnosis of coronary artery disease: CART model. *Computer Methods and Programs in Biomedicine*, 192, 105400. <https://doi.org/10.1016/j.cmpb.2020.105400>
- Hao, D., Fan, Y., Xiao, W., Liu, R., Pivetti, C., Walimbe, T., ... Wang, A. (2020). Rapid endothelialization of small diameter vascular grafts by a bioactive integrin-binding ligand specifically targeting endothelial progenitor cells and endothelial cells. *Acta Biomaterialia*, 108, 178–193. <https://doi.org/10.1016/j.actbio.2020.03.005>
- Zhang, F., Bambharoliya, T., Xie, Y., Liu, L., Celik, H., Wang, L., ... King, M. W. (2021). A hybrid vascular graft harnessing the superior mechanical properties of synthetic fibers and the biological performance of collagen filaments. *Materials Science and Engineering C*, 118(May 2020), 111418. <https://doi.org/10.1016/j.msec.2020.111418>
- Spadaccio, C., Nappi, F., De Marco, F., Sedati, P., Sutherland, F. W. H., Chello, M., ... Rainer, A. (2016). Preliminary in vivo evaluation of a hybrid armored vascular graft combining electrospinning and additive manufacturing techniques. *Drug Target Insights*, 10, 1–7. <https://doi.org/10.4137/DTI.s35202>
- Yalcin, I., Horakova, J., Mikes, P., Sadikoglu, T. G., Domin, R., & Lukas, D. (2014). Design of Polycaprolactone Vascular Grafts. *Journal of Industrial Textiles*, 45(5). <https://doi.org/10.1177/1528083714540701>
- Oztemur, J., & Yalcin-Enis, I. (2021). Development of biodegradable webs of PLA/PCL blends prepared via electrospinning: Morphological, chemical, and thermal characterization. *Journal of Biomedical Materials Research - Part B Applied Biomaterials*, 109(11), 1844–1856. <https://doi.org/10.1002/jbm.b.34846>
- Oztemur, J., & Yalcin Enis, I. (2020). The Role of Biopolymer Selection in the Design of Electrospun Small Caliber Vascular Grafts to Replace the Native Arterial Structure. In A. Hayaloğlu (Ed.), *Theory and Research in Engineering* (First, pp. 167–192). Gece Kitaplığı.
- Hiob, M. A., She, S., Muiznieks, L. D., & Weiss, A. S. (2017). Biomaterials and Modifications in the Development of Small-Diameter Vascular Grafts. *ACS Biomaterials Science and Engineering*, 3(5), 712–723. <https://doi.org/10.1021/acsbiomaterials.6b00220>
- Konig, G., McAllister, T. N., Dusserre, N., Garrido, S. A., Ilycan, C., Marini, A., ... L'Heureux, N. (2009). Mechanical properties of completely autologous human tissue engineered blood vessels compared to human saphenous vein and mammary artery. *Biomaterials*, 30(8), 1542–1550. <https://doi.org/10.1016/j.biomaterials.2008.11.011>
- Zamani, M., Khafaji, M., Najji, M., Vossoughi, M., Alemzadeh, I., & Haghhighipour, N. (2017). A Biomimetic Heparinized Composite Silk-Based Vascular Scaffold with sustained Antithrombogenicity. *Scientific Reports*, 7(1), 1–14. <https://doi.org/10.1038/s41598-017-04510-1>

11. Gao, J., Chen, S., Tang, D., Jiang, L., Shi, J., & Wang, S. (2019). Mechanical Properties and Degradability of Electrospun PCL/PLGA Blended Scaffolds as Vascular Grafts. *Transactions of Tianjin University*, 25(2), 152–160. <https://doi.org/10.1007/s12209-018-0152-8>
12. Yalcin Enis, I., Horakova, J., Gok Sadikoglu, T., Novak, O., & Lukas, D. (2017). Mechanical investigation of bilayer vascular grafts electrospun from aliphatic polyesters. *Polymers for Advanced Technologies*, 28(2), 201–213. <https://doi.org/10.1002/pat.3875>
13. McClure, M. J., Sell, S. A., Ayres, C. E., Simpson, D. G., & Bowlin, G. L. (2009). Electrospinning-aligned and random polydioxanone-polycaprolactone-silk fibroin-blended scaffolds: Geometry for a vascular matrix. *Biomedical Materials*, 4(5). <https://doi.org/10.1088/1748-6041/4/5/055010>
14. Grasl, C., Stoiber, M., Röhrich, M., Moscato, F., Bergmeister, H., & Schima, H. (2021). Electrospinning of small diameter vascular grafts with preferential fiber directions and comparison of their mechanical behavior with native rat aortas. *Materials Science and Engineering C*, 124(October 2020). <https://doi.org/10.1016/j.msec.2021.112085>
15. De Valence, S., Tille, J. C., Giliberto, J. P., Mrowczynski, W., Gurny, R., Walpoth, B. H., & Möller, M. (2012). Advantages of bilayered vascular grafts for surgical applicability and tissue regeneration. *Acta Biomaterialia*, 8(11), 3914–3920. <https://doi.org/10.1016/j.actbio.2012.06.035>
16. Pawar, R. P., Tekale, S. U., Shisodia, S. U., Totre, J. T., & Domb, A. J. (2014). Biomedical Applications of Poly (Lactic Acid ). 40–51.

# FABRICATION AND CHARACTERIZATION OF ELECTROSPUN ANTHOCYANIN-LOADED POLYLACTIDE NANOFIBERS

PALAK HANDAN\* AND KAYA OGLU BURÇAK KARAGÜZEL

Istanbul Technical University, Faculty of Textile Technologies and Design, Department of Textile Engineering, Gumussuyu Campus, Inonu Cad., No. 65, Istanbul, Turkey

## ABSTRACT

In this study, morphological, chemical and thermal characteristics of biobased and biodegradable anthocyanin-loaded polylactide (PLA) nanofibrous membranes were investigated. To prepare electrospinning solutions, PLA was dissolved at a concentration of 10% (wv<sup>-1</sup>) in a solvent system of chloroform/dimethylformamide (75/25% vv<sup>-1</sup>), and anthocyanin at different concentrations (1, 2, and 3% wv<sup>-1</sup>) was added into the polymer solutions. The prepared solutions were electrospun by using a single syringe electrospinning setup. The morphological, chemical and thermal structure of the neat and anthocyanin-loaded PLA nanofibrous membranes were characterized via Scanning Electron Microscopy (SEM), Fourier Transform Infrared Spectroscopy (FT-IR), and Differential Scanning Calorimetry (DSC), respectively. The FT-IR spectra proved the incorporation of anthocyanin into nanofibrous membranes successfully. It was observed that when anthocyanin was added into the polymer solution; bead-free nanofibers were produced, and when the concentration of anthocyanin was increased, mean fiber diameter increased as well. In addition, anthocyanin loading did not affect the crystallization behavior of PLA; however, the glass transition temperature (T<sub>g</sub>) of the nanofibrous membranes including no anthocyanin in the structure was higher than those of the other membranes including anthocyanin.

## KEYWORDS

Polylactide (PLA); Anthocyanin; Nanofibers; Electrospinning; Bio-based.

\* Corresponding author: Palak H., e-mail: [palakh@itu.edu.tr](mailto:palakh@itu.edu.tr)

## INTRODUCTION

Electrospinning is a practical technique to fabricate ultrafine polymer fibers in different diameters ranging from nanometers to micrometers by applying an electric field on the polymer solution. Electrospun nanofibrous membranes (ENMs) show unique characteristics, i.e., high specific surface area, high porosity, small pore size and high absorbance capacity [1]. ENMs can also be produced by incorporating various compounds such as pigments, nanoparticles, antimicrobials and drugs into the structure to improve their properties for use in different application areas.

The need of using sustainable and biobased polymers increases globally due to environmental concerns. PLA is a biobased, biodegradable and biocompatible aliphatic polyester, which is derived from renewable resources, i.e., corn starch and sugar cane. Due to its good mechanical and thermal properties, PLA is used in various engineering applications instead of petroleum-based polymers i.e., polyethylene terephthalate (PET) and polystyrene (PS) [12]. PLA was also used in the

development of electrospun nanofibrous mats for biosensors [2], active food packaging [3,4,6,10] and pH indicator [7,9] applications.

Anthocyanin from natural sources, i.e., black carrots, red cabbage, grape, blueberry, etc., is a water-soluble, non-toxic and commercially available natural pigment. It is stable against photodegradation and color resistant at higher temperatures. In addition, anthocyanin has strong bioactivities, including antioxidant, anti-inflammatory, antibacterial activities [14]. It is mostly used for developing halochromic/pH-sensitive materials since it is able to change its color with the change of pH [8,14].

In this study, it is aimed to develop biobased-biodegradable anthocyanin-loaded PLA nanofibrous membranes, and reveal the effect of anthocyanin loading on the morphological, chemical and thermal characteristics of the membranes. The proposed anthocyanin-loaded nanofibrous membranes have a potential to be further developed as pH-sensitive ENMs for protective clothing, filtration, wound dressings, and food packaging applications.

**Table 1.** Properties of the PLA grade [12].

Grade	D-content (mol%)	Melt flow rate g/10min (210°C)	Molecular weight (kg/mol)	Polydispersity index
4060D (Amorphous)	12	7-10	190	1.9

**Table 2.** Properties of the solvents.

Solvent	Boiling Point (°C)	Dielectric constant ( $\epsilon$ )	Hansen solubility parameter, $\delta$ (MPa <sup>1/2</sup> )
DMF	153	36.70	24.2
CHL	61	4.80	18.7

## EXPERIMENTAL

### Materials

Commercial grade of PLA (4060D) was supplied from NatureWorks LLC (USA) (Table 1). Chloroform (CHL, molecular weight: 119.38 g/mol, 99% purity, Sigma-Aldrich) and N,N-dimethylformamide (DMF, molecular weight: 73.09 g/mol, 99% purity, Sigma-Aldrich) were used as solvents (Table 2). Black carrot anthocyanin in powder form was supplied from GemmaNatural (Turkey).

### Methods

The polymer solutions were prepared by dissolving PLA at a concentration of 10% (wv<sup>-1</sup>) in a binary solvent system (CHL/DMF: 75/25% vv<sup>-1</sup>) for 4h at 50°C [4]. Anthocyanin at different concentrations (1, 2, and 3% wv<sup>-1</sup>) was magnetically stirred in DMF for 2h. Then, it was added into the polymer solutions, and final polymer solutions including anthocyanin were ultrasonicated for 1h, then magnetically stirred for 16h at room temperature.

The prepared polymer solutions were used in an electrospinning device of Nanospinner24 (Inovenso) for producing nanofibrous mats. The applied voltage was in a range of 10-12 kV and tip-to-collector distance and feed rate were fixed at 12-13 cm and 2.5 ml/h, respectively. The nanofibrous mats were electrospun and deposited on a cylindrical rotary collector rotating at 60 rpm. Electrospun nanofibrous mats were produced at room temperature with a relative humidity (RH) of ~40-50%.

The morphology of nanofibrous membranes was examined with a Tescan Vega3 scanning electron microscope (SEM). Before imaging, samples were placed into a Quorum Sputter Coater to be coated with a thin layer of Au/Pd for 2 min. To measure the diameter of the nanofibers, SEM images were analyzed with ImageJ software. 100 measurements were taken on each sample, and average nanofiber diameters were calculated. In order to identify the bonds and functional groups of nanofibrous mats,

Perkin Elmer Spectrum 65 FTIR-ATR spectrometer was used. In order to analyze the thermal and crystallization behavior of nanofibrous membranes, a differential scanning calorimetry (DSC), Perkin Elmer DSC400, was used. The samples were heated from 25°C to 200°C at a heating rate of 10°C/min and then cooled to 25°C at a rate of 10°C/min.

## RESULTS AND DISCUSSION

### Morphological analysis

SEM images of electrospun nanofibers are shown in Fig. 1(a-d). Bead formation was observed on the PLA nanofibers (Fig. 1a) since an inherent amorphous structure led to lower levels of polymer chain entanglement [13]. On the other hand, the viscosity increased after 1% wv<sup>-1</sup> anthocyanin was added into the polymer solution; thus, bead-free uniform nanofibers were produced (Fig. 1b), and the mean fiber diameter increased from 327 ± 101 nm to 481 ± 90 nm. Similarly, once the concentration of anthocyanin was increased to 2% (Fig. 1c), and 3% (wv<sup>-1</sup>) (Fig. 1d), uniform fibers having a larger mean diameter, i.e., 590 ± 130 nm and 629 ± 86 nm respectively, were produced.

### FT-IR spectrum analysis

Figure 2a shows the FT-IR spectra of PLA and anthocyanin, whereas Figure 2b shows the FT-IR spectra of nanofibrous PLA membranes without any additive, and with anthocyanin. The spectra of nanofibrous membranes were similar to the spectrum of PLA since it is the dominant component of the nanofibrous membranes. Since the anthocyanin concentration was the highest, the specific band of anthocyanin at 3279 cm<sup>-1</sup> was mainly remarkable in the FT-IR spectrum of PLA+3% anthocyanin membrane. Relatively strong bands were observed in the region of 1400 cm<sup>-1</sup> to 1080 cm<sup>-1</sup> for the nanofibrous membranes containing anthocyanin, proving the formation of C-O asymmetric stretching, C-O-C and CH<sub>2</sub> vibrations groups in the structure [5].

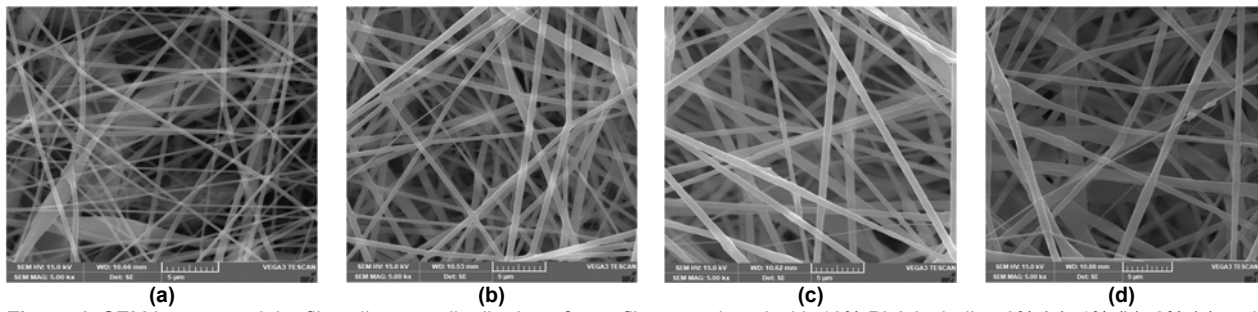


**Figure 1.** SEM images and the fiber diameter distribution of nanofibers produced with 10% PLA including 0% (a), 1% (b), 2% (c) and 3% (d) ( $wv^{-1}$ ) anthocyanin.

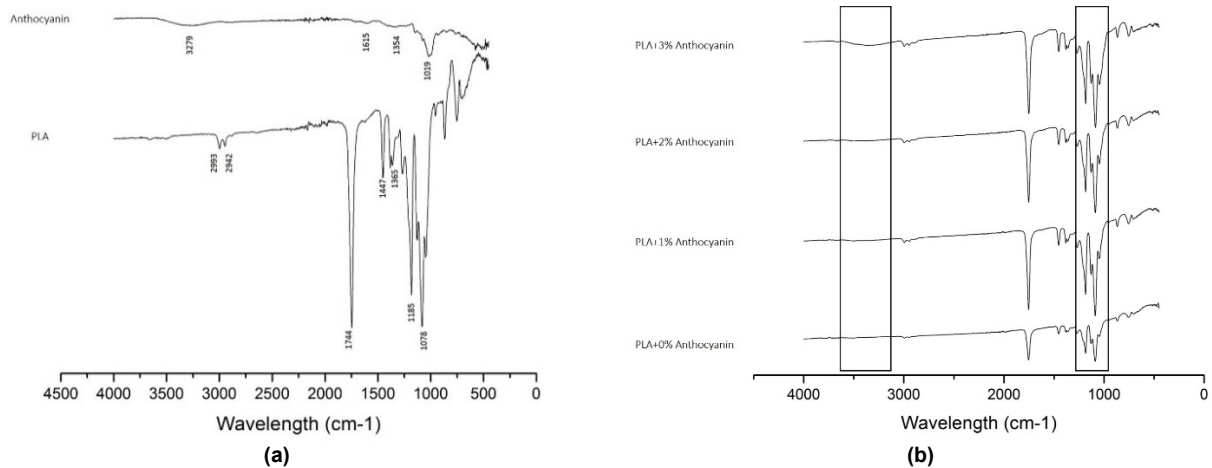


**Figure 2.** (a) FT-IR spectra of PLA and anthocyanin, (b) FT-IR spectra of nanofibrous PLA mats with and without anthocyanin loading.

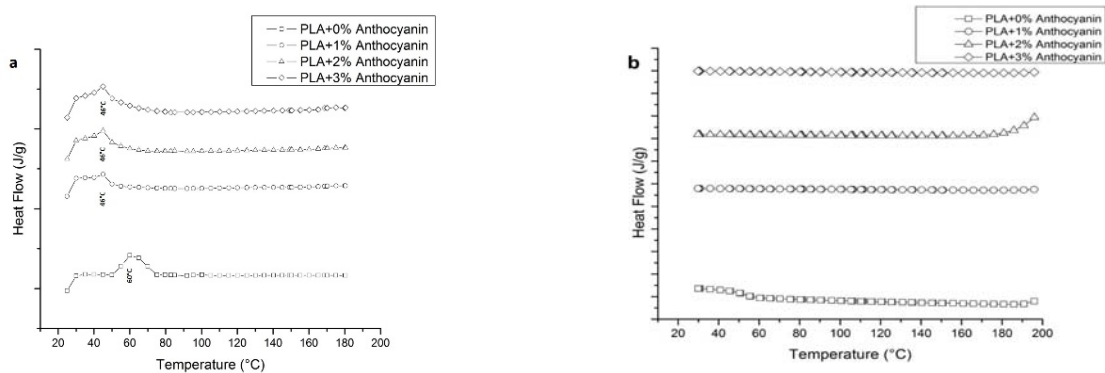


**Figure 3.** Differential scanning calorimetry heating (a) and cooling (b) thermograms of nanofibrous mats.

## CONCLUSIONS

In this study, anthocyanin-loaded PLA based nanofibrous membranes were successfully produced by electrospinning method. SEM analysis indicated that PLA fibers were obtained at nanoscale. When the concentration of anthocyanin was increased, uniform fibers having a larger mean diameter were produced. FTIR analysis indicated that the spectra are mainly dominated by the characteristic peaks of PLA. The main peak of anthocyanin was also observed in the spectra, which means that it was successfully loaded into the nanofibrous membranes. The addition of anthocyanin did not affect the crystallization behaviour of PLA, and

nanofibrous membranes did not show any crystallinity. The  $T_g$  of nanofibrous membrane which has no anthocyanin in the structure was higher than those of the other membranes containing anthocyanin due to plasticizing effect of the anthocyanin pigment. It was concluded that anthocyanin loading did not have a negative effect on the characteristic properties of PLA based nanofibrous membranes.

For further studies, the proposed anthocyanin-loaded nanofibrous membranes can be developed as pH-sensitive ENMs for the applications areas of tissue engineering, protective clothing, filtration, and food packaging.

**Acknowledgements:** Authors acknowledge Istanbul Technical University Scientific Research Projects Fund under Grant No. BAP 43661 for the financial support.

## REFERENCES

- Agarwal, A., Raheja, A., Natarajan, T. S., & Chandra, T. S. (2012). Development of universal pH sensing electrospun nanofibers. *Sensors and Actuators, B: Chemical*, 161(1), 1097–1101. <https://doi.org/10.1016/j.snb.2011.12.027>
- Aliheidari, N., Aliahmad, N., Agarwal, M., et al. (2019). Electrospun nanofibers for label-free sensor applications. *Sensors*, 19(16): 3587. <http://dx.doi.org/10.3390/s19163587>
- Altan, A., Aytac, Z., & Uyar, T. (2018). "Carvacrol loaded electrospun fibrous films from zein and poly(lactic acid) for active food packaging", *Food Hydrocolloids*, 81, 48–59. <https://doi.org/10.1016/j.foodhyd.2018.02.028>
- Aydogdu, A., Yildiz, E., Ayhan, Z., Aydogdu, Y., Sumnu, G., & Sahin, S. (2019). "Nanostructured poly(lactic acid)/soy protein/HPMC films by electrospinning for potential applications in food industry", *European Polymer Journal*, 112, 477–486. <http://dx.doi.org/10.1016/j.eurpolymj.2019.01.006>
- Jaleel, K.A., Zubair, J.A., and Masa, J. M. A.-B. (2017). Effects of natural pigments on the poly(methyl methacrylate) biopolymer. *J Cancer Sci Ther*, 9(1).
- Kayaci, F., Umu, C., Tekinay, T. & Uyar, T. (2013). "Antibacterial electrospun poly(lactic acid) (pla) nanofibrous webs incorporating triclosan/cyclodextrin inclusion complexes", *J. Agric. Food Chem.* 61, 3901–3908. <https://doi.org/10.1021/jf400440b>
- Kuntzler, S.G, Costa, J.A.V, Brizio, A.P.D.R., & de Morais, M.G. (2020). Development of a colorimetric pH indicator using nano fibers containing *Spirulina* sp. LEB 18, *Food Chemistry*, 328, 126768. <https://doi.org/10.1016/j.foodchem.2020.126768>
- Maftoonazad, N., & Ramaswamy, H. (2019). Design and testing of an electrospun nanofiber mat as a pH biosensor and monitor the pH associated quality in fresh date fruit (Rutab). *Polymer Testing*, 75, 76–84. <https://dx.doi.org/10.1016/j.polymertesting.2019.01.011>
- Moreira, J. B., Terra, A. L. M., Costa, J. A. V., & Morais, M. G. de. (2018). "Development of pH indicator from PLA/PEO ultrafine fibers containing pigment of microalgae origin", *International Journal of Biological Macromolecules*, 118, 1855–1862. <https://doi.org/10.1016/j.ijbiomac.2018.07.028>
- Munteanu, B.S, Aytac, Z., Pricope, G.M., Uyar, T. & Vasile, C. (2014). "Polylactic acid (PLA)/Silver-NP/VitaminE bionanocomposite electrospun nanofibers with antibacterial and antioxidant activity", *J Nanopart Res*, 16:2643. <https://doi.org/10.1007/s11051-014-2643-4>
- Natureworks Ingeo (2022, October) <https://www.natureworkslc.com/Products>
- Nofar, M., Maani, A., Sojoudi, H., Heuzey, M. C., & Carreau, P. J. (2015). Interfacial and rheological properties of PLA/PBAT and PLA/PBSA blends and their morphological stability under shear flow. *Journal of Rheology*, 59(2), 317–333. <http://dx.doi.org/10.1122/1.4905714>
- Palak, H., Güler, E., Nofar, M., & Karagüzel Kayaoğlu, B. (2022). Effects of D-lactide content and molecular weight on the morphological, thermal, and mechanical properties of electrospun nanofiber polylactide mats. *Journal of Industrial Textiles*, 51(2S), 3030S–3056S. <https://doi.org/10.1177/15280837221090260>
- Prietto, L., Pinto, V.Z., El Halal, S.L.M., Morais, M.G., et al. (2007). Ultrafine fibers of zein and anthocyanins as natural pH indicator. *Journal of the Science of Food and Agriculture*, 98, 2735-2741. <https://doi.org/10.1002/jsfa.8769>
- Sun, X. Zhoua, T. Weia, C., Lan, W., Zhao, Y. et al. (2018) Antibacterial effect and mechanism of anthocyanin rich Chinese wild blueberry extract on various foodborne pathogens, *Food Control*, 94 155-161. <https://doi.org/10.1016/j.foodcont.2018.07.012>

# IMPROVING LOCAL THERMAL COMFORT IN BUILDINGS: A STUDY OF PROPERTIES OF HEATING TEXTILE COMPOSITES IN CONSTRUCTION INDUSTRY

KANIA ANNA\* AND BARBURSKI MARCIN

Lodz University of Technology, Faculty of Material Technologies and Textile Design, Institute of Architecture of Textiles, ul. Żeromskiego 116, 90-543 Łódź, Poland

## ABSTRACT

The focus of this study is to analyze heating and insulating properties of textiles utilized in the construction industry. Research regarding textile heating composites typically centers around their use in the fashion industry and personal thermal comfort. Therefore, the study focuses on the application of textile heating composites as a method for improving the local thermal comfort of the user. The aim of this project was to analyze and describe the heating and insulating properties of electroconductive yarns and insulating textiles used in the construction industry. This goal was achieved by building physical samples that underwent heating tests. The next step was to compare the examined properties and select the best combination of yarn and fabric, which was then tested in the target environment. It was concluded that the best heating results are achieved with steel thread embroidered on fiberglass mesh and combined with extruded polystyrene that can be used to improve the local thermal comfort of the user.

## KEYWORDS

Electroconductive yarns; Heating; Embroidery; Personal thermal comfort; Composite; Building.

---

\* Corresponding author: Barburski M., e-mail: [marcin.barburski@p.lodz.pl](mailto:marcin.barburski@p.lodz.pl)

## INTRODUCTION

The search for new materials with better and better properties has led to the creation of a new group of materials known as composite materials. When designing innovative composite materials, they consider the operating conditions and the loads under which they will work. The rapidly growing industry related to the production of composite combines issues in the field of textiles, metallurgy, mechanics and chemistry of polymers, and plastics processing. [4]

A special field of composites is the combination of textiles and electronics, known as textronics. Programmable products can be produced through technical embroidery, weaving, or wreathing, and thanks to the use of flat textile products, they are flexible and portable. Popular applications of textronics are actively heating clothes or garments that measure basic life parameters. [1], [8], [10].

Heating textile composites have been described and tested mainly in the application of the fashion industry and personal thermal comfort products. [2], [9] For building heating usually used are classic heating systems with radiators connected directly to the power plant or to local water heating systems. [5], [7] Floor heating is used less frequently, usually

in combination with one of the aforementioned heating methods, as an additional element increasing the local thermal comfort of the user. [11]

Thermal comfort is a mental state in which a person subjectively feels a sense of warmth. It depends on two kinds of factors:

- Thermal conditions, including air temperature, humidity, air movement, and radiant temperature, e.g., cool air near a window.
- Workers' individual personal factors, such as level of physical activity and clothing. Physical factors such as weight, gender, and age are also important variables. [6]

## EXPERIMENTAL

### Materials and fabrication procedures

A steel thread with a nominal electrical resistance of 27 $\Omega$  per meter, a silvered thread with a nominal electrical resistance of 80 $\Omega$  per meter, and a carbon rowing of unknown nominal electrical resistance were used to create a technical embroidery on a fiberglass mesh of 330g/m<sup>2</sup> density and 30mm thick extruded polystyrene was used as insulation material, covered with 5mm thick expanded

polystyrene with an aluminum layer on top (Figure 1C). The polystyrene was combined with a designated glue, and the fiberglass mesh with the embroidery was then placed on top of it (Figure 1B) using heat-resistant and nonconducting glue. All fitting packet was covered by Jacquard woven fabric. (Figure 1A) The first samples were made with a single thread as shown in Figure 2, in a shape of a square with 50 cm long sides and 1 cm distance between single lines for steel and silvered threads. The pattern was adjusted accordingly for the carbon rowing with 2 cm distance between the lines. Next samples were made with multiple threads, as shown in Figure 3, also in a shape of a square and 1 cm distance between single lines for steel and silvered threads, but with 30 cm long sides. The pattern was adjusted accordingly for the carbon roving with 1,5 cm distance between the lines. In samples made with the pattern from Figure 2, the ends were connected directly to the energy source, while in samples made with the pattern from Figure 3, the ends were connected to form a parallel circuit, and then connected to the power source. Samples were then covered with a layer of jacquard woven fabrics made by Marta Rzeźniczak (Institute of Architecture of Textile, Lodz University of Technology).

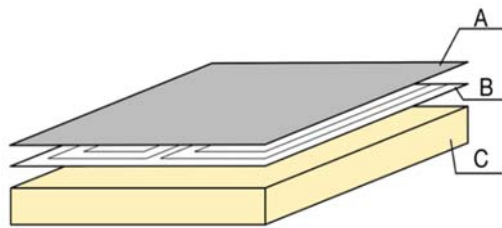


**Figure 1.** Schematics of samples. A – Jacquard woven fabric, B – heating embroidery on fiberglass mesh, C – extruded polystyrene.

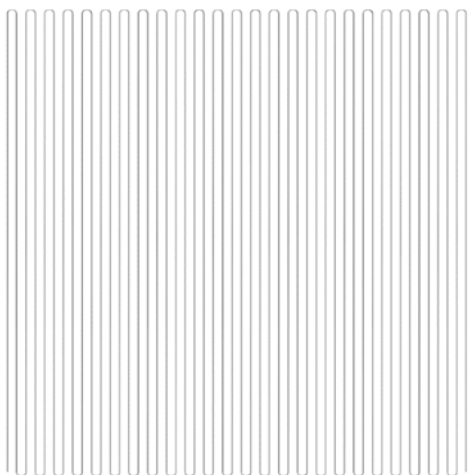


**Figure 2.** Pattern used to make first samples.

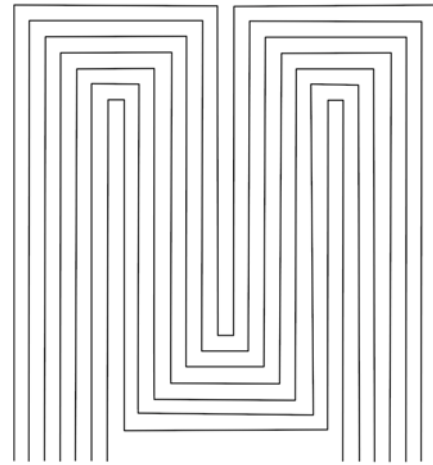


**Figure 3.** Pattern used to make second samples

## Experimental procedures

First samples were tested to measure the electric resistance and the minimum voltage needed for a heating effect. Then after adjusting the pattern, samples were made in different configurations: 1) steel thread embroidered on fiberglass mesh, 2) embroidery on fiberglass mesh attached to polystyrene, 3) embroidery on fiberglass mesh attached to polystyrene and covered with the jacquard. Corresponding samples were made using carbon fiber. The samples were then connected individually to a DC power source with an effective voltage of 22V and were investigated under thermal camera ThermaCAM E65 for maximal temperature, the time needed to reach maximal temperature, and the time needed for cooling down to a temperature of 24°C. The temperature of the environment was 21,2°C. Then the steel thread sample covered with jacquard was tested for current-voltage characteristics and temperature as a function of voltage using the same DC source as before. The active power of the system was calculated using the current-voltage characteristic. The sample was also tested for heat conduction coefficient to see whether the embroidery and jacquard influenced the declared coefficient of extruded polystyrene (XPS).

## RESULTS AND DISCUSSION

### Minimal voltage

The samples were tested for approximate electric resistance to estimate the minimum voltage needed for the heating effect. The results were as follows: steel thread – 550Ω, carbon fiber - 640Ω, silvered thread - 3300Ω. Because of the significantly bigger resistance of the silvered thread, it was eliminated from further research as ineffective. The minimum voltage needed for the heating effect oscillated between 240V-300V. To reduce voltage to safe quantities, the pattern was adjusted to accommodate shorter lengths of threads and parallel circuits.

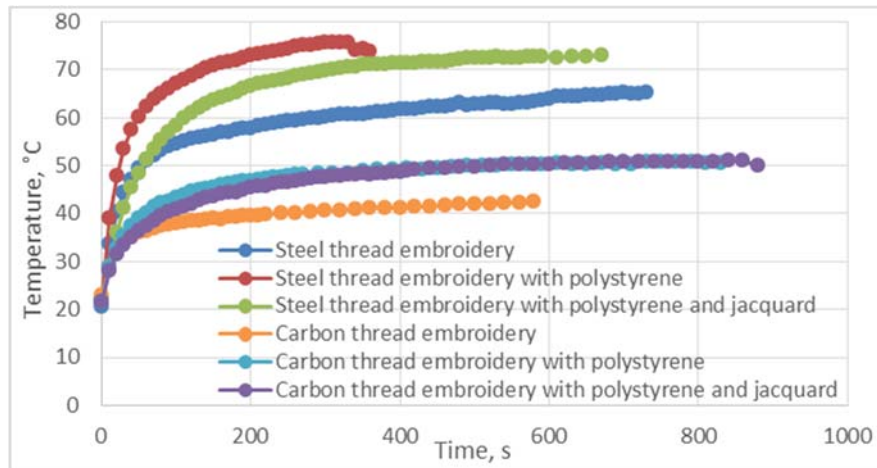


Figure 4. Comparison of temperatures and heating times of different samples.

Table 1. Results of observation under a thermal camera.

Lp	Sample	Maximal reached temperature, °C	Heating time, s	Cooling time, s
1	Steel thread embroidery	65,3	740	240
2	Steel thread embroidery with polystyrene	75,7	360	679
3	Steel thread embroidery with polystyrene and jacquard	72,9	670	943
4	Carbon thread embroidery	42,4	580	191
5	Carbon thread embroidery with polystyrene	50,9	830	567
6	Carbon thread embroidery with polystyrene and jacquard	51	880	732

### Thermal camera observation

Samples made with the adjusted pattern were observed under a thermal camera, as shown in Figure 4 and Table 1. The best results were achieved with steel thread covered with jacquard woven fabric. Despite longer heating time than just extruded polystyrene with steel thread embroidery on fiberglass mesh, it achieves a similar temperature and is more user-friendly – the electroconductive threads are covered, so there is no danger of accidental burn or short circuit. The carbon rowing heated up to lower temperatures needed more time to reach maximum temperature and cooled down faster. Overall, steel thread performed better, with shorter times of heating up and longer times of cooldown. The jacquard cover didn't have a big impact on the maximum temperature, slightly changing the heating curve in comparison to just the embroidery and polystyrene combination (Figure 4).

### Steel thread sample with jacquard woven fabric covering

After comparing results from previous tests, it was concluded that further research will be conducted on a sample made with steel thread with the jacquard covering. As shown in Figure 5, the maximal measured temperature within safe for humans voltages was 93°C. Apart from the initial heating voltage between 0V and 10V, the dependence

between voltage and temperature is linear (Figure 6). It may prove to be useful in further research and developing control systems. The current-voltage characteristic on Figure 5. demonstrates that there are no statistically important differences in resistance due to heating. It was used to calculate the active power of the sample, as shown in Table 2. Comparing it with the power needed to heat a square meter of a room [3] it may be concluded that there should not be a significant difference between the energy efficiency of radiators and the presented composite.

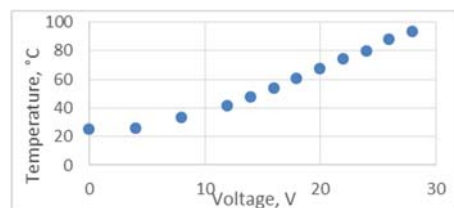


Figure 5. Temperature as a function of voltage for steel thread embroidery on fiberglass mesh with XPS and jacquard woven fabric.

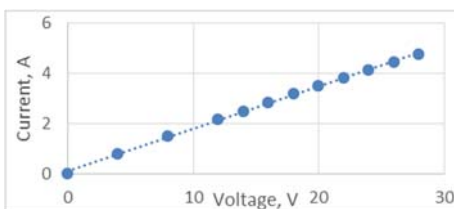


Figure 6. Current-voltage characteristic for steel thread embroidery on fiberglass mesh with XPS and jacquard woven fabric cover.

**Table 2.** Active power as function of time.

<b>Temperature °C</b>	25,8	32,8	41,5	47,5	53,8	60,6	67	74,2	79,5	87,5	93
<b>Active power W</b>	3,04	11,89	25,97	34,4	45,12	57,02	70,04	83,6	98,88	114,92	132,16

## CONCLUSIONS

The presented study showcased the heating potential and characteristics of different electro-conductive threads. The samples were made using steel thread, silvered thread, and carbon roving, which were embroidered on fiberglass mesh. Then they were glued on extruded polystyrene and covered with jacquard woven fabric. Their electric resistance, heating potential and time, cooling time, and temperature as a function of voltage were measured. Current-voltage characteristic was made and used to calculate the active power of the sample. The main results are summarized below:

1. After comparing electric resistance and maximal temperatures reached by different threads, the steel thread was chosen as the overall best material for heating purposes.
2. There is no statistically significant difference between the performances of the sample on extruded polystyrene with the jacquard woven fabric cover and the one without the cover.
3. The studied composite has comparable active power to those of typical radiators, therefore being an equally energy-efficient source of heating.

Considering all the above, it can be concluded, that textile composites are a good mode of improving local thermal comfort.

**Acknowledgements:** *The authors would like to thank Witold Grymin from the Department of Building Materials Physics and Sustainable Design, Lodz University of Technology for supporting them during this work and helping in laboratory work with a full of patience and kindness. The article was written when the first author was a student of E2TOP project at Lodz University of Technology.*

## REFERENCES

1. Bonaldi, R.R. (2018). High Performance Apparel. Woodhead Publishing (Cambridge)  
<https://doi.org/10.1016/C2015-0-01391-0>
2. Couto, S., Campos, J.B.L.M., Neves, S.F., Mayor, T.S., (2015). Advances in the optimisation of apparel heating products: A numerical approach to study heat transport through a blanket with an embedded smart heating system, Applied Thermal Engineering, 87  
<https://doi.org/10.1016/j.applthermaleng.2015.05.035>
3. Kacznow, S. (2022). Dobór mocy grzejników. Retrieved October 20, 2022. [www.egrzejniki.pl](http://www.egrzejniki.pl)
4. Long, A. C. (2007). Composites Forming Technologies. Woodhead Publishing (Cambridge)
5. Łukasiewicz, E., Shamoushaki, M. (2017). Heating potential of undeveloped geothermal water intakes in Poland in the context of sustainable development and air protection, Water Resources and Industry, 27  
<https://doi.org/10.1016/j.wri.2022.100175>
6. Pawłowski, K. (2017). Projektowanie ścian w budownictwie energooszczędnym. Grupa Medium (Warszawa)
7. Szulgowska-Zgrzywa, M., Piechurski, K., Stefanowicz, E., Baborska-Narozny, M. (2022). Multi-criteria assessment of the scenarios of changing the heating system in apartments in historical buildings in Wrocław (Poland) – Case study, Energy and Buildings, 254  
<https://doi.org/10.1016/j.enbuild.2021.111611>
8. Tunakova, V., Gregr, J. (2010). Electrical conductivity measurements of fibers and yarns. Retrieved October 20, 2022. [www.researchgate.net](http://www.researchgate.net)
9. Wang, F., Kang, Z., Zhou, J. (2019). Model validation and parametric study on a personal heating clothing system (PHCS) to help occupants attain thermal comfort in unheated buildings, Building and Environment, 162  
<http://dx.doi.org/10.1016/j.buildenv.2019.106308>
10. Xue, P., Tao, X., Leung, M., Zhang, H. (2005). Wearable Electronics and Photonics. Woodhead Publishing (Cambridge)
11. Zembrowski, J. (2017). Sekrety tworzenia murowanych domów bez błędów. Biuro Doradztwa Budowlanego (Białystok)

# DESIGN AND INVESTIGATION THE OPERATION OF TEXTILE BASED ELECTRODES FOR ELECTROTHERAPY

AGHADAVOOD ROYA<sup>1\*</sup>, SHAHBAZ ZAHRA<sup>2</sup>, KHEIRI TAHEREH<sup>2</sup>, SHANBEH MOHSEN<sup>2</sup> AND MARTINEK RADEK<sup>1</sup>

<sup>1</sup> VSB - Technical University of Ostrava, Department of Cybernetics and Biomedical Engineering, 17.listopadu 2172/15, 70800, Ostrava-Poruba, Czech Republic

<sup>2</sup> Isfahan University of Technology, Department of Textile Engineering, Isfahan 84156-83111, Iran

## ABSTRACT

Electrostimulation is a way of treatment various nerve and muscle injuries as well as acute and chronic pain conditions. The electrotherapy which is increasingly used in physiotherapy, muscle is exposed to an electrical pulse in order to activate excitable tissue using external electrodes with the aim of building muscle strength, enhancement healing, improvement in patient's mobility or reducing pain. Textile based electrodes are significantly noticed in the aspects of being flexible and re-usable and no needs of hydrogels, thereby avoiding skin irritation and allergic reactions and enhancing user comfort. This article presents a kind of textile based electrodes made of conductive yarns containing stainless steel/polyester blend fiber. The embroidery technique was used to prepare the textile based electrodes. Samples were examined on 10 people with pain in their bodies in a hospital without being moisturised. The purpose of this study is to assess the performance of 3 different textile based electrodes, considering the conductivity of the yarns which have been used to produce textile based electrodes, the usefulness of them for electrotherapy and comparing them with rubber electrodes commonly are used in clinics regularly.

## KEYWORDS

Electrostimulation; Electrotherapy; Rubber electrode; Textile electrodes; Conductive yarn; Embroidery.

\* Corresponding author: Aghadavood R., e-mail: [roya.aghadavod.marmani.st@vsb.cz](mailto:roya.aghadavod.marmani.st@vsb.cz)

## INTRODUCTION

"Smart textiles" are novel topics in research area which is related to new generation of fiber assemblies and apparel systems that are able to react with, sense and be adapted to surrounding conditions or stimuli in a manual or programmed manner. Fiber and also textile based electronics have extreme flexibility as well as wearing comfort. In addition, their fabrication is low-cost and have environmentally friendly process by means of conventional facilities, often with no need of special conditions. The most relevant definition of smart textiles is textiles that interact external situations [7]. To date, conductive textiles or in another words electro-conductive textiles have wide variety of applications in smart textiles are currently under investigation by many researchers. There are three ways to make a fabric conductive, using conductive fiber materials, conductive fiber coatings, or conductive coating or finishing methods on the whole textile fabrics [2].

Electrotherapy involves a wide range of techniques and devices and used as longterm treatment for post-acute rehabilitation patients delivered over a

period of eight to sixteen weeks. In this type of therapy human body is exposed to a low-level current in order to become activated or stimulated. In contrast of internal electrodes used with in the body surface electrodes are applied on the skin. Among surface electrodes, the disposable rubber electrodes, need using an additional hydrogel or electrode cream as an electrolyte interface between the skin and the electrode in order to improve skin contact and ensure a continuous current flow. As well as investigating the contact between the electrode and human skin, natural changes in the skin such as changes of humidity, temperature, structure should be paid attention. The surface resistance of the electrode must be in a small value and also it is one of the most significant parameters of a proper electro stimulation process. In order to have a lower surface resistance yarns characterised by high conductivity for instance silver polyamide yarns or cotton yarns wrapped round by stainless steel can be used [10].

Previous works investigated suitable stimulation parameters using TENS electrodes, designed garments able to deliver functional electrical stimulation [9]. In spite of the majority medical use

of rubber electrodes, they have been found to cause skin irritation, shocking and skin burns in some patients. While wearable conductive textile electrodes provide alternative, skin comfort and high elasticity for users. Baheti et al. dealt with the deposition of silver particle onto knitted fabrics for possible application in electrotherapy. A knitted fabric with deposited silver particles was used in electrotherapy and its operation on some properties as well as electrical conductivity, physiological comfort, antibacterial, and durability were investigated. When there is a variety of human body movements small electrical resistance changes were observed during the extension to 80% and as the results, it can be noticed that the electrical resistance will increase significantly after the 90% extension. Besides, as other findings of this paper, it can be noted that no significant changes in fabric properties such as air permeability, water vapor permeability, fabric porosity, and conductivity were observed [1]. Three types of knitwear with a similar surface weight with different raw material composition were fabricated by Skrzetuska et al. Embroidery machine and film printing were used in stimulating electrode fabrication. Friction, washing and mechanical tests were investigated. As a result, they found that the best textile material for film printing process in electrode fabrication is viscose knitwear[8]. Garments with the ability to deliver functional electrical stimulation were designed by Moineau et al. Electrodes knitted by means of conductive yarn were moistened before use[6]. Another study on dry and wet textile electrodes in electrotherapy demonstrated that using dry electrodes can cause pain when the current is in a low range; on the other hand, the wet textile based electrodes which were tested alongside the dry and common hydrogel electrodes showed no sign of pain during the process which is due to pain-sensing fiber that can be activated more feasible with the dry electrodes than the wet and hydrogel ones [11]. Considering the differences between wet and dry electrodes, there is another study which confirms the preference of wet textile electrodes over the dry ones. Euler et al has compared six various of knitted electrodes in wet and dry state. The study shows that wet electrodes have less contact impedance than dry knitted electrodes. From the results it can be noted that dry textile electrodes have their best performance with an uneven surface. At the same time the wet textile based electrodes are more

acceptable with a smooth surface. Nevertheless it is noticed that the dry textile based electrodes performance can be improved by putting pressure on the system[3]. Liu et al in a novel study has investigated a textile based electrode for electrotherapy which had an acceptable result in reducing pain on subjects[5]. Hunold et al has investigated a novel textile based electrode which is integrated with flexible caps; also a comparison between these novel electrodes and conventional rubber electrodes were studied. The results showed that the flexible cap used with textile based electrodes made them more comfortable as wearable electrodes[4].

## EXPERIMENTAL

### Materials

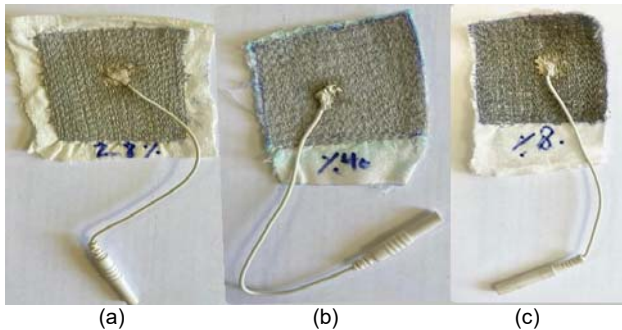
In this study textile based electrodes are made of Stainless steel/polyester staple fiber blend yarn (produced by Xiamen JL-fiber Science and Technology Co. Ltd., Xiamen, China). The fineness of stainless-steel fiber was 12 microns. Properties of the conductive yarns are presented in Table 1. Electrodes were made on a stretchable woven fabric in 6\*6 square centimeter dimension. The weave design of this fabric was plain. Mass per unit area of the used fabric was 0.0113 g / cm<sup>2</sup>. A couple of electrodes were prepared from each yarn, one of them as phase and the other one as zero, therefore we had six samples that their features are noted in Table 2. Surface electrical resistance of each electrode were measured by using a four probe. The warp yarn of based woven fabric was multifilament Polyester/Spandex(75den/20den) intermingled yarn. Weft yarn was Polyester/viscose(65/35%) ring spun yarn with linear density of 20 tex. The connector attached to the surface of each electrode by using conductive silver glue. Rubber electrodes has been used as reference one in order to evaluate the performance of the textile based electrodes. Prepared textile based electrodes are shown in Fig 1. A two-channel Berjis ST-90 physiotherapy system was used as an electricity resource to provide electrical current. That provided electrical current transferred to the surface of the textile based electrode through a wire which used as a connector. The rubber electrode is shown in Fig 2.

**Table 1.** Properties of the yarn

Yarn Code \ Properties	Blend Ratio (Stainless steel/PET)	Strength (cN/Tex)	Linear Resistance ( $\Omega/cm$ )	Diameter ( $\mu m$ )	Extension (%)
A	80%/20%	32.22	5.31	447.14	6.78
B	40%/60%	120.05	23.07	249.46	3.24
C	28%/72%	125.84	29.82	248.25	3.08

**Table 2.** Properties of the samples

Electrode Code	Yarn Code	Surface electrical resistance ( $\Omega/square$ )	Weight (g)	Thickness (mm)
1	A	2.25	1.83	1.28
2	B	16.6	1.09	0.95
3	C	26	1.72	1.15

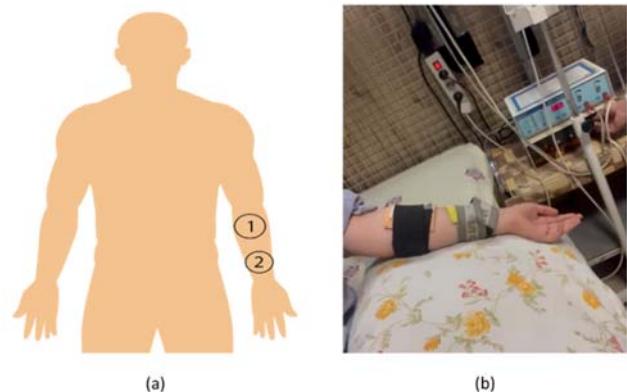

**Figure 1.** Textile based electrodes: (a): The electrode from yarn C and its connector, (b): The electrode from yarn B and its connector, (c): The electrode from yarn A and its connector

**Figure 2.** Rubber electrode

## Methods

In this study conductive yarns containing 28, 40 and 80 percent of stainless steel fibers and 72, 60 and 20 percent of polyester fibers, respectively were used to develop textile based electrodes with the dimension of 6\*6 square centimeter. Conductive yarns were embroidered on mentioned fabric by means of Jack JK-9100B sewing machine. Moreover, connectors have been used in order to connect the textile electrodes to the two-channel Berjis ST-90 physiotherapy system. Textile based electrodes were placed on different parts of patient's body such as patient's arm, leg, calf, knee and back.

As an example, electrodes position on the patient's arm is illustrated in Fig 3(a) and also Fig 3(b) shows textile based electrodes which was worn around the forearm of one of the authors. These textile based electrodes were located in wet sponge pads. Spongy pads are shown in Fig 4.


**Figure 3.** (a) electrodes positions on the patient's arm, (b) clinical test of textile based electrodes on forearm position.

**Figure 4.** Spong pads.

## RESULTS AND DISCUSSION

In our experiments we compared the performance of textile based electrodes with conventional rubber ones. Results showed that textile based electrodes had a comparable performance with rubber electrodes during the electrotherapy. We confirmed that the textile based electrodes had a desirable current during the electrotherapy for all the patients on all parts of their bodies. According to the results, textile based electrodes illustrated similar electrical current with rubber electrodes as the patients were therapied and no clear differences has been observed in the performance of rubber and textile based electrodes. The electrical conductivity of electrodes could be one of the main factors which has been considered in this study. The result revealed that the electrical current using dry textile electrodes did not increased as the conductivity increased and transferred current did not change. All the textile based electrodes with different conductivity performed equally.

## CONCLUSIONS

In this study textile based electrodes, which prepared by swing conductive stainless steel yarns on a stretchable woven fabric by using Jack JK-9100B sewing machine, have been presented as an alternative for conventional rubber electrodes. Both electrodes were placed in a pad and no skin irritation was observed while using pad. The results showed that textile electrodes performed well throughout the therapy. Furthermore, according to the result, increasing the conductivity won't lead to improve textile electrodes efficiency in transferring the electrical current. Compared to the rubber electrodes prepared electrodes exhibited similar and comparable performance. It seems that the use of textile based electrodes for using in electrotherapy instead of conventional electrodes has many potential and in future we aim at work on the life time and durability of these electrodes and also effect of dimension and structure of them on their performance.

**Acknowledgements:** This article was supported by the Ministry of Education of the Czech Republic Project No. SP2022/34, SP2022/6.

## REFERENCES

1. Ali, A., Baheti, V., Militky, J., & Khan, Z. (2018). Utility of silver-coated fabrics as electrodes in electrotherapy applications. *Journal of Applied Polymer Science*, 135(23), 46357. <http://dx.doi.org/10.1002/app.46357>
2. Ehrmann, A., & Blachowicz, T. (2017). Conductive yarns, fabrics, and coatings. In *Examination of Textiles with Mathematical and Physical Methods* (pp. 13-29). Springer, Cham. [https://doi.org/10.1007/978-3-319-47408-3\\_2](https://doi.org/10.1007/978-3-319-47408-3_2)
3. Euler, L., Guo, L., & Persson, N. K. (2021). Textile electrodes: Influence of knitting construction and pressure on the contact impedance. *Sensors*, 21(5), 1578. <https://doi.org/10.3390/s21051578>
4. Hunold, A., Ortega, D., Schellhorn, K., & Hauelsen, J. (2020). Novel flexible cap for application of transcranial electrical stimulation: a usability study. *Biomedical engineering online*, 19(1), 1-11. <https://doi.org/10.1186/s12938-020-00792-1>
5. Liu, M., Ward, T., Young, D., Matos, H., Wei, Y., Adams, J., & Yang, K. (2020). Electronic textiles based wearable electrotherapy for pain relief. *Sensors and Actuators A: Physical*, 303, 111701. <http://dx.doi.org/10.1016/j.sna.2019.111701>
6. Moineau, B., Marquez-Chin, C., Alizadeh-Meghraz, M., & Popovic, M. R. (2019). Garments for functional electrical stimulation: design and proofs of concept. *Journal of Rehabilitation and Assistive Technologies Engineering*, 6, 2055668319854340. <https://doi.org/10.1177/2055668319854340>
7. Persson, N. K., Martinez, J. G., Zhong, Y., Maziz, A., & Jager, E. W. (2018). Actuating textiles: next generation of smart textiles. *Advanced Materials Technologies*, 3(10), 1700397. <https://doi.org/10.1002/admt.201700397>
8. Skrzetuska, E., Michalak, D., & Krucińska, I. (2021). Design and analysis of electrodes for electrostimulation (TENS) using the technique of film printing and embroidery in textiles. *Sensors*, 21(14), 4789. <https://doi.org/10.3390/s21144789>
9. Tao, X. (Ed.). (2015). *Handbook of smart textiles* (pp. 293-316). Singapore, Springer. <http://dx.doi.org/10.1007/978-981-4451-45-1>
10. Tokarska, M. (2011). Research of Textile Electrodes for Electrotherapy. *Fibres & Textiles in Eastern Europe*, 19(5), 88.
11. Zhou, H., Lu, Y., Chen, W., Wu, Z., Zou, H., Krundel, L., & Li, G. (2015). Stimulating the comfort of textile electrodes in wearable neuromuscular electrical stimulation. *Sensors*, 15(7), 17241-17257. <https://doi.org/10.3390/s150717241>

# SOLUTION BLOWN OF PLA NANOFIBER CONTAINING OZONATED MORMODICA OIL AND ITS MICROCAPSULES TO OBTAIN ANTIBACTERIAL MEDICAL TEXTILES SURFACES

PEKTAŞ KORAY<sup>1\*</sup>, BALCI ONUR<sup>1</sup> AND ORHAN MEHMET<sup>2</sup>

<sup>1</sup> Kahramanmaraş Sütçü İmam University, Faculty of Engineering and Architecture, Textile Engineering Department, Avşar Campus, 46100, Onikişubat/ Kahramanmaraş, Turkey

<sup>2</sup> Uludağ University, Faculty of Engineering and Architecture, Textile Engineering Department, Görükle Campus, 16059, Nilüfer/ Bursa, Turkey

## ABSTRACT

In the scope of the study, it was aimed to obtain antibacterial nanofiber surfaces containing Momordica oil, its ozonated oil form and its microcapsules forms. First of all, Momordica oil was exposed to ozone gas for 135 min. After that, crude and ozonated mormodica oil were microencapsulated by using simple coacervation. Subsequently, %10 PLA polymer solution were prepared and used for obtaining PLA nanofiber surface by using solution blowing spinning. Besides, PLA polymer solution were mixed with crude mormodica oil, ozonated mormodica oil and their microcapsules forms and then these solutions were spun by using solution blowing spinning. Obtained ozonated oil, microcapsules and nanofiber surfaces were characterized via measurement of total unsaturated fatty acid amount in the oils, scanning electron microscope, FT-IR analysis and antibacterial activity test. The data showed that mormodica oil were ozonated. Microencapsulation process was done successfully and obtained nanofiber containing mormodica oil and its microcapsules. Moreover antibacterial activity showed that mormodica oil and ozonated mormodica oil showed antibacterial activity against to *S.aureus* and *E.coli* bacteria according to the disc diffusion method. The nanofiber surfaces containing ozonated oil and its microcapsules showed antibacterial activity against to *S.aureus* and *E.coli* bacteria according to the ASTM E 2149-01 method. As a result, it was obtained biodegradable nanofiber containing microcapsules and showing antibacterial activity.

## KEYWORDS

Solution blowing spinning; PLA; Ozonated oil; Microencapsulation; Antibacterial activity.

---

\* Corresponding author: Pektaş K., e-mail: [koraypektas@ksu.edu.tr](mailto:koraypektas@ksu.edu.tr)

## INTRODUCTION

Recently, the ozone (O<sub>3</sub>) is applied to treat many illnesses such as cellulite, burnt, ulcer, chronic wounds, immune system illnesses etc. On examining these treatments, it is seen that the ozone is used both directly and ozonated vegetable oils in treatment of illnesses. However, comparing to ozone gas and the ozonated water, the ozonated oils have an advantage that the ozone is bonded to oil via unsaturated fatty acids. Thus, the ozone could be stored as ozonide and its effect goes a long [1-3]. The ozonides, which show anti-bacterial and anti-fungal activity, carry O<sub>2</sub> into lesion without sparking off skin irritation [4].

On the other hand, the microencapsulation is a preferable method to transfer ozonated oil onto textile surfaces. The microencapsulation is a caging method that liquid or solid particles, which are

located small droplets, are hindered in a thin film. The microencapsulation is formed by many methods such as in-situ polymerization, interfacial polymerization, coacervation, spray drying etc. [1,5]. But the coacervation methods are common to encapsulate oils among them [6].

Solution blown technique is a spinning method that inspired from both meltblown and electro spinning method, generate micro and nanofiber surfaces [7]. On examining literature on solution blowing spinning, there are much more studies on nanofiber spinning while there are a few studies on medical textile surfaces [8-11].

In this study, it was aimed to obtain biodegradable antibacterial nanofiber surfaces containing Momordica oil, its ozonated oil form and its microcapsules forms. To get these functionality, mormodica oil, ozonated mormodica oil and their microcapsules were mixed PLA polymer solution

and spun together. After that, a set of tests and analyses were employed both mormodica oil and obtained nanofiber surface.

## EXPERIMENTAL

### Materials

In the scope of this study, mormodica oil and its ozonated form were used as an active material. Arabic gum was used as shell material for microencapsulation process. PLA polymer was used for obtaining biodegradable nanofiber surfaces. Chloroform was used for dissolving the PLA polymer. 30 g/m<sup>2</sup> Polypropylene non-woven surfaces was used as a ground surface to collect PLA nanofiber.

### Methods

Crude mormodica oil were exposed to ozone gas for 135 min in a glass reaction column and then ozonated mormodica oil obtained (Figure 1).

As for the microencapsulation of the crude and ozonated mormodica oil, simple coacervation method was used and flow chart of the microencapsulation process was given in Figure 2.

Solution blowing spinning was used for obtaining PLA nanofiber. With this purpose, 10g PLA polymer was dissolved in the chloroform (100ml) for 2 hours at 60 °C. Then the polymer solution was cooled to room temperature. After that solution blowing spinning parameters were adjusted and PLA nanofiber were obtained. To obtain PLA nanofiber

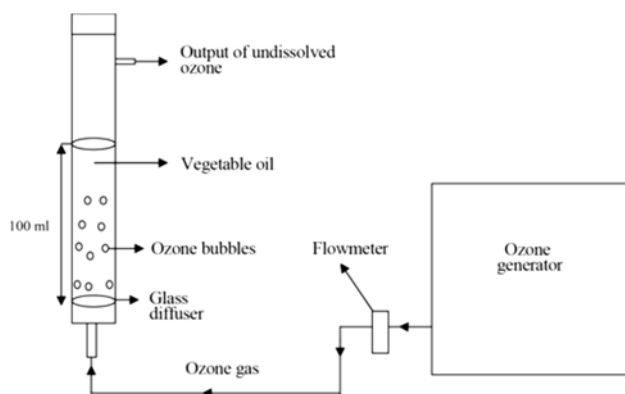


Figure 1. Schematic drawing of the ozonation process.

containing oil and microcapsules, 1 ml oil or microcapsule solution poured into the 20 ml PLA polymer solution. Then fiber spinning containing oil or microcapsules were employed. Fiber spinning parameter of the solution blowing spinning were given below.

- Solution feeding rate: 10ml/h.
- Air pressure: 2 bar
- Working distance: 37 cm
- Working time: 30 min.
- Distance between inner and outer nozzle: 2 mm

As for the characterization of the oils, total unsaturated fatty acid amount was determined by using GC and FT-IR analyses was done to observe change of the spectrum after ozonation process. Besides, disc diffusion method was used for investigating antibacterial activity of the oils. SEM images were taken for observe nanofiber morphology. Antibacterial activity of the nanofiber surfaces was analyzed according to the ASTM E 2149-01.

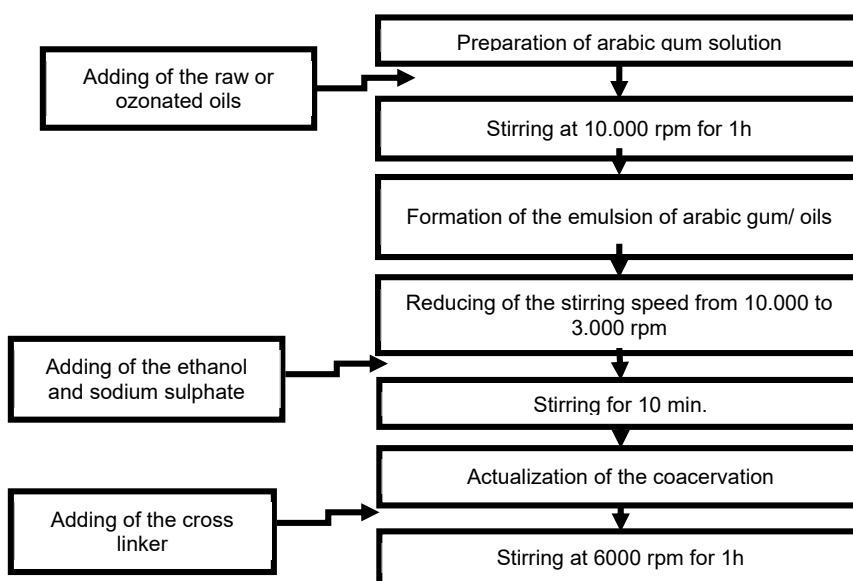


Figure 2. Flow chart of the microencapsulation process.

## RESULTS AND DISCUSSION

Total unsaturated fatty acid amounts of the oil were given in Table 1.

Total unsaturated fatty acid amount of the oils showed that unsaturated fatty acid amount decreased after ozonation process. Because the bound of the =C-H in the crude oil were broken and replace C-O bound. during the ozonation process. To support this hypothesis, FT-IR spectrum of the oil were investigated. FT-IR spectrum of the oil (Figure 3) showed that C-O bound was seen at  $1100\text{cm}^{-1}$  after ozonation process and it was proof of the ozonation of the mormodica oil was done successful.

On examining of the antibacterial activity of the crude and ozonated mormodica oil (Table 2), it was seen that both of them had antibacterial activity against to both gram negative (*E.coli*) and gram positive (*S.aureus*) bacteria with different inhibition zone. Besides, it was seen that antibacterial activity of the ozonated mormodica oil was higher than the crude one.

After characterization of the mormodica oil and ozonated one, PLA nanofiber surface were observed via SEM images. Upon observing of the PLA nanofiber morphology, it was seen that ground non-woven surfaces had micrometer fiber diameter while crude PLA fiber, containing oil and microcapsules ones had nanometer fiber diameter but some beads formations were observed. It was thought that nanofiber spinning parameter could change to hinder bead formations. Moreover, it was seen that microcapsules in the PLA nanofiber were seen as spherical shape.

**Table 1.** Total unsaturated fatty acid amount of the oils.

Unsaturated fatty acid (%)	Mormodica oil	Ozonated mormodica oil
Oleic acid	42,457	11,413
Linoleic acid	38,949	3.309
Total unsaturated fatty acid amount	81,406	14,722

**Table 2.** Antibacterial activity of the crude and ozonated mormodica oil.

Oil Sample	Inhibition zone diameter (mm)	
	<i>S.aureus</i>	<i>E.coli</i>
Crude mormodica oil	100	100
Ozanated mormodica oil	160	130

Antibacterial activity of the polypropylene non-woven and nanofiber surface against to gram negative (*E.coli*) and gram positive (*S.aureus*) bacteria showed that all surface had the antibacterial activity. However, of all the sample, PLA nanofiber containing crude mormodica oil and ozonated one had higher antibacterial activity against to *S.aureus*. On the other hand all sample did not show antibacterial activity against to *E.coli* (Table 3). This situation could be explained by lack of the amount of oil in the nanofiber. Because it was seen that antibacterial activity of the oil increased in tandem with the escalating of the oil amount according to the disc diffusion method. Thus, the more oil is contained in the nanofiber, the more antibacterial activity is observed.

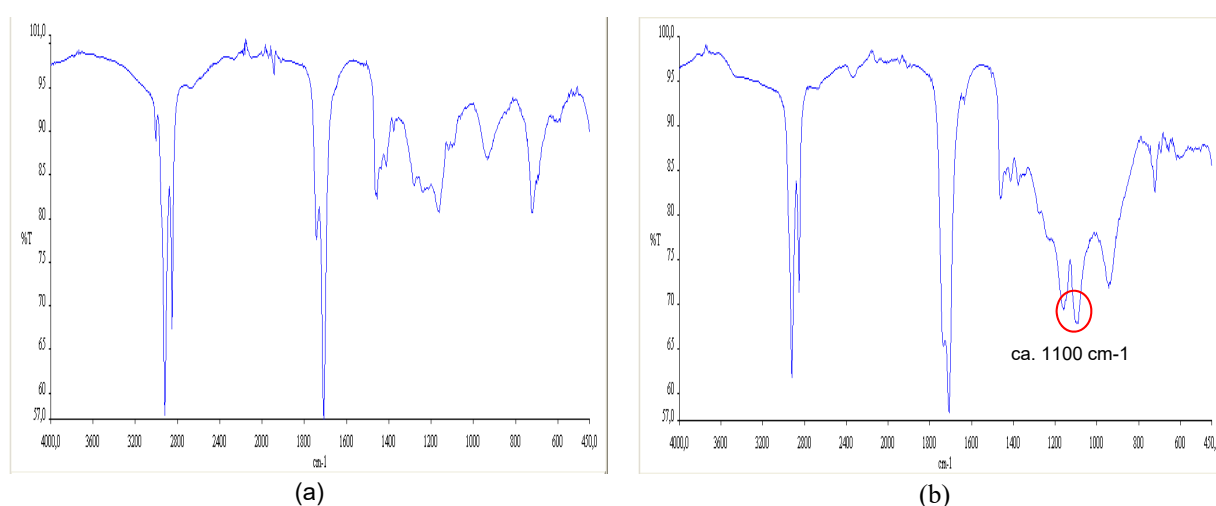


**Figure 3.** FT-IR spectrum of the oil a.mormodica oil b. ozonated mormodica oil.

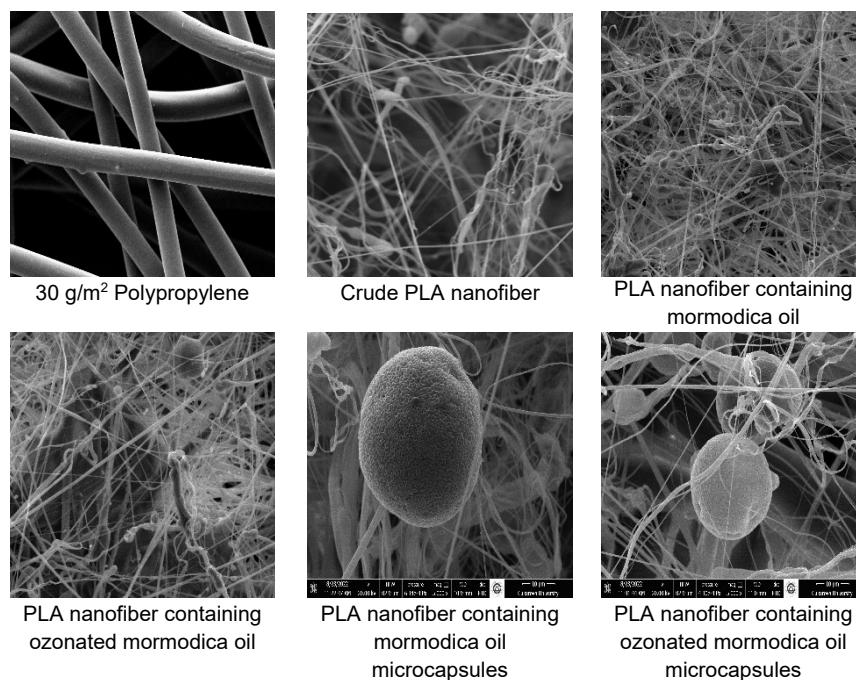


Figure 4. SEM images of the nanofiber.

Table 3. Antibacterial activity of the non-woven and nanofiber surfaces.

Sample	Bacteria reduction/proliferation (%)	
	<i>S.aureus</i>	<i>E.coli</i>
Polypropylene ground non-woven surface	-88,25	-11,48
PLA nanofiber	-83,51	-12,41
PLA nanofiber containing mormodica oil	-99,37	-11,11
PLA nanofiber containing ozonated mormodica oil	-100,00	-40,74
PLA nanofiber containing mormodica oil micro capsules	-81,40	-11,67
PLA nanofiber containing ozonated mormodica oil micro capsules	-98,72	-10,19

## CONCLUSIONS

In the scope of this study, ozonated oil showing antibacterial activity were obtained. After that, crude and ozonated mormodica oil were microencapsulated via simple coacervation successfully. PLA nanofibers were spun by solution blowing spinning. Moreover, PLA nanofiber containing oil and microcapsules were spun successfully but some beads formation in the surfaces was observed. Nevertheless, All surface show antibacterial activity against to *S.aureus* while they did not show antibacterial activity against to *E.coli*. For further studies, it is thought that fiber formation parameters of the solution blowing spinning for PLA polymer will investigate deeply and will try to obtain antibacterial activity of the surfaces against to gram negative bacteria (*E.coli*).

**Acknowledgements:** This study (5220045) is funded by The Scientific and Technological Research Council of Turkey, Republic of Turkey (TUBITAK). We would like to thank warmly TUBITAK for supporting this study.

## REFERENCES

- Beşen, B. S., Güneşoğlu, C., Balci, O., & Sütçü, K. (2016). Antibacterial Finishing of 100% Cotton Fabric with  $\beta$ -Cyclodextrin-Ozonated Olive Oil Inclusion Complex. *AATCC Journal of Research*, 3(6), 12–18. <https://doi.org/10.14504/ajr.3.6.3>
- Beşen, B. S., Güneşoğlu, C., Balci, O., Sütçü, K., Balci, O., Güneşoğlu, C., İrem Tatlı, İ. (2016). Obtaining medical textiles including microcapsules of the ozonated vegetable oils. *AATCC Journal of Research*, 3(6), 12–18. <https://doi.org/10.1007/s12221-017-1212-8>
- Sancar BEŞEN, B., Balci, O., Orhan, M., Güneşoğlu, C., İrem TATLI, İ., Sütçü İmam Üniversitesi, K., ... Botanik Anabilim Dalı, F. (2015). Ozonlanmış Yağlar ile İşlem Uygulanmış Dokusuz Yüzeylerin Antibakteriyel Etkinliklerinin İncelenmesi An Investigation on Antibacterial Activities of Nonwovens Treated with Ozonated Oils. *Journal of Textiles and Engineer*, 22(100), 25. <https://doi.org/10.7216/1300759920152210003>
- Öcal, E., (2013), Ozon Yağının Kapsül Formasyonu Üzerindeki Etkisi. Uzmanlık Tezi. Hacettepe Üniversitesi Tıp Fakültesi. Ankara. s.14
- Karthikeyan, M., Ramachandran, T., Shanmugasundaram, O.L., (2014), "Synthesis, Characterization, and Development of Thermally Enhanced Cotton Fabric Using Nanoencapsulated Phase Change Materials Containing Paraffin Wax", *The Journal of The Textile Institute*, <https://doi.org/10.1080/00405000.2014.886368>
- Özyıldız, F., Karagönüllü, S., Basal, G., Uzel, A., Bayraktar, O., (2012), "Micro-encapsulation of Ozonated Red Pepper Seed Oil with Antimicrobial Activity and Application to Nonwoven Fabric", *The Society for Applied*

- Microbiology, *Letters in Applied Microbiology*, vol.56, pp.168-179.  
<https://doi.org/10.1111/lam.12028>
7. Medeiros, E. S., Glenn, G. M., Klamczynski, A. P., Orts, W. J., & Mattoso, L. H. C. (2009). Solution blow spinning: A new method to produce micro- and nanofibers from polymer solutions. *Journal of Applied Polymer Science*, 113(4), 2322–2330.  
<https://doi.org/10.1002/app.30275>
  8. Calisir, M. D., & Kiliç, A. (2020). A comparative study on SiO<sub>2</sub> nanofiber production via two novel non-electrospinning methods: Centrifugal spinning vs solution blowing. *Materials Letters*, 258, 126751.  
<https://doi.org/10.1016/j.matlet.2019.126751>
  9. Polat, Y., Calisir, M., Gungor, M., Sagirli, M. N., Atakan, R., Akgul, Y., ... Kiliç, A. (2019). Solution blown nanofibrous air filters modified with glass microparticles. *Journal of Industrial Textiles*, 1–14.  
<https://doi.org/10.1177/1528083719888674>
  10. Shi, L., Zhuang, X., Tao, X., Cheng, B., & Kang, W. (2013). Solution blowing nylon 6 nanofiber mats for air filtration. *Fibers and Polymers*, 14(9), 1485–1490.  
<https://doi.org/10.1007/s12221-013-1485-5>
  11. Sinha-Ray, S., Sinha-Ray, S., Yarin, A. L., & Pourdeyhimi, B. (2015). Application of solution-blown 20-50nm nanofibers in filtration of nanoparticles: The efficient van der Waals collectors. *Journal of Membrane Science*, 485, 132–150.  
<https://doi.org/10.1016/j.memsci.2015.02.026>
  12. Liu, Y., Zhang, G., Zhuang, X., Li, S., Shi, L., Kang, W., ... Xu, X. (2019). Solution blown nylon 6 nanofibrous membrane as scaffold for nanofiltration. *Polymers*, 11(2), 1–15.  
<https://doi.org/10.3390/POLYM11020364>

# CHITOSAN ADDED COMPOSITE VISCOSE YARN AND ITS POTENTIAL APPLICATION FOR DENIM FABRIC DEVELOPMENT

KORKMAZ AHMET<sup>1\*</sup> AND BABAARSLAN OSMAN<sup>2</sup>

<sup>1</sup> R&D Department, Çalılık Denim Textile AŞ., Yeşilyurt, Malatya, Turkey

<sup>2</sup> Cukurova University, Department of Textile Engineering, Adana, Turkey

## ABSTRACT

The rapid increase in consumption has led to the decrease and even extinction of natural resources on earth. The textile industry also has an important place in terms of consumption. The transition to more sustainable biodegradable products instead of established fossil-based materials has increased rapidly due to textile manufacturers and related industries, legal regulations, social responsibility commitments and increasing ecological awareness of customers. Developing new environmentally friendly, biodegradable material groups with new technologies or by modifying existing technologies has been the main goal of many researchers. In this context, we aimed to develop denim fabric that is effective against strong hospital bacteria by using the yarn containing biopolymer chitosan as a weft in denim production. Chitosan finds wide application in the textile industry due to its biodegradability, antibacterial activity and many more functionalities. Chitosan is used in biomedical textile applications in the textile industry, either as a wound healing, hemostatic (blood stopper), antibacterial, antifungal, either alone or modified to various derivatives or combined with other materials. In this context, instead of using chitosan as a coating material in our studies, chitosan-containing yarn was used in the production of denim fabric in order to distribute the chitosan more homogeneously and to increase the washing resistance. As a result, it was determined that the denim fabric developed by using chitosan-based yarn in weft in denim production reduces hospital bacteria (MRSA-Methicillin resistant staphylococcus aureus) by > 99%.

## KEYWORDS

Chitosan; Antibacterial; Denim fabric; Biodegradability; MRSA; Medical textiles.

---

\* Corresponding author: Korkmaz A., e-mail: [ahmet.korkmaz@calikdenim.com.tr](mailto:ahmet.korkmaz@calikdenim.com.tr), [teksob@cu.edu.tr](mailto:teksob@cu.edu.tr)

## INTRODUCTION

Seafood producing companies around the world throw large quantities of crab and shrimp shells into the environment without reuse. In recent years, intensive studies of researchers about the reuse of wastes has also included shrimp and crab shells, and these wastes are evaluated by chemical or biological methods and new products are obtained. Chitin and its most important derivative, chitosan, are among the products obtained in this way. The wastes of the shrimps, whose meat is separated in the processing plants, constitute approximately 40-56% of the total product. Shell wastes also contain very valuable bioactive components such as antioxidants, peptones, amino acids, peptides, proteins, minerals, enzymes, lipids and other beneficial nutrients. The raw material requirement for the production of chitin is met from shrimp (56,000 tons), various shellfish (39,000 tons),

mushrooms (32000 tons), oysters (23000 tons). In Figure 1, the production process of the chitin is shown.

Chitosan is a biopolymer obtained by deacetylation of chitin ( $\beta$ -(1-4)-poly-N-acetyl-D-glucosamine), which is the most common in nature after cellulose. In Figure 2, the production process of the chitin with the chemical method is shown.

Chitosan, a natural biopolymer with biocompatible, non-toxic and antibacterial properties, can be used in different forms such as solution, powder, fiber and film [12]. The reason for the analgesic effect of chitosan is due to its polycationic structure. The biodegradability of chitosan is due to the fact that chitosan is not only a polymer carrying amino groups, but also a polysaccharide, which as a result contains brittle glycosidic bonds. [7].



Figure 1. Production process of chitin [5].

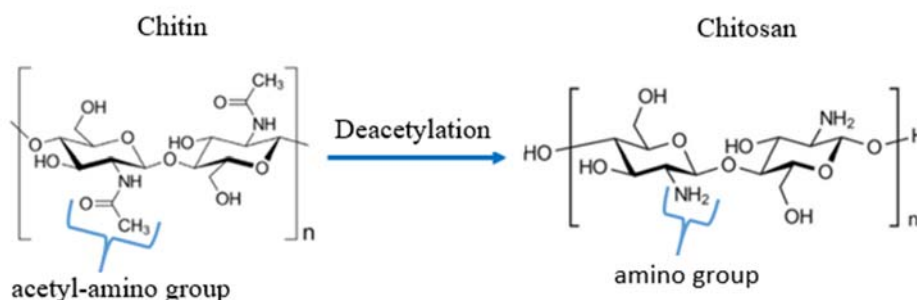


Figure 2. Chitosan from chitin via deacetylation [5].

The presence of amino groups in the chitosan structure (Figure 3) distinguishes it from chitin, and this difference gives the polymer many special properties. The amino groups in the chitosan structure can be protonated by providing solubility in diluted acidic aqueous solutions. In contrast, the practical applications of chitin, if any, are extremely limited due to its poor solubility [2].

In addition, due to these amino groups, chitosan efficiently complexes various species such as metal ions and is therefore often used in wastewater treatment, purification by recovery of heavy metals (Rinaudo 2006). The hemostatic property of chitosan can also be associated with the presence of positive charges present in chitosan. This is because the membranes of red blood cells are negatively charged and therefore can interact with the positively charged chitosan. The fact that chitin has less hemostatic properties than chitosan tends to confirm this explanation [2].

Chitosan can be converted into many forms such as hydrogel, sponge, membrane, film, depending on the area of use. As it is known, sponges are open-pore foams and can absorb large amounts of liquid due to their microporosity. Chitosan-based sponges are mostly used as wound-healing materials, as they can absorb wound exudates while aiding tissue regeneration. Chitosan sponges also find application in bone tissue engineering as filling material [9, 8].

Stegmaier et al. investigated the use of chitosan as a sizing agent with appropriate modification in the textile industry. As a result of these studies, economic and ecological advantages in sizing have been demonstrated by increasing the weaving efficiency based on the reduction of yarn breaks with chitosan-based sizing [11].

The use of chitosan as an absorbent in the removal of dyes to treat textile wastes has been investigated. In this context, chitosan was found to be very effective in removing dianix orange S-G, a disperse

dye, from wastewater. Dye removal was carried out using the ability of chitosan to dissolve in acidic medium and reform in basic medium [14].

Chitosan has been used as an aid to increase the uptake of anionic dyes in textile dyeing. Chitosan is used instead of salt in reactive dye dyeing of cotton fabric. Cellulosic fiber takes a negative charge in the aqueous medium and repels the negatively charged dye anion during dyeing. Such repulsion between fiber and dye is avoided by using salt in the dyebath for reactive dyes.

By treating cotton fabric with chitosan, Ashenafi et al. revealed that surface modification of cotton provides better dyeing properties and the best possibility for salt-free dyeing of cotton may be the use of chitosan [1].

Erdoğan et al. aimed to develop a new generation of environmentally friendly antibacterial finishes by using chitosan as a binder for nano-silver coatings. In the study, chitosan formed a colorless film and formed a matrix that allowed nano-Ag particles to accumulate homogeneously on the fabric surface, and as a result, a very strong anti-bacterial effect was observed [4].

Chitosan can be crosslinked with cellulose using polycarboxylic acids, thus providing better bonding between chitosan and cotton fabric. A good wrinkle recovery was obtained in cotton as a result of the cross-linking of chitosan and cellulose by polycarboxylic acids [13].

Ivanova et al. developed super hydrophobic and anti-bacterial textiles using chitosan-based nanoparticles for biomedical applications (6). In their studies, Raeisi obtained superhydrophobic cotton fabrics by using chitosan and titanium dioxide (TiO<sub>2</sub>) nanocomposites [10].

MRSA (also known as supervirus) stands for methicillin-resistant *Staphylococcus*. MRSA is a "staph" germ (bacteria) that does not get better with

the type of antibiotics that usually cure staph infections. These kind of staph germs are spread by skin-to-skin contact. Healthcare personnels or visitors to a hospital may carry staph germs on their body which can spread to a patient. After entering to the body through open wounds, burns or cuts can this staph germ spread to bones, joints, the blood, or any organ, such as the lungs, heart, or brain and can cause serious health problems. If we list the groups at risk in addition to healthcare personnel: athletes who share items such as towels or razors, draggie, people who had surgery in the past year, children in day care, members of the military.

Denim is a textile product that can be worn by people of all ages and kinds. From this point of view we aimed to developed a denim fabric, which controbute to reduction of super virus MRSA spreading among both healthcare personnel, hospital visitors and above mentioned people at risk. In line with this purpose we used chitosan containing weft yarn in denim.

**EXPERIMENTAL**

**Materials**

The application of chitosan to cotton fabrics has mostly been in the form of microcapsules of powdered chitosan or in the form of coating by dissolving in acid. In order to make chitosan more homogeneous and permanent in denim fabric, chitosan-based yarn was supplied in this study. For the denim production was used Ne 30/1 chitosan-based yarn as weft.

The physical properties of chitosan containing yarn as weft in denim production are shown in Table 1. When yarns are compared especially in terms of hardness and elongation, it is seen that chitosan-based yarn is better.

**Methods**

The developed denim with chitosan rayon yarn and cotton yarn in weft is weaved according to procedure in Table 2. The processes applied to the weaved denim fabrics are summarized in Figure 3.

**Table 1.** The physical properties of in denim production used yarn.

Yarn	Ne	%U	Hairness	Elongation	Stiffness
Chitosan viscose yarn	30/1	10,1	4,73	9,21	17,96
Combed cotton yarn	30/1	10,5	5	5,5	15,5-16

**Table 2.** Weaving procedure.

	Warp Yarn	Warp Yarn Number Ne	Weft Yarn	Weft Yarn Number Ne	Weft density	Weaving Type	Warp Wire Count	Comb Width	Comb No/Number of wire through
<b>Sample 2</b>	%100 CO	20/1	%100 CO	30/1	27,5	3/1 Z	5880	210	140/2
<b>Sample 1</b>	%100 CO	20/1	Chitosan based	30/1	27,5	3/1 Z	5096	182	70/4

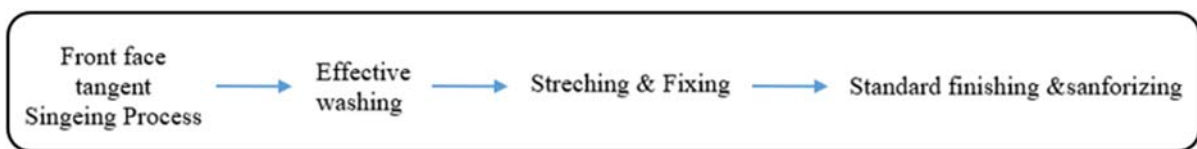


**Figure 3.** Applied processes to the weaved denim fabric.

**RESULTS AND DISCUSSION**

FT-IR Analysis of chitosan containing yarn

The FT-IR spectra for commercial chitosan powder in comparison with chitosan rayon yarn, which is used as weft in denim is illustrated in Fig. 4. The main characteristic peaks of commercial chitosan powder are at 3357 (-OH & -NH stretch), 2974 (C-H stretch), 1647 and (N-H bend), 1374 (bridge O stretch), and 1024 cm<sup>-1</sup>(C-O stretch). Whereas the main corresponding peaks of chitosan rayon yarn

were at 3350, 2880, 1652, 1378 and 1024 cm<sup>-1</sup> respectively.

SEM/analysis

To compare the structure of the chitosan containing rayon yarn with cotton yarn cross-section of fibers were studied using SEM. When the cross-section images of chitosan containing yarn are compared with commercial viscose rayon fiber product, the similarity can be seen in figure 6. The both fibre have close to circular cross-section.

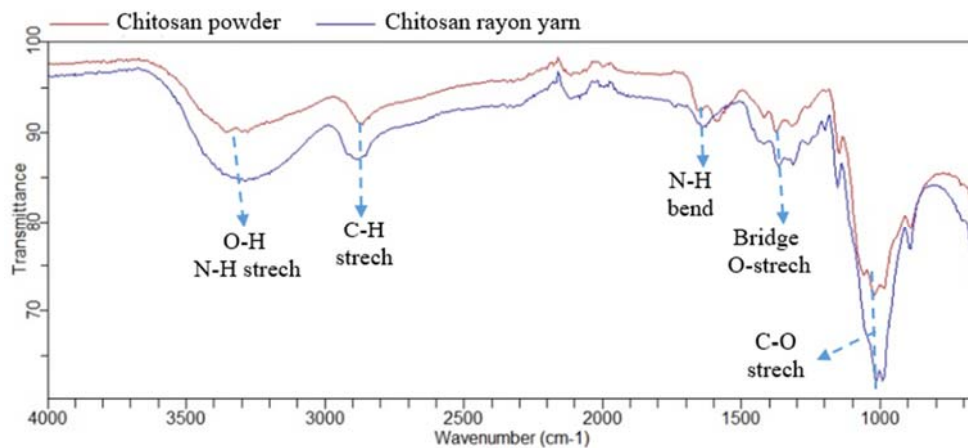


Figure 4. FT-IR spectra of commercial chitosan powder and chitosan viscose yarn.

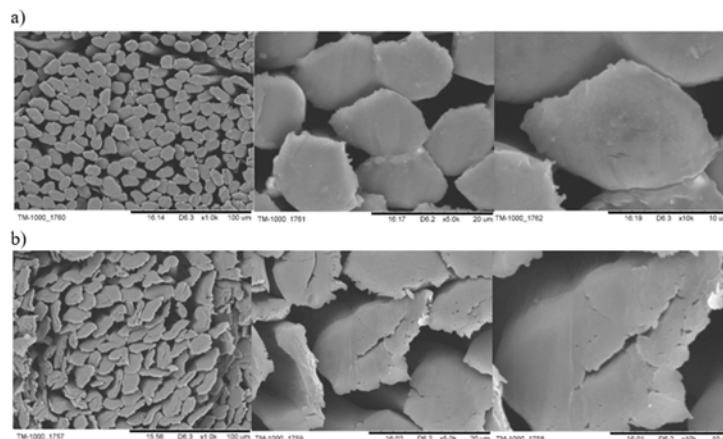


Figure 5. SEM Pictures of: (a) Cross section of chitosan containing rayon yarn Ne 30/1 (1000/5000/10000), (b) Cross section of cotton yarn Ne 30/1, (1000/5000/10000).

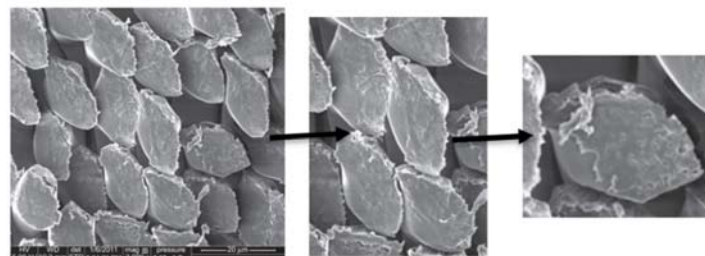


Figure 6. Lyocell rayon fiber cross-sectional view SEM [3].

Physical Properties of Weaved Denim

The weaved two denim fabrics with the same warp and different weft were compared relates to their physical properties. Dry-wash crocking results of both fabrics seems to be practically same. According to tear result of chitosan containing yarn compared with Ne 30/1 cotton yarn in weft is more durable than cotton yarn (Table 3).

Determination of antibacterial activity: The antibacterial activity of developed denim with chitosan containing yarn in weft was determined according to AATCC 100:2019 standards with the test organism staphylococcus aureus MRSA (ATCC 33591) in Intertek Testing Services Taiwan Ltd. As can be seen from the result in Table 3, the super

bacteria MRSA is reduced by more than 99.92 % on the developed denim fabric.

After 24 hours of incubation the reduction in methicillin staphylococcus aureus MRSA (ATCC 33591) is depicted in Figure 7.

The positively charged ions provided by Chitosan concentrate on the surface of the fabric and provide antibacterial protection to the fabric. When bacteria containing negative ions come into contact with the chitosan surface on the fabric; The positively charged ions bind to the bacteria and cause their enzymes to break down. The enzymes are then unable to produce energy, which inhibits the bacteria from multiplying and the bacteria eventually die.

**Table 3:** Physical Properties of weaved denim.

Weft Yarn	WEIGHT		WEIGHT		CROCKING		STIFFNESS	pH	TENSILE ( kgf )		TEAR ( grf )	
	DRY	WASH	DRY	WASH	DRY	WET			WARP	WEFT	WARP	WEFT
	gr/m <sup>2</sup>	gr/m <sup>2</sup>	oz/yd <sup>2</sup>	oz/Yd <sup>2</sup>								
Ne 30/1 Chitosan containing	176	177	5,2	5,2	2-3	1-2	0,28	4,54	43	24	3588	2936
Ne 30/1 Cotton	189	173	5,6	5,1	3	1-2	0,25	4,87	40	26	3719	2675

**Table 4.** Antibacterial activity test result of developed denim fabric.

Name Of Test Bacteria (Strain Number)	<i>Methicillin resistant staphylococcus aureus</i> (ATCC 33591)
The number of bacteria recovered from the inoculated viability control fabric swatches immediately after inoculation ("0" contact time) (D)	1.5 X10 <sup>5</sup> CFU/Sample
The number of bacteria recovered from the inoculated viability control fabric swatches incubated over 24 hours contact period (B)	1.8 X10 <sup>7</sup> CFU/Sample
The number of bacteria recovered from the inoculated tested sample swatches immediately after inoculation ("0" contact time) (C)	1.3 X10 <sup>5</sup> CFU/Sample
The number of bacteria recovered from the inoculated tested sample swatches incubated over 24 hours contact period (A)	<100 CFU/Sample
Growth value (F)	2.08
Percent reduction of Bacteria (R)	>99.92%

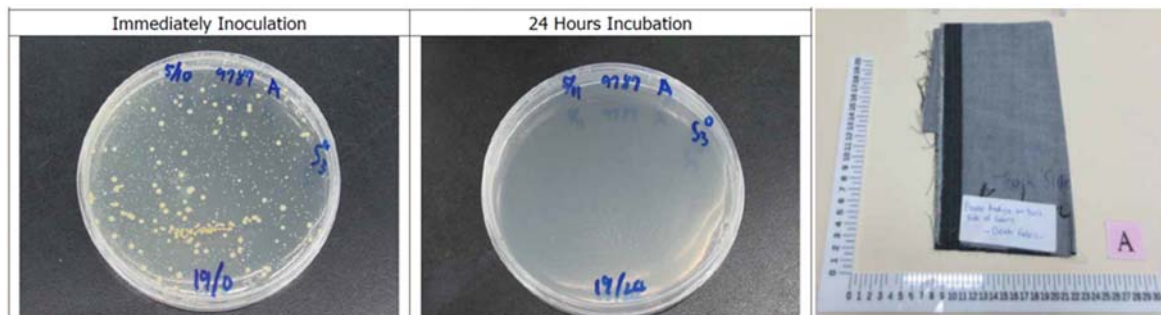


**Figure 7.** Reduction of MRSA after 24 hours incubation.

## CONCLUSIONS

Chitosan is a biopolymer with biocompatible, non-toxic and antibacterial properties which is the most common in nature after cellulose. In this work, it is aimed to create a denim fabric containing chitosan rayon yarn. For this purpose, we provided with wet spinning method produced chitosan containing yarn in order to use as weft yarn in denim. The antibacterial activity of developed denim with chitosan containing yarn in weft was determined according to AATCC 100:2019 standards with the test organism staphylococcus aureus MRSA (ATCC 33591) in Intertek Testing Services Taiwan Ltd. The super bacteria MRSA is reduced by more than 99.92 % on the developed denim fabric. As far as we know, it exists any study in the literature related to the use of chitosan as weft yarn in denim related to

activity gains methicillin staphylococcus aureus MRSA (ATCC 33591).

Denim is a textile product that can be worn by people of all ages and kinds. From this point of view we succeed to developed a denim fabric, which controbute to reduction of super virus MRSA spreading among both healthcare personnel, hospital visitors and soldiers, athletes at risk. If this product is used by healthcare personnel or hospital visitors can protect their health and reduce the casualties of patients caused by MRSA nosocomial infections, and reduce huge medical expenses.

**Acknowledgements:** ÇALIK DENİM TEKSTİL A.Ş., which provides all kinds of technical and administrative support during the management and execution phases of this study. We would like to thank the management.

## REFERENCES

1. Bethlehem, A., Studies on dyeing properties of chitosan modified cellulosic fiber, *Journal of Textile Engineering & Fashion Technology*. 2020;6(1):37–42.  
<http://dx.doi.org/10.15406/jteft.2020.06.00224>
2. Croisier, F., 2013, Chitosan-based biomaterials for tissue engineering *European Polymer Journal* 49 (2013) 780–792  
<http://dx.doi.org/10.1016/j.eurpolymj.2012.12.009>
3. Chen, J., 2015. Synthetic textile fibers: regenerated cellulose fibers. In: Sinclair, R. (Ed.), *Textiles and Fashion*. Woodhead Publishing in Association with the Textile Institute.  
<http://dx.doi.org/10.1016/B978-1-84569-931-4.00004-0>
4. Erdoğan, S., Textilefinishing with chitosan and silver nanoparticles against *Escherichia coli* ATCC 8739, *Trakya University Journal of Natural Sciences*, 21(1): 21-32, 2020 ISSN 2147-0294, e-ISSN 2528-9691  
<https://doi.org/10.23902/trkjinat.641367>
5. Kuzgun N., Chitosan Production, Chitosan Properties and Usage Areas., *Türk Bilimsel Derlemeler Dergisi* 6 (2): 16-21, 2013
6. Ivanova, N.A., Superhydrophobic chitosan-based coatings for textile processing, *Applied Surface Science* 263 (2012) 783–787  
<https://doi.org/10.1016/j.apsusc.2012.09.173>
7. Ibrahim, H. M., 2015, Concepts, Compounds and the Alternatives of Antibacterials, Chitosan as a Biomaterial — Structure, Properties, and Electrospun Nanofibers. 10.5772/59522(Chapter 4)  
<https://dx.doi.org/10.5772/61300>
8. Lee Y-M, Park Y-J, Lee S-J, Ku Y, Han S-B, Choi S-M, et al. Tissue engineered bone formation using chitosan/tricalcium phosphate sponges. *J Periodontol* 2000;71:410–7.  
<https://doi.org/10.1902/jop.2000.71.3.410>
9. Costa-Pinto AR, Reis RL, Neves NM. Scaffolds based bone tissue engineering: the role of chitosan. *Tissue Eng Part B*, 2011;17:331–47.  
<https://doi.org/10.1089/ten.teb.2010.0704>
10. Raeisi, M., Superhydrophobic cotton fabrics coated by chitosan and titanium dioxide nanoparticles with enhanced antibacterial and UV-protecting properties *International Journal of Biological Macromolecules* 171 (2021) 158–165  
<https://doi.org/10.1016/j.ijbiomac.2020.12.220>
11. Stegmaier, T., Chitosan – A Sizing Agent in Fabric Production – Development and Ecological Evaluation, *Clean* 2008, 36 (3), 279 – 286  
<http://dx.doi.org/10.1002/clen.200700013>
12. Şahan, G., 2014, Kitosan biyopolimerinin formları ve tekstil uygulamaları, XIII. Uluslararası İzmir Tekstil ve Hazır Giyim Sempozyumu,170
13. Sunder, Edwin A., 2014, Croslinking of Chitosan with Cotton using Polycarboxylic Acids, *International Journal of Engineering Research & Technology (IJERT)*, ISSN: 2278-0181, Vol 3 Issue 4,
14. Vithanage, A.H., 2015, Textile Dye Removal in Wastewater Using Chitosan, *Annual Sessions of IESL*, pp. [1 - 10], [doi:10.4028/www.scientific.net /AMR.610-613.3394](https://doi.org/10.4028/www.scientific.net/AMR.610.613.3394)

# DESIGN OF ELECTRONICALLY CONTROLLED JACQUARD MACHINE FOR MULTI-SHED WEAVING MACHINES

ARSOY RAŞIT<sup>1\*</sup> AND ASLAN SELÇUK<sup>2</sup>

<sup>1</sup> Kafkas University, Faculty of fine arts, Department of Textile and Fashion Design, Kars 36000, Turkey

<sup>2</sup> Kafkas University, Fine Arts Vocational School, Department of Design, Kars 36000, Turkey

## ABSTRACT

The Jacquard shed opening system, which makes it possible to open the shed by controlling the warp threads in groups and obtain different designs and shapes, differs from other shed opening systems in that each group of warp threads and each of them can be controlled as needed. The various warp movements, which are limited by the number of frames in other shedding systems, are limited by the number of sinkers in the Jacquard system. Since all known Jacquard shedding systems are designed for operation with single shed weaving machines, they cannot be used for shedding on multiple weaving machines. In this study, a new electronically controlled jacquard machine for multiple shed weaving machines was developed, which eliminates this problem and enables the opening of the weaving compartments by controlling the warp threads individually in multiple shed weaving machines, thus allowing the weaving of all known jacquard fabric patterns.

The technological and kinematic schemes of the jacquard machine were prepared taking into account the type of fabric to be produced, the operating principles of the weft insertion and shedding mechanisms to be used in the machine to be developed, and the expectations for improving the technical and economic indicators of the machine.

The electronically controlled pattern reading system, which consists of modules in the machine, converts the electronic data into mechanical data to ensure shedding. In the cam shedding mechanism, which transmits motion to the knives in the form of a stepped shaft in the multiple weaving machine, the warp threads are placed on the knives so that they can move vertically. They are controlled by specially structured sinkers which, in contact with the blades, move from the lower to the upper state with the help of the blades and from the upper to the lower state with the help of springs. When the warp threads are to remain in the upper position according to the pattern, the sinkers are interlocked by electromagnets to form an undulating nozzle corresponding to the fabric pattern.

By arranging the interlocking projections along the sinker, it is possible to match the density of the sinker to the density of the warp threads.

Since the machine allows weaving of all known jacquard fabrics, the problem of not being able to produce weaves other than the rag foot weave, which is considered one of the major drawbacks of multiple shed weaving machines, has been solved.

## KEYWORDS

Jacquard; Shed; Weaving; Plate; Thread.

---

\* Corresponding author: Arsoy R., e-mail: [rasitarsoy@gmail.com](mailto:rasitarsoy@gmail.com)

## INTRODUCTION

The Jacquard shed opening system, which makes it possible to open the shed by controlling the warp threads in groups and obtain different designs and shapes, differs from other shed opening systems in that each group of warp threads and each of them can be controlled as needed [1, 2, 3, 11]. The various warp movements, which are limited by the number of frames in other shedding systems, are limited by the number of sinkers in the Jacquard system.

According to motion control systems, Jacquard machines can be mechanically and electronically controlled. Today, electronic control systems are used in all Jacquard machines.

To enable the production of more complex patterns, research is being carried out into the design of Jacquard machines that allow individual control of the warp threads.

In the invention of Jonathan F. McIntyre, information is given on the construction of an electronically

controlled device that can control the warp threads individually [7].

Walter Keim and Kurt Jhile did the work on an electromagnetic basis. A common electromagnet between the hooks is used to control the shed in a certain position according to the scheme. The electromagnet is attached to the case so that it can be tilted or pivoted about an axis. In the pattern reading position, each hook moves mechanically to approach the pole of the electromagnet, especially to lean against it [9].

Chi Zhang introduced the basic design technologies of jacquard knitting integrated control system, the structure of integrated control system. The results of this project provided some theoretical and practical implications for the development of electronic jacquard control system [4].

M. Kaplan's project involved the manufacture, development and improvement of a prototype pattern loom using a Jacquard shedding machine. It was found that a more complex pattern could be produced by individual manipulation of the warp threads using the Jacquard mechanism [6].

Since all known Jacquard shedding systems are designed to operate on single shed weaving machines, they cannot be used for shedding on multiple shed weaving machines.

In this paper, information is given on the design structure of a new Jacquard machine for multiple shed weaving machines, developed by me, which eliminates this problem and enables shedding by controlling the warp threads one by one on multiple shed weaving machines, allowing all known Jacquard fabric patterns to be woven.

## MATERIALS AND METHODS

The development of a new Jacquard machine requires in-depth knowledge of fabric theory and extensive knowledge of existing designs of known Jacquard machines and mechanisms. Due to the necessity of performing these operations and the complexity of the Jacquard machine design, care was taken to ensure that the design steps listed below were fully implemented in the design [11, 21]:

1. For the design of the Jacquard machine, the technological task was developed. At the same time, the characteristics of the technological process were carefully studied and the mechanical properties of the new machine were critically evaluated;

The design structures of existing Jacquard machines were studied, patents and technical literature were studied to determine the functionality of the machine

to be designed, the main directions of its production perspective and the development prospects;

2. The technological and kinematic schemes of the jacquard machine were prepared taking into account the type of fabric to be produced, the operating principles of the weft insertion and shedding mechanisms to be used in the machine to be developed, and the expectations for improving the technical and economic indicators of the machine;

Figure 1 shows the technology diagram of the wave shed fabric forming system [21]. The shuttle 9 carrying the weft 10 moves at constant speed in the direction shown in the figure in a nozzle A which opens in front of it and closes behind it in a wave-like manner. The number of sheds depends on the dimensions of the shuttle and the width of the fabric. The fabric forming process is realized by compressing the weft threads introduced into the shed to the fabric line with the help of the special weaving blade number 11 in wave motion.

It is not so easy to transfer the movement to the shuttles in the closed shed. Many methods have been proposed for this purpose. One of the methods is to use the weight of the shuttle as the force that stabilizes the shuttle in the shed. When the teeth of the weaving blade number 11 move from left to right, the shuttles move in the horizontal direction at a certain speed under the influence of the friction force.

The main technical scheme of the machine is similar to the known technical schemes. The warp yarns No. 2 opening from the warp beam No. 1 pass through the warp bridge No.3, the warp control system No. 6 and the shafts No. 4, 6, through the eyelets of the reeds No. 8 attached to the frames No. 7 of the shedding mechanism and through the comb teeth No. 11 and reach the fabric forming zone. After the finished fabric has passed the fabric tension shaft No. 12, it is wound onto the fabric beam No. 13.

The motion on the frames is transmitted by the shed forming mechanism No. 15 and the motion on the card teeth No. 11 is transmitted by the weaving blade mechanism No. 14.

When forming a shed, several frames are used to form the shed in the shape of a wave and to allow wave-like movement of the shed along the width of the warp threads.

The main advantages of this technology are that the fabric formation is similar to the classical methods, the machine works at low speeds and has a high efficiency.

The main disadvantage of this technology is that it can be used only for the production of one type of fabrics, namely rag fabrics [1, 21, 24].

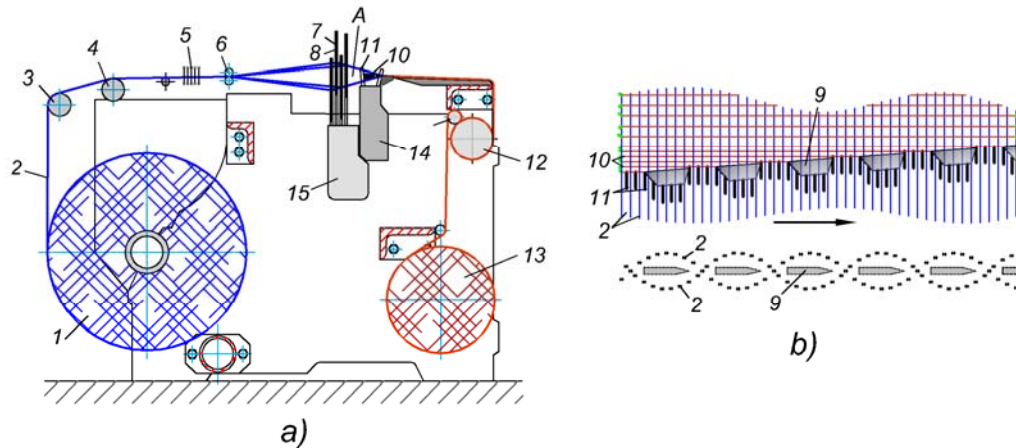


**Figure 1.** Technological scheme of the multiphase weaving machine with wave shed: a) technological scheme; b) threading the weft threads through the shed.

### Presentation of the newly developed machine.

In this study, a new electronically controlled Jacquard machine for multiple shed weaving machines was designed by analyzing the design structures of existing Jacquard machines, patents on the design of shedding systems of multiple shed weaving machines, technical literature and publications on this subject in technical journals [10-22, 24].

In order to make the working principle of the designed Jacquard machine easy to understand, the machine is presented with seven technical drawings:

Fig. 2 - General view of the Jacquard machine mounted on the weaving machine and B-B cross-section of the machine in the front view plane;

Fig. 3 - A-A cross-section of the Jacquard machine in the left view plane;

Fig. 4 - Schematic describing the operation of the electronically controlled interlock mechanism;

Fig. 5 - Cross-section C-C illustrating the assembly and guiding of the sinkers;

Fig. 6- Scheme explaining the formation of the wavy nozzle on the machine;

Fig. 7 - Three-dimensional view of the Jacquard machine explaining its structure and operation;

Fig. 8 - Three-dimensional view of the sinker.

The movement to the Jacquard machine is transmitted from the main shaft of the weaving machine through a 17-18 bevel gear. The machine consists of a computerized electronically controlled pattern reading system, a cam mechanism numbered 4-5 that transmits a wave-like motion to the knives, and a system that transmits motion from the knives to the warp threads according to the pattern.

In the shedding mechanism with cams No. 4-5 transmitting a stepped wave-like motion to the drop wires No. 6, the warp threads No. 1 are placed on the drop wires in such a way that they can move vertically from the lower to the upper layer of the drop wires with the help of the springs 16, in the opposite direction, from the upper layer to the lower layer, they are guided by the specially structured sinkers 8 in contact with the drop wires 6.

The design structure of the sinkers, which transmit the movement to the warp threads depending on the pattern, is shown in Figure 8. The plate, made of thin steel bar, has a locking projection E at the lower end and a slot D at the other end, through which the knives can move freely when the sinkers are locked.

The electronically controlled pattern reading system consists of No. 9 modules. The task of the modules in the machine is to convert the electronic data into mechanical data (the pattern in the computer into a mechanical movement) to ensure the formation of the nozzle. This operation is performed by the electromagnet No. 11 with the latches No. 10. When the warp threads are to remain in the upper position according to the pattern, a magnetic field is generated with the help of the given electric current, and the latches are mobilized. The end of the latch 10, which is pulled and rotated during magnetization, enters the slot E opened on the board and ensures that it is locked and the warp threads remain in the upper position. When the warp threads are to be lowered, the power supply to the module is interrupted. In this case, the end of the pawl rotating in the negative direction comes out of the slot with the help of the spring 12 and the sinker is released and moves together with the knife to the lower position. Lowering of the sinker together with the knife is ensured by the spring 16 connected to the sinker by the thread No. 15.

The number of electronic control modules corresponds to the number of sinkers used in the machine. Since the width of the modules is greater than the thickness of the blanks, the modules are

arranged in several rows. The number of rows is specified in the pattern.

Figure 6 shows that a stepped, corrugated nozzle is formed in the machine. The number of stages of the nozzle depends on the number of blades that form the nozzle. It is recommended that this number is above 8.

In cross-section A-A in the left view plane of the machine, the number of blades is indicated as six, and in Figure 7, which explains the three-dimensional view of the machine, the number of blades is indicated as four to make the figure understandable.

To ensure a high density of platinum, two blades are attached to each arm. Thus, if the sinker thickness is 0.25 mm and the distance between the sinkers is 0.5 mm, the warp density is assumed to be 40 per 1 cm.

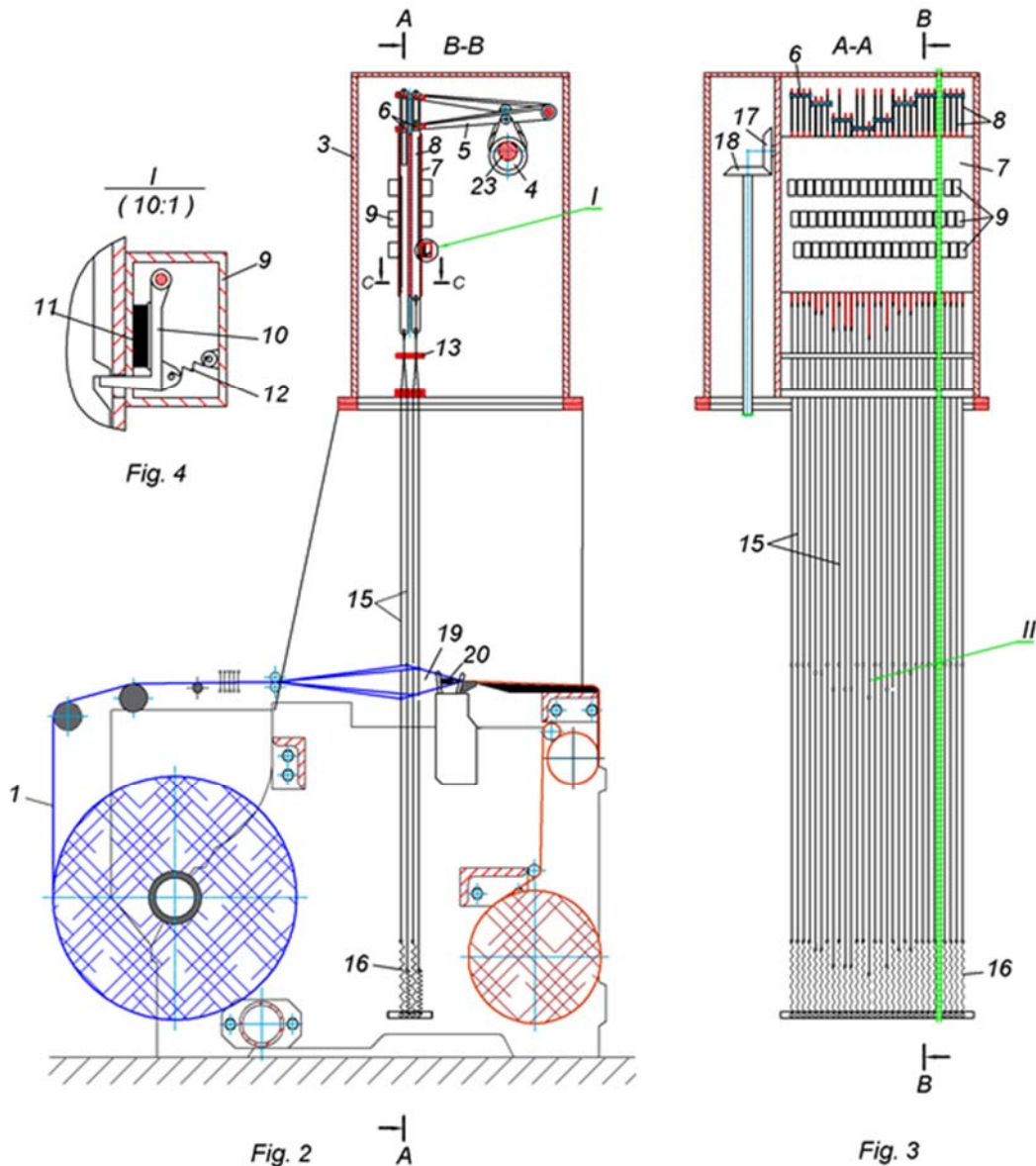
The eccentrics No. 4 mounted on the spindle No. 23, driven by the main spindle of the loom in a ratio of

1:1, perform a rotational movement and transmit a displacement in the vertical direction corresponding to the height of the shed to the blades 6 arranged at the ends of the arms 5 (Fig. 2).

In order to obtain a mountain-shaped nozzle, the eccentrics No. 4 are arranged on the shaft at equal angles according to the number of blades forming the stepped nozzle. If we express the number of blades with  $n$ , the insertion angle of the eccentrics results from the equation  $\phi = 360^\circ/n$ .

The infinite wave-like movement of the blades is transmitted to the warp threads via the sinkers (8) and the threads 15, which connect the warp threads to the sinkers.

The positions of the shuttles No. 20 and the warp threads in the shaft nozzle are shown in Figures 6 and 7.



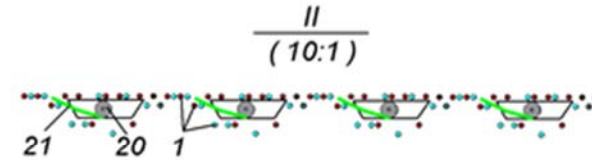
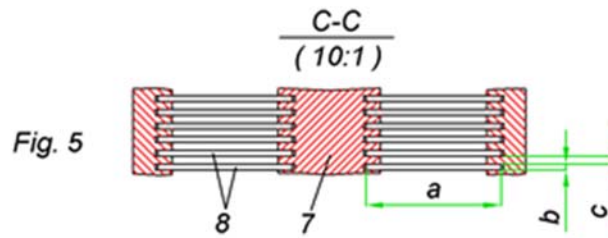


Fig. 6

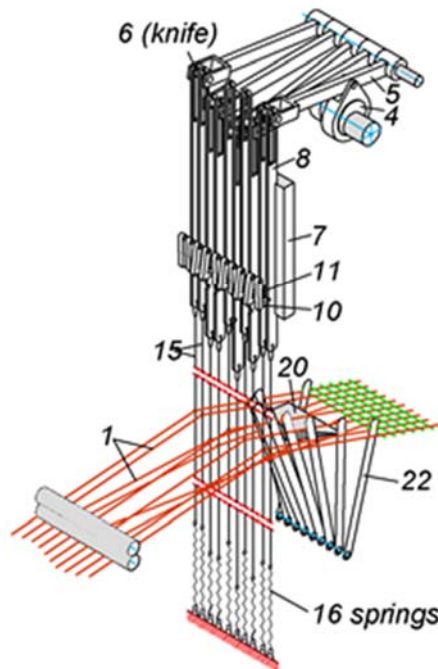


Fig. 7



Fig. 8

## RESULTS

1. In the cam shedding mechanism (4,5), which transmits motion to the knives (6) in the form of a stepped shaft in the multiple weaving machine, the warp threads (1) are placed on the knives so that they can move vertically. They are controlled by specially structured sinkers (8) which, in contact with the blades, move from the lower to the upper state with the help of the blades (6) and from the upper to the lower state with the help of springs (16). When the warp threads are to remain in the upper position according to the pattern, the sinkers are interlocked by electromagnets (10, 11) to form an undulating nozzle corresponding to the fabric pattern.

2. By arranging the interlocking projections (E) along the sinker, it is possible to match the density of the sinker to the density of the warp threads.

3. Since the machine allows weaving of all known jacquard fabrics, the problem of not being able to produce weaves other than the rag foot weave, which is considered one of the major drawbacks of multiple shed weaving machines, has been solved.

## REFERENCES

1. Adanur, S. (2001). Handbook of Weaving (1st ed.). CRC Press.  
<https://doi.org/10.1201/9780429135828>
2. Başer G. (2004. )Dokuma Tekniği ve Sanatı. Punto Yayınları, Cilt 1, İzmir.
3. Eren R. (2009). Dokuma Temel Bilgileri. U.Ü. Mühendislik-Mimarlık Fakültesi Tekstil Mühendisliği Bölümü ders notları.
4. Chi Zhang, Jiangang Zhang, Xiaoguang Wu, Chengjun Zhang. (2010). Key Technology in Embedded Control System of Jacquard Knitting. International Conference on Mechatronics and Automation August, 4-7, Xi'an, China.
5. Nithya G., Sriha P., Gopika N.P. (2022). Design of PIC Microcontroller based Automatic Control System for Electronic Jacquard Mechanism. International Journal of Electrical Engineering and Technology. ISSN 2249-3085, Volume 12, Number 1, pp. 55-61.
6. Kaplan M., Ala D.M., Çelik N. (2019). Design of an Electronic Jacquard Sampling Loom. İcontex, 2nd international congress of innovative textile, ss 66-69.
7. Keim W., Jhile K. (1990). Hook Control Device for an Open Shed Jacquard Machine. Patent Number: 4,936,357. Date of Patent: Jun. 26.
8. Jonathan F. M., Malcolm G. B., Ian T. (1995). Electrically Controlled Jacquard Selection Apparatus. Patent Number: 5,464,046. Date of Patent: Nov. 7
9. Panneerselvam R. G., Yuvaraj D., Bhanu V. (2020). Use of indigenous electronic jacquard in handloom for weaving fashionable silk sarees. Dogo Rangsang Research Journal, UGC Care Group I Journal, ISSN : 2347-7180, Vol-10, Issue-07, No. 16 July.
10. Браун Д. (2004). Patent RU2359076C2. (FR), Зевообразующее устройство, ткацкий станок, Оборудованный таким устройством, и способ образования зева с использованием такого устройства
11. Буданов К.Д., Мартиросов А.А., Попов Э.А., Туваева А.А. (1975). Расчет и проектирование текстильного оборудования. Учебное пособие. — М.: Машиностроение, 390 с.
12. Галкин А.А. Ковалев Г.И. Губин В.В. Сидоров В.Ю. Галкин А.А. Малафеев Р.М. (2000). Зевообразующее устройство ткацкого станка с волнообразно подвижным зевом. Patent RU2177057C1.
13. Губин В.В. Ковалев Г.И. Галкин А.А. Сидоров В.Ю.Малафеев Р.М. (2000). Устройство управления жаккардовым зевообразующим механизмом ткацкого станка с волнообразно подвижным зевом. Patent RU2178471C1.
14. Ковалев Г.И. Макаров В.А. Комаров Ю.И. (1976). Зевообразующее устройство ткацкого станка с волнообразно подвижным зевом. Patent SU669772A1.
15. Ковалев Г.И. Галкин А.А. Сидоров В.Ю.Губин В.В. Галкин А.А. Малафеев Р.М. (2000). Зеленская В.В. Зевообразующее устройство ткацкого станка с волнообразно подвижным зевом. Patent RU2173358C1.
16. Ковалев Г. И., Лоцилин Е. Д. (1989). Зевообразующее устройство ткацкого станка с волнообразно подвижным зевом. Patent SU1677105A1.
17. Люциано К. (1982). Зевообразовательный механизм для ткацкого станка с волнообразно подвижным зевом. Patent SU1313357A3.
18. Люциано К. (1982). Зевообразующее устройство для ткацкого станка с волнообразным подвижным зевом. Patent SU1313357A3.
19. Люциано К. (1982). Зевообразующее устройство ткацкого станка с волнообразно подвижным зевом. Patent SU1313357.
20. Мартынкин Ф. Ф., Виноградов И. Г., Колосова Т. И. (1980). Зевообразовательный механизм для ткацкого станка с волнообразно подвижным зевом. Patent SU973679A1.
21. Талавашек О., Сватый В. (1985). Бесчелночные ткацкие станки. Пер. с чеш. - М.: Легпромбытиздат, 335 с.
22. Хайнрих М., Вернер Х. (1972). Зевообразовательный механизм для ткацкого станка с волнообразно подвижным зевом. Patent SU557129A1.
23. <https://www.derstekstil.name.tr/dokuma-makinelerinin-ana-elemanlari.html>
24. <https://www.derstekstil.name.tr/jakarli-agizlik-acma-sistemleri.html>

# THERMAL AGING EFFECT ON THE PHYSIO-MECHANICAL PROPERTIES OF TEXTILES USED FOR THE REINFORCEMENT OF CONVEYOR BELTS

LEMMI TSEGAYE SH. AND BARBURSKI MARCIN \*

Lodz University of Technology, Faculty of Material Technologies and Textile Design, Institute of Architecture of Textiles, Stefana Żeromskiego 116, 90-924, Lodz, Poland

## ABSTRACT

The use of textiles produced from high tenacity (HT) polyester yarns as a reinforcement material in the mechanical rubber goods industries, mainly in the conveyor belt, is extensively increasing due to their high tensile strength, flexibility, thermal stability, modulus of elasticity, and light weightness. To achieve the desired property of a conveyor belt, the reinforcement components undergo various processing stages; among those stages vulcanizing the reinforcement materials under high temperatures is the crucial process that determines the physical and mechanical properties of the conveyor belt. The main aim of this work was to analyze the effect of vulcanization parameters on the physio-mechanical properties of high tenacity polyester yarns and fabrics that are utilized to reinforce a conveyor belt. An extensive experimental study was conducted on a pre-activated HT polyester yarn of different linear densities and woven fabrics produced for the purpose of conveyor belt reinforcement by subjecting the yarns and fabrics to various aging temperatures for a certain period of aging time. Following the experiments, a comprehensive study and analysis were conducted on the tensile property of the yarns and fabrics. The finding revealed that thermal aging has an immense impact on determining the tensile strength and elongation of the yarn and woven fabric, which also has a direct influence on the properties of the conveyor belt. The analysis of experimental test results of polyester yarns and woven fabrics revealed that vulcanizing textile-reinforced conveyor belt at high temperatures (220 °C) could deteriorate the tensile strength and increase the elongation at break of the yarn, fabric, or belt.

## KEYWORDS

Polyester; Yarn; Woven fabric; Conveyor belt; Vulcanization; Tensile strength.

---

\* Corresponding author: Barburski M., e-mail: [marcin.barbusrki@p.lodz.pl](mailto:marcin.barbusrki@p.lodz.pl)

## INTRODUCTION

Nowadays, the demand for bulk materials transportation in mining, agriculture, construction, transport, power, and other industries with higher efficiency and reasonable transportation cost advances the revolution of conveyor belt technology. Thus, the requirement for lightweight conveyor belts in these sectors is immensely increasing, and textile-rubber reinforcement technology is coming to hand in modern heavy-duty transporting technology. In modern mechanical rubber reinforcement technology, primarily for conveyor belt reinforcement, textiles woven from a high tenacity polyester yarn in a warp direction and polyamide 66 in a weft direction are widely utilized. This is due to the fact that high-tenacity polyester yarn offers significant performance advantages over natural, regenerated, and other synthetic fibers. High warp modulus, which reduces fabric stretch and

expansion under a load, superior tear resistance, and high tensile strength are some of these characteristics. Additionally, high-tenacity polyester is less sensitive to moisture and rot conditions; consequently, conveyor belt durability in these environmental circumstances is good [1].

The high demand of industries for lightweight conveyor belts draws the attention of many scholars to research how various processing parameters can influence the composition of the conveyor belt properties. Barburski et al. [2] investigated the impact of heat treatment on the woven fabrics used as a carcass of the conveyor belt at different production stages of the conveyor belt. The study revealed that fabric weave structure and duration of thermal treatment have an influence on the physical properties of the woven fabric. Amr et al. [3] also studied the effect of the number of plies of the reinforcing material, the speed, and the loading

direction on the tensile property of textile-reinforced conveyor belts using the Taguchi method. Rudawska et al. [4] also analyzed the impact of temperature and humidity on the tensile property of textile-reinforced conveyor belts. Lemmi et al. [1] [5] in detail investigated the effects of thermal aging and vulcanization parameters on the tensile strength, elongation, and surface structure of the polyester yarn, EP woven fabric, and multi-ply conveyor belts. Also, different researchers provided fundamental information concerning the conveyor belt design and woven fabric structure used for the intent of conveyor belt reinforcement [6][7]. In previous works various scholars researched in the area of factors that affect the properties of conveyor belt [8-13]. However, the effect of vulcanization process on the mechanical properties of textiles used for the reinforcement of conveyor has been left behind. The main goal of this work was to analyze the effect of vulcanization parameters on the physio-mechanical properties of high tenacity polyester yarns and fabrics that are utilized to reinforce a conveyor belt.

## MATERIALS AND METHODS

### Materials

In order to analyze the thermal aging effect on the properties of textiles used for the reinforcement of mechanical rubber goods, especially conveyor belts, a comprehensive study was conducted on high tenacity polyester(poly(ethylene terephthalate)) yarn and technical fabrics woven from HT polyester yarn in a warp direction and polyamide 66 yarn in the weft direction. The yarn and fabric samples were supplied by Kordárna, A.s company, the Czech Republic. The detailed property of the yarns and fabrics used to conduct this work is provided in Tables 1 and 2, respectively.

**Table 1.** Properties of High Tenacity Polyester Yarn sample [1].

Yarn type	Property				
	Linear density (tex)	Breaking force (N)	Breaking tenacity (cN/tex)	Elongation at break (%)	Hot air shrinkage (%)
High Tenacity Polyester	110	89.90	81.00	13.50	5.50

**Table 2.** Properties of Technical dipped woven fabric sample [1].

Fabric Type	Fabric Properties						
	Warp Yarn	Weft Yarn	Warp Count Ends/cm	Weft Count Picks/cm	Mass per unit Area (g/m <sup>2</sup> )	Crimp of Warp (%)	Weave Type
EP 200 - Dipped*	Polyester	PA 66	9.10 ± 0.25	4.50 ± 0.15	631 ± 10	2.50	Plain weave

\* E-HT polyester yarn, P- Polyamide 66, 200 – nominal strength of the fabric sample in kNm<sup>-1</sup>. Dipped- the sample was dipped in resorcinol–formaldehyde–latex (RFL) solution to enhance the adhesiveness of the textile to rubber material.

## Methods

Determining the impact of vulcanization process parameters on the tensile property of the conveyor belt carcass is difficult because of the complex structural composition of the conveyor belt. In this work, the following methods were employed to ascertain the effect of thermal aging on the properties of textile fabrics and yarns. High-tenacity polyester yarn and EP woven fabric samples were aged under the thermal aging temperature of 140, 160, and 220 °C for a duration of 35 minutes in an industrial oven. Following that, a multi-ply conveyor belt reinforced with a woven fabric of the same parameter was produced. The vulcanization temperature and duration used to vulcanize the conveyor belt was similar to the thermal aging used to age the fabric samples. Besides this, the samples used to reinforce the belt have the same property as the fabric samples on which the thermal aging investigation was conducted. Finally, the fabric samples were removed from the belt (Figure 1) to analyze the effect of the vulcanization process on the properties of the fabric used to reinforce the belt. The tensile property of the yarn and fabric samples pre-and post-thermal aging were tested in accordance with ISO 2062:2009 [14] and ISO 13934-1:2013 [15]. A Zwick/Roell tensile testing machine with a constant rate of extension, 2.5kN load cell, 250 mm/min crosshead speed, and a gauge length of 250mm was used to test the tensile property of the yarn samples. Also, for the tensile property testing of woven fabrics, the Zwick/Roell tensile testing machine of 150 kN load cell, testing the speed of 100 mm/min with a mechanical extensometer and the specimen width of 50 mm and 250 mm length between clamps were used. All experimental tests were conducted in standard laboratory conditions.



Figure 1. Woven fabric removed from conveyor belt reinforcement [1].

## RESULTS AND DISCUSSION

### The effect of thermal aging parameters on the tenacity and percentage elongation of high tenacity polyester yarn

By altering the aging temperatures, the impact of thermal aging factors on the tenacity of polyester yarn was studied. As shown in Figure 2, there were no considerable changes in the tenacity of the yarn samples aged at 160 °C and 200 °C compared to the tenacity of the unaged yarn.

However, compared to the tenacity of the unaged yarn samples, the tenacity of yarn samples aged at 220 °C was drastically decreased. This indicates that the aging of polyester yarns way above its glass transition temperature ( $\approx 180$  °C) and around the melting point ( $\approx 260$  °C) can degrade the tenacity of the yarn.

However, as shown in Figure 3, the aging of polyester yarns above the fiber's glass transition increases the yarn's percentage elongation. Unlike the tenacity, the percentage elongation of the yarn is incremented as the aging temperature approaches to the melting point of the yarn.

### Influence of thermal aging parameters on the tensile strength of woven fabrics

In Figure 4, the impact of thermal aging on the woven fabrics aged in an industrial oven and the fabric removed from a conveyor belt post-vulcanization process were compared. Regardless of the thermal aging medium, the tensile strength of the fabric samples was degraded compared to the unaged fabric samples.

Nevertheless, severe deterioration of the fabric's tensile strength was observed for the samples aged at 220 °C in the case of both mediums of aging. Moreover, the samples removed from the vulcanized

conveyor belt were almost destroyed at 220 °C; this discrepancy resulted from the fact that the fabrics aged in the oven were aged under no pressure, whereas the fabric used as the carcass of the conveyor belt was vulcanized under high pressure, which affects the tensile strength of the fabric. Therefore, vulcanizing of EP textile reinforced conveyor at or above 220 °C cannot be recommended regardless of the vulcanization duration.

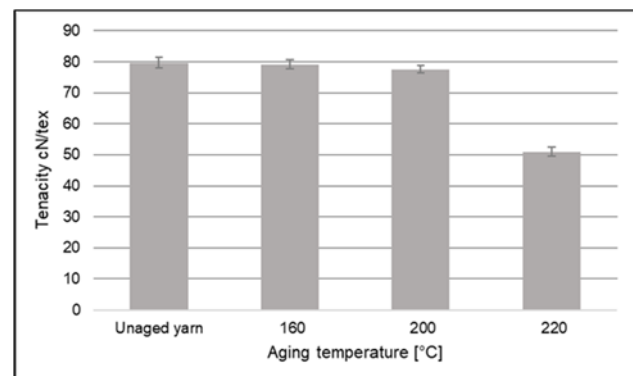


Figure 2. Impact of thermal aging on the tenacity of HT polyester yarn.

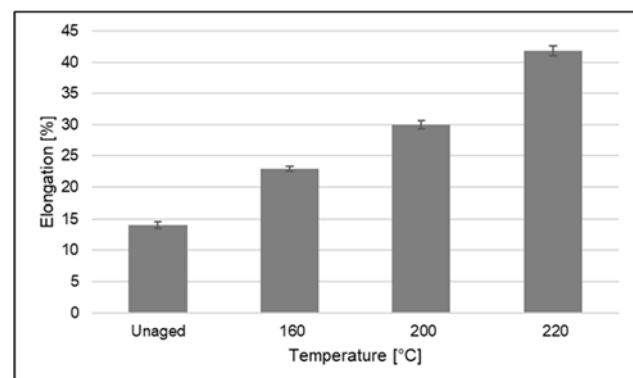
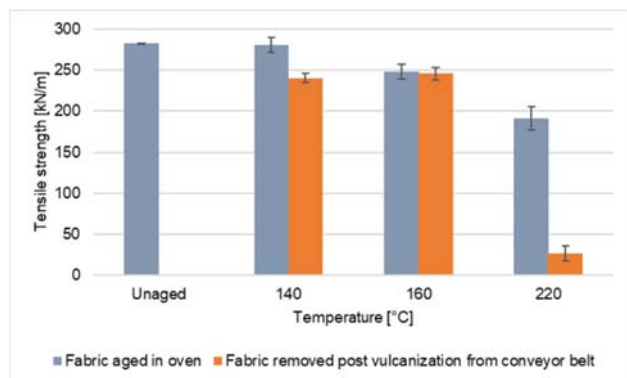
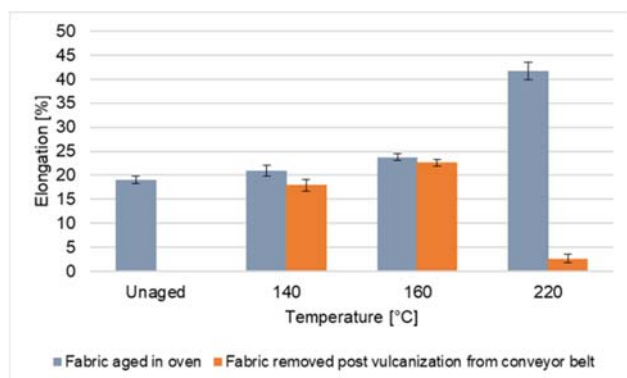


Figure 3. Effect of thermal aging on the percentage elongation of yarn.



**Figure 4.** Effect of thermal aging on the tensile strength of the woven fabric.



**Figure 5.** Effect of thermal aging on elongation of woven fabric.

## Impact of thermal aging on the elongation of woven fabric

In determining the performance of the conveyor belt in varying stress levels, the percentage elongation of the conveyor belt has a significant impact. Hence, this property must be scrutinized during material choice for the reinforcement of the belt. As shown in Figure 5, the percentage elongation of the fabrics aged below  $T_g$  temperature of polyester ( $\approx 180$  °C) was around 5% higher compared to the unaged fabric. However, the fabric samples aged in an industrial oven at 220 °C were highly elongated, which is not recommended for the conveyor belt design. In order to reduce power fluctuation on the drive sharing of rollers, increase the service life of the belt and prevent the driving motor from burning out, always a conveyor belt with low percentage elongation is recommended. In addition, the elongation of the sample removed from the conveyor belt was fully deteriorated at 220 °C due to the fact that the sample was broken under a minor applied force.

## CONCLUSIONS

The influence of aging temperature on the tensile properties of high tenacity polyester yarn and EP fabric was investigated by subjecting the yarn and fabric samples to different aging conditions used in the normal vulcanization process of conveyor belts. From the experimental results obtained, the tensile strength and percentage elongation of the polyester

yarn and EP fabric is highly dependent on the aging temperature. Irrespective of the aging stage and medium of aging, the tensile strength of the samples subjected to thermal aging at 220 °C was decreased. However, the percentage elongation of yarn and EP fabric samples aged in an industrial oven was shown higher percentage elongation, but the elongation of the sample removed from the conveyor belt vulcanized at 220 °C was lower than expected. Therefore, vulcanizing a conveyor belt reinforced by EP woven fabric at or above 220 °C is not recommended as it deteriorates the tensile property of the conveyor belt's constituent materials. Therefore, from the experimental analysis conducted, the optimum temperature to vulcanize EP reinforced conveyor belt is 160 °C for the duration of 35 minutes, depending on the number of plies of the conveyor belt.

**Acknowledgements:** The authors are grateful for the support provided by Sempertans Bełchatów Sp. z o.o R&D department for providing the laboratory equipment needed to accomplish the goal of this work. This paper was completed while the first author was a Doctoral Candidate in the Interdisciplinary Doctoral School at the Lodz University of Technology, Poland

## REFERENCES

- Lemmi, T.S.; Barbuski, M.; Kabziński, A.; Frkacz, K. (2021). Effect of thermal aging on the mechanical properties of high tenacity polyester yarn. *Materials*, 14(1666), pp.1-11, <https://doi.org/10.3390/ma14071666>.
- Barbuski, M.; Góralczyk, M.; Snycerski, M. (2015). Analysis of changes in the internal structure of PA6.6/PET fabrics of different weave patterns under heat treatment. *Fibres Text. East. Eur.*, 23, 46–51, <http://dx.doi.org/10.5604/12303666.1152722>
- Ali, A.A.; Abdellah, M.Y.; Hassan, M.K.; Mohamed, S.T. (2018). Optimization of tensile strength of reinforced rubber using Taguchi method. *Int. J. Sci. Eng. Res.*, 9, 180–186.
- Rudawska, A.; Madleňák, R.; Madleňáková, L.; Drożdźiel, P. (2020). Investigation of the effect of operational factors on conveyor belt mechanical properties. *Appl. Sci.*, 10, 4201, <https://doi.org/10.3390/app10124201>.
- Lemmi, T.S.; Barbuski, M.; Kabziński, A.; Frkacz, K. (2021). Effect of thermal aging on the mechanical properties of high tenacity polyester yarn. *Materials*, 14, 1666, <https://doi.org/10.3390/ma14071666>.
- Kabziński, A. (2010). Rubber textile composites. Application of fabrics in conveyor belts. *Tech. Wyr. Włókiennicze*, 18, 59–63.
- Naga, K.; Ananth, S.; Rakesh, V.; Visweswarao, P. K. (2013). Design and selecting the proper conveyor-belt. *Int. J. Adv. Eng. Technol. E*, IV, 43–49.
- Bajda, M.; Hardygóra, M. (2021). Analysis of reasons for reduced strength of multiply conveyor belt splices. *Energies*, 14, 1-21, 1512, <https://doi.org/10.3390/en14051512>.
- Ambriško, L.; Marasová, D.; Grendel, P. (2016). Determination the effect of factors affecting the tensile strength of fabric conveyor belts. *Maint. Reliab.*, 18, 1, 110–116, <http://dx.doi.org/10.17531/ein.2016.1.14>.
- Alvarez, A. A.; Alexander, A.; Soto, R.; Luís, J.; Rivera, V.; Concepción, A. D. (2021). Adhesion quality assessment of textile conveyor belts through experimental methods and

11. mathematical modeling. *Qual. Manag.*, 22, 181, 64–67.
11. Chou, C. S.; Liu, C. L.; Chuang, W. C. (2013). Optimum conditions for vulcanizing a fabric conveyor belt with better adhesive strength and less abrasion. *Mater. Des.*, 44, 172–178, <https://doi.org/10.1016/j.matdes.2012.07.029>
12. Yao, Y.; Zhang B. (2020). Influence of the elastic modulus of a conveyor belt on the power allocation of multi-drive conveyors. *PLoS One*, 15, 7, 1–16, <https://doi.org/10.1371/journal.pone.0235768>
13. Rudawska, A.; Madleňák, R.; Madleňáková, L.; Drożdziel, P. (2020) Investigation of the effect of operational factors on conveyor belt mechanical properties. *Appl. Sci.*, 10, 12, 1–17, <https://doi.org/10.3390/app10124201>.
14. ISO. Textiles—yarns from packages—determination of single-end breaking force and elongation at break using constant rate of extension (CRE) tester; ISO 2062:2009; ISO: Geneva, Switzerland, 2009.
15. ISO. Textiles—Tensile Properties of Fabrics—Part 1: Determination of Maximum Force and Elongation at Maximum Force Using the Strip Method; ISO 13934-1:2013; ISO: Geneva, Switzerland, 2013.

# INVESTIGATING THE APPLICATION OF TERRA DYE ON COTTON KNITTED FABRICS

SOOCHETA ANAGHA VAIDYA\* AND BHUNDOO SANSKRITA SINGH

University of Mauritius, Department of Applied Sustainability and Enterprise Development, Reduit, Mauritius

## ABSTRACT

Today, sustainable textile dyeing technologies are being researched with a purpose of developing eco-friendly dyes that are cost effective and resource efficient. Natural Earth Pigments also known as native earth pigments, earth colours, earth ochres, iron oxide pigments etc. come from naturally occurring minerals, typically iron oxide or manganese oxide. Terra dye is a sustainable and environment friendly dye which has been derived from pigmented earth and without the use of harsh toxic chemicals. It is 100% natural, obtained from the extraction of minerals. The study investigates the application of 'Terra dye' on cotton knitted fabrics. 100% Cotton Jersey and 100% Cotton Fleece fabrics were used. The terra dyed fabrics were tested for their properties of colour uptake, bleeding, rubbing fastness, resistance to light and washing fastness. The effect of different fixing agents was investigated. The results of the lab trials and testing, conclude that Terra dye has good prospects of being used in dyeing.

## KEYWORDS

Application; Natural Earth Pigments; Terra Dye; 100% Cotton fabrics.

---

\* Corresponding author: Soocheta A.V., e-mail: [a.soocheta@uom.ac.mu](mailto:a.soocheta@uom.ac.mu)

## INTRODUCTION

New sustainable textile dyeing technologies are being researched and developed with the aim of developing sustainable dyes that are more cost effective, resource efficient causing no harm to the planet. (TS Jeans Care, 2022). Terra is the Latin name for the earth. It is the name of the Goddess that protects the planet. The name has a direct connection to the innovative eco-friendly earth dyes. Terra dye is a sustainable and environment friendly dye which has been derived from pigmented earths and with no use of harsh toxic chemicals. It is 100% natural as it is obtained from the extraction of minerals. Through the process of grinding, geological material can become a pigment powder. Mineral deposits present give colouration to the earth pigments. Earth pigments are insoluble in water and are physically and chemically unaffected by the mediums they mix with. Furthermore, it caters for 50% water savings and 50% less use of energy as compared to a conventional pigment dye. Terra dye has some inherent disadvantages. This pigment dye may not be harmful to the environment but processes such as mining and quarrying required during extraction of earth pigments may be highly polluting. Dyes collected from natural earth pigments may lead to a variance in the colour of the dye due

to factors contributing to the source itself such as climate, location of earth pigment and volcanic eruptions.

Mauritius, is a volcanic island. It has at Chamarel a rare and impressive geological phenomenon of the seven coloured. As seen in figure 1 the colours of the earth are blend together, like ochre and mauve, brown and pink, and shade in-between. The colours are seen to move from brown to ochre, from mauve to pink and into dozens of variations. The island with such diversified earth colour palatte provide scope for exploring terra dyes. The study investigates the application of 'Terra dye' on 100% Cotton Jersey and 100% Cotton Fleece knitted fabrics.

## EXPERIMENTAL METHOD

### Materials

100% Greige cotton jersey and cotton fleece knitted fabrics were used (Figure 2.1 (a) (b)). Five Terra dyes as seen n figure 2.2 (a) (b) (c) (d) (e), trade names "Giallo Artiglieria" (Yellow), "Verde Similcromo" (Green), "Rosso Laccato Scuro" (Pink), "Rosso Ercolano" (Red Earth) and "Mineral Black" were utilised. The Terra dyes and fabrics were provided by Consolidated Fabrics Ltd.



Figure 2.1 (a) (b). Greige Cotton Jersey and Fleece knitted fabric



a) Giallo Artiglieria (Yellow) b) Verde Similcromo (Green) c) Rosso Laccato Scuro (Pink)



(d) Rosso Ercolano (Red Earth) (e) Mineral Black

Figure 2.2 a) b) c) d) e). Terra Dyes

### Pre-treatment of Fabric

**Semi Bleach:** The fabrics were semi bleached in a Fong's industrial dyeing machine as shown in Figure 2.3. Machine was preheated at 50°C for 10 minutes and 158 Litres of water was filled. 160g of Ronwet, a wetting agent, was added. 25 kgs of the fabric was loaded. 160 g of Imerol NFL, a detergent, 64 g of Prestogen FCB, a stabiliser and 32 g of Ronlube, an anti-crease, was added into the machine. After 5 mins, 633g of liquid Caustic Soda was poured into the bath. 640g of Hydrogen Peroxide was added and the temperature was increased at 3°C per minute until it reached 110°C. for 20 minutes. Nevocid, an acid, was injected into machine trough pipe system. The pH was maintained between 6-7. 64g of Bactosol, a peroxide added to neutralize the liquor. The fabric was rinsed with water and dried

**Scouring:** A batch 4 kg fabric was scoured in Rotary machine as shown in Figure 2.4 (a) & (b) with 0.50g/L Asutol and 60g Ronwet, wetting agent to remove impurities present before proceeding with dyeing. The Cotton Jersey and Cotton Fleece

fabrics scoured as per the scouring profile seen in Figure 2.5.



Figure 2.3. Pretreatment



Figure 2.4 (a) & (b). Scouring process in Rotary

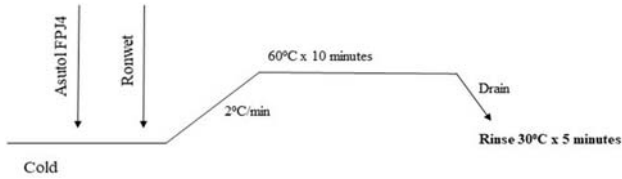


Figure 2.5. Scouring Profile (Adapted - Tropic Knits Washplant Dyehouse Recipe Card, 2022)

### Dyeing of Cotton Fabrics with Terra Dyes

120 L of cold water was filled into the Rotary machine. 120 grams of Terra dye pigment was mixed with 1 litre of cold water until the pigment was completely diffused into the water. The dye was then poured slowly into the machine through a strainer to filter remaining undissolved dye pigments. The machine was run for 15 minutes and temperature raised to 60°C. The steam valve was opened to allow steam to be gradually released at 1°C per minute from the steam pipe into the machine to control even dyeing. After 15 minutes, hydro extraction was carried out in which the dyed water was drained out of the machine.

The fabrics were rinsed twice with cold water for 5 minutes. 120g of Acasoft, a softener was then added at 40°C and machine was run for further 10 minutes. The fabrics were dried. Figure 2.6. shows the dyeing profile used for Terra dyeing.

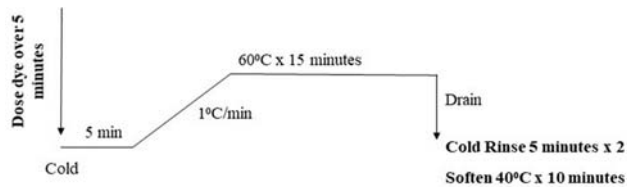


Figure 2.6. Dyeing Profile Terra dye (Adapted -Tropic Knits Washplant-Dyehouse Recipe card, 2022).

### Dyeing of Cotton Fabrics with Terra Dyes using Cationisation method

1 kg of Cotton Jersey and Cotton Fleece were dyed with Terra dye trade name “Sand” which is of a yellow Ochre colour. Cationisation method involves the use of binder, to fix the dye pigment onto the fabric and achieve good colourfastness.

**Scouring:** The fabrics were scoured with 0.50 g/L Asutol prior to dyeing using the scouring profile as seen in Figure 2.7. After hydro extraction, the machine was filled with 30 litres of water to proceed with cationisation.

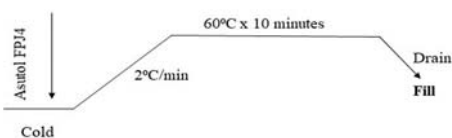


Figure 2.7. Scouring Profile (Adapted -Tropic Knits Washplant - Dyehouse Recipe Card, 2022)

**Cationisation:** 30 grams of Dye prep (Binder) was well diluted, filtered and poured into the Rotary machine and the machine was run for 3 minutes. The machine was heated to 50°C at 2°C per minute. Machine was run for 15 minutes at 50°C. After 15 minutes, 30 grams of Soda Ash was added and machine was run for another 15 minutes. The pH was maintained in the range of 8-10. Hydro extraction was carried out before cold rinsing for 5 minutes twice. Cationisation profile is seen in Figure 2.8.

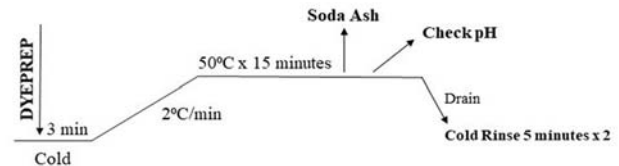


Figure 2.8. Cationisation Profile (Adapted- Tropic Knits Washplant - Dyehouse Recipe Card, 2022)

**Pigmentation:** Machine was filled with cold water. 6 grams of Acetic acid added and run for 5 minutes. The pH was maintained at 4.5 before dosing 100 grams of dye pigment into the machine. Machine was heated 1°C per minute to a temperature of 50°C for 20 minutes. 60 grams of Fixacryl CFD, a dye fixer, was added and machine was run for 10 minutes. Water was drained and fabric was cold rinsed for 5 minutes. Figure 2.9 shows the pigmentation profile.

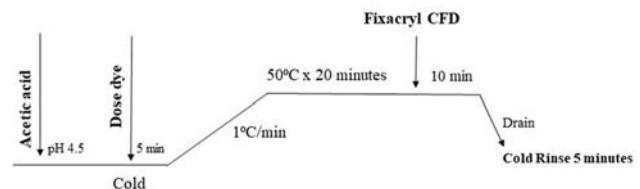


Figure 2.9. Pigmentation profile (Adapted -Tropic Knits Washplant - Dyehouse Recipe Card, 2022).

**Softening:** Fresh cold water was filled in machine. pH of water was adjusted to 5.5-6 by adding acid and machine was run for 3 mins (Figure 2.10). 40 grams of Acaflakes RT New, softener, was added to the bath. The machine was heated at 2°C per minute to a temperature of 40°C and run for 10 minutes. Hydro extraction was carried out and the fabrics were tumble dried at 105°C for 60 minutes.

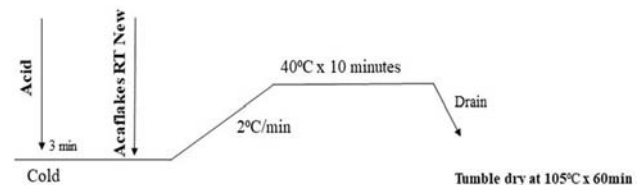


Figure 2.10. Softening profile (Adapted from Tropic Knits Washplant - Dyehouse Recipe Card, 2022).

## Finishing

Dyed fabric samples were padded with different fixatives in separate batches - 200g Sodium Sulphate (Salt), 5 ml Acetic acid, 200g Sodium Carbonate (Soda Ash), 200g Sodium Bicarbonate (Baking Soda) and 40g Hifix, a cationic fixing agent. A rapid pad mangle machine was utilised for padding process.

**Padding:** 1 litre of water was boiled at a temperature of 100°C. 200 grams of Sodium Sulphate was added, stirred continuously to dissolve and allowed to cool. This solution was used for padding and samples were oven dried. Same process was used for each fixative.

## Evaluation

**Grams per Square Metre (GSM):** The GSM of both Cotton Jersey and Fleece were measured when at “greige” state, after semi-bleaching, dyeing and finishing process. The fabrics were ring cut matched with circular standard template and weighted on an electronic balance.

**Pantone CAPSURE:** Pantone Capsure apparatus Figure 2.11 was utilised to match dye colour of fabric with pantone colour libraries to obtain colour name and code.

**Rubbing Fastness:** Dyed Cotton Jersey and Fleece specimens were cut in dimension 25cm x 5 cm for both dry and wet rubbing test. The test was carried out in a crock meter whereby the rubbing fringe was

covered with a dry crocking cloth and held in position with a spring clip. Fabric specimen was placed on rubbing area and was held by the clamping device’s pins passing through the fabric and into holes on the base. Along the warp direction, the fringe was moved forth and back 10 times in 10 seconds at the rate of one turn per second. Same procedure is carried out for wet rubbing test. In the latter case, the crocking cloth is wetted, squeezed and dried at room temperature after rubbing which was later matched with greyscale for assessing staining. (Figure 2.12)

**Wash Fastness:** Microfiber was sewn on top of all dyed samples. Soap solution was prepared with 5g of ECE detergent and 2g of Sodium Carbonate per litre of water. Solution of liquor ratio 50:1 was poured in each container for each sample and was put in machine at 60°C for 30 minutes and was flat dried (Figure 2.13). Samples were assessed with greyscale for staining.

**Light Fastness:** Pieces of Blue Wool was stick onto a piece of cardboard of dimension 12.8 cm x 4.9 cm and was used to act as control. On 5 other pieces of cardboard, the dyed samples were cut and glued. The machine was set for 103 hours. Samples were cross-checked each 6 hours for any colour change. Changes in colour were matched with greyscale standard in a light cabinet. The blue wool had to fade to a contrast equal to a grade of 2/3 according greyscale. (Figure 2.14(a) (b)).



Figure 2.11. Pantone.



Figure 2.12. Samples Rub fastness.

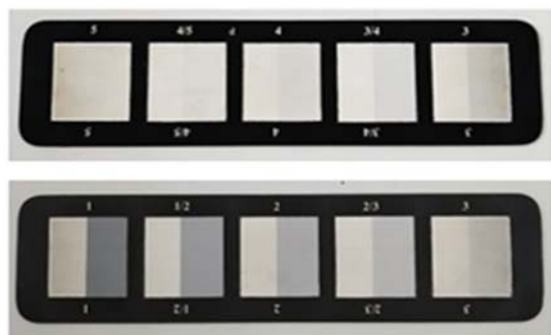


Figure 2.13. Assessing crocking cloth with greyscale for staining.



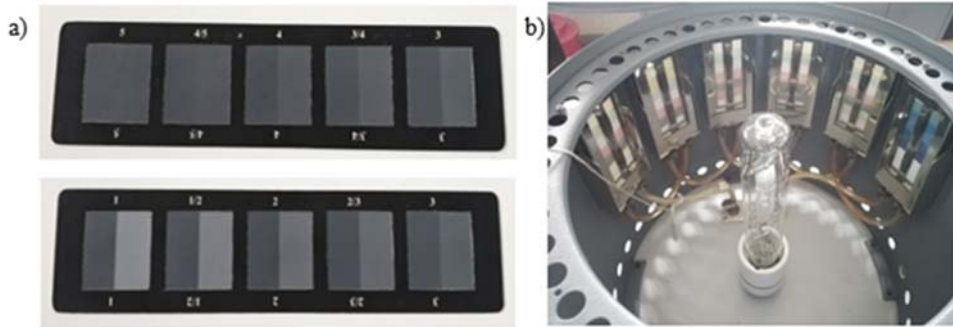


Figure 2.14 (a) Greyscale for assessing colour change (b) Samples in light fastness machine.

**RESULTS AND DISCUSSION**

**Pre-treatment of Fabric**

**Semi-bleaching:** With visual inspection, a major change in fabric colour can be observed. The natural yellowish brown colour the fabric was removed to a uniform degree of whiteness. (Figure 3.1 (a) & (b)).



Figure 3.1 (a) (b). Semi-bleached Cotton Jersey and Fleece fabric.

**Fabric Mass weight loss:** Table 3.1 shows the weight loss occurred due to the amount of fibres being treated with the addition of Hydrogen peroxide(H<sub>2</sub>O<sub>2</sub>) during semi-bleach process. It can be observed that weight loss for Fleece is less than Jersey fabric.

Table 3.1 Mass of Fabric.

Fabric Type	Before Semi-bleaching	After Semi-bleaching
100% Cotton Jersey	25 kg	21.5 kg
100% Cotton Fleece	25 kg	22 kg

**Spectrophotometric Whiteness Test**

As seen in figure 3.2 (a) (b), a Standard Whiteness of 72.42 was obtained for semi-bleached Cotton fleece and 70.63 for jersey fabric.

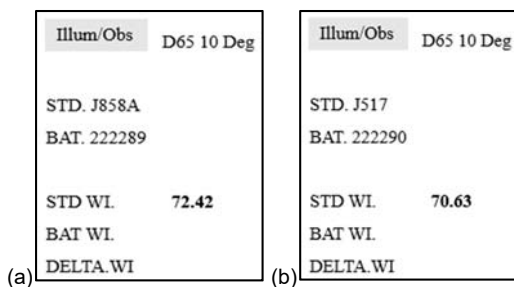


Figure 3.2 (a) (b) Whiteness test Datacolour Spectrophotometer.

- Illum/Obs D65 10 Deg refers to a light source name which is a simulation of natural day light.
- STD refers to standard of fabric.
- BAT refers to the batch number of fabric lot.
- STD WI refers to the Standard Whiteness

**Dyeing with Terra dyes**

Table 3.2 shows the colour codes and names obtained for the jersey and fleece cotton fabrics dyed with terra dyes. Pantone CAPSURE apparatus was used to obtain the colour codes and names.

**Padding and Finishing**

**Padding process with Sodium Sulphate:** Rosso Ercolano and Mineral black was seen to bleed colour in the bath. For lighter dye shades, no major change was observed in the solution during padding process. White patches of salt were observed on fabric surface after being oven dried and fabric feel became rough.

**Padding process with Sodium Carbonate:** Slight bleeding was observed for light coloured samples whereas dark shade bleed much more. Fabric were smooth after drying with showed no tendency of curling.

**Padding process with Sodium Bicarbonate, Acetic acid & Cationic Fixing agent:** Darker dye shades continued to bleed. Fabric remained soft with good drape with even dyeing. Similar results were achieved for acetic acid and cationic fixing agent.

**Grams per Square Metre (GSM)**

It can be observed that both fabrics gained weight after semi-bleaching process. This may be due to the fact that curling tendency of knitted fabrics and shrinkage occurred increased the weight. Furthermore, an additional increase in GSM was observed after dyeing due to the reason that the dye pigment weight has add up to the fabric weight. Fleece fabric is gaining more mass due to its compact and thick structure. GSM has increased much more after the addition of fixatives, and fabrics have become much heavier.

**Table 3.2:** Pantone Color and Code.

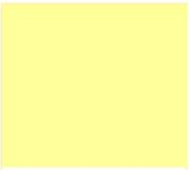
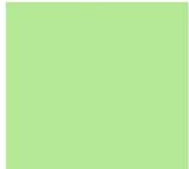
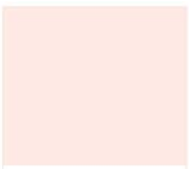
Terra Dye	Jersey Cotton	Fleece Cotton
Giallo Artiglieria (Yellow)	 PANTONE 12-0817 TCX Apricot Gelato	 PANTONE 12-0822 TCX Golden Fleece
Verde Similcromo (Green)	 PANTONE 13-6208 TCX Bok Choy	 PANTONE 15-6315 TCX Smoke Green
Rosso Laccato Scuro (Pink)	 PANTONE 13-1904 TCX Chalk Pink	 PANTONE 14-1905 TCX Lotus
Rosso Ercolano (Red Earth)	 PANTONE 16-1522 TCX Rose Dawn	 PANTONE 16-1516 TCX Cameo Brown
Mineral Black	 PANTONE 18-4005 TCX Steel Gray	 PANTONE 18-5203 TCX Pewter
Sand (With Binder)	 PANTONE 13-1025 TCX Impala	 PANTONE 14-0936 TCX Sahara Sun



Figure 3.3 (a) (b). Dry and Wet Rub fastness for treated fabrics.

## Dry and Wet Rubbing Fastness of Terra dyes

In the greyscale, the fastness ratings range from 1 (Poor) to 5 (Excellent). Very good results (3.5-4.5) were obtained for all dry rub tests indicating that less staining occurred with amount of unfixed dyes present in fabric. However, for wet rubbing, an average wet rubbing fastness (3) was obtained for non-treated fabrics as unfixed dyes dissolved in water and stained the crocking cloth. Small fuzzy balls(pills) of fibres can be seen on crocking cloth. On the other hand, lighter shade samples treated with Sodium Sulphate, Sodium Carbonate, Sodium Bicarbonate, Acetic acid and Cationic fixing agent obtained excellent results (4-4.5). Only the darker shades wet rubbing fastness could not have been improved with addition of fixatives. (Figure 3.3 (a) (b)).

## Results for Wash Fastness test

Staining on microfiber were assessed with greyscale in order to determine whether the dye used stains other fibres and whether garment with this dye can be washed together in washing machine at home. (Table 3.3). Non-treated terra dye samples slightly stained almost all fibres. Lighter shades did not stain

the multifibre when compared to darker shades. For the Sodium Sulphate samples, the white salt patches present on fabric was washed away. For Sodium Carbonate, Sodium Bicarbonate and Acetic acid, quite good results were obtained as dye shade strength was the same after washing and did not bleed much. Lighter dye shades did not affect the multifibre at all. Excellent results were achieved for cationic fixing agent samples as no major staining was observed

## Light Fastness test

After being exposed to UV light for 103 hours, the samples (Figure 3.4.) were assessed with colour change greyscale. The obtained results are seen in Table 3.4. Slight colour changes could be observed in lighter samples whereas a major colour difference was observed in darker samples. The darker the colour, the more the fading away of the shade is noticeable. Sodium Carbonate and Bicarbonate samples fairly resisted to light. Presence of salt in sample has made the colour to fade more rapidly compared to the other samples. Samples with Acetic acid and Cationic fixing agent resulted in good resistance to light.

Table 3.3 Fastness to washing test results.

Sample Type	Dye Colour	Staining on Multifibre					
		Acetate	Cotton	Nylon	Polyester	Acrylic	Wool
Non-treated	Yellow Jersey	5 (No change)					
	Yellow Fleece	4/5	4/5	3( Pink)	4/5	4/5	4/5
	Green Jersey	5 (No change)					
	Green Fleece	5 (No change)					
	Pink Jersey	4/5	5	4/5	4/5	5 (No change)	
	Pink Fleece	4/5	4/5	4	4/5	4/5	4/5
	Red Jersey	5 (No change)		4/5	4/5	4/5	4/5
	Red Fleece	4	4/5	4	4/5	4/5	4
	Black Jersey	4/5	4/5	4/5	4/5	5 (No change)	
	Black Fleece	4/5	4/5	4/5	4/5	4/5	5
	Sand Jersey	5 (No change)					
	Sand Fleece	5 (No change)					
Sodium Sulphate	Yellow Jersey	5 (No change)					
	Yellow Fleece	5 (No change)					
	Green Jersey	5 (No change)					
	Green Fleece	5 (No change)					
	Pink Jersey	5 (No change)		4/5	4/5	5 (No change)	
	Pink Fleece	5 (No change)		4/5	4/5	5 (No change)	
	Red Jersey	4/5	5	5	4/5	4/5	5
	Red Fleece	4/5	4/5	4/5	4/5	4/5	5
	Black Jersey	5	5	4/5	5	5	5
	Black Fleece	4/5	4/5	4/5	4/5	4/5	4/5
Sodium Carbonate	Yellow Jersey	5 (No change)					
	Yellow Fleece	5 (No change)					
	Green Jersey	5 (No change)					
	Green Fleece	5 (No change)					
	Pink Jersey	4/5	5	4/5	5 (No change)		
	Pink Fleece	4/5	5	4/5	5 (No change)		
	Red Jersey	4/5	5	4/5	5 (No change)		
	Red Fleece	4/5	4/5	4/5	4/5	4/5	5
	Black Jersey	5 (No change)					
	Black Fleece	4/5	4/5	4/5	4/5	4/5	5
Sodium Bicarbonate	Yellow Jersey	5 (No change)					
	Yellow Fleece	5 (No change)					
	Green Jersey	5 (No change)					
	Green Fleece	5 (No change)					
	Pink Jersey	4/5	5	4/5	5	4/5	5
	Pink Fleece	4/5			5 (No change)		
	Red Jersey	4/5		5 (No change)			
	Red Fleece	4/5					
	Black Jersey	5 (No change)					
	Black Fleece	4/5			5 (No change)		
Acetic Acid	Yellow Jersey	5 (No change)					
	Yellow Fleece	5 (No change)					
	Green Jersey	5 (No change)					
	Green Fleece	5 (No change)					
	Pink Jersey	4/5	5	4/5		5 (No change)	
	Pink Fleece	4/5			5 (No change)		
	Red Jersey	4/5		5 (No change)			
	Red Fleece	4	4/5			5	
	Black Jersey	4/5					
	Black Fleece	4/5					
Cationic Fixing agent	Yellow Jersey	5 (No change)					
	Yellow Fleece	5 (No change)					
	Green Jersey	5 (No change)					
	Green Fleece	5 (No change)					
	Pink Jersey	5 (No change)					
	Pink Fleece	5 (No change)					
	Red Jersey	4/5	5 (No change)			4/5	5
	Red Fleece	4	4/5	4	4	4/5	
	Black Jersey	4/5					
	Black Fleece	4/5					



Figure 3.4 Samples after light fastness.

Table 3.4 Light fastness test results.

Number of hours	Non-treated	Sodium Sulphate	Sodium Carbonate	Sodium Bicarbonate	Acetic acid	Cationic Fixing agent
<b>Light dye shades</b>						
6 hours	5	4/5	4/5	5	4/5	5
18 hours	5	4	4/5	5	4/5	5
42 hours	4/5	4	4	4/5	4/5	4/5
103 hours	4/5	3/4	4	4	4	4/5
<b>Dark dye shades</b>						
6 hours	4/5	4/5	4/5	5	4/5	5
18 hours	4	3/4	4	5	4/5	5
42 hours	3/4	3	3/4	4/5	4/5	4/5
103 hours	3	2/3	3	4	4	4/5

## CONCLUSIONS

This study has provided an in-depth understanding of Terra dye. The study investigates the application of 'Terra dye' on 100% Cotton Jersey and 100% Cotton Fleece knitted fabrics. The fabrics were semi bleached in an industrial dyeing machine with Asutol and Ronwet to remove impurities present before dyeing. Data colour spectrophotometer was used to test the degree of whiteness. The scoured fabrics were dyed in a rotary dyeing machine. Five colours of Terra dye namely Giallo Artiglieria (Yellow), Verde Similcromo (Green), Rosso Laccato Scuro (Pink), Rosso Ercolano (Red Earth) and Mineral Black (Black) were used. The fabrics were rinsed thoroughly and treated with Acasoft, softener. The dyed fabrics were treated with fixing agents namely Sodium Sulphate (Salt), Acetic acid, Sodium Carbonate (Soda Ash), Sodium Bicarbonate (Baking Soda) and Hifix, a cationic fixing agent using the rapid padding mangle. Dyeing using the Cationisation method was carried out with 'Sand Terra dye'. Cationisation method involved the use of binder to fix the dye pigment onto fabric surface to achieve good colourfastness. Pantone Capsure apparatus was utilised to match the fabric dye colour with pantone colour libraries and obtain the pantone colour name and code. Very good results were obtained for all dry rub tests and an average wet rubbing fastness was observed that stained the crocking cloth. The dye could not achieve darker colour strength or fix the dye pigments permanently on the fabric surface. It was seen that the bleeding of dye from the fabric could be reduced by use of cationisation method and cationic fixing agent. Samples with Acetic acid and Cationic fixing agent

resulted in good resistance to light. The results of the lab trials and testing, conclude that Terra dye has good prospects of being used in dyeing. These Eco-friendly pigments obtained from natural sources show potential to make it into the mainstream fashion.

**Acknowledgements:** Acknowledgements are due to Mr Shiva Chinappen CDL Knits Ltd for arranging and providing with the required materials, equipment and facilities; Mr M. Seeburn for providing dyeing facilities at the Wash plant of Tropic Knits Ltd.; Mr V. Jeepah for assisting with the dyeing processes.

## REFERENCES

- Corbman, b., 1985. Textiles. 6th ed. New york: Macgraw-hill, pp.107-255
- Dr Mukhopadhyay, S., 2022. The polymer system of cotton.
- Esteve-Turrillas, F. and de la Guardia, M., 2017. Environmental impact of Recover cotton in textile industry. Resources, Conservation and Recycling, 116, pp.107-115. <https://doi.org/10.1016/j.resconrec.2016.09.034>
- Fao.org. 2016. FAOSTAT. [online] Available at: <<https://www.fao.org/faostat/en/>> [Accessed 18 January 2022].
- Fibre2fashion.com. 2022. Bleaching of Cotton Textile Material - Bleaching Of Cotton Fibre. [online] Available at: <<https://www.fibre2fashion.com/industry-article/7071/problems-in-bleaching-for-cotton-textile-material>> [Accessed 20 April 2022].
- KEMI, Swedish Chemicals Agency, 2016. Hazardous chemical substances in textiles. Arkitektkopia, Stockholm 2016.
- Kerr, J., 2022. Soil Morphological Characteristics — MARLIN - Septic Tank Cleaning, Inspection, Installation, and Repair. [online] MARLIN - Septic Tank Cleaning, Inspection, Installation, and Repair. Available at: <<https://www.marlinw.com/understanding-onsite-wastewater/2019/7/19/soil-morphological-characteristics>> [Accessed 8 January 2022].
- Mondal, M., 2021. Fundamentals of natural fibres and textiles. Duxford: Woodhead Publishing.

- <https://doi.org/10.1016/C2019-0-03400-0>
9. Orvis, 2022. Terra Dye Organic Cotton Scoopneck Short-Sleeved Tee. [online] Orvis.com. Available at: <<https://www.orvis.com/terra-dye-organic-cotton-scoopneck-short-sleeved-tee/29CN.html>> [Accessed 16 January 2022].
  10. Pantone.com. 2022. PANTONE® USA | PANTONE® - Find a Pantone Color | Quick Online Color Tool. [online] Available at: <<https://www.pantone.com/connect/14-0936-TCX>> [Accessed 15 June 2022].
  11. Shawn, A., 2021. chemical Composition of Cotton Fiber. [online] Textile Learner. Available at: <<https://textilelearner.net/chemical-composition-of-cotton-fiber/>> [Accessed 16 January 2022].
  12. Soil Survey Manual, 1951 [ebook] U.S Department of Agriculture Miscellaneous Publication, pp.238-240. Available at: <<https://books.google.mu/books?id=8JJzAAAAIAAJ&printsec=frontcover#v=onepage&q&f=false>> [Accessed 15 January 2022].
  13. The Earth Pigments Company, LLC. 2022. A Brief Look on Pigments Through the Ages. [online] Available at: <<https://www.earthpigments.com/blog/a-brief-look-on-pigments-through-the-ages/>> [Accessed 10 January 2022].
  14. Tsjeanscare.wixsite.com. 2022. [online] Available at: <<https://tsjeanscare.wixsite.com/tsjeanscare/researchanddevelopment>> [Accessed 14 March 2022].
  15. Willis, S. 2021. How Sustainable Dyeing is Changing the Textile Industry. [online] Available at: <<https://www.pluginandplaytechcenter.com/resources/how-sustainable-dyeing-changing-textile-industry/>> [Accessed 11 February 2022].
  16. Zaitex, 2022. ZETATERRA eco-friendly dyes from natural resources. [online] zaitexfashion.com. Available at: <<https://zaitexfashion.com/zetaterra>> [Accessed 29 July 2022].

# NOVEL ELASTIC WARP KNITTED FABRIC WITH PERFORATION

MELNYK LIUDMYLA\* AND KYZYMCHUK OLENA

Kyiv National University of Technologies and Design, Ukraine, Nemyrovycha-Danchenko str. 2, Kyiv, 01011, Ukraine

## ABSTRACT

The aim of this project is to create novel elastic knitted materials with improved comfort for medical products. In this context, warp knitted structures were produced using different weft threads laying in. The elastic warp knitted fabric produced with transverse weft threads for the whole width was used as a reference sample. It is widely used in medical products. Laying in weft threads with a partial set according to a certain repeat allows us to get structures in which there is no connection in adjacent wales in certain places. This leads to the formation of through holes in the structure. As a result of increased permeability, comfort properties are improving. The structure, functional and comfort properties of developed and reference elastic warp knitted fabrics were investigated. It was found that novel elastic fabrics have higher values of comfort indicators and provide the necessary functional properties.

## KEYWORDS

Elastic fabric; Warp knitting; Permeability; Perforation.

---

\* Corresponding author: Melnyk L., e-mail: [melnik.lm@knuvd.edu.ua](mailto:melnik.lm@knuvd.edu.ua)

## INTRODUCTION

The demand for such medical products as bandages and corsets is growing every year [0]. For the treatment of diseases of the thoracic, lumbar and sacral regions, simple medicines are not enough, but also supportive devices are needed. The manufacturing of textile products for preventive and rehabilitation purposes is relevant in the socio-economic aspect as well. They allow you to normalize body motion and human well-being; to ensure the limits of a normal state in the life cycle, to preserve health, and to prevent future disease development. The history of the creation and development of medical and preventive products goes back decades, during which the product designs have undergone significant changes. They gained the greatest development with the appearance of elastic textile bands and fabrics [0].

Different textile technology (braiding, weaving, knitting, and non-weaving) are used for the manufacture of medical products. Knitting is the most promising method because of favorable technical and economic indicators as well as product quality [0]. Knitted fabrics with their huge variety of interlooping, differences in the raw material composition, stitch density, thickness, and so on have got a wide range of physical-mechanical and

comfort properties. In addition, they also ensure a good fit for the different shapes of the body surface.

High stretchability and elasticity are the main functional properties of knitted fabric for rehabilitation products. It is provided by the use of elastomers such as polyurethane or latex threads and is determined by their location. In weft knitting, elastomeric threads are used as a transverse weft (coursewise stretching fabric) [0] or for loops formation (bi-stretching fabric) [0], while in warp knitting, elastomeric threads are usually vertically laid (walewise stretching fabric) [0]. It should be noted that the warp-knitted band manufactured on the Crochet knitting machine is the preferred material for corsets and bandages [0]. The pillar stitch with the closed loop is ground interlooping. The elastomer threads are laid longitudinally in every wale and positioned between the loop's overlap and underlap. They are fed into knitting zone with up to 270% pre-elongation. The weft filling yarns are used for connecting the separate chains into the fabric and are laid for the whole width on both sides of elastomeric threads to cover them better. Such fabric has very compact structure (Figure 1) with high stitch density vertically as a result of elastomer relaxation after knitting.

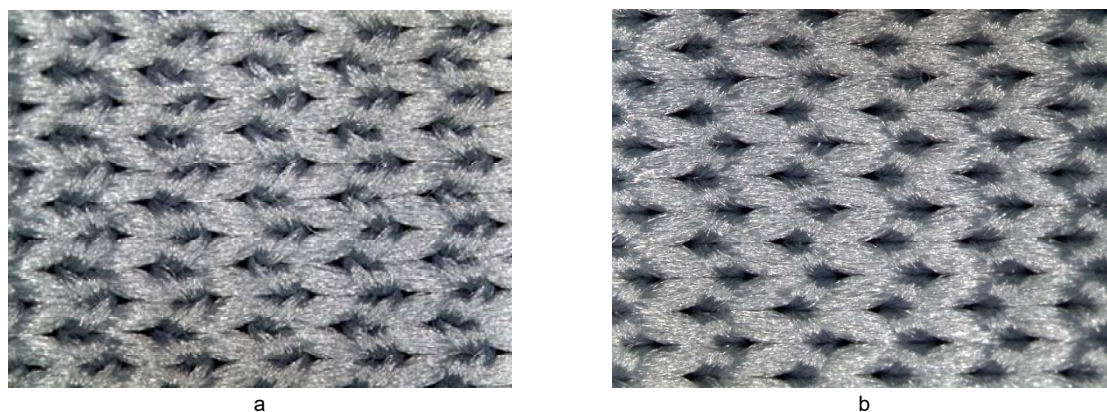


Figure 1. Photos of elastic warp knitted fabric: (a) – face side; (b) – back side.

The comfort is the second important aspect of developing elastic materials for medical and preventive products [0]. is a complex parameter because it involves both objective (permeability, hygroscopicity, thermal conductivity) and subjective (individual human approach) scores [0]. It is paid considerable attention now. These requirements are usually provided by the raw material composition [0].

The goal of this research is to develop novel elastic warp knitted material with through holes in terms of improving the permeability and future providing a higher comfort level of medical products.

## EXPERIMENTAL PART

### Materials

Four fabric variants differ by transvers weft (Table 1) were produced on 15-gauge T.C.H crochet knitting machine. Technological parameters as yarn feeding tension, fabric takedown load, and the number of used needles were kept constant for all samples.

The 16.7 tex polyester threads are used as ground (1<sup>st</sup> guide bar) for pillar stitches (Fig. 2.a) and 0.8 mm diameter polyurethan threads (3<sup>rd</sup> guide bar) are used as longitudinal elastomer component (Fig. 2.b). Both guide bars are fully threaded.

The 33.4 tex (96 filaments) polyester threads of 2-ply (A variant) and 4-ply (B variant) were used as weft in transverse direction. In order to create novel structure and to study the effect of interlooping on fabric properties two variants of weft yarn laying-in repeat were used:

- the whole width weft (W variant) introduced by special feeders on both sides of elastomer threads in opposite directions (reference samples);
- the patterned weft (P variant) introduced by incomplete (1 in, 5 out) guide bars (Figure 3) on both sides of elastomer threads in same directions (novel structure).

The lapping diagrams on figures 2 and 3 were created by using Warp Knitting Pattern Editor of TexMind [0].

Table 1. Elastic warp knitted fabric.

Cod	Linear density of weft thread	Variant of weft
AW	33.4 tex * 2	whole width
AP	33.4 tex * 2	patterned
BW	33.4 tex * 4	whole width
BP	33.4 tex * 4	patterned

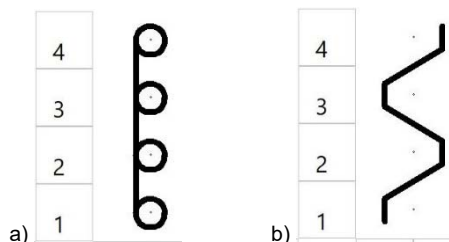


Figure 2. Lapping diagram: a – 1<sup>st</sup> guide bar (pillar stitch); b – 3<sup>rd</sup> guide bar (elastomer thread).

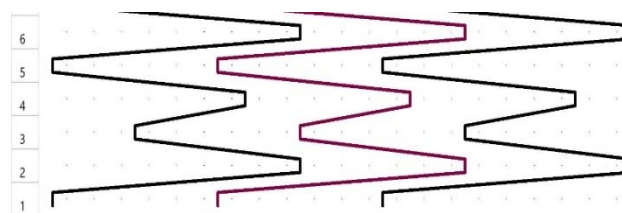
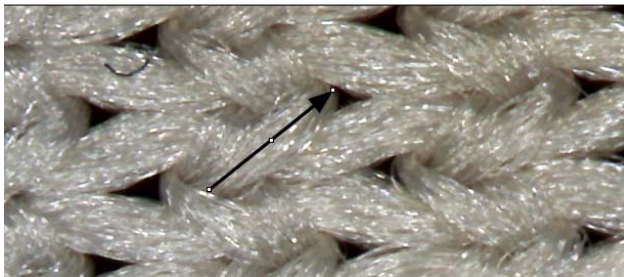
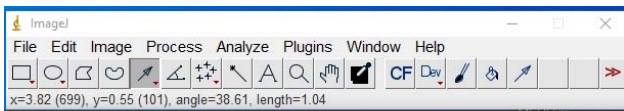


Figure 3. Lapping diagram for: 2<sup>nd</sup> and 4<sup>th</sup> guide bars (patterned weft).

## Methods

The structural properties of the fabrics were tested using the following standards: BS EN 14971:2006 [0] for stitch density, ISO 5084: 1996 [0] for thickness, and ASTM D3776 [0] for mass per unit area. The mean value for 10 parallel measurements were used for result analyses.

Photos of fabrics were taken on a digital microscope Microsafe ShinyVision MM-2288-5X-BN. Loop size and hole areas were measured by ImageJ software (Figure 4). The mean value for 10 parallel measurements were used for result analyses.



**Figure 4.** Measurement with ImageJ software.

The study of stretchability and elasticity of elastic warp-knitted fabric was performed according to BS EN ISO 20932-1:2020 [0] on Zwick Roell Z010. Required cycling limits are the following: gauge length settings 100 mm; the number of cycles 5; cycling load 35 N, recovery period 30 min. 3 specimens (300 mm x 50 mm) were tested for each fabric's variant. The following indicators are calculated from obtained data: elongation, permanent deformation, recovered elongation and elastic recovery.

Comfort properties of the fabrics were tested using the following standard methods:

- Air permeability is according ISO 9237:1995 [0] on Textest FX 3300 (pressure of 100 Pa and sample area of 20 cm<sup>2</sup>). Each fabric sample was tested 10 times.

- Thermal conductivity is according ISO 8301:1991 [0] on Alambeta (Sensora instruments). Each fabric sample was tested 3 times.
- Water vapour resistance is according TS EN ISO 11092:2014 [0] on Permetest. Each fabric sample was tested 5 times.

## RESULTS AND DISCUSSION

### Fabric structure

The fabrics with the patterned weft yarns (variants AP and BP) have got through holes in 3rd and 4th courses of repeat at places where no connection between the two adjacent weft yarns (Figure 3). The photos of fabric after knitting and relaxation during 48 hours in standard environmental conditions (20 °C and 101 kPa) are presented in Figure 5. The measurement results of stitch size and hole areas are presented in Table 2.

As a result of the analysis of the stitch size (loop's width and height), it was established that the novel fabrics with perforation correspond to the reference elastic warp-knitted fabrics. There is a difference in loop positioning only. For fabric with a 2-ply weft yarn, the loop skeleton is more inclined to the horizontal line. It is the result of both the total linear density of weft yarn and better conditions for elastomer relaxation.

It should be noted that the size of the through holes is larger for AP fabric despite the smaller loop's height. It is because the ticker weft yarn in BP fabric fills the part of a hole.

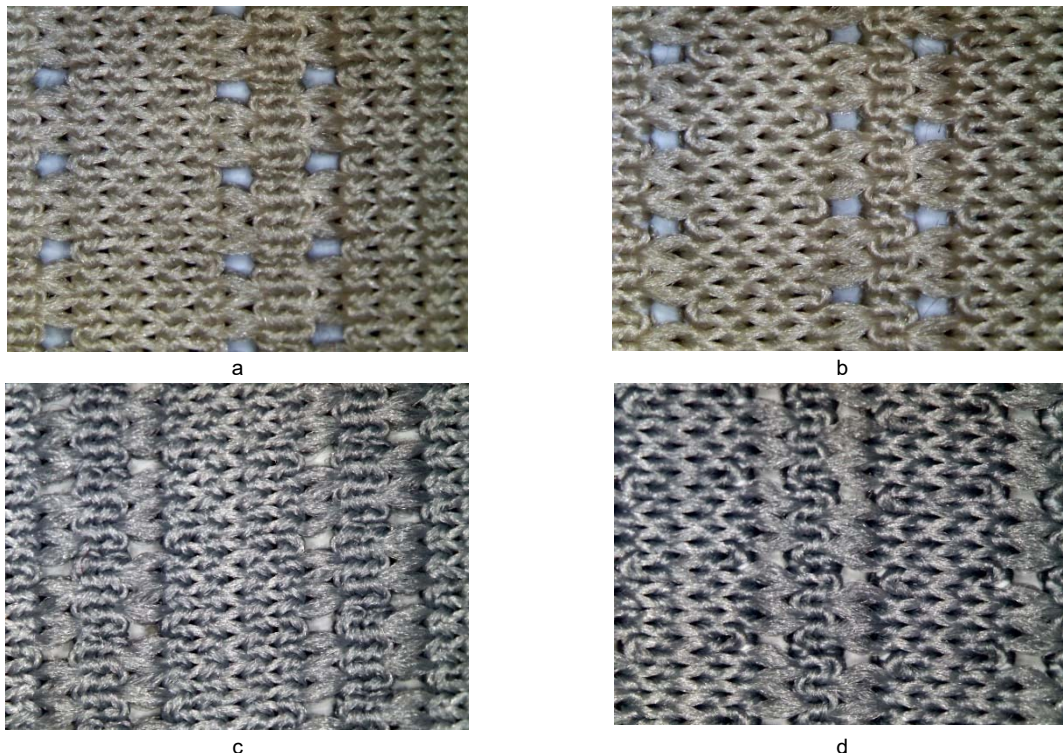


**Figure 5.** Photos of novel elastic warp knitted fabric: (a) – AP face side; (b) – AP back side; (c) – BP face side; (d) – BP back side.

**Table 2.** Stitch size and hole area of elastic warp knitted fabric.

Cod	Loop's width, W [mm]	Loop's height, W [mm]	Angle to horizontal [°]	Hole's area, S [mm <sup>2</sup> ]
Reference samples				
AW	1.05	0.76	38.8	-
BW	0.96	0.76	42.9	-
Developed structure				
AP	1.04	0.73	38.7	0.74 ± 0.01
BP	1.01	0.79	40.3	0.45 ± 0.01

**Table 3.** Parameters of elastic warp knitted fabric.

Cod	Stitch length [mm]			Stitch density per 100 mm		Thickness [mm]	Mass per unit area [g/sq.m]
	loop	elastomer	weft	wales	courses		
Reference samples							
AW	5,50 ± 0,01	0.50	1.67 ± 0.01	62	204 ± 3	1.48 ± 0.01	809.4 ± 4.2
BW	5,82 ± 0,01	0.53	1.70 ± 0.01	62	168 ± 2	1.68 ± 0.02	947.7 ± 4.6
Developed structure							
AP	5,56 ± 0,02	0.51	1.50 ± 0.02	62	193 ± 3	1.69 ± 0.02	794.2 ± 4.0
BP	5,79 ± 0,02	0.51	1.51 ± 0.02	62	186 ± 3	1.78 ± 0.02	886.0 ± 4.6

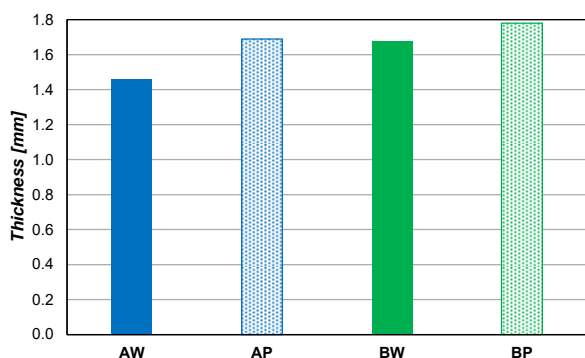


**Figure 6.** The thickness of elastic warp knitted fabric.

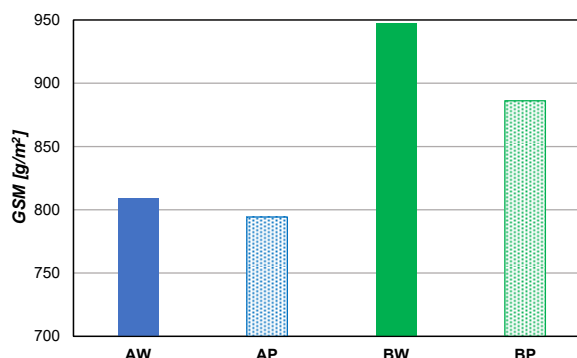


**Figure 7.** The mass of elastic warp knitted fabric.

### Structural parameters

The structural parameters of elastic warp knitted fabrics are presented in Table 3.

The total linear density of weft threads affects the stitch length. The loop's length for fabrics with 4-ply weft yarn is 5.5 % longer than for fabrics with 2-ply weft yarn. The length of elastomer per stitch for BP fabric is longer than for AP fabric as well. Research results show that weft yarn repeat affects its length only. The weft length per stitch for developed fabrics is 10% less than that for reference ones.

It is obvious that all knitted fabrics have the same stitch density horizontally (62 wales per 100 mm) because the distance between the wales is determined by the needle pitch. There is difference in stitch density vertically. For the reference samples the density of BW fabric is 35 stitches (17 %) less than AW fabric. The difference for developed structure is not so big. It is only 7 stitches (4 %).

As for thickness, the fabrics with 4-ply weft yarn are thicker than the corresponding fabrics with 2-ply weft yarn (Figure 6). It was found that developed fabrics are thicker than reference ones. It is the result of the overlapping of two weft threads in the contact areas. Developed elastic warp-knitted fabrics have reduced mass (Figure 7) that leads to a decrease in materials consumption and weight of the final product.

### Elasticity

The research results for elasticity of elastic warp knitted fabric are presented in Table 4. They show that both reference and novel elastic warp knitted fabric with perforation provides a high level of stretchability and elasticity. The fabrics' elongation is more than 140 [%] and only for the AP variant is 127 [%] but it is quite high. A permanent deformation does not exceed 3 [%]. All studied elastic warp knitted fabrics provide high level of elasticity: elastic recovery is more than 98%.

**Table 4.** Elasticity of elastic warp knitted fabrics.

Cod	Elongation, S [%]	Permanent deformation, C [%]	Recovered elongation, D [%]	Elastic recovery, R [%]
Reference samples				
AW	147 ± 2	2.3 ± 0.3	144	98.4
BW	142 ± 3	0.3 ± 0.0	142	99.8
Developed structure				
AP	127 ± 1	1.7 ± 0.3	125	98.7
BP	142 ± 3	3.0 ± 0.5	139	97.9

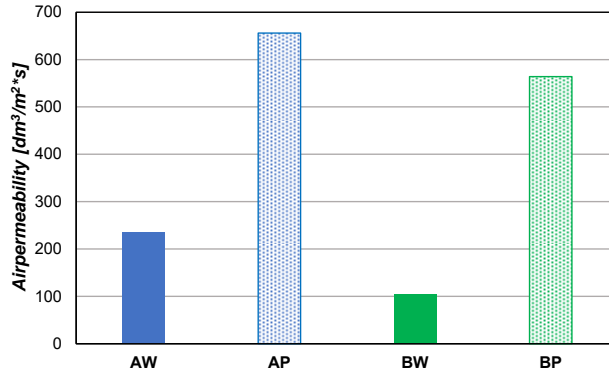


**Figure 8.** The air permeability of elastic warp knitted fabric.

**Table 5.** Water vapor properties of elastic warp knitted fabrics.

Cod	Relative Water Vapour Permeability, RWVP [%]	Water Vapour Resistance, Ret [Pa·m²·W⁻¹]
Reference samples		
AW	30 ± 1.1	10.7 ± 0.43
BW	31 ± 1.1	12.9 ± 0.54
Developed structure		
AP	41 ± 1.2	8.1 ± 0.25
BP	33 ± 0.8	9.6 ± 0.48

**Table 6.** Thermal properties of elastic warp knitted fabrics.

Cod	Thermal conductivity coefficient $\lambda \cdot 10^3$ [W·m⁻¹·K⁻¹]	Thermal diffusivity coefficient, $a \cdot 10^{-6}$ [m²·c⁻¹]	Thermal absorptivity coefficient, $b$ [W·s¹/²·m⁻²·K⁻¹]	Thermal resistivity coefficient, $R \cdot 10^{-3}$ [K·m²·W⁻¹]
Reference samples				
AW	76.3 ± 0.9	0.105 ± 0.009	236 ± 7	19.2 ± 0.3
BW	78.7 ± 0.6	0.056 ± 0.003	333 ± 7	20.6 ± 0.2
Developed structure				
AP	66.1 ± 0.7	0.071 ± 0.003	248 ± 3	25.6 ± 0.2
BP	63.7 ± 0.6	0.095 ± 0.001	206 ± 2	28.0 ± 0.3

**Air permeability**

The results of the fabrics` air permeability testing are presented in Figure 8. Predictably, novel fabrics have much greater value because of through holes. The value is greater for fabrics with 2-ply weft yarn both reference and developed structures.

**Water vapor permeability**

Research results obtained at the Permetest instrument are presented in Table 5.

The reference elastic warp knitted fabrics AW and BW have 30-31% relative water vapour permeability

(RWVP) that is not affected by the total linear density of transverse weft threads. The novel elastic warp knitted fabrics has improved water vapour permeability that depends on the total linear density of transverse weft threads. AW sample has 8% higher RWVP compared to BP sample.

The Water Vapour Resistance coefficient (Ret) of novel elastic warp knitted fabrics is lower compared to reference samples. It allows developed fabric to be used in medical products for moderate efforts. They are more pleasant to wear during physical activity.

## Thermal properties

Research results obtained at the Alambeta instrument are presented in Table 6.

The decrease in the thermal conductivity coefficient and the increase in the thermal resistance coefficient indicate the lower thermal insulation properties for novel elastic warp-knitted fabrics (AP and BP). As described before, the novel fabric is developed for medical products used daily and worn on underwear or even on the body directly. In this case, the lower thermal insulation properties lead to improving the comfort of products.

## CONCLUSIONS

Taking into account the fact that elastic warp-knitted fabrics are widely used for the production of medical support products, new structures with perforations were developed. In contrast to the widespread fabrics with the whole-width weft, weft threads are laid according to a certain repeat and used incomplete threading of the guide bar. Through holes are formed in courses where there are no contacts between two adjacent weft threads. The conducted research showed that the main functional properties of the novel fabrics (stretchability and elasticity) correspond to the properties of the reference fabrics. Due to the presence of perforations, the comfort of the products is improved: air and water vapour permeability indicators have significantly increased and thermal protection indicators have decreased.

**Acknowledgements:** *This research was done at Ege University within the 2221 project "Research and Development of Comfortable Elastic Textile Materials as a Medical Support Product" with support from The Scientific and Technological Research Council of Turkey. The authors would like to thank Philipp Schwartz Initiative for Ukrainian scientist as well for supporting the future development of project at Technical University Dresden.*

## REFERENCES

1. IMARC Group, Medical Textiles Market: Global Industry Trends, Share, Size, Growth, Opportunity and Forecast 2022-2027 (<https://www.imarcgroup.com/medical-textiles-market>)
2. Melnyk L.M., Kyzymchuk O.P. (2012) The utilization of elastic knitted materials in the medical-preventive goods. Bulletin of Kyiv National University of Technologies and Design, 4, 139-145. – in Ukrainian
3. Sadhan Chandra R. (2012). 27 - Scope of knitting in the manufacture of medical textiles. In: Sadhan Chandra R, editor. Fundamentals and Advances in Knitting Technology: Woodhead Publishing India, 326-9. [https://doi.org/10.1533/9780857095558\\_326](https://doi.org/10.1533/9780857095558_326)
4. Kyzymchuk, O. & Melnyk, L. (2016). Influence of miss knit repeat on parameters and properties of elasticized knitted fabric, IOP Conf. Series: Materials Science and Engineering, 141, 012006. <http://dx.doi.org/10.1088/1757-899X/141/1/012006>
5. Pavko-Cuden A. (2010) Parameters of Compact Single Weft Knitted Structure (Part 2): Loop Modules and Munden Constants – Compact and Supercompact Structure. Tekstilec, 53 (10–12), 259–272
6. Kyzymchuk, O., Melnyk, L., Arabuli, S. (2020). Study of Elastic Warp Knitted Bands: Production and Properties. Tekstilec, 63(2), 113-23. [DOI: 10.14502/Tekstilec2020.63.113-123](https://doi.org/10.14502/Tekstilec2020.63.113-123)
7. Kyzymchuk, O., Melnyk, L. (2018) Stretch properties of elastic knitted fabric with pillar stitch. Journal of Engineered Fibers and Fabrics, 13 (4): 1-10. <https://doi.org/10.1177/1558925018820722>
8. Ng Sau-Fun, Hui Chi-Leung & Wong Lai-Fan (2011) Development of medical garments and apparel for the elderly and the disabled, Textile Progress, 43:4, 235-285, <https://doi.org/10.1080/00405167.2011.573240>
9. Mallikarjunan K., Senior L. (2011) Comfort and Thermo Physiological Characteristics of Multilayered Fabrics for Medical Textiles, Journal of Textile and Apparel, Technology and Management, 7 (1), 1–15.
10. Oglakcioglu N. (2016) Design of functional knitted fabrics for medical corsets with high clothing comfort characteristics. Journal of Industrial Textiles. 45(5), 1009-1025. <https://doi.org/10.1177/1528083714551438>
11. Warp Knitting Pattern Editor. TexMind. Web site: <http://texmind.com/wp/products/warp-knitting-software/>
12. BS EN 14971:2006 Textiles. Knitted fabrics. Determination of number of stitches per unit of length and unit area
13. ISO 5084: 1996 Textiles - Determination of thickness of textiles and textile products
14. ASTM D3776. Standard Test Methods for Mass Per Unit Area (Weight) of Fabric.
15. BS EN ISO 20932-1:2020+A1:2021 Textiles. Determination of the elasticity of fabrics. Strip tests.
16. ISO 9237:1995, Textiles -- Determination of the permeability of fabrics to air
17. ISO 8301:1991 Thermal insulation; determination of steady-state thermal resistance and related properties; heat flow meter apparatus.
18. TS EN ISO 11092:2014 Textiles. Physiological effects. Measurement of thermal and water-vapour resistance under steady-state conditions

# INVESTIGATION OF STRUCTURAL AND PERFORMANCE PROPERTIES OF HEMP-CONTAINING KNITTED FABRICS WITH DIFFERENT COMPOSITIONS

SEN KORHAN<sup>1\*</sup>, KAYA AYSEGUL<sup>2</sup> AND KANIK GOKSU<sup>2</sup>

<sup>1</sup> TYH Uluslararası Tekstil Pazarlama A.Ş., Istanbul R&D Center, Oruc Reis Street No:7, P.O. Box 34197, Istanbul, Turkey

<sup>2</sup> TYH Tekstil Istanbul R&D Center Istanbul, Turkey

## ABSTRACT

The growing relevance of sustainable materials has increased the importance of hemp-containing products obtained from natural fibers. When the raw materials used in the garment industry are examined, it is observed that the market share of hemp-containing fibers is low in percentage. Researching the production techniques and methods of fabrics to be obtained from hemp fiber and adapting them to the use of clothing will contribute significantly to the development of the hemp product range. It is aimed that these fabrics to be developed will pass tests in accordance with end-consumer standards. In this study, structural and performance properties of hemp fiber were examined and alternatives were produced instead of conventional methods for a sustainable world. In line with the sustainability strategy, there are advantages of hemp fibers in terms of water consumption, environmental impact compared to cotton fiber. Within the scope, studies were carried out to develop single jersey knitted fabrics by hemp- containing at different compositions such as 70 % cotton/ 30 %hemp, 80 % cotton/ 20 %hemp and 90 % cotton/ 10 %hemp, %100 cotton fabric having the similar structural properties was taken as a control sample. As a result, prototype tests were performed considering the structural and performance properties of the developed fabrics.

## KEYWORDS

Textile Ecology; Sustainability; Hemp Fiber; Cotton Fiber; Knitting; Water Consumption.

---

\* Corresponding author: Sen K., e-mail: [korhansen@tyh.com.tr](mailto:korhansen@tyh.com.tr)

## INTRODUCTION

The textile and apparel industry, which is one of the most important requirements of people, should continue its activities by considering human and environmental health and, accordingly, sustainable development. The concept of "textile ecology" is important to ensure sustainability in the textile industry. In this context, hemp, a biodegradable fiber, has come to the fore again [1].

Due to its many environmentally friendly features, the use of hemp fiber in sustainable textile design and production also allows it to be evaluated within the scope of slow and ecological fashion. There are many studies conducted on reusing hemp fibers by recycling them with chemical methods, and this shows its sustainability. Hemp is a more environmentally friendly, economical and sustainable type of raw material compared to similar raw materials [2].

Hemp is an industrial plant which has an annual, herbaceous and multi-use potential in the cannabis. Cannabis is a woody annual plant from the

Cannabaceae family. Today, there are two subspecies of hemp. These are; *Cannabis sativa* and *Cannabis indica*. The type that is important for industrial applications and used in fiber production is *Cannabis sativa*. [3].

Since it does not demand much water, it contributes to the protection of water resources. It produces a high amount of oxygen and does not require pesticides and fertilization as it does not have any agricultural pests. Hemp acts as a carbon sink due to CO<sub>2</sub> absorption, and it has been revealed that hemp plants help maintain strong soil structure, protecting them against landslides due to their roots located at a depth of about 1 meter underneath. According to the related literature, compared to cotton cultivation, it was determined that the water footprint of industrial hemp (2719 l/kg) is less than 1/3 of the water footprint of cotton (10000 l/kg) [4].

On the other hand, it has been observed that 60% of hemp is returned to the soil as a nutrient when dried in the field. In this context, literature research has shown that the environmental impact of hemp raw materials is low and can be an important resource in

ensuring sustainability in the textile industry. Looking at the physical structure of hemp fiber, hemp fiber has a hollow structure. It has a large lumen and this lumen constitutes approximately 1/2 - 1/3 of the total cross-sectional area. It is larger than ramie, flax, and cotton. Since there are many hydrophilic molecules that can easily combine water molecules, hemp fiber has good moisture absorption with a commercial moisture value of 10.8%. It also has a much higher moisture holding capacity than cotton fiber with a commercial moisture value of 8.5%. Hemp fiber with a polygonal cross-section has a hollow structure with a lot of air inside, which can increase insulation. At the same time, it effectively prevents the formation of anaerobic bacteria. Hemp fiber can block up to 90% of ultraviolet sunlight without any treatment, and this is because of its high lignin content, which can absorb ultraviolet light [5-7].

Within the scope, the development studies with a composition of 70 % cotton/ 30 %hemp, 80 % cotton/ 20 %hemp and 90 % cotton/ 10 %hemp single jersey knitted fabrics in navy blue color with Ne number 20/1 were carried out. These fabrics were compared to %100 cotton fabric with similar properties. The mass per unit area value of the cotton fabric is 175 g/m<sup>2</sup> and the width is 185 cm. Procurement studies were carried out to determine

the fabric formulation and content. Since hemp fiber is limited, the duration of the studies has been extended. Fabric development studies were carried out with another supplier.

Defects in raw material production due to the pandemic and the fact that hemp yarn quality is not suitable for knitting made prototype development studies difficult. Since hemp is seen as the cotton fiber of the future, TYH Tekstil attaches importance to the use of hemp- containing yarns. Therefore, despite the failures, the studies continued. As a result, structural and performance tests such as pilling, fastness, fiber analysis (quantitative/microscopic count- qualitative method) and bursting strength were made on the developed fabrics and comparisons were made between both fabrics.

## EXPERIMENTAL

### Materials

Single jersey knitted fabrics with Ne 20/1 yarn counts in different weights and compositions from natural fibers were used in this study. The structural parameters of the fabric samples used in this study are listed in Table 1.

Table 1. Properties of TYH fabrics.

Properties of Fabrics	Fabric-1	Fabric-2	Fabric-3	Fabric-4
Raw Material	100% cotton	90 % Cotton 10 %Hemp	80 % Cotton 20 %Hemp	70 % Cotton 30 %Hemp
Type Knitting	Single jersey			
Unit Weight (gr/m <sup>2</sup> )	175	170	170	160
Yarn Count (Ne)	20/1			
Color	Navy Blue- 654-860.qtx 			

Table 2. Tests and Standards.

Test	Standard
Washing Fastness (Gyrowash)	ISO 105 C06 AIS
Rubbing Fastness (Dry-Wet)	EN ISO 105 – X12
Water Fastness	EN ISO 105 – E01
Perspiration Fastness	EN ISO 105 – E05
pH	ISO 3071 – 1980
ICI Pilling Box	ISO 12945 – 1
Pilling Martin Dale	EN ISO 12947
Fiber Analysis (quantitative/microscopic count)	AATCC 20 A
Fiber Analysis (qualitative method)	TS 4739:1986 (Metot:1)
Bursting Strength	ISO 13938-2:2019

## Methods

To ensure compatibility between fabrics, first of all, the structural properties of the developed fabrics were evaluated. Washing fastness, rubbing fastness (dry and wet), water fastness, perspiration fastness, pH tests, pilling test with ICI Pilling Box and Pilling Martin Dale were performed. In addition, fiber analysis (quantitative/microscopic count- qualitative method), bursting strength test was determined. Test sample fabrics were adjusted according to standard conditions before test and analyzes ( $21 \pm 1$  °C,  $65 \pm 2\%$  relative humidity).

In this study, these tests applied to the fabrics have been conducted in accordance with certain standards. Tests and related standards are given in Table 2.

Hemp-containing yarns could not be knitted due to the strength problem. Both yarns created bursting images during knitting. Yarn repair works were started by checking the strength, pilling and fastness values of the fabrics and improving the production conditions of the yarns. It has been observed that the working performance is low during knitting due to waiting after fixation with yarns. The fixation is a process performed to provide yarn relaxation and proper working form.

The drier the environment in the waiting conditions of the yarn, the shorter the deterioration of this form. If the standard weather conditions (closed warehouses out of the sun) are provided, it is not affected by the waiting period. When the incoming yarns were examined, it was observed that they were subject to the post-shipment transfer process and the yarn was very dry. This situation directly

affects the breaking and working performance. Double fixation was applied for improvement studies. It has been tried to improve the working performances by re-transferring-fixing the yarns.

## RESULTS AND DISCUSSION

Fastness is a color strength of textile product to withstand the factors encountered during both its production and use. It is a major quality feature in dyed textile products. Knowing the fastness of the textile material is important for the preparation of care labels [8]. Thus, washing fastness, rubbing fastness (dry and wet), water fastness, perspiration fastness and pH tests were applied. Table 3 shows the results of these testing. These tests were carried out in the company's laboratory. As can be seen from Table 3, it was determined that the developed knitted fabrics presented good fastness results. Test results were evaluated according to the company's acceptance value and customer criteria.

In addition, the pilling problem, one of the important problems in textile, disturbing both the producer and the consumer and also affecting the fabric quality. Test devices and methods used together with the factors affecting pilling are also very important in terms of evaluating the pilling performance of fabrics [9]. In this context, as a fabric pilling analysis, Martin Dale test according to EN ISO 12947 standard and ICI Pilling Box test according to ISO 12945-1 standard were performed on the developed knitted fabrics as seen in Table 3. Martin Dale test results were determined as 3/4 and 4, ICI Pilling Box test as 4. These results have been accepted as valid according to standards.

**Table 3.** Structural Tests of the fabrics and results.

Physical Test	Fabric-1	Fabric-2	Fabric-3	Fabric-4
Washing Fastness	4/5	4/5	4/5	4
Dry Rubbing Fastness	4/5	4	4/5	4/5
Wet Rubbing Fastness	3/4	4	4	4
Water Fastness	4/5	4	4	3/4
Perspiration Fastness	4/5	4	4/5	4
pH	6.8	6.9	6.9	6.8
ICI Pilling Box	4	4	4	3/4
Pilling Martin Dale	4	3/4	4	3

**Table 4.** Performance tests of the fabrics and results.

Performance Test	Fabric-1	Fabric-2	Fabric-3	Fabric-4
Bursting Strength, (kPa)	603.3	489.2	525.95	460.05
Distance To Burst, (mm)	16.1	10.6	10.8	10.5

In the literature, effect of the parameters, affecting the evenness also mechanical and structural properties of blended yarns with different hemp compositions, and the regression equation between blending ratio and yarn mechanical property was investigated. Based on this equation, blended yarns were produced in different compositions by using polyester, hemp and cotton fibers in the experiment. When the results were examined, it was observed that the unevenness of the hemp blended yarn increased as the hemp fiber ratio in the yarn increased. Since hemp fiber has longer fiber length, higher initial modulus, irregular fiber cross-section and greater surface friction than polyester and cotton, in addition to its stiffness, its distribution in the yarn is greatly affected by the content. Due to its mechanical properties, hemp fiber is affected by its distribution in the yarn. It has been found that, due to their smooth surface and low holding force, they are easy to slide from each other, although they have high strength when stretched. It has also been observed that when hemp fiber is blended with polyester and cotton in specific rate, the adhesive strength increases again under the effect of twisting [7, 10].

Bursting strength test were performed in the relevant parts of the product as a performance test. In this context, the performance tests of the fabrics are presented in Table 4.

Examining the test results, the rigid structure of the hemp fiber improves the strength of the fabric up to a certain point, and when that point is exceeded, hemp fibers begin to fall out. Thus, it reduces strength and more fiber fall out occurred in the Fabric-4 (70 % Cotton/ 30 %Hemp) compared to others. In the test results, it was observed that the Fabric-3 (80 % Cotton/ 20 %Hemp) gave ideal results close to cotton. In terms of structural properties, the Fabric-3 (80 % Cotton/ 20 %Hemp) gave better results than other hemp blended fabrics. This fabric can be an alternative fabric to cotton fibers. The optical microscope images of hemp and cotton fibers are shown in Figure 1.



Figure 1. Structure of cotton/hemp fibers

The fibers in the middle in the image are hemp fibers, as seen in the Figure 1. Under a microscope a cotton fiber looks like a twisted ribbon or a collapsed and twisted ribbon or a collapsed and twisted tube. These twists are called convolutions [11]. Hemp has more twisted ribbon than cotton fiber.

During the growth phase of the plant, there is no change in the number of fibers, but the length of the fiber's increases. In the hemp plant, the fiber thickness increases from the stem down. The fiber lengths are determined by the distance between the ribbon. The glossy hemp fibers are yellow-brown, and the cross-section of the fiber is polygonal [7, 12].

## CONCLUSIONS

The fact that the products obtained from synthetic fibers are petroleum-based increase the CO<sub>2</sub> emission and carbon footprint. Natural fibers are mostly preferred in clothing products used in our daily lives. On the other hand, hemp fibers have become an alternative to cotton since the cultivation process of cotton fibers, which is the most preferred natural fiber, includes abundant irrigation and pesticide and chemical fertilizer applications that cause many health problems. For this purpose, TYH Tekstil has given importance to research and development studies in this field, considering hemp fibers as the cotton of the future.

Many problems have been encountered in hemp fiber, from the fiber stage to the fabric stage. Despite all the problems, fabrics have been developed. Studies were carried out to develop single jersey knitted fabrics from blending raw materials containing hemp at different composition such as 70 % cotton/ 30 %hemp, 80 % cotton/ 20 %hemp and 90 % cotton/ 10 %hemp, %100 cotton fabric having the similar structural properties was taken as a control sample. The structural and performance properties of the fabrics developed in the test results are evaluated. Results show that compared to other hemp-containing knitted fabrics, 80% cotton/ 20% hemp blended knitted fabric was considered more suitable for use in knitting. Consequently, this study reveals that composition is not the decisive factor, although it is commonly assumed that the strength reduces as the hemp ratio increase. The rigid structure of the hemp fiber improves the strength of the fabric up to a certain point, and when that point is exceeded, hemp fibers begin to fall out. Thus, it reduces strength and more fiber fall out occurred in the Fabric-4 (70 % Cotton/ 30 %Hemp) compared to others.

Hemp fiber is very popular nowadays due to the rising of environmental concerns. This popularity depends on its ecological properties and superior daily usage performance. This paper gives

information about hemp fiber properties and its advantages. The aim of this paper is to highlight the importance of hemp-containing textiles for today's world textile market. As a suggestion, in the light of this study, experiments can be made on different fabric compositions to find the rate at which fiber fall out starts. Factors affecting the fall out can be determined and studies can be carried out to solve this problem. As a result, its use can be spread by increasing the hemp mixture to the highest possible rate. It's observed that defects are related to strength properties according to performance test in this study. TYH Tekstil Istanbul R&D Center is open to cooperate for innovative studies and suggestions.

**Acknowledgements:** *This study is conducting in an apparel company's R&D Center as an R&D project. This work would not have been possible without his endless support of dear Mr. Mehmet Kaya, the director of TYH Tekstil A.Ş. We are especially indebted to him and TYH Tekstil. We would also like to show my gratitude to all of those with whom We have had the pleasure to work during this study and other related projects.*

## REFERENCES

1. Kumar, R. (2017). Prospects Of Sustainable Fashion Design Innovation. International Journal of Textile and Fashion Technology, Volume 7, Issue 6, 5-14. <http://dx.doi.org/10.24247/ijftfdec20172>
2. Gedik, G., Avinc, O., (2020). Hemp Fiber as a Sustainable Raw Material Source for Textile Industry: Can We Use Its Potential for More Eco-Friendly Production? Sustainability in the Textile and Apparel Industries, 87–109. [http://dx.doi.org/10.1007/978-3-030-38541-5\\_4](http://dx.doi.org/10.1007/978-3-030-38541-5_4)
3. Kurtuldu, E., Ismal, Ö.E. (2019). The Fiber Appreciated Again in Sustainable Textile Production and Design: Hemp (in Turkish). Faculty of Fine Arts Art Journal, Volume 12, Issue 24, 694- 718.
4. Averink, J. (2015). Global water footprint of industrial hemp textile (Master's thesis, University of Twente).
5. Ahmed, F., Islam, Z., Mahmud, S., Sarker, E., Islam, R. (2022). Hemp as a potential raw material toward a sustainable world: A review. Heliyon. Volume 8, Issue 1. 1-15. <https://doi.org/10.1016/j.heliyon.2022.e08753>
6. Zimniewska, M. Hemp Fibre Properties and Processing Target Textile: A Review. Materials 2022, 15, 1901. <https://doi.org/10.3390/ma15051901>
7. Kaya, S., Oner, E. (2020). Production, Characteristics and Applications of Hemp Fibres in Textile Industry (in Turkish). The Journal of Graduate School of Natural and Applied Sciences of Mehmet Akif Ersoy University Volume 11, Issue 1 108-123. <http://dx.doi.org/10.29048/makufebed.693406>
8. Tolek, S., Kadem, F.D. (2016). An investigation on color analysis and Fastness properties of the denim fabric Dyed with a different method (in Turkish). Tekstil ve Konfeksiyon, Volume 26, Issue 2, 199-204.
9. Okur, A. (1998). Pilling of fabrics: formation, affecting factors and testing methods (in Turkish). Tekstil ve Mühendis, Volume 45-46, 10-18.
10. Zhang, H., Zhang, J., Gao, Y. (2014). Study on the relationship between blending ratio and performance of hemp/polyester yarn. Journal of Natural Fibers, Volume 11, Issue 2, 136-143. <https://doi.org/10.1080/15440478.2013.861780>
11. Mondal, I.H. (2021). Fundamentals of Natural Fibres and Textiles. A volume in The Textile Institute Book Series, Cover for Fundamentals of Natural Fibres and Textiles. <https://doi.org/10.1016/C2019-0-03400-0>
12. Gedik, G., Avinç, O. O., Yavas, A. (2010). Hemp Fiber Properties and Its Advantages in Textile Industry (in Turkish). Electronic Journal of Textile Technologies, Volume 4, Issue 3, 39-48.

# POLYACRYLONITRILE NONWOVENS FOR THE PRODUCTION OF CARBON MATERIALS SUPPORTING THE REGENERATION OF BONE AND CARTILAGE TISSUES

BOGUŃ MACIEJ<sup>1\*</sup>, ŚLEDZIŃSKA KATARZYNA<sup>1</sup>, GIEŁDOWSKA MAŁGORZATA<sup>1</sup>, KRÓL PAULINA<sup>1</sup>, KAMIŃSKA IRENA<sup>1</sup> AND MAGDZIARZ SYLWIA<sup>1,2</sup>

<sup>1</sup> Łukasiewicz Research Network, Lodz Institute of Technology, 19/27 Marii Skłodowskiej-Curie, Lodz, Poland

<sup>2</sup> Institute of Organic Chemistry, Faculty of Chemistry, Lodz University of Technology, 116 Zeromskiego, 90-924 Lodz, Poland

## ABSTRACT

The influence of the change in surface weight on the physical properties of oxidized polyacrylonitrile precursor nonwovens intended for the production of carbon materials used in tissue engineering was studied. Thermal insulation properties of the nonwovens and their behavior during incubation in phosphate buffered saline (PBS) were investigated. Initial carbonization tests showed that from the point of view of carbonization and further application of carbon materials, the most effective was the use of a surface weight of about 120 g/m<sup>2</sup>. At the same time, for the research conducted on the incubation of nonwovens in PBS, no significant change in the pH of the solution was found.

## KEYWORDS

Polyacrylonitrile fibers; Nonwovens; PBS incubation; Thermal insulation properties.

---

\* Corresponding author: Boguń M., e-mail: [maciej.bogun@lit.lukasiewicz.gov.pl](mailto:maciej.bogun@lit.lukasiewicz.gov.pl)

## INTRODUCTION

One of directions in the development of contemporary medicine is the search for new materials that will support the process of tissue regeneration. Among these types of materials, carbon fibers, carbon nanostructures and composites with their participation are of particular importance. They have been used in many solutions in modern medicine [1-5]. In this case, it is important to properly select both the carbon fiber precursor and the carbonization process itself so that the produced carbon structure and its properties are appropriate for the intended purpose [6,7]. When thermal insulation properties of precursor nonwovens are known, it is possible to select the most favorable conditions for the carbonization process in order to obtain a carbon nonwoven fabric with the same chemical structure in the entire bulk. This is extremely important from the point of view of medical application of carbon nonwovens, which will constitute the scaffolding of hybrid carbon-polymer biomaterials. At the same time, knowledge of the impact of the carbonization process on the liquid absorption capacity, changes in pH and conductivity of the incubated medium allows us to shape the behavior of the biomaterial in vitro and in vivo.

The aim of this study was to examine thermal insulation properties of the produced precursor nonwovens with two surface weights and to investigate the incubation of the nonwovens in a phosphate-buffered saline (PBS) solution.

## EXPERIMENTAL

### Materials

Oxidized polyacrylonitrile fibers from Toray (Hungary) were used for the production of nonwovens. Figure 1 shows a cross-section and longitudinal view of the fibers used. Medical grade phosphate-buffered saline solution (PBS) was used for incubation tests.

### Methods

The nonwovens were produced using a mechanical fleece forming system with a laboratory carding machine. Then, the obtained fleece was subjected to the needling process on a HEUER type ROM 30LP/120/11/900 needle punching machine.

Measurements of the surface topography (SEM analysis) of the materials were carried out on a VEGA3 TESCAN (Tescan Osay Holding, Brno, Czech Republic).

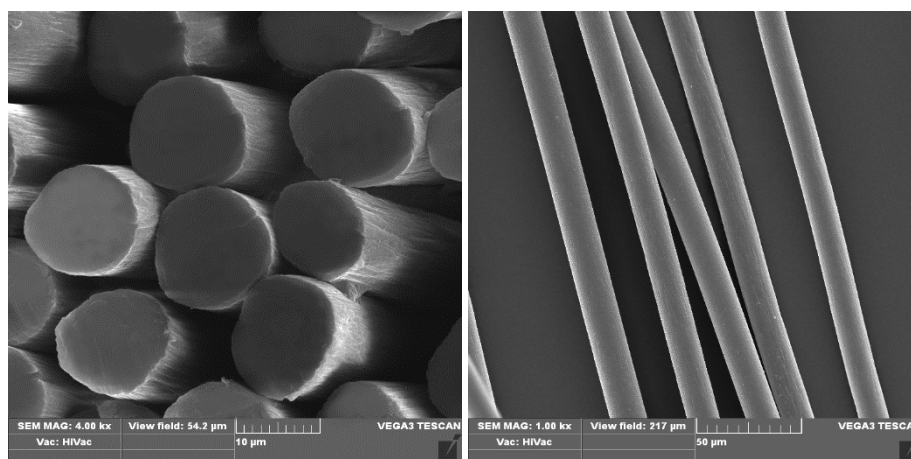


Figure 1. SEM pictures of the precursor fibers used.

Table 1. Thermal insulation parameters for precursor nonwovens.

Sample	$\lambda$ Wm <sup>-1</sup> K <sup>-1</sup>	a m <sup>2</sup> s <sup>-1</sup>	b Wm <sup>-2</sup> s <sup>1/2</sup> K <sup>-1</sup>	r Km <sup>2</sup> W <sup>-1</sup>	h mm	p -	q <sub>max</sub> Wm <sup>-2</sup>
OPAN 120	0,0368 ±0,0006	6,61E-07 ±1,04E-07	45,6 ±3,1	0,0712 ±0,0006	2,62 ±0,04	3,70 ±0,32	0,531 ±0,046
OPAN 600	0,0475 ±0,0019	4,37E-07 ±1,19E-07	73,1 ±8,3	0,1302 ±0,0066	6,17 ±0,16	5,86 ±0,78	0,528 ±0,065

where:  $\lambda$  – thermal conductivity; a – thermal diffusivity; b – thermal absorption; r – thermal resistance; h – thickness; p – the quotient of the maximum and stationary heat flow; q<sub>max</sub> – maximum heat flow.

To test the thermal insulation properties, the Alambeta device (Sensora, Czech Republic) was used, by means of which thermal conductivity, thermal diffusivity, thermal absorption, thermal resistance, quotient of the maximum and stationary heat flow density were measured.

The incubation of the nonwovens in PBS was examined at specific intervals. The pH and conductivity of the incubated medium was determined with an immersion probe.

## RESULTS AND DISCUSSION

The study of thermal insulation properties shows that an increase of the surface weight from 120 g/m<sup>2</sup> to 600 g/m<sup>2</sup> causes an increase in thermal insulation parameters. This is typical because of a similar structure of the material used and differences in its thickness. There are significant differences in all tested thermal insulation parameters. The exception is heat flow density, which is at a similar level for both surface weights (Table 1). When analyzing results of the test and carrying out the process of carbonization of nonwovens, it should be stated that the increase of the surface weight results in quality deterioration of the produced carbon materials. It should be noted, however, that in the case of medical use of this type of biomaterial, the carbonization process is carried out to a temperature 1200°C. At the same time, as part of the work, research was carried out on the incubation of the produced nonwovens in the PBS medium at various intervals. Figures 2 and 3 show the results of

changes in pH and conductivity of the incubated medium after keeping the nonwovens in it for various periods.

The conducted research shows that the surface weight is of no great importance for the pH of the medium. In both cases, the change of pH ranges from 6 to 7. On the other hand, in the case of conductivity, the influence of the surface weight of the nonwoven on changes of this parameter is visible. The incubation medium in which the nonwovens with a lower surface weight were kept shows an increase in conductivity over time, unlike the medium in which the nonwovens with a surface weight of 600 g/m<sup>2</sup> were incubated.

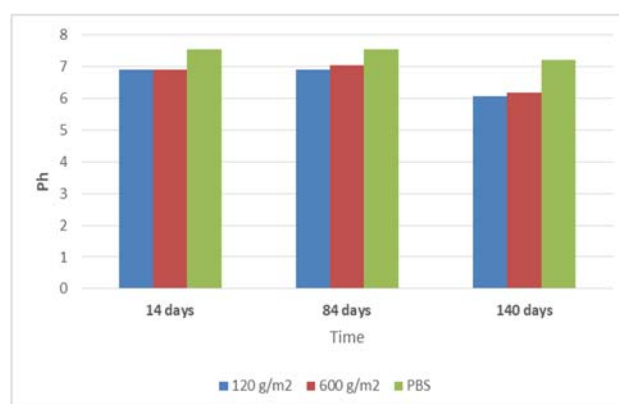
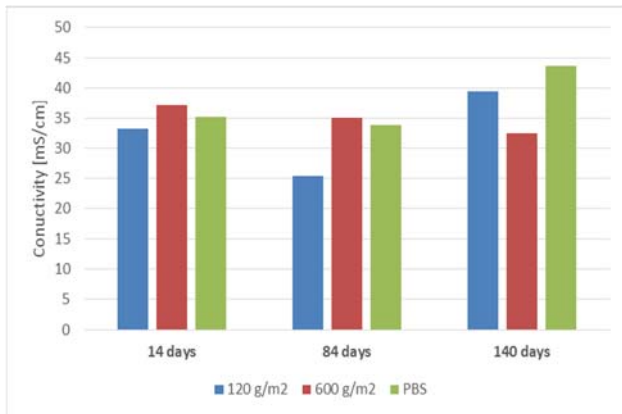


Figure 2. Changes in the pH of the incubation medium over time.



**Figure 3.** Changes in the conductivity of the incubation medium over time.

## CONCLUSIONS

It follows from the research on thermal insulation properties that the surface weight of nonwovens can have a significant influence on the carbonization effectiveness. This may result in differences in the properties of the carbon material in the entire bulk. In the case of medical use of carbon structures, it is important that the carbon structure produced during the carbonization process is homogeneous. In this case, the lack of homogeneity in the chemical structure may result in the formation of inflammations *in vivo*. Research on the incubation of nonwovens with different surface weights in the assumed time intervals showed differences in the parameters tested. Therefore, it is important to reconcile many opposing interdependencies in the design of biomaterials, so that the material constructed in this case, being a type of GBR membrane (guide bone regeneration), contributes to the effective process of tissue regeneration.

**Acknowledgements:** This research was funded by the National Science Centre, Poland, grant number UMO-2018/31/B/ST8/02418.

## REFERENCES

- Frączyk, J., Magdziarz, S., Stodolak-Zych, E., Dzierzkowska E., Puchowicz, D., Kamińska, I., Giełdowska, M., Boguń, M. (2021), Chemical Modification as a Method of Improving Biocompatibility of Carbon Nonwovens. *Materials* 14(12), 3198  
<https://doi.org/10.3390%2Fma14123198>
- Rajzer I., Rom, M., Błażewicz, M. (2010), Production of carbon fibres modified with ceramic powders for medical applications. *Fibers and Polymers* 11, 615-624  
<http://dx.doi.org/10.1007/s12221-010-0615-8>
- Trabelsi, M., Mamun A., Klöcker, M., Sabantina, L., Großberchode, Ch., Blachowicz, T., Ehrmann, A. (2019), Increased mechanical properties of carbon nanofiber mats for possible medical applications. *Fibers* 7(11), 98  
<https://doi.org/10.3390/fib7110098>
- Yadav, D., Amini, F., Ehrmann, A. (2020), Recent advances in carbon nanofibers and their applications – a review. (*European Polymer Journal* 138, 109963  
<https://doi.org/10.1016/j.eurpolymj.2020.109963>
- Chua, C.Y.X., Liu, H.-Ch., Di Trani, N., Susnjar, A., Ho, J., Scorrano, G., Rhudy, J., Sizovs, A., Lolli, G., Hernandez, N., Nucci, M.C, Cicalo, R., Ferrari, M., Grattoni, A. (2021), Carbon fiber reinforced polymers for implantable medical devices. *Biomaterials* 271, 120719  
<https://doi.org/10.1016/j.biomaterials.2021.120719>
- Fraczek-Szczypta, A., Rabiej, S., Szparaga, G., Pabjanczyk-Wlaziło, E., Krol, P., Brzezinska, M., Błażewicz, S., Bogun, M. (2015), The structure and properties of the carbon non-wovens modified with bioactive nanoceramics for medical applications. *Materials Science & Engineering C: Materials for Biological Applications* 51, 336-345  
<https://doi.org/10.1016/j.msec.2015.03.021>
- Morawska-Chochół, A., Domalik-Pyzik, P., Menaszek, E., Sterna, J., Bielecki, W., Bonecka, J., Boguń, M., Chłopek, J. (2018), Biodegradable intramedullary nails reinforced with carbon and alginate fibers: *in vitro* and *in vivo* biocompatibility. *Journal Applied Biomaterials&Functional Materials* 16(1), 36-41  
<https://doi.org/10.5301/jabfm.5000370>

# IDENTIFYING THE MATERIALS IN ARCHAEOLOGICAL TEXTILES

BŘEZINOVÁ HELENA<sup>1\*</sup>, PECHOČIAKOVÁ MIROSLAVA<sup>2</sup> AND GRABMÜLLEROVÁ JANA<sup>2</sup>

<sup>1</sup> Institute of Archaeology of the Czech Academy of Sciences, Prague, Czech Republic

<sup>2</sup> Technical University of Liberec, Faculty of Textile Engineering, Liberec, Czech Republic

## ABSTRACT

Given their organic origin, textiles rank among the rarest archaeological finds. While the vast majority of these artefacts are preserved as small fragments or mineralised remnants, their detailed textile technology study provides interesting and important information about the use of textile techniques and the quality of processing. The most important information concerns the utilised textile materials, but for degraded textiles, these materials are among the most difficult information to obtain. Image analysis using electron microscopy (SEM) is a significant aide in this pursuit.

## KEYWORDS

Archaeological textiles; Raw material; SEM; Image analyses.

\* Corresponding author: Březinová H., e-mail: [brezinova@arup.cas.cz](mailto:brezinova@arup.cas.cz)

## INTRODUCTION

Textiles from the prehistoric and medieval periods occur in archaeological contexts mainly as small fragments or mineralised remnants. Their professional evaluation by means of a textile-technological study provides a great deal of important information about the historical development of textile production, with the spectrum of textile raw materials ranking among the basic data produced by this research. The possibility of determining the raw material is directly related to the state of preservation of the textile fibres or the degree of degradation of the characteristic structure of individual types of fibres. In addition to optical microscopy, fibres are identified using various analytical methods connected with fibre sampling and an evaluation employing spectra of standards (e.g., infrared spectroscopy, Raman spectroscopy) [2]. Image analysis using electron microscopy (SEM) produces very good results. The advantage of this method is the possibility to analyse microscopic samples of textile fragments.

## SEM

SEM analysis was conducted using a TESCAN VEGA3 raster electron microscope. The SEM depicts the studied item by means of a thin electron probe formed and swept by the microscope tube. The majority of the imaging qualities of the microscope depend on the parameters of this electron probe: the size of the electron track, the aperture angle and the current in the probe. The

current in the probe is determined by the number of electrons passing through the probe at a given moment. The microscope tube is an electron optical device that forms and positions the electron probe. A system of magnetic lenses and apertures forms the resulting beam used to display the studied item.

## SELECTED RESULTS

A joint project conducted in 2012–2022 by the Institute of Archaeology of the Czech Academy of Sciences, Prague, and the Faculty of Textile Engineering analysed several dozen textile samples from archaeological excavations. The most interesting and important results in the establishment of textile materials – a major contribution to knowledge of the historical development of textile production in this country – came from the following three finds:

- a fragment of wool fabric on a bronze bracelet from the Tursko-Těšina site, which is one of the oldest finds of wool textiles in Europe, dates to the early phase of the Early Bronze Age [4];
- a mineralised remnant of fabric from nettle fibres preserved on an iron artefact from the 9<sup>th</sup> century from Břeclav-Pohansko, which is the first evidence in the Czech environment of the use of nettle in textile production [3];
- a minute fragment of silk fabric on a small piece of sheet metal from the important Great Moravian site in Mikulčice, which is highly significant and clear

confirmation of the presence of luxury silk fabrics imported into the environment of elite society from the Byzantine Empire [1].

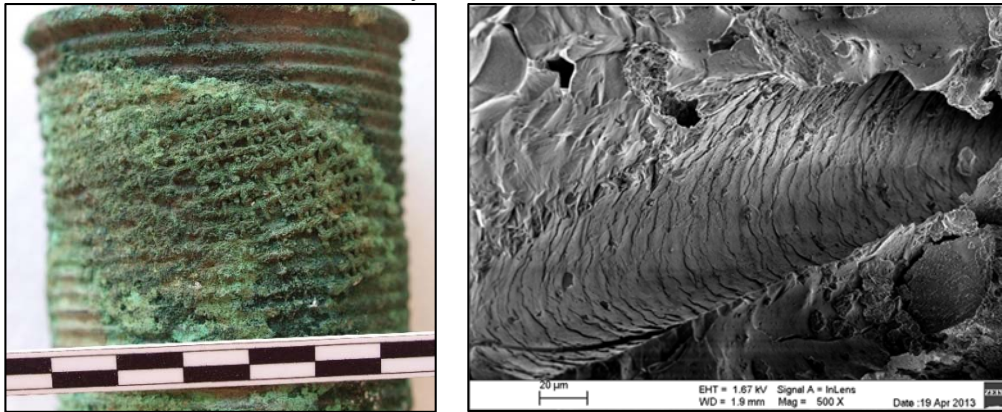


**Figure 1.** A mineralised fragment of wool fabric preserved on a bronze bracelet; Early Bronze Age Tursko-Těšina; ©Institute of Archaeology of the Czech Academy of Sciences, Prague. Imprint of wool fibre, clearly visible imprints of scales on the surface of the fibre.

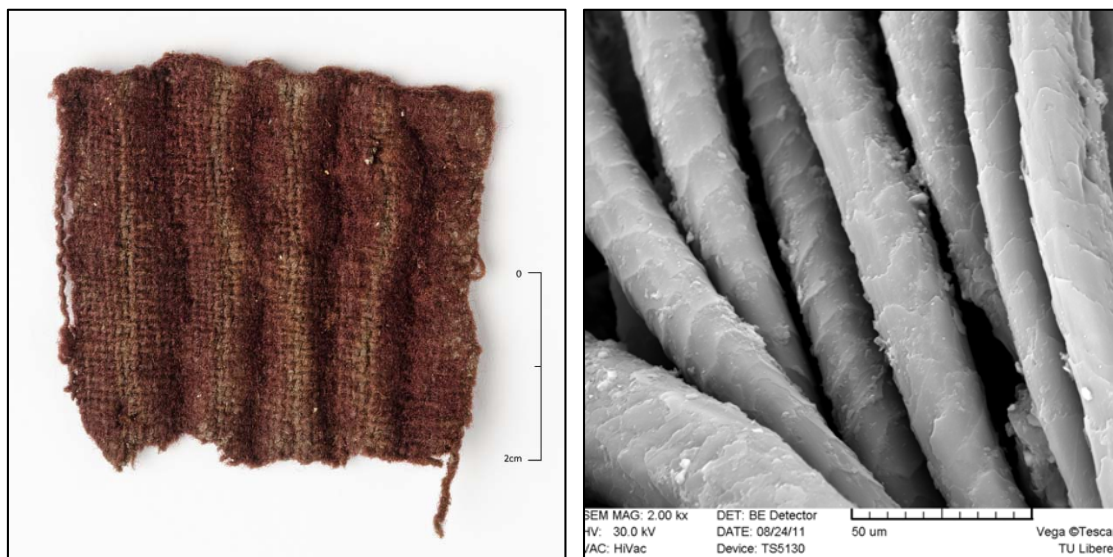


**Figure 2.** The fragment of wool fabric comes from the archaeological excavation of a medieval dump in the centre of Prague; ©Institute of Archaeology of the Czech Academy of Sciences, Prague. Fibres of “domestic wool” (containing fibres of varying fineness: guard hair, undercoat, intermediate hair).

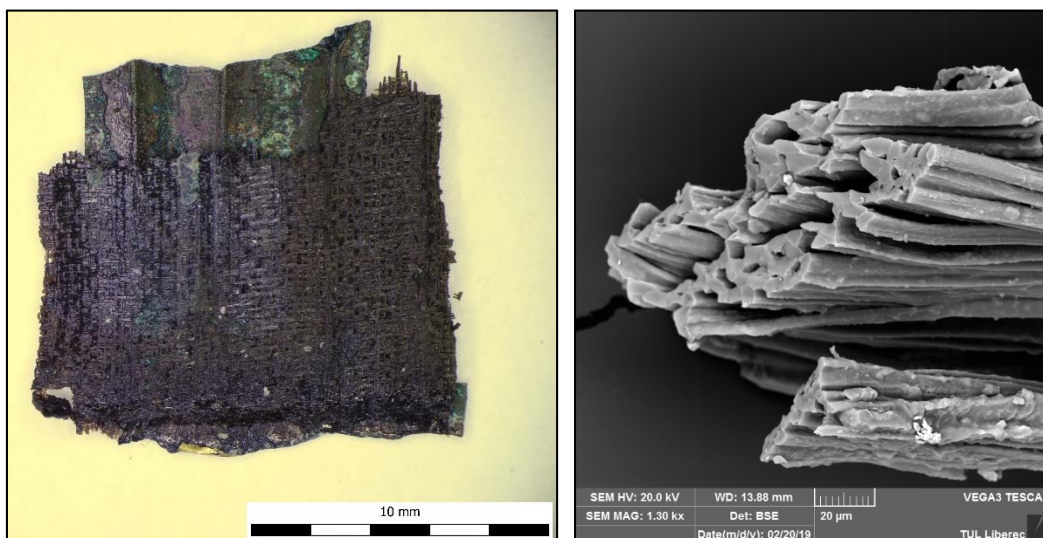


**Figure 3.** A fragment of silk fabric preserved on a small piece of sheet metal from the Great Moravian agglomeration in Mikulčice; ©Institute of Archaeology of the Czech Academy of Sciences, Brno; silk fibres, with the clearly visible typical shape of the fibre cross-section – a triangle with rounded vertices, also fineness of fibre is very typical.

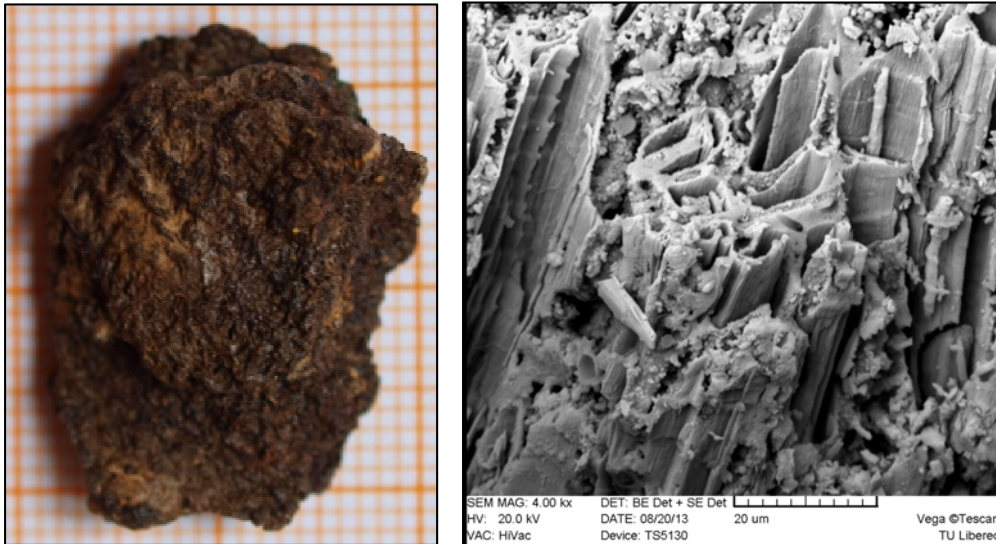


**Figure 4.** A mineralised fragment of fabric made from nettle fibres; Great Moravian hillfort of Břeclav-Pohansko; ©Department of Archaeology and Museology, Masaryk University Brno. Nettle fibre with the typical traits for bast fibres, which differ from others by the shape of the cross-section and size of the lumen.



**Figure 5.** A fragment of linen fabric preserved on the surface of a gombík (globular hollow pendant) from the early medieval cemetery in Vinoř. ©Department of Archaeology, Charles University; bundles of elementary flax fibres with the typical nodes and sharp edges of the regular 5–7-side cross-section.

## CONCLUSIONS

The use of scanning electron microscopy is an example of important interdisciplinary and institutional collaboration playing a major role in expanding our knowledge of the history of textile production. Archaeological textile finds document the earliest phase in the development of this craft, which was always a key production activity. The study of textile production using the latest technical equipment is a common practice in archaeology throughout Europe today.

Knowledge of contemporary material engineering can be successfully used to identify fibre fragments. The fibres of natural origin show typical traits (cross-section shape, size and shape of interior “hollows”, the surface pattern, fibre fineness) and are the same for the given fibres. If it is not possible to use other

methods for the identification of a find due to its limited amount, contamination by other material, etc., image analysis is the only means of determining the textile material.

**Acknowledgements:** *This work was accomplished with support from the grant project of the Czech Science Foundation GA ČR 19-00166S “Textiles from Archaeological Contexts at Prague Castle – Relics of Czech Rulers, Their Family Members and Church Dignitaries.”*

## REFERENCES

1. Březinová, H. (2013). Finds of textile fragments and evidence of textile production at a major excavation site of the Great Moravia in Mikulčice (South Moravia, Czech Republic). In: Banck-Burges, J., Nübold, C (Eds.). NESAT XI. The North European Symposium for Archaeological Textiles. Verlag Marie Leidorf (Rahden/Westf.), 193–196.
2. Březinová, H. – Kohout, D. – Bravermanová, M. – Otavská, V. – Selmi Wallisová, M. (2016). *Středověké*

- textilní a barvířské technologie. Soubor textilních fragmentů z odpadních vrstev z Nového Města pražského. (Medieval Textiles and Dyeing Technologies. An Assemblage of Textile Fragments from the Waste Layers of Prague's New Town). Institute of Archaeology of the Czech Academy of Sciences, Prague.
3. Březinová, H. – Přichystalová, R. (2014): Úvahy o textilní výrobě na Pohansku na základě analýzy nálezů textilních fragmentů a předmětů souvisejících se spřádáním a tkaním. (An Examination of Textile Production at Pohansko on the Basis of an Analysis of Textile Fragments and Artefacts Connected with Spinning and Weaving). Památky archeologické, CV, 2014, 155–214.
  4. Štolcová, T. – Březinová, H. (2018): Textile Fragments from the Bronze Age Site of Tursko-Těšina, Czech Republic (Included in Rast-Eicher, A.: In the Beginning was the Fibre). In: Sofaer, J. (ed.). Considering Creativity. Creativity, Knowledge and Practice in Bronze Age Europe. Archaeopress Archaeology, 121–123.

# STANDARDISING THE SAMPLE PREPARATION FOR ANALYSIS OF FIBRES AND PARTICLES BY STATIC IMAGE ANALYSIS

FISCHER HOLGER<sup>1\*</sup>, SIGMUND INA<sup>2</sup>, HARTWIG PETRA<sup>1</sup>, DEDERER ESTHER<sup>1</sup> AND MASCHINSKI ANNETT<sup>2</sup>

<sup>1</sup> Faserinstitut Bremen e.V. FIBRE, Bremen, Germany

<sup>2</sup> Sächsisches Textilforschungsinstitut e.V. STFI, Chemnitz, Germany

## ABSTRACT

Static image analysis is known as a versatile method, which is in use for characterisation i.e. of fibres, nonwovens, textile recyclates etc. Due to incomplete standardization (esp. in the area of sample preparation) the usage is actually limited. Within the project StaPAFaB two research institutes are engaged to compile a reference manual listing typical classes of materials and optimised methods of sample preparation for each of them. This will be combined with recommendations for reasonable parameters in image acquisition / processing and possible limitations for each type of material. Aim is to enable reproducible and consistent analyses on an inter-laboratory level as well as to reduce the demand of time for the analyses. This article focuses on typical classes of textile materials and adapted methods to enable their quick and reliable sample preparation.

## KEYWORDS

Image analysis; Sample preparation; Textile fibres; Recycled fibres.

---

\* Corresponding author: Fischer H., e-mail: [fischer@faserinstitut.de](mailto:fischer@faserinstitut.de)

## INTRODUCTION

Static image analysis delivers more detailed results than e.g. sieving. Namely there are distributions instead of average values for length, width and several shape factors. As for all analytical methods, standardisation is an essential prerequisite for reproducibility as well as for comparability of the results. Unfortunately, up to now standardisation has taken place only incompletely for static image analysis. ISO 9276–1 to –6 [1] define parameters for evaluation and graphical presentation of the results. Image acquisition and calibration of the experimental setup is only specifically described by the equipment suppliers. This does not cover the way how to prepare samples for the static image analysis.

Consequently this leads to problems in commercial and research laboratories. Static image analysis is a useful method for universal access to parameters like size and shape of a wide range of materials, combined with statistical analysis. This misleads to a frequent use of this method for new questions and single research samples. Finally different ways of

sample preparation, combined with various parameters in image acquisition and analysis lead to strongly different results. This guarantees neither a reproducibility of results in one laboratory, nor comparable results between different laboratories. On the other hand it is known from inter-laboratorial round trials, that a well-described procedure can guarantee identical results within a small tolerance [2].

To overcome the problems in the area of sample preparation, the project StaPAFaB has been started, where two research institutes are engaged to compile a reference manual listing typical classes of materials and optimised methods of sample preparation for each of them. The manual will comprise different types of sample preparation as well-documented guideline for scientists and practitioners. This article presents results for typical 'easy' and 'complicated' sample materials to give a first insight into the project aims.

## DEFINITION OF MATERIAL CLASSES

Typical sample Materials have been collected during the project and have been classified according to a newly set-up scheme (cf. Figure 1) allowing to find easily adequate methods of preparing samples for analysis. The material classes are:

- **particles with free-flowing property**, e.g. powders, small crystals (minerals), granules, rice husks etc. Main criterion: these particles do not stick together.
- **particles with limited free-flowing property**, e.g. short fibres, shives etc. Main criterion: these particles tend to stick together slightly, but can be separated non-destructively by small mechanical action.
- **single fibres**, which are not short fibres (see above). Main criterion: the length must be smaller than the max. scanner image length.
- **roving snippets**, e.g. cut-offs from processing high performance fibres (glass, carbon, etc.). Main criterion: the snippets are stable enough for either sieving or at least manual separation using tweezers.
- **recyclates** (consisting of several material fractions): depending on structure several options are possible.

Each material class is sub-divided into groups. For each group possible methods of preparation are specified and recommendations are given.

For a correct assignment of a sample to the most relevant group and best fitting preparation method it is essential to know, what the aim of the analysis is and which parameters have to be analysed. Otherwise the preparation time and number of parameters to analyse may exceed your budget and time! In experience of the authors each hour of discussion with the sample supplier can save two or more hours working with the samples.

Based on this information it is easy to assign each sample material to one of the groups and then to select the preparation method fitting best to analyse the parameters required by the sample supplier. A typical example for saving time and efforts is a fibre sample (class: single fibres). In the worst case there is only manual preparation possible to analyse length and crimp of each fibre. In the best case the fibres can be cut to short fibres and the width distribution can easily be analysed.

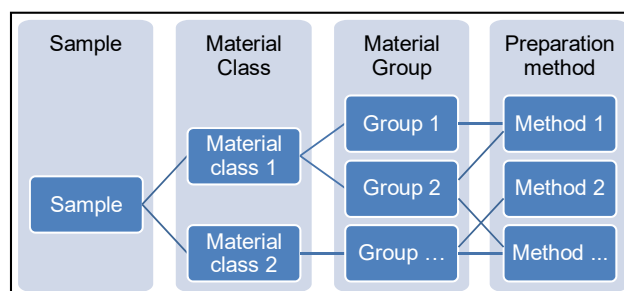


Figure 1. Scheme of material classification to identify adequate method(s) for sample preparation

## EXAMPLES FOR SAMPLE PREPARATION OF DIFFERENT MATERIAL CLASSES

Within this section typical examples are given for an easy sample preparation using the dispersion by sieving (cf. section 3.1) as well as a quick separation method for complex recycle mixtures enabling at least access to essential data of composition (cf. section 3.2).

### Example #1: 'easy' sample preparation

As described in the previous section, recommendations for different Materials may end up in the same preparation method. This is the case for e.g.:

- Short cut fibres ('flock fibres') <2 mm length: material class 'single fibres', group short fibres, within the group described as case of 'short enough to exhibit free-flowing property'
- Sand or minerals (Aluminiumtrihydroxide 'ATH', Soda etc.) in dry state: material class 'particles with free-flowing property', group dry powders

For both of them use of a sieve as aid for dispersion is recommended, assisted by shaking or use of a brush. In Figure 2 (a) the experimental setup is shown in brief: a spoon and/or spatula to distribute the sample on the sieve, a brush for additional dispersion, and an analytical sieve in adequate mesh size. To guarantee a reproducibility of the results, the sieve must be certified to a standard like ISO 3310-1 [3]. Some preceding trials are recommended to identify the optimal sieve size: if a sample passes directly through the sieve, the mesh size is too big. If the sample remains (nearly) completely on top of the sieve and does not pass even under vibration, the sieve size is too small. If the sample has a large size distribution, it may be necessary to use two or more sieves to fractionize the sample. In this case the complete sample must be analysed in several images to obtain a valid result representing the sample correctly.

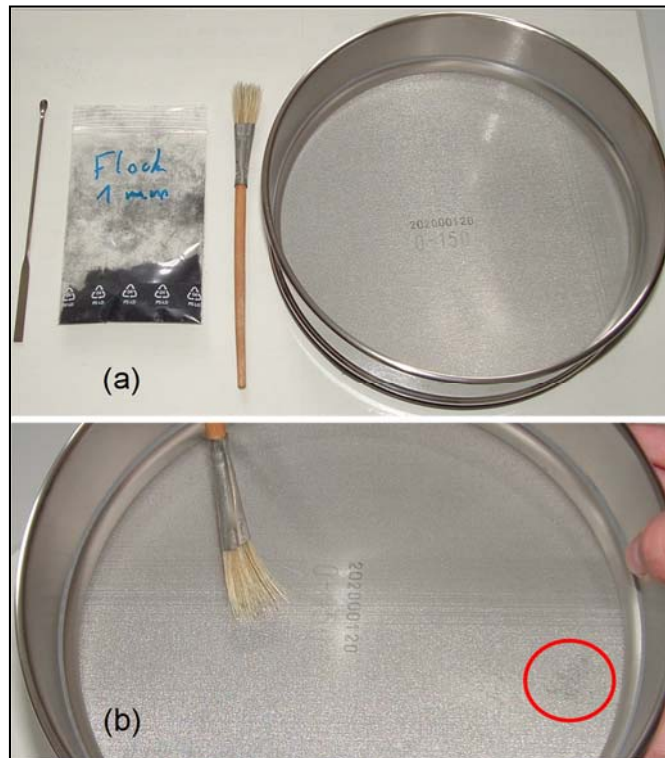


**Figure 2.** (a) Flock sample, tools and sieve for preparation and (b) dispersing by brush with flock agglomerate still to disperse in red circle.

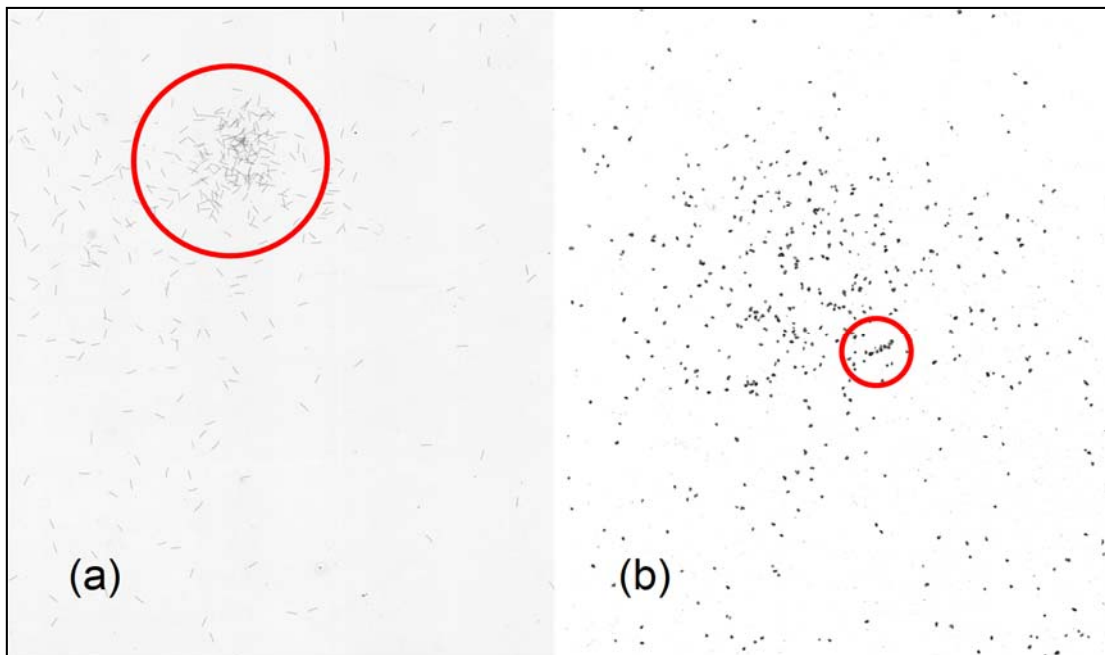


**Figure 3.** Acquired images of (a) flock fibres of figure 2 and (b) sugar particles. Red circles indicate remaining agglomerates which should be excluded from analysis.

For sample preparation mostly it is sufficient to position the sieve above the scanner or a transparent foil, which is later transported into the scanner. Then the sample is distributed over the sieve by the spatula or spoon. Finally the particles can be dispersed by using a brush as shown in Figure 2 (b). Agglomerates of sample particles have to be dispersed carefully in order to achieve a good distribution for scanning. If particles remain on the

sieve, they must be transferred to a second transparent foil to be analysed as additional image to guarantee an analysis of the complete sample.

In Figure 3 the greyscale scans of two particle sample are presented as typical examples for the sample types listed above: (a) flock fibres of figure 2 with 1 mm of nominal length representing short fibres and (b) sugar particles as example of crystalline particles.

Both samples exhibit a good dispersion of the particles over the image. But, in both samples there are small regions with insufficient dispersion, indicated by red circles. For the image analysis it is essential, that there are not too much overlapping particles. In general it is not possible to analyse these overlaps correctly, and thus they must be excluded from the analysis. For the sample preparation this means, that either the particles in these regions may be separated manually (only reasonable for large particles), or they must be excluded from the subsequent analysis.

Finally the images can be loaded into the desired image analysis software to perform the analysis of the desired parameters. For short fibres this is typically width and length, while for particles it is typically the grain size, aspect ratio etc.

## Example #2 / complex sample preparation

Textile recyclates often consist of different fractions. Thus there was normally only the time-consuming possibility of manual separation and subsequent analysis of each fraction. Within the project a new approach using compressed air to separate the fractions has been developed. It enables a quick approach to at least rough analysis of the shares.

The experimental setup (cf. Figure 4 a & b) is simply using a sampling bag 42 x 21 cm and a commercial airbrush pistol (a). The sample here is cotton from T-shirts after the tearing process. After separating the agglomerate (b) the bag has to be transported horizontally to a flatbed scanner to acquire a greyscale image (cf. Figure 4 c). The fractions fabrics, yarns and fibres can now be easily identified and quantified by their gray scale values. In this case the fabrics appear black, represented by the greyscale values 0 to 50, while the yarn pieces are

dark grey, represented by the greyscale values 51 to 140. The fibres appear light grey, represented by the greyscale values 141 to 200. Values above 200 to 255 represent the background.

The exact limits of the different fractions vary for different recyclates depending on structure, colour and degree of disintegration. Thus the greyscale limits for the different fractions should be defined individually. Now it is easy to analyse the greyscale histogram, using e.g. free software like ImageJ [4]. Typically not more than 5 – 10% of the pixels should be particles to avoid too strong overlapping. From these pixels the share of the different fractions can be calculated in %, representing roughly the mass shares.

As a second example a carpet recyclate after separation in compressed air is shown in Figure 5 with (a) photograph and (b) greyscale scan. For this material the same approach for assessing the shares of different fractions is possible. In this case not only the fabrics (carpet backing), but as well the tufting yarn appear black. For this reason they can only be counted as one fraction. Finer yarns from the backing and fibres are the other fractions evaluable.

Summing up, by this method of sample preparation it is easily possible to access the share of fractions in textile recyclates. This is important to control the efficiency of the tearing process and gives information necessary to decide, if the degree of disintegration is sufficient.

In principle, some more parameters like size and shape distribution of the fabric fragments or width distribution of the fibres can be analysed.

Other options like length distribution of the yarn pieces and fibres would be only available after manual sample separation.

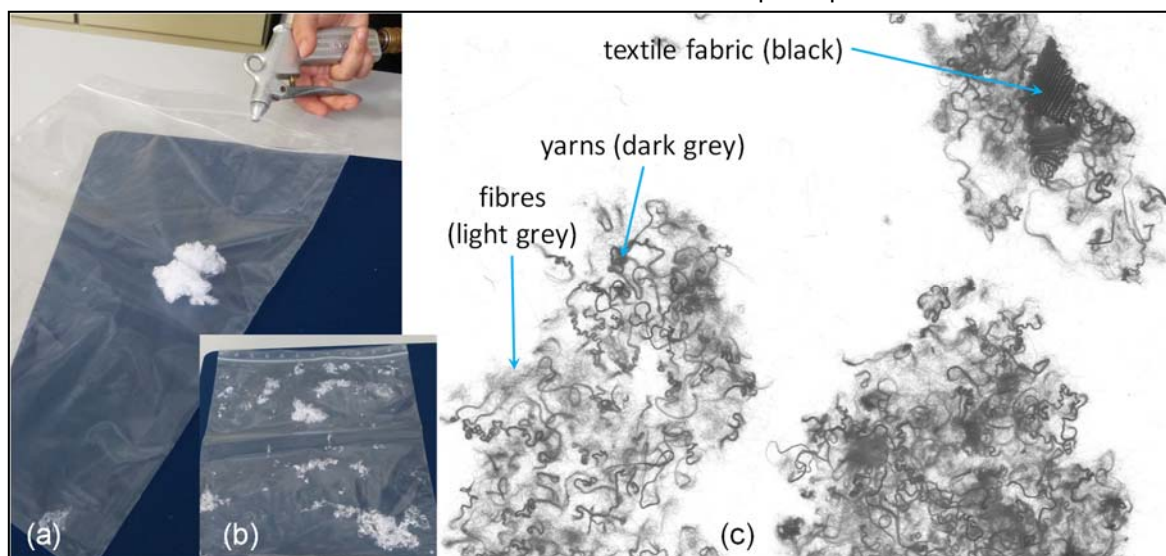


**Figure 4.** (a) agglomerate of recycled textile in sampling bag, (b) after separation by compressed air and (c) resulting grayscale image in sampling bag with fabrics in black, yarns in dark gray and fibres in light gray.

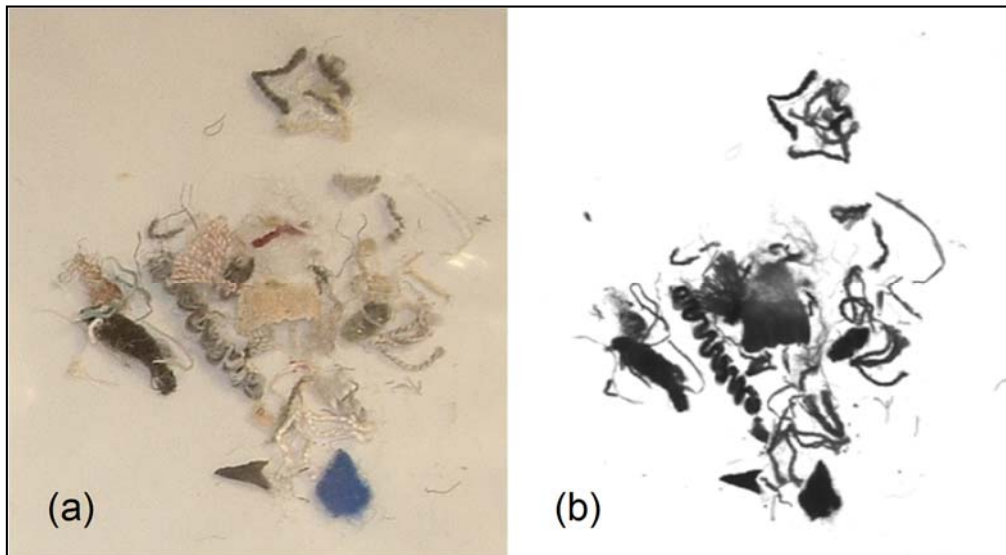


Figure 5. Agglomerate of recycled carpet, (a) photograph and (b) grayscale scan.

## CONCLUSIONS & OUTLOOK

Within the project StaPAFaB a scheme has been set-up for quick and reliable sample preparation for static image analysis. The project work led to progress in sample preparation techniques especially in the field of textile recyclates. At the beginning of the StaPAFaB project the only method to prepare samples from these recyclates was manual separation, demanding up to >1 day per sample. Using the compressed air method described here it is possible to prepare a sample within minutes, which is good enough to assess the parameters important for the tearing process.

In order to disseminate the results to a broad circle of interested scientists as well as practitioners, a public workshop will take place in January 2023 in Bremen / DE for everybody interested in these topics. In addition, the project results will be published in April 2023 as a reference manual listing typical classes of materials and optimised methods of sample preparation for each of them.

**Acknowledgement.** *The authors are much indebted to the federal ministry of economic affairs and climate action for funding this research within the programme INNO-KOM (No. 49VF200016 & 49VF200017).*

Supported by:



on the basis of a decision  
by the German Bundestag

## REFERENCES

1. International Organization for Standardization ISO (ed.). ISO 9276-1:1998-06: Representation of results of particle size analysis - Part 1: Graphical representation. ISO, Geneva, CH 1998.
2. Fischer, H.; Haag, K. & Müssig, J. (2016). Standardisation & Harmonisation of the Length Analysis of Flock Fibres by Scanner-based Image Analysis. *Melliand International* 22(1), 16 – 18. ISSN 0947-9163.
3. International Organization for Standardization ISO (ed.). ISO 3310-1:2016-08: Test sieves - Technical requirements and testing - Part 1: Test sieves of metal wire cloth. ISO, Geneva, CH 2016.
4. National Institutes of Health. ImageJ Image Processing and Analysis in Java. <https://imagej.nih.gov/ij/download.html> . Accessed 2022-10-14.

# SURFACE ROUGHNESS OF POLYAMIDE KNITTED FABRICS

TOMOVSKA ELENA<sup>1\*</sup> AND HES LUBOS<sup>2</sup>

<sup>1</sup> University "Ss. Cyril and Methodius", Faculty of Technology and Metallurgy, Department of Textile Engineering, Ruger Boskovic 16, 1000 Skopje, Macedonia

<sup>2</sup> Technical University of Liberec, Faculty of Textile Engineering, Department of Textile Evaluation, Studentská 2, 461 17 Liberec, Czech Republic

## ABSTRACT

Fabrics are never ideally smooth. Their texture varies between fine and coarse, quantified through the surface's vertical deviation. Fabric roughness, or its opposite smoothness, is employed as measure of the surface texture of fabrics. In general, texture depends upon fiber properties, yarn count, yarn twist, and fabric structure and fabric design). This research aims to determine the limitations in visual perception of surface roughness in comparison to objective surface roughness measurements of low weight polyamide fabrics. Subjective evaluation is used for the visual assessment, while instrumental measurement of the properties was conducted using a noncontact laser profilometer. Subjective evaluation was conducted by a panel of forty untrained evaluators on a sample of seven polyamide knitted fabrics with different yarn count and composition. The roughness profile parameters were measured using Talysurf CLI 500 according to ISO 4827. Although the surface roughness measured as arithmetic mean deviation (Ra) and roughness through visual inspection of the fabric are correlated, instrumental measurements of roughness are more precise. Differences in the surface roughness arising from significantly different yarn structures will be observed, while those due to the knitted fabric structure are negligible in visual inspection.

## KEYWORDS

Texture; Surface roughness; Knitted fabrics; Visual inspection.

---

\* Corresponding author: Tomovska E., e-mail: [etomovska@tmf.ukim.edu.mk](mailto:etomovska@tmf.ukim.edu.mk)

## INTRODUCTION

Surface roughness is a tactile property of fabrics that has been widely investigated by many researchers for both woven and knitted fabrics. The research application is mainly dedicated to defining the sensorial or tactile comfort. Tactile comfort properties are complex concepts which include dimensional changes at small forces such as tensile, shear, compression, and bending, surface properties (friction and roughness) and warm/cool feeling evaluate via the Kawabata evaluation system [5]. Numerous research works [1,2,3,4,6] have studied the effect of different fiber materials, fiber blended ratios, fiber morphology, yarn properties, finishing treatments, and fabric constructions on the hand feel properties of knitted fabrics. Furthermore, surface roughness has been used to distinguish between various types of structures [7].

This research aims to investigate the visually perceived surface roughness and luster of pantyhose fabrics. Subjective evaluation is used for

the visual assessment, while instrumental measurements of the properties was used to obtain objective fabric parameters.

## EXPERIMENTAL

### Materials

Samples were knitted from commercially available yarns on industrial circular knitting machine with four systems, diameter of four inches and 400 needles. The physical and structural properties of the samples are presented in Table 1. The pure polyamide knits single jersey, while the addition of elastane was through knitted hopsack structure. Sample S22T was with increased luster, in a plated knit from a covered elastane yarn and a trilobal increased luster filament. The samples are made of fine filaments, with low weight and high cover factor. Figure 1 shows the microscopic images of selected samples, taken on Olympus BX51 microscope at a magnification of 5×.

Table 1. Sample structure.

Sample		S5E	S17P	S17E	S22PP	S44CE	S78CE	S22T
Yarn count (dtex)		5.5/2	17/3	17/3	22/5	44/13	78/24	22/5
Density	Wales (cm-1)	28.6	42.9	33.3	23.8	23.8	28.6	23.8
	Courses (cm-1)	28.1	24.6	28.1	31.6	21.1	24.6	35.1
Sample code: Number-yarn count, P- polyamide 6.6, PP- polyamide 6, E-polyamide-bare elastane blend, CE- polyamide-covered elastane blend								

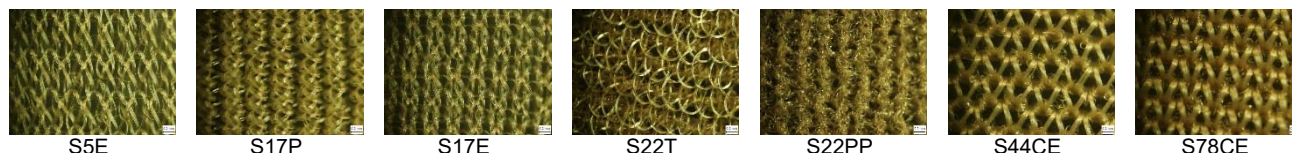


Figure 1. Microscopy of samples.

### Methods

Subjective evaluation was conducted on a knee-height leg model. To standardize the evaluation, evaluators were asked to describe the shin part of the leg. The model was placed in a black viewing cabinet (length 60cm, height 50m, depth 45cm), with a D-65 light source, illuminating the leg surface under a 15° angle. Samples were evaluated from a distance of 1.5m. The evaluators were 40 women aged 20 to 60, with normal visual acuity. A semantic differential method in a five-scoring system was used to assess texture, evaluated by bipolar opposites of rough-smooth and uneven-even.

To evaluate surface roughness, Talysurf CLI 500, a noncontact laser profilometer was used. Roughness profile parameters were measured according to ISO 4827. For global evaluation of the roughness amplitude profile the arithmetic mean deviation (Ra, µm) in wales and courses direction on a length of 5±0.05mm was used. This measurement quantifies the absolute values of the profile variations (peaks and valleys) from the mean line in the evaluation length. However, Ra does not give information on the shape of the profile. Therefore, a pseudo-color map was used to assess the reasons for variation of the surface.

### RESULTS AND DISCUSSION

The results of the subjective and objective evaluation of pantyhose are presented on Figures 2 and 3. A Pearson correlation coefficient of 0.79 was found between the visually perceived roughness (VR) and the instrumentally measured roughness (Ra) in the wales direction, while a lower correlation (Pr=0.69) was found in the course direction. This points out two important differences between the visual and haptic assessment of fabric. Firstly, the correlation between visual assessment and roughness measurements is not strong. Small

differences in roughness that may be instrumentally measured will escape the human eye. Secondly, the direction of viewing will influence the surface roughness visual perception, as lower correlation was found in the courses direction. As roughness is a three-dimensional property assessment of the fabrics can be made despite directionality.

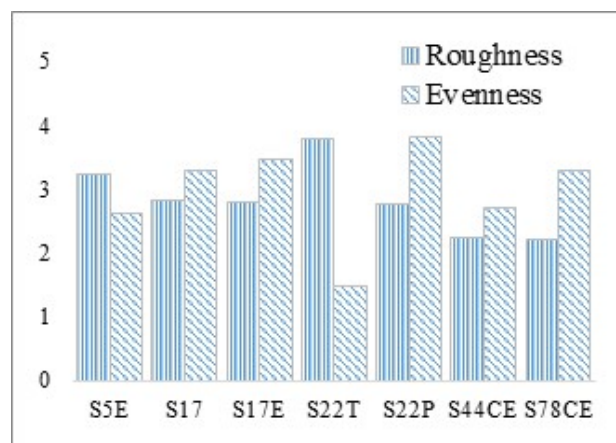


Figure 2. Visual assessment of pantyhose roughness and evenness.

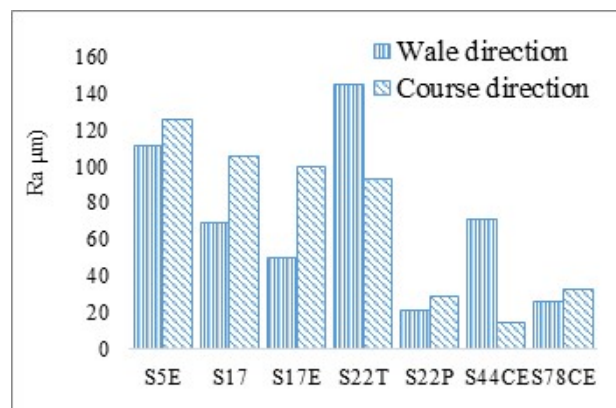


Figure 3. Arithmetic mean deviation of the roughness profile.

When examining the values presented in figure 3 S22T is a clear outlier. Unlike the rest of the series which is knit of smooth multifilament yarns, this sample was made of a single covered yarn with an addition of a profiled trilobal filament, thus the uneven structure of the yarn contributes to surface roughness. However, in the objective assessment of the surface roughness an additional outlier was found with sample S44CE. To examine the differences in the surface roughness figure 4 a) and b) presents a pseudo-color map of the two samples. The map the roughness profile of the sample to a color spectrum, with peaks shown as red-white and valleys shown as red green. As can be seen on the representation of the pseudo-color map for sample S22T the roughness in the sample is due to the uneven distribution of peaks and valleys in the sample, caused by the covered yarn, as well as the protrusions of the trilobal filament. On the other hand, the sample S44CE has a fairly even structure with deep valleys occurring periodically, consistent with the knitted structure and the loop shapes within it. The roughness of knitted fabrics comes from the applied yarn, as well as the structure of the fabric, with the former having greater influence on the visual perception of fabrics.

When the outlier sample S22T is removed from the analysis a correlation coefficient of 0.9 is obtained between visually assessed surface roughness and yarn count. However, low correlation (0.54) existed between objectively measured Ra and the yarn

count. To illustrate this difference pseudo-color maps of fine filament pantyhose of 17dtex (S17P and S17E) and coarse filament pantyhose (S78CE) are presented on figure 4 c), d) and e). As can be seen from the figure increased yarn count contributes to less differences in height along the roughness profile of a surface, creating a closed, smooth surface. This is due to the even packing of filaments within the loop structure when the yarn count increases. The presence of elastane yarns in the knit (S17E) stabilizes the loop structure, leading to a more even distribution of the peaks and valleys on the fabric surface compared to a sample with no elastane (S17P). Even though these differences in surface can be seen via instrumental analysis, they are not perceivable visually in real conditions of wear.

Furthermore, during visual assessment of pantyhose yarn count is a more important parameter compared to fiber composition, as can be seen by the assessment of sample S22PP made of PA6 in 22dtex. In the visual assessment of the set this sample is seen to have similar roughness to samples with fine yarn count of 17dtex. However, due to the fiber composition the roughness Ra of the sample are closer to those of coarser yarns. Although the difference in roughness caused by different fiber composition will influence the general surface related properties, such as comfort it will not be immediately visually perceivable.

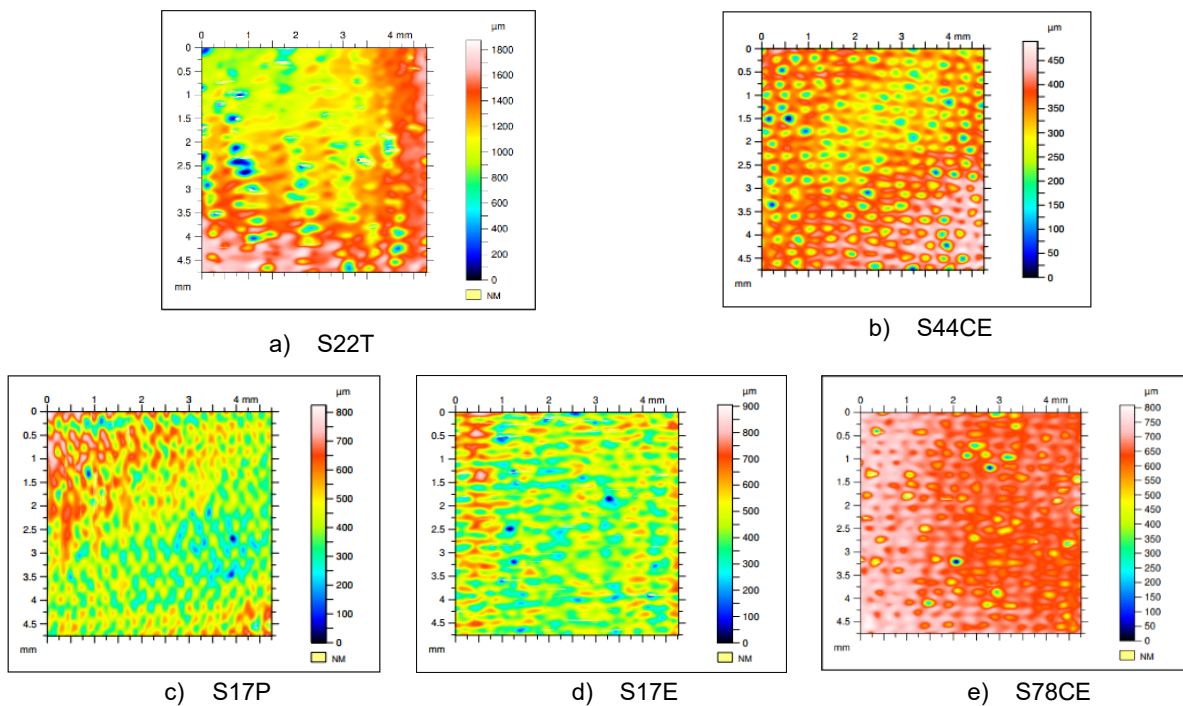


**Figure 4.** Pseudo color maps of samples.

## CONCLUSIONS

This study investigated roughness as a property of knitted fabrics. Although the measured arithmetic mean deviation (Ra) the surface roughness and roughness through visual inspection of the fabric are correlated, instrumental measurements of roughness are more precise. Differences in the surface roughness arising from significantly different yarn structures will be observed, while those due to the knitted fabric structure are negligible in visual inspection.

**Acknowledgements:** *The authors would like to thank the Vishegrad Fund for providing a mobility grant for this research.*

## REFERENCES

1. Atalie, D., Gideon, R. K., Ferede, A., Tesinova, P., Lenfeldova, I. (2021): Tactile Comfort and Low-Stress Mechanical Properties of Half-Bleached Knitted Fabrics Made from Cotton Yarns with Different Parameters, *Journal of Natural Fibers*, 18(11), 1699-171.1  
<https://doi.org/10.1080/15440478.2019.1697989>
2. Balci Kilic, G., Okur, A. (2018). Effect of yarn characteristics on surface properties of knitted fabrics. *Textile Research Journal*, 89 (12).  
<https://doi.org/10.1177/0040517518797337>
3. Demiryürek, O., D. Uysaltürk. (2013). Thermal comfort properties of Viloft/cotton and Viloft/polyester blended knitted fabrics. *Textile Research Journal* 83 (16):1740-53.  
<https://doi.org/10.1177/0040517513478458>
4. Mahar, T.J., Wang, H., Postle R. (2013). A review of fabric tactile properties and their subjective assessment for next-to-skin knitted fabrics. *The Journal of The Textile Institute*, 104:6, 572-589.  
<https://doi.org/10.1080/00405000.2013.774947>
5. Mooneghi, S. A., S. Saharkhiz, and S. M. H. Varkiani. 2014. Surface roughness evaluation of textile fabrics: A literature review. *Journal of Engineered Fibers and Fabrics* 9 (2):1-18.  
<https://doi.org/10.1177/155892501400900201>
6. Vasile, S., Malengier, B., De Raeve, A., Deruyck, F., (2017). Influence of selected production parameters on the hand of mattress knitted fabrics assessed by the Fabric Touch Tester. *Textile Research Journal*, 89(1).  
<https://doi.org/10.1177/0040517517736471>
7. Vassiliadis, S.G. and Provatidis, C.G. (2004), "Structural characterization of textile fabrics using surface roughness data", *International Journal of Clothing Science and Technology*, Vol. 16 No. 5, pp. 445-457.  
<http://dx.doi.org/10.1108/09556220410554633>

## AIMS AND SCOPES

“Vlákna a Textil” is a peer-reviewed scientific journal serving the fields of fibers, textile structures and fiber-based products including research, production, processing, and applications.

The birth of this journal is connected with three institutions, Research Institute for Man-Made Fibers, Svit (VÚCHV), Research Institute of Chemistry of Textiles (VÚTCH) in Žilina and Department of Fibers and Textiles at the Faculty of Chemical Technology, Slovak Technical University in Bratislava, having a joint intention to provide, utilize and deposit results obtained through the research, development and production activities dealing with the aforementioned scopes. „Vlákna a Textil“ journal has been launched as a consequence of a joining of existing magazines „Chemické vlákna“ (VÚCHV) and „Textil a chémia“ (VÚTCH). Their tradition should provide a good framework for the new journal with the main aim to create a closer link between the basic element of the product - fibre and its fabric - textile.

Since its founding in 1994, the journal introduces new concepts, innovative technologies and better understanding of textile materials (physics and chemistry of fiber forming polymers), processes (technological, chemical and finishing), garment technology and its evaluation (analysis, testing and quality control) including non-traditional applications, such as technical textiles, composites, smart textiles or garment, and nano applications among others. The journal publishes original research papers and reviews. Original papers should present a significant advance in the understanding or application of materials and/or textile structures made of them.

# VLÁKNA A TEXTIL

Volume 30, Issue 1, April 2023

## CONTENT

- 5 SAJJADIEH SABA, SAFARI FATEME, GHALEBI BAHARE AND SHANBEH MOHSEN  
EFFECT OF TENSILE FATIGUE CYCLIC LOADING ON PERFORMANCE OF TEXTILE-BASED STRAIN SENSORS
- 11 ŞARAFNAL DILEK AND BABAARSLAN OSMAN  
INVESTIGATION OF THE USAGE OF ALTERNATIVE NEW GENERATION ECO-FRIENDLY FIBER BLENDS IN SYNTHETIC BASED DENIM FABRICS
- 18 KOÇAMAN RECEP TÜRKAY, PUTZKE ENRICO AND FICKER FRANK  
WEAVEABILITY OF SPACER/DISTANCE FABRICS WITH HIGH PERFORMANCE FIBERS ON A TECHNICAL DOUBLE RAPIER JACQUARD WEAVING LOOM USING LANCETS
- 24 FANG JIAHUI, KYOSEV YORDAN KONSTADINOV, LI YULING AND MA YANXUE  
SIMULATION OF THE SEGMENT FILLING INSERTION FABRICS AT THE YARN LEVEL
- 30 BOŇKOVÁ KAROLÍNA  
NUMERICAL MODELLING OF TEXTILE STRUCTURES: POTENTIAL AND LIMITS
- 36 İNCE MEHMET ERDEM, İNANIR SEVGI AND ERDOĞAN ESRA KUMSAL  
COMFORTABLE AND PROTECTIVE HYBRID WEFT-KNIT PLATED FABRIC FROM GLASS AND WOOL/ACRYLIC YARNS
- 42 LIU HAIJANG, KYOSEV YORDAN AND JIANG GAOMING  
PATTERN RELATED ISSUES IN THE MODELLING OF DEFORMED OVER SURFACE WARP KNITTED STRUCTURES WITH LONGER UNDERLAPS
- 49 PONECKA AGATA, BARBURSKI MARCIN, FRANZ DAVID, CUARTERO JESÚS AND MIRALBES RAMON  
NEW SOLUTIONS IN THE PRODUCTION OF COMPOSITES - MECHANICAL PROPERTIES OF COMPOSITES REINFORCED WITH TECHNICAL EMBROIDERY AND WOVEN FABRIC MADE OF FLAX FIBERS
- 54 GABEN MAHDI AND GOLDFELD YISKA  
DETECTING DAMAGED ZONES ALONG SMART SELF-SENSORY CARBON BASED TRC BY TDR
- 61 YOSEF LIDOR AND GOLDFELD YISKA  
INTELLIGENT TEXTILE AND FIBER REINFORCED MPC COMPOSITES FOR SHM
- 67 ÖZDEMİR SUZAN, ÖZTEMUR JANSET, SEZGİN HANDE AND YALÇIN-ENİS İPEK  
THE EFFECT OF POLYMER TYPE AND FIBER ORIENTATION ON THE COMPLIANCE PROPERTIES OF ELECTROSPUN VASCULAR GRAFTS
- 72 ÖZTEMUR JANSET, ÖZDEMİR SUZAN, SEZGİN HANDE AND YALÇIN-ENİS İPEK  
A PRELIMINARY STUDY EXAMINING THE BURST STRENGTH OF VASCULAR TUBULAR SCAFFOLDS
- 76 PALAK HANCI AND KAYAĞLU BURÇAK KARAGÖZEL  
FABRICATION AND CHARACTERIZATION OF ELECTROSPUN ANTHOCYANIN-LOADED POLYLACTIDE NANOFIBERS
- 80 KANIA ANNA AND BARBURSKI MARCIN  
IMPROVING LOCAL THERMAL COMFORT IN BUILDINGS: A STUDY OF PROPERTIES OF HEATING TEXTILE COMPOSITES IN CONSTRUCTION INDUSTRY
- 84 AGHADAVOOD ROYA, SHAHBAZ ZAHRA, KHERI TAHEREH, SHANBEH MOHSEN AND MARTINEK RADEK  
DESIGN AND INVESTIGATION THE OPERATION OF TEXTILE BASED ELECTRODES FOR ELECTROTHERAPY
- 88 PEKTAŞ KORAY, BALCI ONUR AND ORHAN MEHMET  
SOLUTION BLOWN OF PLA NANOFIBER CONTAINING OZONATED MORMODICA OIL AND ITS MICROCAPSULES TO OBTAIN ANTIBACTERIAL MEDICAL TEXTILES SURFACES
- 93 KORKMAZ AHMET AND BABAARSLAN OSMAN  
CHITOSAN ADDED COMPOSITE VISCOSE YARN AND ITS POTENTIAL APPLICATION FOR DENIM FABRIC DEVELOPMENT
- 99 ARSOY RAŞIT AND ASLAN SELÇUK  
DESIGN OF ELECTRONICALLY CONTROLLED JACQUARD MACHINE FOR MULTI-SHED WEAVING MACHINES
- 105 LEMMI TSEGAYE SH. AND BARBURSKI MARCIN  
THERMAL AGING EFFECT ON THE PHYSIO-MECHANICAL PROPERTIES OF TEXTILES USED FOR THE REINFORCEMENT OF CONVEYOR BELTS
- 110 SOOCHETA ANAGHA VAIDYA AND BHUNDOO SANSKRITA SINGH  
INVESTIGATING THE APPLICATION OF TERRA DYE ON COTTON KNITTED FABRICS
- 120 MELNYK LUDMYLA AND KYZYMCHUK OLENA  
NOVEL ELASTIC WARP KNITTED FABRIC WITH PERFORATION
- 126 SEN KORHAN, KAYA AYSEGUL AND KANIK GOKSU  
INVESTIGATION OF STRUCTURAL AND PERFORMANCE PROPERTIES OF HEMP-CONTAINING KNITTED FABRICS WITH DIFFERENT COMPOSITIONS
- 131 BOGUŃ MACIEJ, ŚLEDZIŃSKA KATARZYNA, GIEŁDOWSKA MAŁGORZATA, KRÓL PAULINA, KAMIŃSKA IRENA AND MAGDZARZ SYLWIA  
POLYACRYLONITRILE NONWOVENS FOR THE PRODUCTION OF CARBON MATERIALS SUPPORTING THE REGENERATION OF BONE AND CARTILAGE TISSUES
- 134 BŘEZINOVÁ HELENA, PECHOČIAKOVÁ MIROSLAVA AND GRABMÜLLEROVÁ JANA  
IDENTIFYING THE MATERIALS IN ARCHAEOLOGICAL TEXTILES
- 138 FISCHER HOLGER, SIGMUND INA, HARTWIG PETRA, DEDERER ESTHER AND MASCHINSKI ANNETT  
STANDARDISING THE SAMPLE PREPARATION FOR ANALYSIS OF FIBRES AND PARTICLES BY STATIC IMAGE ANALYSIS
- 143 TOMOVSKA ELENA AND HES LUBOS  
SURFACE ROUGHNESS OF POLYAMIDE KNITTED FABRICS

